การวิเคราะห์โครงข่ายเคลื่อนที่ความจุสูงที่มีเซลล์ขนาดเล็กหนาแน่นภายในอาคารสามมิติ

นายโรนี่ คูเมอร์ ซาฮา

วิทยานิพนธ์นี้เป็นส่วนหนึ่งของการศึกษาตามหลักสูตรปริญญาวิศวกรรมศาสตรดุษฎีบัณฑิต
สาขาวิชาวิศวกรรมไฟฟ้า ภาควิชาวิศวกรรมไฟฟ้า
คณะวิศวกรรมศาสตร์ จุฬาลงกรณ์มหาวิทยาลัย
ปีการศึกษา 2559

ANALYSIS OF HIGH CAPACITY MOBILE NETWORK WITH 3D IN-BUILDING DENSE SMALL CELL

Mr. Rony Kumer Saha

A Dissertation Submitted in Partial Fulfillment of the Requirements
for the Degree of Doctor of Philosophy Program in Electrical Engineering
Department of Electrical Engineering
Faculty of Engineering
Chulalongkorn University
Academic Year 2016

Thesis Title	ANALYSIS OF HIGH CAPACITY MOBILE NETWORK WITH 3D IN-BUILDING DENSE SMALL CELL
By	Mr. Rony Kumer Saha
Field of Study	Electrical Engineering
Thesis Advisor	Associate Professor Chaodit Aswakul, Ph.D.

Accepted by the Faculty of Engineering, Chulalongkorn University in Partial Fulfillment of the Requirements for the Doctoral Degree

.....Dean of the Faculty of Engineering
(Associate Professor Supot Teachavorasinskun, D.Eng.)

THESIS COMMITTEE

.....Chairman
(Associate Professor Watit Benjapolakul, D.Eng.)
.....Thesis Advisor
(Associate Professor Chaodit Aswakul, Ph.D.)
.....Examiner
(Associate Professor Lunchakorn Wuttisittikulkij, Ph.D.)
.....Examiner
(Yan Zhao, Ph.D.)
.....External Examiner
(Professor Yusheng Ji, Dr.Eng.)

โรนี่ คูเมอร์ ซาฮา : การวิเคราะห์โครงข่ายเคลื่อนที่ความจุสูงที่มีเซลล์ขนาดเล็กหนาแน่นภายในอาคารสามมิติ (ANALYSIS OF HIGH CAPACITY MOBILE NETWORK WITH 3D IN-BUILDING DENSE SMALL CELL) อ.ที่ปรึกษาวิทยานิพนธ์หลัก: เชาวน์ดิศ อัศวกุล, 333 หน้า.

วิทยานิพนธ์ฉบับนี้มุ่งตอบสนองความต้องการสร้างความจุให้สูงขึ้นในโครงข่ายเคลื่อนที่ยุคหน้า (เอนจีเมมเอน) นั่นคือ เทคโนโลยียุคที่ห้า ด้วยเซลล์ขนาดเล็ก เช่น เซลล์เฟมโต ซึ่งถูกติดตั้งสำหรับพื้นที่ให้บริการภายในอาคารสามมิติโดยการใช้กระบวนการต่าง ๆ เช่น การจัดการสัญญาณรบกวนระหว่างช่องสัญญาณ, การกำกับใช้ระยะทางขั้นต่ำระหว่างสถานีฐานที่ติดกัน, การใช้สเปกตรัมซ้ำและการแยกระนาบควบคุมกับระนาบผู้ใช้ (ระนาบซี-ยู) ของเซลล์เฟมโต ในปัจจุบันนั้นโครงข่ายเคลื่อนที่อื่น ๆ มีลักษณะทั่วไปอันหนึ่งคือสถาปัตยกรรมที่ระนาบ ซี-ยู ติดกันอย่างแน่นซึ่งนำไปสู่ปัญหาต่าง ๆ ในโครงข่ายเซลล์ขนาดเล็ก เช่น การจัดการสัญญาณรบกวนที่มีความซับซ้อน ข้อจำกัดนี้ได้นำไปสู่การพัฒนาสถาปัตยกรรมการแบ่งระนาบ ซี-ยู (ซียูเอสเอ) โดยการทำให้ระนาบ ซี-ยู นั้นแยกออกจากกัน นอกจากนี้ในโครงข่ายเคลื่อนที่เซลลูลาร์ต่าง ๆ นั้นทราฟฟิกข้อมูลส่วนใหญ่ถูกสร้างขึ้นภายในพื้นที่ครอบคลุมบริการในอาคาร ซึ่งเป็นสถานการณ์หลักในเมืองซึ่งมีอาคารสูงหลายชั้นอยู่โดยทั่วไป และการแพร่กระจายคลื่นวิทยุในสถานการณ์สามมิตินั้นมีความซับซ้อนมากกว่าในกรณีสองมิติอย่างมาก ด้วยเหตุนี้จึงนำไปสู่ประเด็นสำคัญต่าง ๆ เช่น การจำลองสถาปัตยกรรมโครงข่ายเซลล์ขนาดเล็กและการกำหนดลักษณะเฉพาะสัญญาณรบกวน, การพัฒนากลยุทธ์การแบ่งทรัพยากรและการใช้ซ้ำ ตลอดจนการวิเคราะห์ขีดจำกัดในการเพิ่มความหนาแน่นเซลล์ขนาดเล็ก และการพัฒนาของเทคนิคออกแบบใหม่สำหรับโครงข่ายเซลล์ขนาดเล็กภายในอาคารสามมิติ งานวิจัยในวิทยานิพนธ์ฉบับนี้ได้พิจารณาประเด็นต่าง ๆ เหล่านี้

ผลงานโดยเฉพาะที่ได้นำเสนอไว้ในวิทยานิพนธ์มีดังนี้: (i) การทบทวนเทคโนโลยีสนับสนุนต่าง ๆ เพื่อเสนอกรอบความคิดของพัฒนาการสถาปัตยกรรมโครงข่ายเคลื่อนที่ยุคหน้าเพื่อให้ได้ความจุของโครงข่ายตามที่คาดหวังไว้ สำหรับโครงข่ายเซลล์เป็นศูนย์กลางนั้นงานวิจัยนี้ได้นำเสนอ (ii) ขั้นตอนวิธีเพื่อจัดกำหนดการและการใช้ความถี่ซ้ำ (เอฟอาเอสเอ) ซึ่งใช้การประสานงานเพื่อปรับปรุงสัญญาณรบกวนระหว่างเซลล์ (อีไอซีไอซี) ด้วยเฟรมย่อยเกือบว่าง (เอบีเอส) แบบปรับตัวได้ สำหรับการจัดสรรและการใช้ทรัพยากรซ้ำเชิงตั้งฉาก (โออาอาเอ), (iii) แบบจำลองเชิงวิเคราะห์ที่จัดการได้ง่ายสำหรับกำหนดลักษณะเฉพาะสัญญาณรบกวน และการกำกับใช้ระยะทางขั้นต่ำสำหรับการจัดสรรและการใช้ทรัพยากรซ้ำแบบไม่เชิงตั้งฉาก (เอนโออาอาเอ), และ (iv) แนวทางใหม่การจัดกลุ่มด้วยกลยุทธ์ที่นำเสนอเพื่อใช้ทรัพยากรในเซลล์เฟมโตซ้ำภายในอาคารหลายชั้นสามมิติ นอกจากนี้สำหรับโครงข่ายอุปกรณ์เป็นศูนย์กลางนั้นงานวิจัยนี้ได้นำเสนอ (v) สถาปัตยกรรมของอุปกรณ์ผู้ใช้ และเซลล์ขนาดเล็กที่ใช้งานแบนด์หลายช่วงแบบใหม่สำหรับเชื่อมโยงขึ้น/เชื่อมโยงลง และการแยกระนาบ ซี-ยู, (vi) สถาปัตยกรรมของสถานีฐานเซลล์ขนาดเล็ก (เอสซีบีเอส) สำหรับการเปรียบเทียบสมรรถนะของซียูซีเอ และซียูเอสเอ และ (vii) แนวทางการจัดสรรทรัพยากรคลื่นความถี่วิทยุสามมิติแบบรวมศูนย์ และแนวทางจัดกำหนดการสำหรับซียูเอสเอ

ภาควิชา วิศวกรรมไฟฟ้า ลายมือชื่อนิสิต .....

สาขาวิชา วิศวกรรมไฟฟ้า ลายมือชื่อ อ.ที่ปรึกษาหลัก .....

ปีการศึกษา 2559

5771421221 : MAJOR ELECTRICAL ENGINEERING
KEYWORDS: SMALL CELL / 5G MOBILE / NETWORK DENSIFICATION / INTERFERENCE MODELING / RESOURCE ALLOCATION / 3D / IN-BUILDING

RONY KUMER SAHA: ANALYSIS OF HIGH CAPACITY MOBILE NETWORK WITH 3D IN-BUILDING DENSE SMALL CELL. ADVISOR: ASSOC. PROF. CHAODIT ASWAKUL, Ph.D., 333 pp.

This dissertation research emphasizes on achieving high capacity demand of next generation mobile networks (NGMN), i.e. fifth generation (5G), with small cells, i.e. femtocells, deployed in 3-dimensional (3D) indoor coverages by employing such procedures as managing co-channel interference, enforcing a minimum distance, reusing spectrum, and splitting control-plane and user-plane (C-/U-plane) of femtocells. In conventional mobile networks, a common feature is tightly coupled C-/U-plane architecture (CUCA) which is one of the major reasons for most of the problems that small cell network densification faces, e.g. complex interference management. This call for developing a new C-/U-plane split architecture (CUSA) by decoupling C-/U-plane. Further, in cellular mobile networks, most of the data traffic is generated within indoor coverages, mainly in urban environments where an existence of dense high rise multi-floor buildings is a typical scenario. Furthermore, mobile radio propagation in 3D scenario is far more complex than that of 2D scenario. These cause such inevitable issues as small cell network architecture modeling and interference characterization, resource reuse and allocation strategy development, and small cell densification limit characterization to call for their in-depth investigation and the development of new design technique for 3D in-building small cell networks. This dissertation research addresses these aforesaid issues.

More specifically, the following objectives are addressed in this dissertation: (i) a review on enabling technologies for proposing a framework of NGMN architectural evolution to achieve the prospective capacity of NGMN; for cell-centric networks, (ii) an adaptive almost blank subframe (ABS) based enhanced intercell interference coordination (eICIC) enabled frequency reuse and scheduling algorithm (FRSA) for an orthogonal resource reuse and allocation (ORRA), (iii) a tractable analytical model for interference characterization and minimum distance enforcement for non-ORRA (NORRA), and (iv) a novel clustering approach along with developing a number of strategies to reuse resources in femtocells within a 3D multi-floor building; for device-centric networks, (v) a novel multi-band enabled small cell and UE architecture for uplink/downlink (UL/DL) and C-/U-plane splitting, (vi) numerous small cell base station (SCBS) architectures for performance comparisons between CUCA and CUSA, and (vii) a centralized 3D radio resource allocation and scheduling approach for CUSA.

Department:	Electrical Engineering	Student's Signature	.....
Field of Study:	Electrical Engineering	Advisor's Signature	.....
Academic Year:	2016		

ACKNOWLEDGEMENTS

Foremost of all, I would like to outspread my innumerable gratitude to my advisor, Professor (Associate) Chaodit Aswakul, Ph.D., for all the way up to this far I have achieved in the Ph.D. program at Chulalongkorn University. His state-of-the-art approaches, insightful thoughts, meaningful discussions, prompt feedbacks, and beforehand supports are just a few to mention that help shape me toward being an independent researcher. Thank you so very much for occupying yourself with such an extraordinary role during this wonderful journey of my life for achieving Ph.D. degree in Electrical Engineering.

I am indebted to this dissertation research grant funders provided by the 100th Anniversary Chulalongkorn University Fund for Doctoral Scholarship and the Electrical Engineering Ph.D. (EECU-Ph.D.) Honors Program Scholarship, Chulalongkorn University, Bangkok, Thailand.

I would like to thank all the other committee members, including chairman, examiners, and external examiners, of this dissertation research for showing keenness, spending valuable time, and sharing view to help make the research work improved further.

I would also like to thank Professor (Associate) Poompat Saengudomlert, Ph.D., Bangkok University, Thailand for his valuable discussions and comments on the dissertation research and to help improve the quality of the published first journal article on this dissertation research.

Finally, I would like to thank my family and friends for their always reinforcements and supports.

CONTENTS

Page

Page

Page

Page

Page

Page

Page

Page

Page

LIST OF FIGURES

LIST OF TABLES

LIST OF ABBREVIATIONS

Abbreviation	Expansion
2D	2-Dimensional
3D	3-Dimensional
3G	Third Generation
3GPP	Third Generation Partnership Project
4G	Fourth Generation
5G	Fifth Generation
AAF	Average Activation Factor
ABS	Almost Blank Subframe
BS	Base Station
C-/U-plane	Control-plane and User-plane
cFC	Co-channel Femtocell
cFCBS	Co-channel Femtocell Base Station
CH	Cluster Head
CoMP	Coordinated Multi-Point
C-plane	Control-plane
C-RAN	Cloud Radio Access Network
CRPA	Common Resource Pool and Allocation
CSG	Closed Subscriber Group
CSI	Channel State Information
CUCA	C-/U-plane Coupled Architecture
CUSA	C-/U-plane Separation Architecture
dB	Decibel
dBi	Decibel relative to an isotropic radiator
dBm	Decibel-Milliwatts
DBSA	Different BSs based Split Architecture
eICIC	Enhanced Inter-Cell Interference Coordination
FBS	Fully Blank Subframe
FC	Femtocell

FCBS	Femtocell Base Station
FCL	Femtocell Cluster
FD	Frequency-Domain
FFR	Fractional Frequency Reuse
FPP	FBS Pattern Period
FRSA	Frequency Reuse and Scheduling Algorithm
FU	Femto User Equipment
HetNets	Heterogeneous Networks
ICIC	Inter-Cell Interference Coordination
IC-RRM	Inter-Cell RRM
IP	Internet Protocol
LOS	Line-of-Sight
LTE	Long Term Evolution
LTE-Advanced	Long Term Evolution-Advanced
MC	Macrocell
MCBS	Macrocell Base Station
MIMO	Multiple-Input Multiple-Output
MME	Mobility Management Entity
mmWave	Millimeter Wave
MU	Macro UE
NGMN	Next Generation Mobile Networks
NORRA	Non-Orthogonal Resource Reuse and Allocation
OAF	Optimal value of AAF
OPNA	Optimal Number of ABSs
ORPA	Orthogonal Resource Pool and Allocation
ORRA	Orthogonal Resource Reuse and Allocation
PC	Picocell
PCBS	Picocell Base Station
PGW	Packet Data Network Gateway
RA	Random Access
RAN	Radio Access Network

RB	Resource Block
RoE	Region of Exclusion
RRC	Radio Resource Control
SBSA	Single BS based Split Architecture
SC	Small Cell
SDN	Software Defined Network
sFCBS	Serving Femtocell Base Station
SGW	Serving Gateway
SINR	Signal-to-Interference-plus-Noise Ratio
SON	Self-Optimizing Network
TD	Time-Domain
TTI	Transmission Time Interval
UE	User Equipment
UL/DL	Uplink and Downlink
U-plane	User-plane
WiMAX	Worldwide Interoperability for Microwave Access
WSDN	Wireless Software Defined Network

LIST OF NOTATIONS

Notation		Description
$t_{non-FBS}$	≜	A non-FBS
$\boldsymbol{T_{FBS}}$	≜	A set of FBS indices over all FPPs for *Q* TTIs
$\boldsymbol{N_M}$	≜	A set of indices of all MUs
T_{APP}	≜	ABS pattern period
σ_{cc}^{FC}	≜	Aggregate capacity of all FCBSs for co-channel frequency
σ_{df}^{FC}	≜	Aggregate capacity of all FCBSs for different frequency mmWave
$\alpha_{agg,ter}$	≜	Aggregate link interference inter-floor level
$\alpha_{agg,tra}$	≜	Aggregate link interference intra-floor level
$\sigma_i(T_{ABS})$	≜	Aggregate throughputs of all indoor MUs as a function of T_{ABS}
$\sigma_o(T_{ABS})$	≜	Aggregate throughputs of all outdoor MUs as a function of T_{ABS}
φ	≜	An arbitrary ABS pattern
α_{fbs}	≜	An arbitrary FBS pattern
t_{FBS}	≜	An FBS
α	≜	Average activation factor
$\alpha_{off\rightarrow on}$	≜	Average aggregate delay per FPP from switching off-state to on-state of any FCBSs for traffic request processing of any FUs
$\alpha_{on\rightarrow off}$	≜	Average aggregate delay per FPP from switching on-state to off-state of any FCBSs for traffic request processing of any FUs
σ_{avg}^{nsr}	≜	Average network sum rate
γ_{mc}	≜	Average spectral efficiency of a MCBS
γ_{sc}	≜	Average spectral efficiency of a SCBS
B_{mc}	≜	Bandwidth of a MCBS
B_{sc}	≜	Bandwidth of a SCBS
κ	≜	Capacity scaling factor
ζ	≜	Categories of UE in the system

$H_{t,i}$ ≜ Channel response for a link between a UE and a BS at RB = *i* in TTI = *t*

χ_{ter} ≜ Chromatic number inter-floor level

χ_{tra} ≜ Chromatic number intra-floor level

M_{mcbs} ≜ Co-channel low frequency band for both MCBS and FCBSs

x_c ≜ Control signaling traffic (in percentage of U-plane traffic)

L_{ow} ≜ External wall penetration loss

$\alpha_f(\cdot)$ ≜ Floor attenuation factor

M_{fcbs} ≜ High frequency band for FCBSs only

β ≜ Implementation loss factor

$I_{t,i}$ ≜ Interference signal power at any RB = *i* in any TTI = *t*

F_J ≜ Jain's fairness index

$\sigma_{thr,ter}$ ≜ Link capacity constraint inter-floor level

$\sigma_{thr,tra}$ ≜ Link capacity constraint intra-floor level

C_{link} ≜ Link capacity for a point-to-point communication between a MCBS and a UE

σ_{ter} ≜ Link capacity inter-floor level

σ_{tra} ≜ Link capacity intra-floor level

$\alpha_{thr,ter}$ ≜ Link interference constraint inter-floor level

$\alpha_{thr,tra}$ ≜ Link interference constraint intra-floor level

$\alpha_{thr,se}$ ≜ Link spectral efficiency constraint for both intra-and inter-floor level

$\sigma_{ter,se}$ ≜ Link spectral efficiency inter-floor level

$\sigma_{tra,se}$ ≜ Link spectral efficiency intra-floor level

$\sigma_{t,i}$ ≜ Link throughput at RB = *i* in TTI = *t* (bps/Hz)

$C_i^{\max}$ ≜ Maximum aggregate throughput of indoor MUs

$C_o^{\max}$ ≜ Maximum aggregate throughput of outdoor MUs

$y_{\max,ter}$ ≜ Maximum number of cFCBSs for a sFCBS inter-floor level

$y_{\max,tra}$ ≜ Maximum number of cFCBSs for a sFCBS intra-floor level

L ≜ Maximum number of FCLs in a MC coverage for ORRA

Q ≜ Maximum number of TTIs per simulation run time

$d_{\min}$ ≜ Minimum distance between sFU and any cFCBSs

d_{ter}^{*} ≜ Minimum distance inter-floor level

d_{tra}^{*} ≜ Minimum distance intra-floor level

$n_{t,i}$ ≜ Noise power at any RB = i in any TTI = t

n_p ≜ Normalized noise power

$\boldsymbol{T_{ABS}}$ ≜ Number of ABSs in an ABS pattern period

cl_{intra} ≜ Number of clusters per floor

n_{diag} ≜ Number of FCBSs along the diagonal of a square RoE

n_{fl} ≜ Number of floors

fl_{3DR} ≜ Number of floors within the RoE for inter-floor level constraint

T_{FBS} ≜ Number of fully blank subframes per FPP

S_P ≜ Number of PCs in the MC coverage

M_{ncFC} ≜ Number of RBs for all non-cFCBSs

M_C ≜ Number of RBs for the C-plane traffic of all UEs

M_{iMU} ≜ Number of RBs for the U-plane traffic of all indoor MUs

M ≜ Number of RBs in the microwave system bandwidth

m ≜ Number of RBs in the mmWave system bandwidth

M_{UFC} ≜ Number of RBs that can be reused in FCBSs per cluster in CUCA

Ξ_{ter}^{wr} ≜ Number of reused RBs in cFCBSs inter-floor level

Ξ_{tra}^{wr} ≜ Number of reused RBs in cFCBSs intra-floor level

M_{cFC} ≜ Number of reused RBs per cFCBS

T_{FPP} ≜ Number of subframes per FPP

$P(\text{off-state})$ ≜ Off-state probability of the transmit power of a FCBS

$P(\text{on-state})$ ≜ On-state probability of the transmit power of a FCBS

α^{*} ≜ Optimal average activation factor

PL	≜	Path loss
α_s	≜	Percentage average duration of any in-progress active FU traffic per FPP
α_{ns}	≜	Percentage average duration of in-active FU traffic per FPP
x_{cp}	≜	Percentage of C-plane traffic in CUCA
μ_{iM}	≜	Percentage of indoor MUs in the MC coverage
λ_p	≜	Power off-state to on-state transition rate of any FCBSs
μ	≜	Power on-state to off-state transition rate of any FCBSs
η	≜	Power saving factor of any FCBSs
m_{RB}	≜	RB indices
$S_{r,cl}$	≜	RB resources allocated to FCBS *r* of cluster *cl*
$\rho_{t,i}$	≜	Received SINR for a UE at any RB = *i* in any TTI = *t*
ξ	≜	Resource reuse factor
U_T	≜	Reusable time resource utilization factor
$\boldsymbol{T}$	≜	Simulation run time
m_i	≜	Slope of aggregate throughput equation for indoor MUs
m_o	≜	Slope of aggregate throughput equation for outdoor MUs
$p(\cdot)$	≜	State probabilities in the Birth-Death process
C_{sys}	≜	System capacity
σ^{sys}	≜	System level average spectral efficiency (bps/Hz) per RB per TTI
T^*_{ABS}	≜	The value of an OPNA
S_{FS}	≜	Total number of active FCs in the system for ORRA
n_{cl}	≜	Total number of FCBSs in a cluster
N	≜	Total number of MUs
m_{orth}	≜	Total number of orthogonal set of RBs per RoE for static allocation
X_x	≜	Total number of RBs allocated to user *x* over the simulation runtime
P_F	≜	Transmit power of any FC
P_M	≜	Transmit power of any MC

P_P $\triangleq$ Transmit power of any PC

T_w $\triangleq$ Wastage of reusable time resources

CHAPTER 1
INTRODUCTION

This chapter gives an introduction of the dissertation research as a whole. The chapter starts with a background to give a broad idea of the dissertation topic followed by a problem statement that mainly concerns with what is known, unknown, and attempted to be known by the research community. Related works are mentioned by listing relevant state-of-the-art literature to find a research gap and clarify the novelties and merits of the research gap that the dissertation aims to address. Based on the research gap, objectives of the dissertation are stated with scopes and limitations. The chapter ends with a brief outline of the whole dissertation work, which lists out how the objectives are addressed in the subsequent chapters.

1.1 Background

The exponentially growing number of mobile users and an ever-increasing demand of high data rates impose several challenges on current cellular networks, e.g. fourth generation (4G) long term evolution (LTE) network and its evolutions, in terms of a high network capacity and a wide coverage area to meet up the user demand in next generation mobile networks (NGMN), i.e. fifth generation (5G) mobile networks. The major drawbacks that mobile users face from current networks are a non-uniform low data rate, a non-unified quality of experience, a poor end-to-end performance, a weak indoor coverage, an insufficient high mobility performance, and a high cost per bit transfer. Similarly, network operators face a number of difficulties in providing satisfactory services with their current mobile networks, such as provisions of a high network capacity, low latency, high spectral efficiency, large amount of spectrum availability, and low energy consumption.

Moreover, network performances play a significant role on the evolution of a new generation of mobile networks. In mobile wireless networks, the network capacity

has been seen as the main driver for evolution of a number of past generations, e.g. second generation (2G), third generation (3G), and 4G. In a similar trend, achieving a high capacity is considered also the major driver for the evolution of 5G networks. Typically, to address a high capacity demand, network operators consider reducing the distance between a base station (BS) and a user equipment (UE) in order to improve the received signal strength at a UE. A standard practice to reduce cell coverage is to deploy low power nodes such as femtocells (FCs), picocells (PCs) in the coverage of a macrocell (MC). This results in shifting traditional homogeneous networks to more advanced heterogeneous networks (HetNets). A low power node covers a small portion of a MC area, and hence is also termed as a small cell (SC).

Since typically the capacity per unit area increases with the number of SCs, SCs are expected to be deployed as densely as possible, and hence HetNets are thus extended to dense HetNets as one of the potential techniques to address high capacity demand of 5G networks. Besides dense HetNets, the capacity of 5G networks will most likely be driven by spectrum aggregation and spectral efficiency technique. Since microwave frequencies deployed in existing networks are almost saturated, millimeter wave (mmWave) spectrum bands are considered for 5G networks to increase system bandwidth because of usable high spectrum availability in these bands. Many advanced techniques such as enhanced inter-cell interference coordination (eICIC) [1], cooperative communication, and massive multiple-input multiple-output (MIMO) have been proposed as the major enabling technologies to improve spectral efficiency of 5G networks.

Since low power small cell base stations BSs (SCBSs) deployed in a MC coverage can contribute to improving the system capacity of 5G networks, the capacity gain can be improved further if the system bandwidth can be reused as many times as possible. A reuse of system bandwidth depends mainly on two aspects, namely deployment scenarios and SC densities, and is done by co-channel deployment of SCs within a MC. The reuse can be increased significantly by a dense deployment of SCs per unit area. In dense HetNets, an extremely large number of SCs are deployed where the coverages of SCs can even overlap one another. However, this raises the concern of generating a significant level of interference from one cell to another. Interference is one of the major bottlenecks and more severe in dense HetNets than in traditional

homogeneous networks. Major sources of interference in HetNets are unplanned deployment, restricted FC access, and transmission power difference among nodes [1]. FCs are partly deployed by users in an unplanned fashion with almost no consciousness on density, location, and access type of FCs from an operator perspective. If the access type of a FC is configured as closed subscriber group (CSG), interference effect becomes the most severe in comparison with the other access types.

Interference in HetNets can better be managed by using frequency-domain (FD), time-domain (TD), and power control inter-cell interference coordination (ICIC) techniques which are aggregately called as eICIC [1]. In TD eICIC technique, a victim UE is scheduled in TD while interferences from other nodes are reduced. In FD eICIC technique [1], by an orthogonal scheduling of control channels between cells in a reduced bandwidth, interference can be mitigated. In power control eICIC technique, different power control techniques can be applied to SCs [1]. A straightforward way to address the interference effect is to allocate orthogonal frequencies to SCs. However, this approach directly impacts a limited and highly expensive system bandwidth, and hence the achievable system capacity. Another approach is to ensure a very tight coordination among SCs such that the same frequency can be reused among SCs with an appropriate cooperation.

Besides, the propagation in indoor environment appears to be much more uncertain in large scale than in the outdoor environment. Because of a number of effects in 3-dimensional (3D) in-building scenarios, e.g. complex indoor propagation mechanisms (from effects within and outside the building of interest, i.e. direct signal component, reflection from walls and ceilings within the building, and nearby buildings) and diffraction (from edges and along the building surfaces), 3D modeling of indoor propagation is necessary over the mostly practiced 2-dimensional (2D) scenario for SC based dense HetNets. Since most existing approaches to interference management in SC networks are based on 2D model, these approaches cannot capture the aforementioned effects for an accurate in-building interference modeling. For example, many well established and accepted simplified models, which are reasonably applicable in outdoor environments, are not a straightforward extension to apply to indoor environments. Hence, outdoor models, which typically consider 2D scenario or single-floor indoor scenario for the resource reuse and interference management, are

not applicable to indoor 3D in-building scenario. Though there are mainly two approaches to model indoor propagation proposed in existing literature, because of complexity of theoretical models and non-portability of empirical models, a trade-off of these two approaches would be a reasonable choice for developing an indoor model with sufficient accuracy and less complexity to analyze the resource reuse and interference management in indoor SC networks.

One of the noticeable characteristics of current mobile networks is that both the control decision and processing task units exist in the same networking device, e.g. BS, serving gateway (SGW), and packet data network gateway (PGW) nodes in a LTE network. This implies that current mobile networks are based on distributed and coupled control and data planes where each entity distributed over the network is responsible for executing both decision making and processing tasks. This distributed nature of current mobile networks results in manifold challenges as follows:

- complexity in control and management of a network (e.g., a mobility manager needs to coordinate more with an increase in the number of users)
- a poor network efficiency (e.g., it is difficult to update existing devices with advanced solutions)
- non-evolvability (e.g., there are fewer scopes in creating service differentiations between competitors)
- inflexibility (e.g., operators rely on vendor specific solutions to introduce a new feature)

Hence, to address these challenges, network operators seek new solutions [2], and rather than considering the traditional cell-centric control, an advanced device-centric control has been proposed as a new solution [3] in distributed networks, in which the control-plane and user-plane (C-/U-plane) and the uplink and downlink (UL/DL) split architecture is considered, such that various functionalities, e.g. radio resource management, interference mitigation, and mobility control among network nodes can be managed more efficiently than that in cell-centric networks. A more detail discussion on these aforementioned aspects can be found in Chapter 2 and Appendix

A. Hence, to achieve high capacity demand of 5G networks, modeling interference, developing efficient resource reuse and allocation strategies, and defining limit of densification under various constraints in ultra-dense deployment of SCs, particularly in 3D in-building scenario for urban environments using traditional cell-centric and new device-centric network architectures have become crucial research issues that call enormous research attentions for possible solutions.

1.2 Problem statement

The 5G cellular is in its early stage of research and development with no clear direction on how the envisaged high capacity of 5G networks can be achieved. Though several proposals on enabling technologies as aforementioned from various aspects have been introduced in literature, how all these technologies can be applied, controlled, and managed to meet the required 5G capacity as well as what the 5G network architecture will eventually look like to achieve the target capacity is still an open research issue. Based on the trends of enabling technologies, 5G networks are expected to evolve in three major directions, namely, radio access network (RAN) nodes and performance improvement technologies to address the high 5G capacity demand, network programmable capability for the network control, and backhaul networks and network synchronization to enable coordination between nodes for a cost-effective quality of experience performance. Hence, all these trends can be classified into three such directions as RAN node and performance enabler, network control programming platform, and backhaul network platform and synchronization as parallel horizontal evolutionary paths toward 5G networks. All these evolutionary paths need to be vertically integrated to incorporate evolutionary aspects for a full-fledge 5G network architectural evolution.

Network densification is one of the major enablers to achieve the expected capacity and spectral efficiency of 5G networks [4] through reusing resources in SCs such as FCs. Reuse of resources in FCs relies on the inter-FC distance which is a function of co-channel interference generated from neighboring FCs. In urban environments where an existence of thousands of 3D multi-storage buildings is an

obvious scenario, modeling co-channel interference and a minimum distance between FCs in 3D scenario, e.g. office buildings and residential areas, to address high data rate demand of 5G networks has become one of the major growing concerns. Typically, interference in HetNets has been studied considerably in 2D scenario [5]. Modeling 2D interference is simple but not accurate enough since it cannot capture complex combinations of deployment and propagation effect existing in realistic 3D buildings. Authors in [5] investigated the impact of three-dimensionality of FC deployments on cross-and co-tier interferences using realistic building data and showed that the interference effect of FCs in urban 3D scenario is significantly higher than that when considering 2D case and proposed to model HetNets in 3D scenario rather than 2D. Theoretically, the maximum capacity of a SC can be achieved when it is allocated with the whole system bandwidth. However, in practice, it is difficult to achieve, and only a fraction of system bandwidth can be allocated to a SC to overcome co-channel interference. Hence, one of the ways to boost network capacity using a limited spectrum is to allocate as much of system bandwidth as possible to each SC by employing a proper interference management scheme. A FC typically has a limited coverage, and hence we can take this as an advantage by reusing the same frequency simultaneously in more than one FCs forming a FC cluster (FCL) to boost network capacity. However, reusing resources simultaneously in FCs results in a significant amount of co-channel interference if a minimum distance between co-channel FCs (cFCs) is not enforced. A denser FC network causes a higher co-channel interference effect at a UE. Hence, how to model co-channel interference and enforce a minimum distance between cFCs [6], i.e. densification limit, for reusing resources particularly in 3D in-building scenario has become an active research area.

In existing HetNets, a common feature is tightly coupled control-plane (C-plane) and user-plane (U-plane) irrespective of the degree of density and heterogeneity and is one of the major reasons for most of the problems that ND facing, e.g. low energy efficiency, complex interference management, higher signaling overhead and backhaul network requirement, and clumsy mobility management. As the data traffic demand increases, existing networks face problem from providing necessary capacity to transport this growing data traffic demand. To address such capacity requirement, SCs are deployed in the coverage of large MCs. However, tight coupling of the C-/U-plane

of conventional HetNets architecture restricts the flexibility in network operation and performance management. Typically, in conventional HetNets architecture, both MCs and SCs are operated at the same frequency to provide both coverage and data services. Because of tight coupling of the C-/U-plane, BSs need to be always active to ensure ubiquitous coverage even though there is no data traffic demand from UEs and results in a poor resource utilization and unnecessary energy consumption that leads to low energy efficiency (EE). These call for developing a new architecture where C-plane and U-plane are decoupled to switch the BSs on and off depending on the data traffic demand and to ensure always-on connectivity. Such a network architecture is termed as C-/U-plane separation architecture (CUSA) (Figure 1.1).

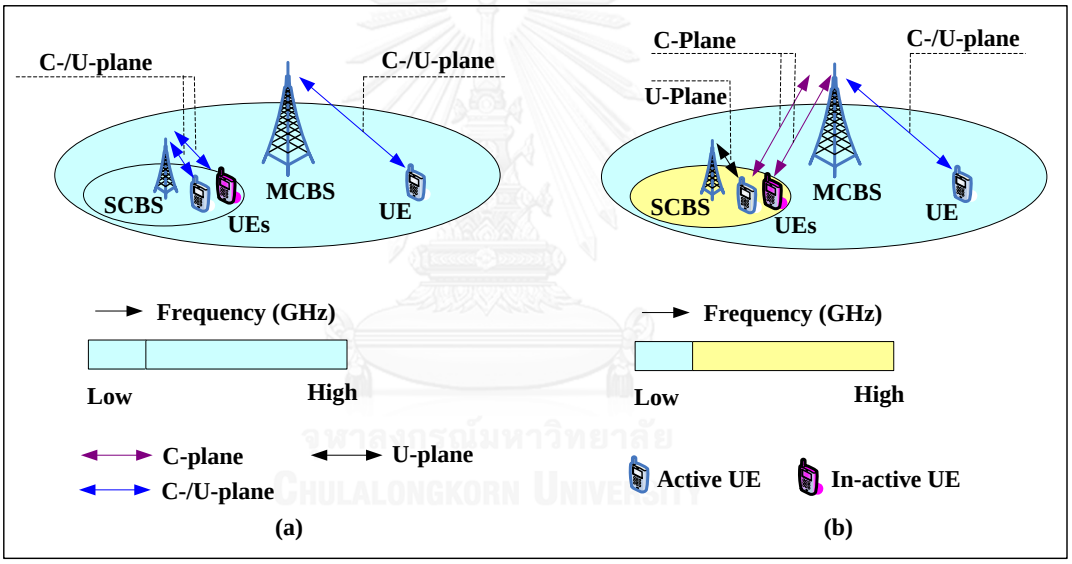

Figure 1.1 : (a) Conventional network architecture; (b) CUSA network architecture [7].

However, in comparison with conventional network architecture where all BSs are always active to overcome coverage holes so that there is no wake up signaling required, and handover procedure is executed by UEs using reference signal received power, the design of signaling network in CUSA is challenging [7]. This is because of the fact that for inactive SCBSs for data services, an optimal SCBS selection from inactive SCBSs and an initialization of wake-up mechanism are required. Since a macrocell BS (MCBS) has no instantaneous channel information of inactive SCBSs, an optimal SCBS selection can be quite challenging, and hence signaling network is more

complex in CUSA than that in conventional network architecture. This raises to do a performance analysis of device-centric networks over cell-centric networks for 5G capacity under constraints, e.g. optimal BS selection and signaling network design.

Overall, the research on ultra-densification is still in its early stage. Fundamental studies such as network architecture, densification limit, efficient radio resources utilization, and interference management need to be investigated for a successful 5G network deployment [8]. Moreover, since most of the data traffic are generated in indoor mainly in urban environments (where an existence of high rise multi-storage buildings is a typical scenario) and the radio propagation in 3D scenario is far more complex than that of the traditional 2D case, interference modeling, resource reuse and allocation, and SC densification limit of such 3D buildings ask a crucial call for deep investigations along with developing novel network design techniques for indoor SCs. For CUSA architecture, some open research questions such as heterogeneous deployment with dual connectivity, channel estimation, and management of discontinuous transmission techniques also need to be answered before considering CUSA architecture over the conventional network architecture [9]. Further, from network architectural aspects, the C-/U-plane separation based dense HetNets are considered promising solutions for a high capacity and an efficient network management of dense HetNets and hence call for immediate research concerns.

1.3 Related works

A few studies have been done towards the direction of surveying enabling technologies for 5G networks, such as [10-11]. However, most of the existing survey articles consider mainly one of the three evolution directions with some additional insights on the others. For example, [10] mainly addressed emerging technologies of the RAN node and performance enabler with an additional insight on software-defined network (SDN). Different from [10], [11] addressed a number of RAN nodes and performance enablers, network virtualization along with additional insights on research challenges regarding such issues as 5G measurement and testing and radio resource management. Although the issues regarding 5G backhaul networks are significant to

enable emerging technologies of other evolutionary directions, these issues remain mostly unaddressed in the existing literatures such as [10-11]. In addition, there is a lack of an architectural evolution framework for 5G networks, which can capture most of the dominant enabling technologies in a systematic approach. Hence, this call for an extensive survey on enabling technologies of NGMN that can capture most of the dominant technologies from a broad set of perspectives and allow developing a systematic framework of the 5G network architectural evolution for achieving expected capacity. For cell-centric networks, a number of existing literatures addressed such issues as modeling interference, enforcing minimum distance, and reusing resources in SCs in 3D in-building scenario for both orthogonal resource reuse and allocation (ORRA) where resource blocks (RBs) are allocated orthogonally to all SCs within a building, and non-ORRA (NORRA) where RBs can be reused more than once in SCs in a building for a given constraint.

For ORRA, an effective solution for 3D in-building coverage is distributed antennas systems (DAS) where antennas of a BS are distributed within a building. Several works studied interference management and resource reuse aspects using DAS in 3D in-building scenarios [12-15]. However, one of the major difficulties with DAS is that each antenna covers typically a larger area than that by a FC, and hence resource reuse and correspondingly overall throughput gain by DAS are lower than that achieved by FC based HetNets [13]. A number of studies also addressed issues of interference management and resource reuse in FCs under 3D in-building scenario. In [5], authors investigated the impact of 3D FC deployments on cross-tier and co-tier interferences using realistic building data and showed that interference effects of urban FCs under 3D are significantly higher than that when considering 2D scenario. Authors in [16] proposed a graph based adaptive FC clustering scheme for inter-FC interference coordination within the same building. Authors in [17] proposed a dynamic clustering based cognitive sub-band allocation scheme to reduce inter-FC interference. FCLs are formed using inter-FC interference graphs, and resources are reused in each disjoint FCL within a building. In [18], authors proposed a semi-static resource allocation scheme where the minimum number of subbands, one for each FC, is computed by solving a node-coloring heuristic algorithm in a multi-floor building over iBuildNet, an indoor network planning and optimization tool. In [19], authors proposed an adaptive

soft frequency reuse scheme where groups of FCs are formed using received signal strength indication from UEs, and different frequency reuse factors and transmission powers are adjusted to mitigate interference. Authors in [20] exploited fractional frequency reuse (FFR) to propose a cooperative transmission and a semi-static interference mitigation scheme for in-building dense FCs. Most of these existing works addressed FC clustering within the same building for resource reuse in FCLs rather than over a large MC coverage. Though authors in [21] addressed FC clustering over a MC coverage, the proposed approach is however limited to 2D scenario and amorphous shape of FCLs. Further, though in reality indoor macro UEs (MUs) cannot get access to CSG femtocell BSs (FCBSs) and interfere with FCBSs and femto UEs (FUs), the existence of indoor MUs within buildings has been overlooked. Hence, no cross-tier interference management mainly in the downlink (DL) between indoor MUs and FUs and the UL between indoor MUs and CSG FCBSs has been addressed. Also, implications on interference from neighboring buildings because of resource reuse has not been emphasized which affects the maximum resource reuse factor per MC. Besides, though in HetNets, FC clustering and resource reuse mostly for two-tier networks in 3D in-building scenario and eICIC for interference management has been studied separately in literature, a combined scheme that can benefit from both eICIC techniques and multi-tier dense HetNets over a large MC coverage has not been addressed yet.

For NORRA, the authors in [16] addressed the issue of interference coordination in 3D in-building scenario for an unplanned deployment of FCs by considering a system with a number of multi-floor buildings each installed densely with FCs in the coverage of a MC. They proposed a graph based interference coordination scheme, and showed that the intra-cell interference of FCs of the same building is the dominant source of interference as compared to the cross-tier interference from MCs and interference from FCs in its neighboring buildings. In [18], the authors proposed a semi static resource allocation scheme based on FFR to avoid interference in 3D multi-floor building using indoor networking and optimization tool, iBuildNet. FCs are considered to locate at different places on different floors with each floor having the same floor plan. They showed that users served by a FCBS on one floor are interfered considerably by a FCBS located on an adjacent floor, and the signals from other floors

make interference effect more complicated in 3D in-building scenario. Authors in [22] proposed to use a BS location model with a minimum cell separation distance to ensure a minimum distance between any two cells in each tier using the Matern hardcore process such that no cell can lie within a predefined minimum distance from any other cell. They investigated the randomness in placement of SCs in 2D network scenario, derived an optimal (lower bound) minimum separation distance between BSs, analyzed numerically the minimum separation distance response as a function of target user density and data rate for different BS densities, and showed that cell coverage can be improved by introducing a minimum separation distance between BSs per tier. Authors in [23] proposed a repulsive cell activation strategy and derived an optimal minimum separation distance between SCs in terms of user density and tier-wise data rate by adopting modified Matern hardcore process to analyze the impact of minimum separation distance on the coverage of SC networks by using a numerical search, which is based on a simple bisection method. Like [22], the authors in [23] also considered self-configuration of BS deployments such that no cell can lie within a minimum separation distance between BSs and showed numerically that a larger target user throughput necessitates a lower minimum separation distance for a given user density, and so is required for a higher user density for a given target user throughput. All these aforementioned works addressed to enforce a minimum distance based on interference statistics around SCBSs, i.e. sensing the presence of neighboring SCBSs to avoid intra- and inter-tier interferences by modeling BS locations as Poisson Point Processes. Further, stochastic geometric approaches have been mainly applied so far in the existing literatures under 2D BS location scenario with a simple homogenous Poisson point process or Matern hardcore process. However, the study under 3D in-building scenario of BS locations existing in practical indoor buildings is not obvious because of complexity and intractability of stochastic analytical closed form expressions.

Further, a good number of existing literatures addressed the issue of CUSA based device-centric networks as one of the major enablers to achieve high indoor capacity. Authors in [7, 9, 24-25] proposed to split C-/U-plane by using different BSs where C-plane is served by the macrocell base station (MCBS) operating typically at a low microwave frequency, whereas U-plane is served by SCBSs, i.e. FCBSs. Each

FCBS is enabled with a single transceiver operating at a high frequency, e.g. mmWave. The authors also proposed a similar SCBS architecture in [4].

Further, the characteristics of traffic generated in the uplink and downlink (UL/DL) and the control-plane and user-plane (C-/U-plane) are asymmetric. The control-plane (C-plane) traffic is bursty and discontinuous, and typically more active during establishing connections. However, the user-plane (U-plane) traffic is typically continuous [26-27]. Furthermore, C-plane and UL traffic volumes are typically lower than that of U-plane and DL respectively. In this regard, authors in [4] proposed to operate C-plane traffic at low microwave frequency and U-plane traffic at high mmWave frequency. Additionally, because of different transmit powers of SCs from a macrocell (MC), decoupling of UL/DL is seen as one of the major changes in 5G to address, e.g. transmit power disparities in UL/DL [28]. Hence, dual connectivity feature of a user equipment (UE) to communicate with two nodes operating at different frequencies was proposed in [29].

However, to the best of our knowledge, no research has yet addressed the problem of interference modeling, resource reuse and allocation, and densification limit of SCs, particularly in 3D in-building scenario, under both traditional cell-centric networks and new split architectures in order to show their comparative performances in terms of, e.g. achievable capacity, of 5G networks, which is proposed to address in this dissertation. More specifically, the objectives mentioned in the next subsection are proposed to carry out in this dissertation.

1.4 Objectives

In this dissertation, the following objectives are proposed to address:

- Carry out an extensive review on enabling technologies in different directions from various perspectives for proposing a framework of the 5G network architectural evolution for the network capacity to give an insight on how all these directions will fit in together under different requirements and constraints,

and what would be the possible best match of these directions in terms of enabling technologies to meet the 5G network capacity demand.

For cell-centric networks,

- ORRA to SCs within a building: Propose a frequency reuse and scheduling algorithm using an adaptive almost blank subframe (ABS) based eICIC technique to reuse frequency resources in FCs deployed in 3D buildings in dense urban environments of a multi-tier network.
- NORRA to SCs within a building for SC network densification limit: Develop a tractable analytical model for interference characterization and minimum distance enforcement to reuse resources in 3D in-building dense SC networks for optimization constraints, namely interference, spectral efficiency, and link capacity.
- Propose a novel clustering approach and a number of resource reuse strategies for dense SC networks deployed in 3D in-building scenario.

For device-centric networks,

- Propose a novel multi-band enabled SC and UE architecture for the UL/DL and the C-/U-plane splitting.
- Develop numerous SCBS architectures for performance comparison between C-/U-plane coupled and split architectures.
- Propose a centralized 3D radio resource allocation and scheduling approach for C-/U-plane split architecture.

1.5 Scopes and limitations

Highlighted briefly, the followings are considered as baseline in carrying out dissertation research:

- *System Model*: A square-grid based FC coverage area where each FCL consists of a number of 2D floors, and each floor consists of a number of square-grid apartments with side length a are considered. Each apartment has one FCBS with a coverage area of $(a \times a)\, m^2$, which is placed in the center of the apartment, and is assumed static. A fixed free space around its building of a FCL and some free spaces between two neighboring FCLs are assumed. Typical values of a = 10 m and a free space of 10 m are assumed. However, in general, a and the value of free space are random variables. A UE per FCBS is considered and placed at the farthest radial distance from the FCBS. A single MC of a corner excited 3-sectored MC site and a number of SCs, including outdoor PCs and indoor FCs are considered. A certain percentage of MUs are distributed non-uniformly within the number of FCLs greater than one. All indoor MUs are served by MC. In addition, a certain percentage of outdoor MUs are offloaded to nearby PCs. FCs are dropped as clustered and deployed only within 3D buildings.
- *Interference management technique*: ABS based eICIC techniques are considered to manage interference between MC-plus-PC tier and FC tier both for NORRA and ORRA schemes. Irrespective of NORRA and ORRA schemes, a basic feature of these schemes is that RBs are reused in FCs only during non-ABSs.
- *Resource scheduling algorithm*: Proportional fair scheduler rather than other simple conventional schedulers such as Round Robin is considered to address multi-user diversity gain from a random and uniform FU distribution, i.e. a highly spread distance distribution between a FU and a serving FCBS (sFCBS), such that the path loss varies significantly at FUs from one to another and non-line-of-sight (non-LOS) components at frequencies below 3 GHz exist. Further, proportional fair scheduler ensures an optimal trade-off between fairness in resource allocation, specifically time and frequency among UEs, and throughput per user performances in comparison with other conventional schedulers.

- *Path loss model*: Rather than choosing sophisticated but computationally complex theoretical models such as ray tracing, simple empirical models recommended for evaluation by the third generation partnership project (3GPP) for modeling indoor FCs are considered. However, because FCs in all FCLs experience the similar signal propagation characteristics, there would not be any significant deviation in performance results from using empirical models that do not necessarily guarantee the transportability between environments.
- *Simulation parameters and assumptions*: The default simulation parameters and assumptions used for system level simulation are based on 3GPP recommendations for system level performance evaluation and are listed in a table which varies accordingly with any particular scenario of investigation. Unless stated explicitly, the default value for any parameter and assumption is considered to use from the mentioned table for any particular simulation scenario.
- *Validity of research results*: The validity of any research result of this dissertation is mainly based on convergence of MATLAB® simulator based simulation results and formulated analytical results.

Finally, in Figure 1.2, the synopsis of the research is depicted in a diagram for a quick visual understanding at one-spot. Each word of the dissertation title is defended by explaining its inclusion reasonably sidewise in the diagram to underpin the novelty of the considered research problems, scopes and contributions. Since the network capacity varies with the degree of application of a particular enabling technology, such a range of variation is shown arbitrarily by dotted lines in the diagram.

1.6 Outline and approach

The dissertation is documented chapter wise in the following order:

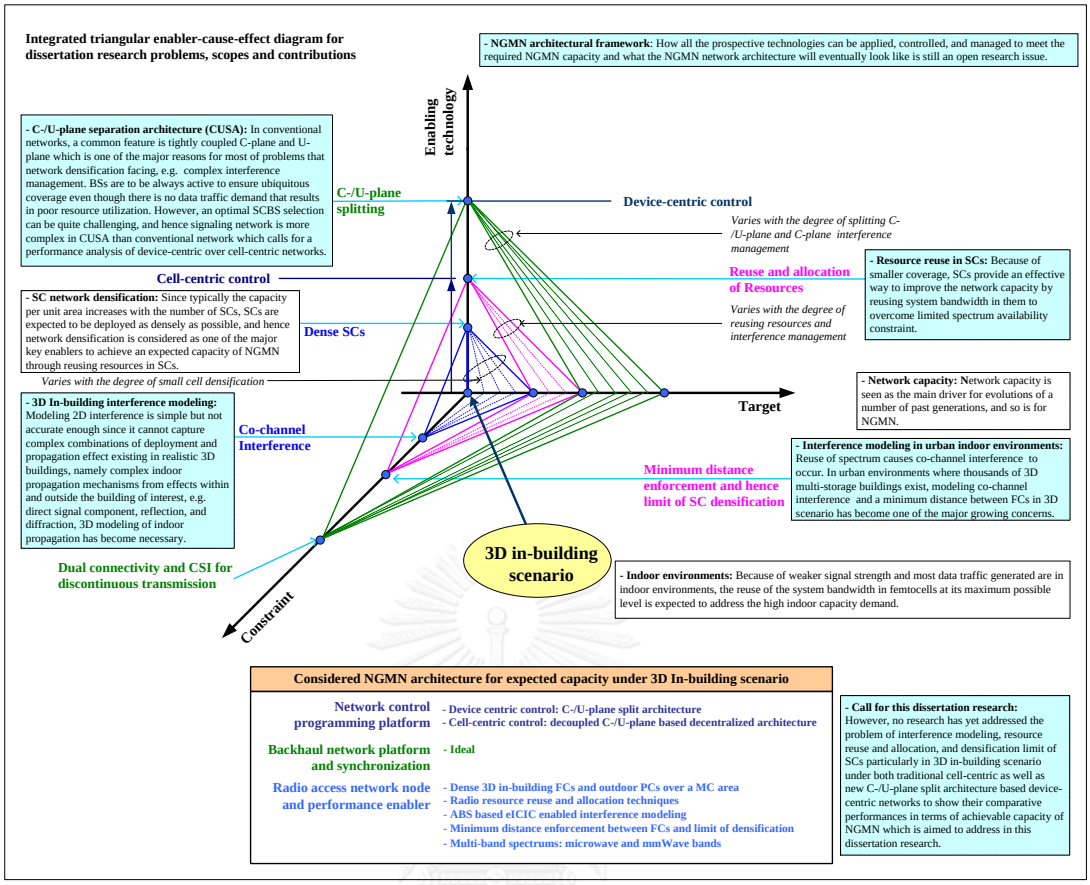

Figure 1.2: One-spot view of the dissertation overall research problems, scopes, and contributions with an integrated triangular enabler-cause-effect diagram.

- In Chapter 1, an introduction to the dissertation is given, including its background, problem statement, related works, objectives, and scopes and limitations.
- In Chapter 2, a review on trends of the existing as well as proposed potential enabling technologies that are expected to shape 5G mobile networks and relevant to the dissertation objectives is discussed, and a brief detail on concepts, theories, techniques, and methods that are considered to use in this research are incorporated in order to gain sufficient background information for an easy of understanding and clarity.
- In Chapter 3, a frequency reuse and scheduling algorithm (FRSA) using an adaptive ABS based eICIC technique that uses ORRA scheme is proposed to reuse frequency resources in FCs deployed in 3D buildings in dense urban

environments of a multi-tier network, including FCs and PCs within a MC coverage. An adaptive optimal number of ABSs (OPNA) scheme for FRSA, and its outperformance over a static OPNA scheme are shown. A schematic of the scheduler implementation for FRSA is also developed.

- In Chapter 4, a novel tractable analytical model for modeling interference in 3D in-building scenario using Wyner model and deriving mathematical expressions for a minimum distance between FCBSs deployed within a building under a number of constraints is proposed. In addition, two strategies to reuse RBs in co-channel FCBSs (cFCBSs) are proposed, and the capacity outperformance with a RR strategy of NORRA over ORRA scheme is shown. With a rough estimation under an example scenario of ultra-dense deployment of FCBSs, it is shown that the prospective desired spectral efficiency of 5G networks can be achieved with the proposed model.
- In Chapter 5, a multi-band enabled FCBS and UE architecture is proposed for splitting the UL/DL as well as the C-/U-plane for 5G mobile networks. For multiple bands, co-channel microwave and different frequency 60 GHz mmWave bands are considered. A number of disruptive architectural design alternatives for 5G mobile networks are presented, including a complete UL/DL splitting as well as a combined UL/DL and C-/U-plane splitting architectures.
- In Chapter 6, numerous SCBS architectures based on the number of transceivers and operating frequency bands existing in a SCBS for serving the C-/U-plane traffic in indoor environments under both the C-/U-plane coupled as well as the C-/U-plane split architectures are discussed and evaluated in terms of the C-/U-plane traffic capacity.
- In Chapter 7, a centralized allocation and scheduling strategy for 3D radio resources, namely time, frequency, and power, for a C-/U-plane split architecture by considering schedulers of all BSs located at a central station is proposed. A fully blank subframe based eICIC to split completely the C-/U-plane such that C-plane can be served only by the MCBS and U-plane by each UE's respective BS is considered.

- In Chapter 8, recommended further studies on the dissertation research are highlighted in terms of concepts and preliminary results.
- The dissertation is concluded in Chapter 9 by pointing out major research approaches, observations, and findings.

In the followings, a number of approaches considered for preparing the dissertation are listed out:

- *Use of information and non-disclosure issues*: Information in this dissertation in any forms, e.g. texts, figures, tables, and algorithms, can be found partially or completely in the published as well as accepted journal and conference articles and hence is used under strict-confidentiality requirement.
- *Chapter structuring*: A generic structure for presenting information mainly in Chapters 3, 4, and 5 is used consistently, including introduction, system model, analytical model, proposed algorithm, simulation assumptions and parameters, implementation, technical and business perspectives, conclusion, and finally a list of references. Further, rather than numbering all equations, only which are needed to refer in later parts of a chapter are mainly numbered. For numbering sections, equations, figures, and tables, of any chapters the following format is used: X dot Y, where X denotes a decimal number of any chapters, whereas Y denotes a decimal number of any sections, equations, and so on as aforementioned.
- *Use of appendices*: A number of appendices are considered to cover required information for completeness and clarity of any issues of chapters.

1.7 Summary

In this chapter, a general introduction of the dissertation is given. Relevant backgrounds in section 1.1 on dense-HetNets, SCBSs, interference in HetNets and its management techniques such as eICIC techniques, indoor signal propagation

environments, 3D modeling of indoor propagation, noticeable characteristics of current mobile networks, cell-centric control, advanced device-centric control, and the C-/U-plane and the UL/DL split architectures are given. In section 1.2, a number of research problems are discussed. Namely, how various proposed enabling technologies can be applied, controlled, and managed to meet the required 5G network capacity as well as what the 5G network architecture will eventually look like to achieve the target capacity are discussed. Further, modeling co-channel interference and enforcing a minimum distance between cFCs, i.e. limit of densification, for reusing resources in 3D in-building scenario are mentioned. The necessity of developing a new architecture with C-/U-plane decoupled is also highlighted. Furthermore, the importance of carrying out performance analysis of device-centric networks over cell-centric networks for 5G network capacity is indicated. As a promising solution for a high capacity network, the C-/U-plane separation architecture based dense HetNets are also pointed out. In section 1.3, related studies to the research problems stated above in existing literature are highlighted for both cell-centric and device-centric networks, and current research gaps are identified. In section 1.4, the objectives of the dissertation are listed, followed by mentioning its relevant scopes and limitations in section 1.5. The chapter ends with giving a chapter wise outline of, and mentioning approaches for documenting, the dissertation in section 1.6.

CHAPTER 2
LITERATURE REVIEW

In this chapter, relevant literature review for this dissertation on necessary concepts and techniques are discussed. Initially, an analysis on the existing as well as the prospective potential enabling technologies for 5G mobile networks is carried out in order to develop a 5G network architectural evolution framework. We then provide a brief discussion on the 3D in-building cellular mobile communications. Important issues of SC deployments such as randomness and 3D in-building modeling practices are highlighted. Further, radio resource allocation strategies and their role on HetNets are discussed. Finally, the chapter ends with a brief discussion on cooperative communication mechanisms for sharing information among BSs in order to improve network capacity. On top of the review in this chapter, a number of relevant background issues are also discussed in Appendix A.

2.1 Incentives and requirements of next generation mobile networks

Internet data traffic through mobile wireless access networks is expected to grow faster than that through traditional fixed access networks [2]. The growth of data usages will continue [30], and an incremental approach to serve user demands will not be sufficient toward meeting mobile network demands by 2020 [31]. Internet protocol (IP) data usage by wireless networks will increase from under 3 Exabyte in 2010 to over 500 Exabyte by 2020 [31]. Internet of Things is expected to dominate over the current practice of human-centric Internet in 5G networks [32]. Nonetheless, with existing networks, it is not possible to address these aforementioned challenges. In this context, 5G mobile network technologies are expected to be standardized around 2020. To address 5G requirements and technologies, there has already been a great attention in research communities. Though there is no exact specification on what 5G networks

will encompass, based on what most people have agreed so far as compared to 4G networks, 5G networks should attain the followings as given in Table 2.1 [31, 33-34].

Table 2.1: 5G mobile network requirements.

Attributes	**Values (compared to 4G networks)**
System capacity	1000 times
Spectral efficiency	10 times
Energy efficiency	10 times
Longer battery life time	10 times
Reduced latency	5 times
Higher number of connecting devices	10-100 times
Reduction in energy per bit as well as cost per bit	100 times
Mobility support	up to 500 km/hr

2.2 5G network architectural evolution framework

In this thesis, a framework of the 5G network architectural evolution for the network capacity is proposed in Figure 2.1 and is detailed in Figure 2.2. Though there are a number of enabling technologies in each evolutionary direction, in order to meet the capacity demand of 5G networks, we limit the scopes of discussion on the enabling technologies as follows in this chapter. However, discussions on a number of enabling technologies, e.g. mmWave, massive MIMO, and SDN, can be found in Appendix A.

- for *RAN node and performance enabler*, MC, PC, and FC based dense HetNets and eICIC based interference management for resource reuse and allocation in 3D in-building scenario,
- for *network control programming platform*, logically distributed programmable network platform, i.e. cell-centric and device-centric networks, and
- for *backhaul network platform and synchronization*, backhaul networks and deployment scenarios and solutions.

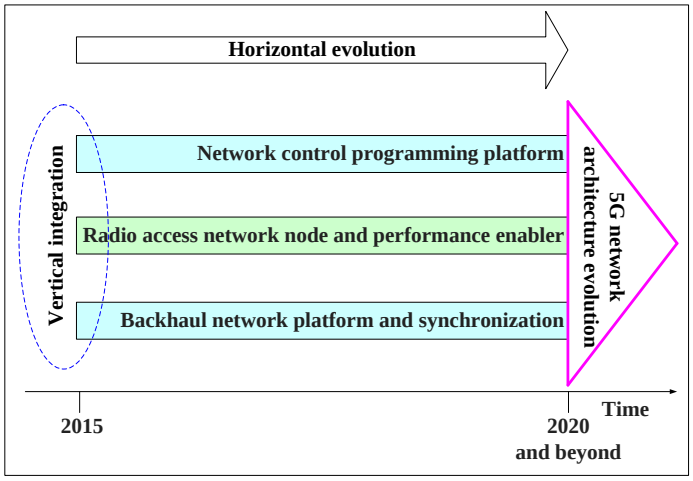

Figure 2.1: 5G network architectural evolution framework.

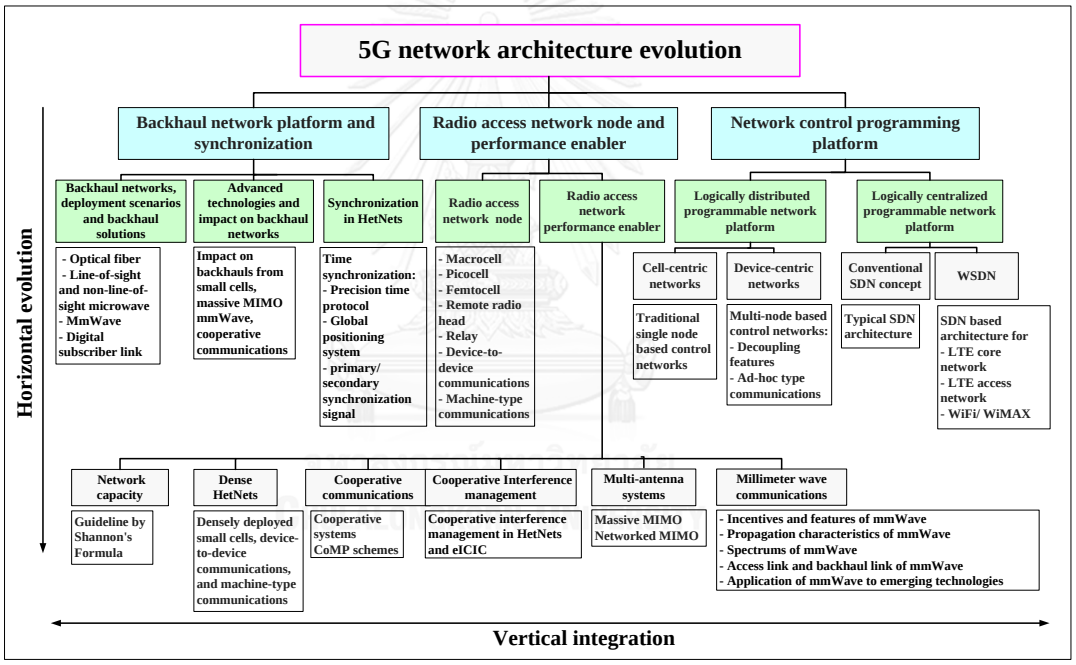

Figure 2.2: Detailed 5G network architectural evolution framework.

2.3 Radio access network node and performance enabler

2.3.1 Radio access network node

The 5G RAN is expected to consist of densely deployed heterogeneous nodes, particularly low power nodes. Network densification with SCs is considered as one of

the prominent approaches to achieve the high capacity of 5G networks where SCs are deployed in the coverage of a MC such that the distance dependent path loss between a UE and a SCBS is reduced to improve the throughput per user. Various types of SCs such as PC, FC, relay node, and remote radio head (RRH) have been standardized by the 3GPP for 4G long term evolution-advanced (LTE-Advanced) systems with a future deployment of device-to-device and machine type communications as parts of beyond LTE-Advanced or 5G systems. Each of these SCs has a number of different characteristics from others in terms of, e.g. transmission power and cell coverage area. Hence, 5G network architectures depend largely on the type and the density of these SCs. Basic features of MC and SCs such as PC, FC, and RRH are discussed as follows.

A MC is usually characterized by a high transmission power, a wide cell coverage, a large number of concurrent user associations, and an open access for all users. Antenna radiation patterns of MCBSs can be either omnidirectional or sectorized. The number of antennas at a MCBS can be multiple, e.g., an evolved nodeB of LTE-Advanced systems with the maximum number of eight antennas in the DL. These evolved nodeBs are connected to each other via X2 backhauls to exchange signaling information, e.g., common control signals using the C-plane and user data information using the U-plane for cooperation.

A PC is a BS with a relatively lower transmission power than that of an evolved nodeB, and correspondingly with a limited cell coverage. A PC usually serves a few tens of users, and is deployed typically in hotspot areas such as shopping mall, bus station. PCs are usually connected to an evolved nodeB with X2 backhauls. The major purpose of deploying a PC is to improve local user throughputs within its periphery and also places where an indoor coverage from a MCBS is poor. Like a MCBS, a picocell BS (PCBS) is also deployed by an operator [1].

A FC is also a low power BS with a transmission power typically less than that of a PC. It is also called as home evolved nodeB [35] in the 3GPP LTE-Advanced, and usually covers a limited area less than that of a PC. Based on the access policy, FCs are usually classified into three types, namely, an open access, a CSG, and a hybrid access [36]. In an open access type, any user can get access to a FC; whereas in a CSG, only a specific group of users are allowed to get an access; and in a hybrid access, a portion of FC resources is restricted for a particular group of users, and the remaining can be

accessed by any user. FCs are usually deployed in indoor coverage areas to improve indoor user throughputs as well as in areas where the received signal strength from a MCBS at a UE is very low or lower than the minimum requirement for establishing and continuing a communication link. FCs use consumers' broadband connections as backhaul links such as digital subscriber line, copper cable, and optical fiber [1].

Similar to a MCBS, a RRH is a high transmission power BS which is usually compact in size and low weight [1]. RRHs are connected to a MCBS via high speed links such as optical fibers, and all control and baseband signal processing tasks are performed for RRHs at MCBSs. The main purpose of RRHs is to distribute the cell coverage by remote BSs such that constraints from site acquisitions [1] can be flexibly tackled. This distributed form of antennas is called DAS which offers an improved link quality, reliability, and coverage because of the more frequent presence of LOS links. A comparative framework of these nodes is shown in Table 2.2 [1, 37].

2.3.2 Radio access network performance enabler

A. Network capacity

A high system capacity is the major requirement for the evolution of 5G networks. With no specific direction on how the envisaged high capacity of 5G networks can be achieved, we intend to exploit the Shannon's capacity formula to point out possible ways to enhance the system capacity of 5G networks. Assume that the link capacity between a UE and a BS is the same as the received throughput at the UE. Using Shannon's capacity formula, the link capacity for a point-to-point communication between a MCBS and a UE considering interference effects at the UE can be expressed as

$$C_{link} = B_{link} \log_2\left(1 + P_{ue} / \left(I_{ue} + n_{ue}\right)\right) \tag{2.1}$$

where P_{ue}, I_{ue}, and n_{ue} are the received signal power, the interference power and the additive white Gaussian noise power respectively at the receiver. B_{link} denotes the link bandwidth.

Table 2.2: A comparative framework of various types of node in HetNets.

Dense HetNet nodes	Specifications attributes				
	Typical transmission power	**Cell coverage**	**RAN backhaul connection**	**Utilization**	**Deployment environment and planning**
MC	46 - 49 dBm	Few kms	LOS microwave, Optical fiber	Network associations for high mobility UE, wide area coverage	Outdoors; planned
PC	23 - 30 dBm	Less than 300 m	LOS microwave, Optical fiber	Data traffic offloading from MCs, indoor and outdoor capacity improvement	Indoors or outdoors; planned
FC	Less than 23 dBm	Less than 50 m	Copper cable, digital subscriber line	Indoor coverage area capacity improvement	Indoors; unplanned
RRH/ DAS	46 dBm [1]	Few kms	Optical fiber	Cooperative gain, handoff reduction	Indoors or outdoors; planned

Assume that there are S links that can be provided with the system bandwidth B_{sys}. For simplicity, assume that all UEs have the same link characteristics such that values of P_{ue}, I_{ue}, and n_{ue} are the same for all UEs. Hence, the system capacity is directly proportional to the link capacity. Consider also that there are more than one antenna at the BS and at the UE such that there exist M_{ue} parallel spatial channels in a link, where M_{ue} = min $\{n_t, n_r\}$ denotes the spatial multiplexing gain, and n_t and n_r denote respectively the number of antennas at the BS and at the UE. Assume that SCs are deployed in the coverage of a MC and are operated with the same system bandwidth, i.e., B_{sys}, such that the bandwidth is reused K_{ue} times to SCs. Hence using (2.1), the system capacity of HetNets for a single MC overlaid by SCs can be given as

$$C_{sys} = K_{ue} M_{ue} B_{sys} \log_2\left(1 + P_{ue}/\left(I_{ue} + n_{ue}\right)\right) \tag{2.2}$$

Note that we implicitly consider that the received power is the same at a UE irrespective of whether the UE is served by a MC or a SC for simplicity and consistency. The assumption is reasonable enough in a sense that the higher transmission power of a MCBS than a SCBS is compensated by good channel conditions between a UE and a SCBS because of lower path loss, higher probability of LOS link, and less fading effect in a SC than a MC. In addition, we assume that the M_{ue} spatial channels have the same capacity. By analyzing (2.2), possible ways to improve each element that eventually contributes to an improvement of the overall system capacity C_{sys} of 5G HetNets can be pointed out and are mentioned in the followings:

- The denser a HetNet, the higher the interference effects through the term I_{ue}.
- By increasing the density of SCs per unit area, more frequency reuse (i.e., higher K_{ue}) can be performed.
- By implementing a massive number of antennas at a MCBS, a large spatial multiplexing gain M_{ue} can be achieved. This implementation of a large number of antennas at a BS is called massive MIMO. In addition to massive MIMO, other advanced technologies such as networked MIMO and DAS can also be used.
- The more the system bandwidth, the higher the system capacity. Since most frequencies below 3 GHz have almost been utilized, possible ways to increase spectrum bandwidths are to aggregate spectrums from mmWave bands, ranging from 3 to 300 GHz. From mmWave spectrum bands, several tens of GHz of bandwidth would be made available for the capacity of 5G networks [3].
- An interference management technique, e.g. eICIC, can be applied to improve signal power P_{ue} and to mitigate interference power I_{ue} at a UE.

In the following subsections, enabling technologies of 1, 2 and 5 are discussed.

B. Dense HetNets

The densification of mobile networks evolves with time as the requirements arise from multiple aspects, e.g. coverage and capacity. In the early stage, the development of mobile networks was based mainly on cell coverage where a large area incorporating both indoor and outdoor environments was considered to be covered by a MC with a high transmit power which was sufficient enough because of mainly voice based low traffic demand. However, with time as the number of mobile users got increased, there was a necessity for a paradigm shift from the coverage limited to the capacity limited network design to address the growing demand of capacity. A typical practice used for years was by splitting a MC into smaller ones, also termed as microcells, to cover mainly high traffic generation areas within a MC. Along with traffic demand, locations of traffic generation were seen substantial, and the traffic generated in indoor surpassed that of outdoor environments.

Now-a-day globally, data traffic demand exceeds voice traffic, and about 65%-70% data traffic [38] generates within indoor environments. Because of a high external wall penetration loss, serving such a huge amount of indoor traffic at a high capacity with indoor BSs rather than outdoor ones becomes crucial. Because of a poor coverage and a low signal transmission capacity within indoor environments by MCs along with a high transmit power requirement of MCs necessitate a shift again in network densification from outdoor to indoor environments where SCs are deployed within indoor environments to cover a small area by each SC to serve indoor UEs at a close-in distance.

Since the capacity demand of 5G networks, is projected to be 1000× that of 4G, an extremely dense deployment of SCs is considered as the major enabler to achieve the required capacity. Such an extremely dense deployment of SCs within indoor environments may shift the existing outside-in approach to a new inside-out approach of BS deployment so that indoor SCBSs can serve close-in low mobility outdoor UEs in addition to indoor UEs, and outdoor MCBSs can serve outdoor high mobility UEs [38]. With time, such shifting paradigms of network densification commensurate with the degree of density of BSs per unit area to cope up with network performance requirements. According to [8], the density of MCBSs in 3G is 4 to 5 BS/km^2, microcell BSs in 4G is 8 to 10 BS/km^2 to improve transmission rates in some parts, i.e. hotspots,

within a MC area, and SCBSs in 5G is 40 to 50 BS/km^2 (expected) to ensure seamless coverage (Figure 2.3).

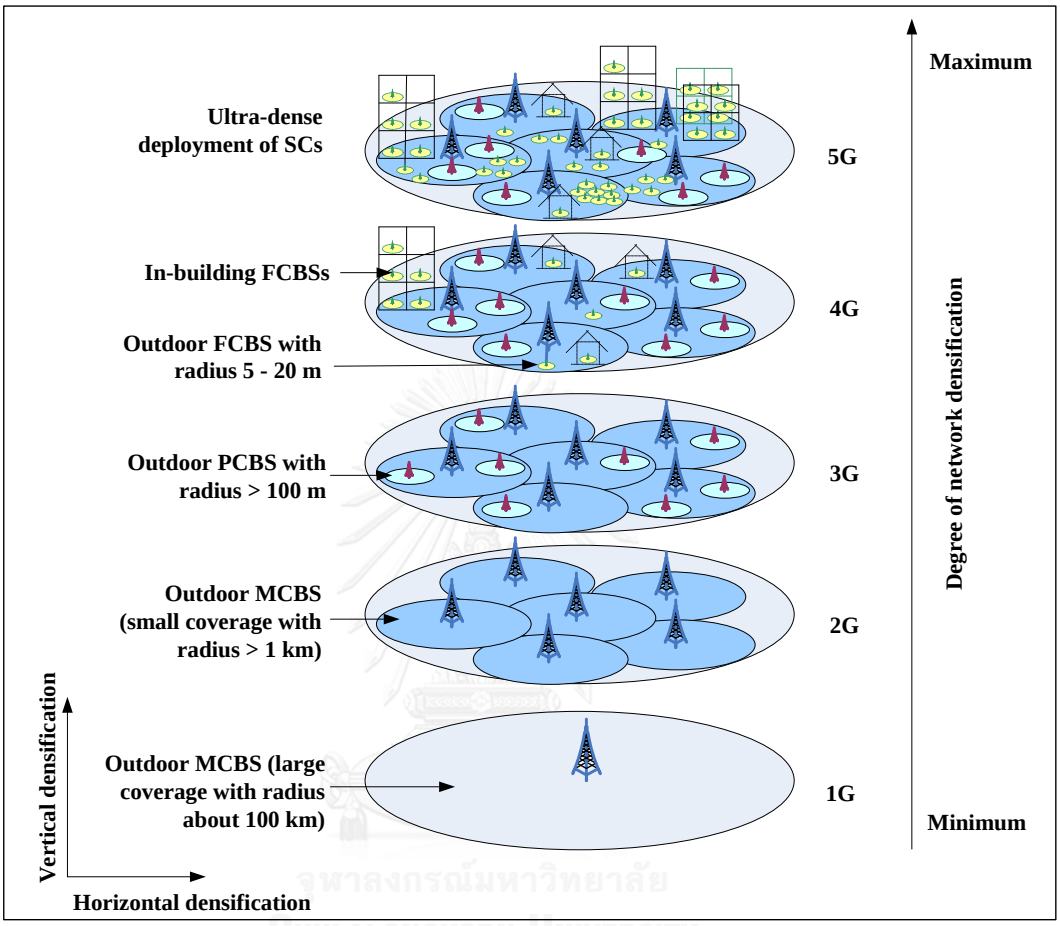

Figure 2.3: Network densification evolution: 1G to 5G (expected).

1. Driver, exploitation and benefits

Though there are mainly three ways the capacity of 5G can be achieved, because the spectrum availability is already scarce, and the spectral efficiency of current networks reaches almost Shannon's limit of capacity, the only option left to improve capacity is the densification of SCs as extremely as possible [38] within the coverage of MCs. SCs take advantages of mainly two aspects, namely a short distance between a SCBS and a UE to enhance signal quality (and hence throughput) and reuse of the same frequency in SCs to improve spectral efficiency [39]. This implies that since a UE throughput is directly proportional to the available transmission channel bandwidth, the

overall SC network capacity improves linearly with the density of SCs. There are various types of SCs that are existing in the current networks such as FCs, PCs, and RRHs. PCs and RRHs are typically used for outdoor hotspot coverages whereas FCs are mainly used for indoor coverages. SC network densification brings a number of benefits, including (i) its allows an intense spatial reuse, (ii) it allocates larger share of the available spectrum to UEs because of the less number of UE per SC, and (iii) it reduces path loss by decreasing distance between a SCBS and a UE [40].

2. Types of HetNets

SCs can be deployed in two ways based on how spectrum resources are assigned to them, namely single-band and multiband deployments. When both MCBS and SCBS operate at the same frequency, i.e. co-channel, the resulting HetNet is termed as underlay HetNet, whereas when they operate at an orthogonal or different frequencies is termed as overlay HetNet. However, when both approaches of deployments is employed to a HetNet, the resulting HetNet can be termed as mixed or hybrid HetNet. Overlay HetNet outperforms underlay HetNet in terms of no cross-tier interference at the cost of additional expensive spectrum use, whereas underlay HetNet outperforms overlay HetNet in terms of high spectral efficiency by reusing spectrum resources in SCs at the expense of increased cross-and co-tier interferences and backhaul overheads for coordination among MCBSs and SCBSs for interference management.

3. Practical limitations and tradeoffs

A number of practical limitations that may affect network densification are outdoor environment, site acquisition, site-to-site distance, physical antenna size for outdoor environment, and external wall penetration loss, internal wall loss, and energy efficient window for indoor environment. In addition, distance dependent path loss exponents, different propagation models, and traffic models also affect network densification [41]. Furthermore, the signal propagation between indoor and outdoor is also affected by modern energy efficient construction materials. As reported in [42],

the average outdoor-indoor penetration loss in modern buildings is about 19-23 dB, whereas for older buildings, the range is about 6-9 dB. Therefore, there is an additional 13-14 dB average penetration loss from modern energy efficient building materials with a peak loss can be as high as 35 dB.

Hence, the densification of SCs has to be properly done since there are a number of tradeoffs from network performance point of view. The more the density of SCs, the less the coverage per SC, that results in a decreased path loss between a SCBS and a UE but an increased interference between UEs. Moreover, the reduced coverage of a SC results in a strong presence of LOS components that degrades gain from multi-user diversity because of near similar channel characteristics of UEs [40]. This implies that there is a limit of densification beyond which the capacity may get saturated even with an increase in SC densification which calls for a systematic view towards the tradeoffs of network densification to define an appropriate density of SCs [40]. Note that although the 2G and 3G mobile systems were noise-limited, and the 4G deployed with multi-antenna technology is interference-limited, because of considering an extreme dense deployment of SCs for 5G, the 5G mobile system will be density-limited [8].

4. Research on dense HetNets

There have already been tremendous considerations on network densification towards 5G networks. A rich amount of researches have already addressed many issues of dense HetNets such as a general overview on dense HetNets in [43], the role of SCs in [44], performances of dense HetNets from various deployment perspectives in [38], coordination of interference in dense HetNets in [45], cooperative distributed radio resource management (RRM) in hyper-dense HetNets in [46], energy efficiency, spectral efficiency, and quality-of-service tradeoffs in [47], coverage analysis of LTE urban HetNets with dense FCs in [48], and a novel architecture using SCs to address machine type communication traffic in [49].

C. Interference management in HetNets

Interference is one of the major bottlenecks and is more severe in dense HetNets than in traditional homogeneous networks. The major sources of interference in HetNets are unplanned deployment, restricted FC access, transmission power difference among nodes, and new techniques such as cell range expansion [1]. In co-channel deployment of a FCBS, a MU close to the coverage of a CSG FCBS is interfered highly by the CSG FCBS in its DL reception as shown in Figure 2.4(a) as the MU is not allowed to get access to the FCBS. Similarly, a MU at far distance (e.g., near cell-edges) from a MCBS transmits in the UL at a high power to compensate the path loss, and hence originates cross-tier interferences by jamming UL transmissions from FUs to a FCBS. Further, the unevenness in transmission powers of different nodes in HetNets is another potential cause of interference. Since a UE usually gets connected to a BS with the highest DL signal strength in its neighbor BSs, a UE prefers to get connected with a MCBS because of its higher transmission power than that of a SCBS, e.g., PCBS. This creates a phenomenon called imbalance in load distribution between cells, and a MCBS is likely to get overloaded almost always even though there are PCBSs around UEs at much shorter distances than those from the MCBS. Moreover, UEs in the near coverage of a PCBS is interfered highly in the DL from the PCBS (Figure 2.4(b)). If a UE near a PCBS is connected to the PCBS, this can help the UE not to suffer from the DL interference since the UE is now communicating with the PCBS and also offloading traffic from the MCBS.

Both offloading problems and the DL interferences for a MU can be addressed by expanding the actual PC area by adding an offset to the reference signal received power of a PCBS which is referred to as cell range expansion [50]. When a PCBS is employed with cell range expansion, a UE receives a higher reference signal received power from the PCBS, and hence more UEs are likely to get connected to the PCBS. This results in more MUs to be offloaded to the PCBS from a MCBS and less DL interferences at a MU. However, those pico UEs (PUs) which are within the expanded cell area of a PCBS are likely to suffer from the DL interferences caused by a MCBS as shown in Figure 2.4(c). This can be overcome by coordinating resource scheduling decisions between a MCBS and a PCBS via backhaul links, e.g. by scheduling orthogonal RBs by a MCBS to MUs near the victim PUs.

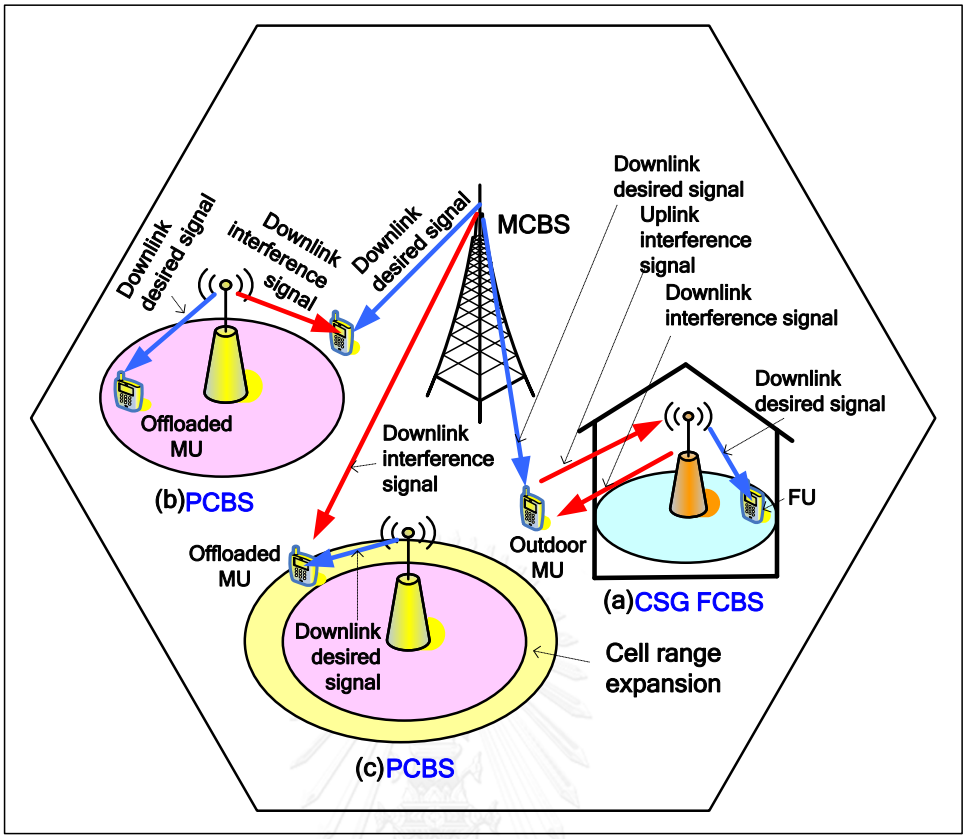

Figure 2.4: Interference in HetNets.

Interferences in HetNets can better be managed by using FD, TD and power control ICIC techniques which are aggregately called as eICIC [1]. In TD eICIC techniques, a victim UE is scheduled in TD while interferences from other nodes are reduced. The use of ABS is one way to address TD eICIC techniques where the victim UE is scheduled during ABSs (Figure 2.5) [1]. As mentioned earlier, interferences from a CSG FCBS s can be overcome by using ABS based eICIC. For example, if a MU is near to the coverage of a CSG FCBS, ABSs can be applied at the FCBS such that the MU will be scheduled only during ABSs. In an ABS, data and control signals are not scheduled; however, only reference signals are scheduled (Figure 2.6). Another approach to address TD eICIC is to apply shifting to the subframe boundary by a number of orthogonal frequency division multiplexing symbols of one BS with respect to the other such that control channels of both BSs do not overlap each other (Figure 2.7). However, control channels of the MU (near the FCBS) are still interfered by data channels of FUs. To overcome this problem, one approach is to mute those overlapped

orthogonal frequency division multiplexing symbols of the FCBS with the control channels of the victim MU. The other approach is to configure subframes of the FCBS as ABSs that overlap control channels of the MU.

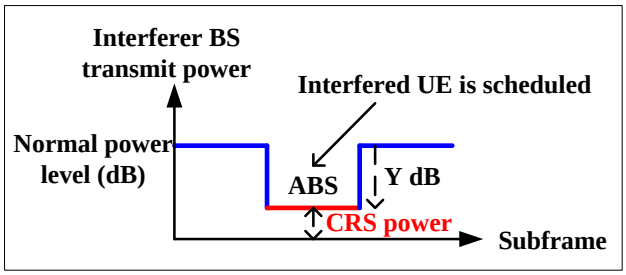

Figure 2.5: Transmit power versus subframe in ABS.

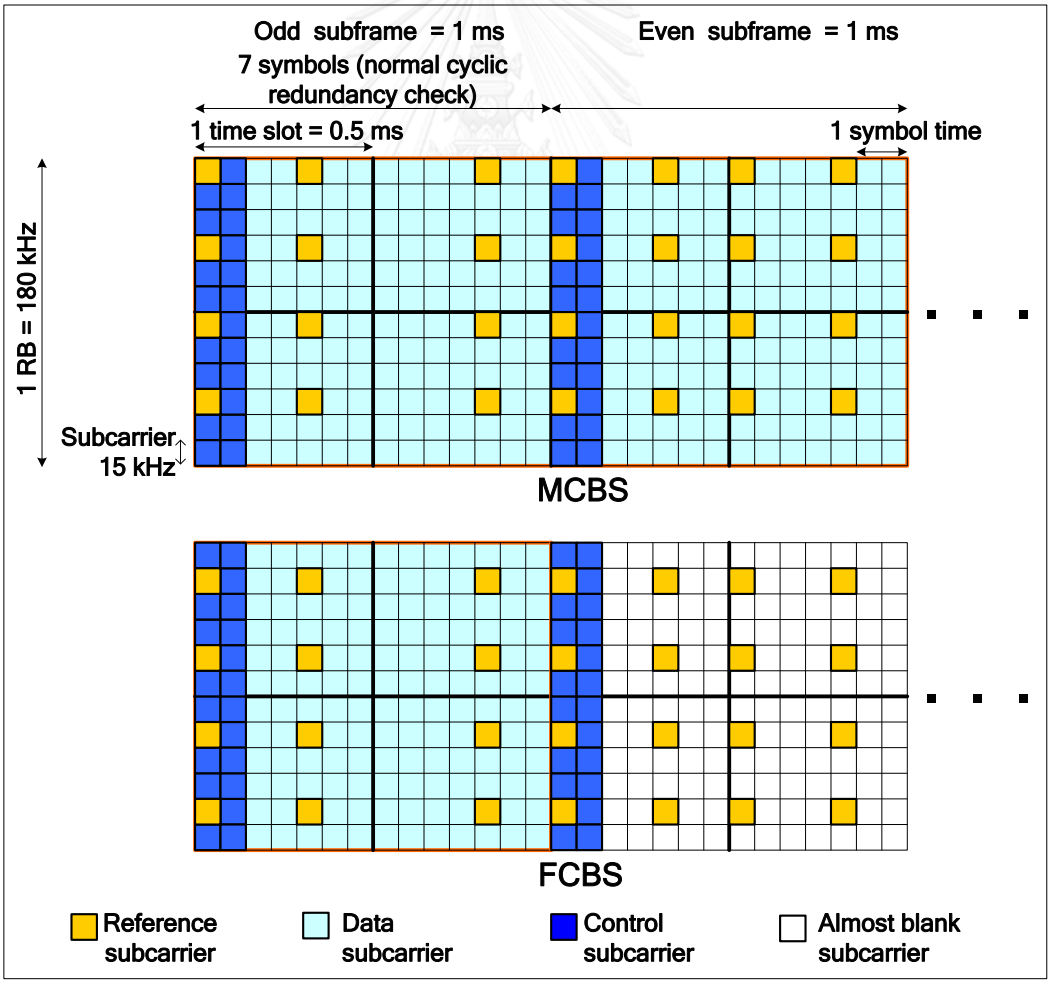

Figure 2.6: ABS based TD eICIC between MCBS and FCBS.

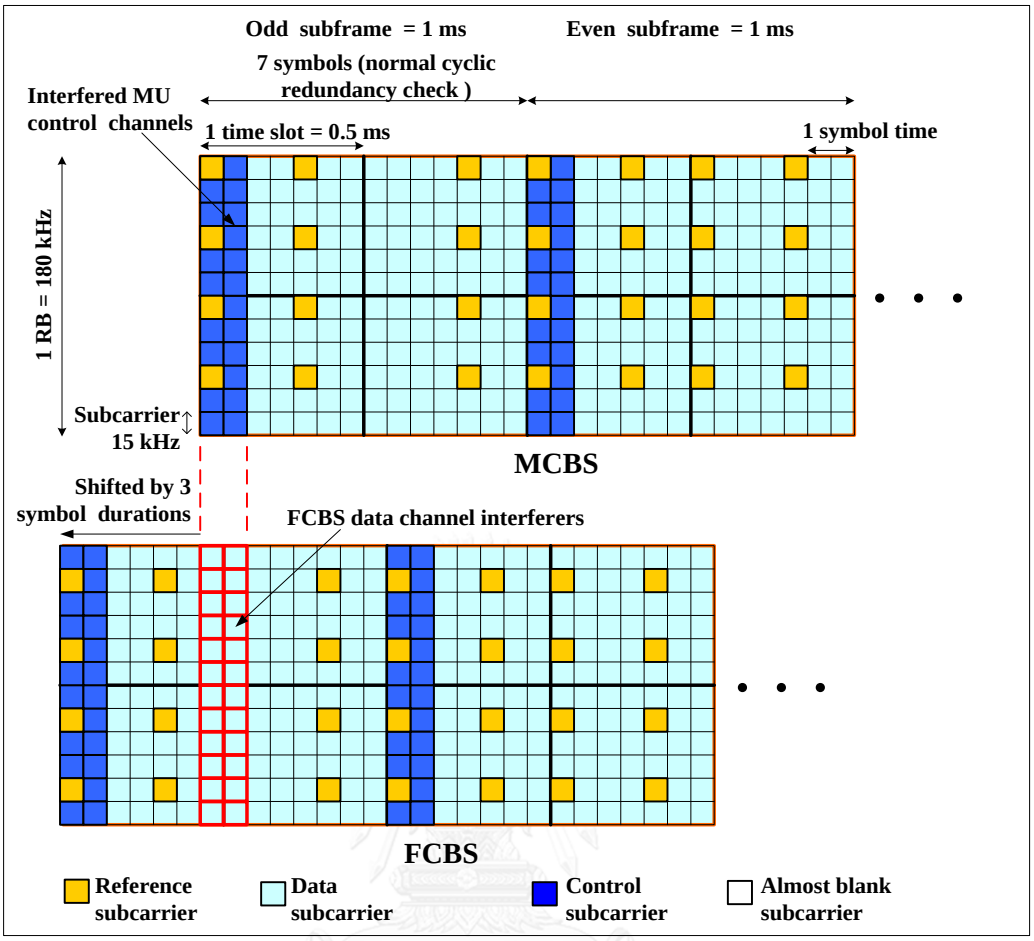

Figure 2.7: FCBS subframes are shifted by 3 symbol durations with respect to that of MU.

In FD eICIC techniques [1], by orthogonal scheduling of control channels between cells in a reduced bandwidth, interferences can be mitigated. Along with a static orthogonalization, a dynamic FD orthogonalization can be performed by detecting a victim UE. An interfered UE can be detected at a BS based on the UE specific measurement reports. The victim UE's BS then informs the interferer BS via backhaul signaling. A victim UE can also be detected by an interferer BS and can coordinate its scheduling decision with the victim UE's BS [1]. In power control eICIC techniques, different power control techniques can be applied to SCs [1]. However, a reduction in transmission power at a FCBS will eventually reduce throughputs of its FUs at the gain of reduced interference for MUs. Some trade-offs can be considered on scenarios of interest such that an optimal power control at SCs can be adopted and may contribute to an overall system capacity improvement.

D. Inter-cell RRM for interference management

Using coordinated multi-point (CoMP), tight inter-cell RRM (IC-RRM) for orthogonal resource assignment such that interference can be managed within limits can be achieved. Two approaches [51] such as centralized and autonomous IC-RRMs can be considered. In centralized IC-RRM, a group of RRHs are connected by high speed backhaul links (e.g., optical fiber) to a centralized BS (also called evolved nodeB). All the baseband signal processing is performed at the evolved nodeB. Radio resources are scheduled at a single point, and scheduling decisions are coordinated among all RRHs such that the interference is mitigated considerably by an orthogonal assignment of resources. This centralized IC-RRM approach is beneficial to HetNets where independent link connections between UL/DL to different nodes can be possible because of the centralized processing at the evolved nodeB. For example, the UL can be connected to a SC, e.g. PC, and the DL is connected to a RRH of the evolved nodeB of a UE. Coordination with the PC can be performed via X2 backhaul with the evolved nodeB. Hence, this in turn mitigates the interference at a UE along with providing necessary UE throughputs in the UL/DL based on necessity.

In autonomous IC-RRM, evolved nodeBs are connected to each other via X2 interface, and relevant information for resource scheduling is exchanged between them such that the interference at a UE, particularly a cell-edge user is minimized. This approach is particularly important for a MU near the coverage of a CSG FCBS where a MU receives weak MCBS signal and is interfered significantly in the DL from the nearby CSG FCBS because of no access to that FCBS. The ICIC gain from this approach employing X2 interface between evolved nodeB and FCBS has been reported in the literature. Figure 2.8 shows an example network architecture for IC-RRM.

2.4 Network control programming platform

The programmable feature of network control is one of the most impactful aspects toward the evolution of 5G networks. The traditional way of

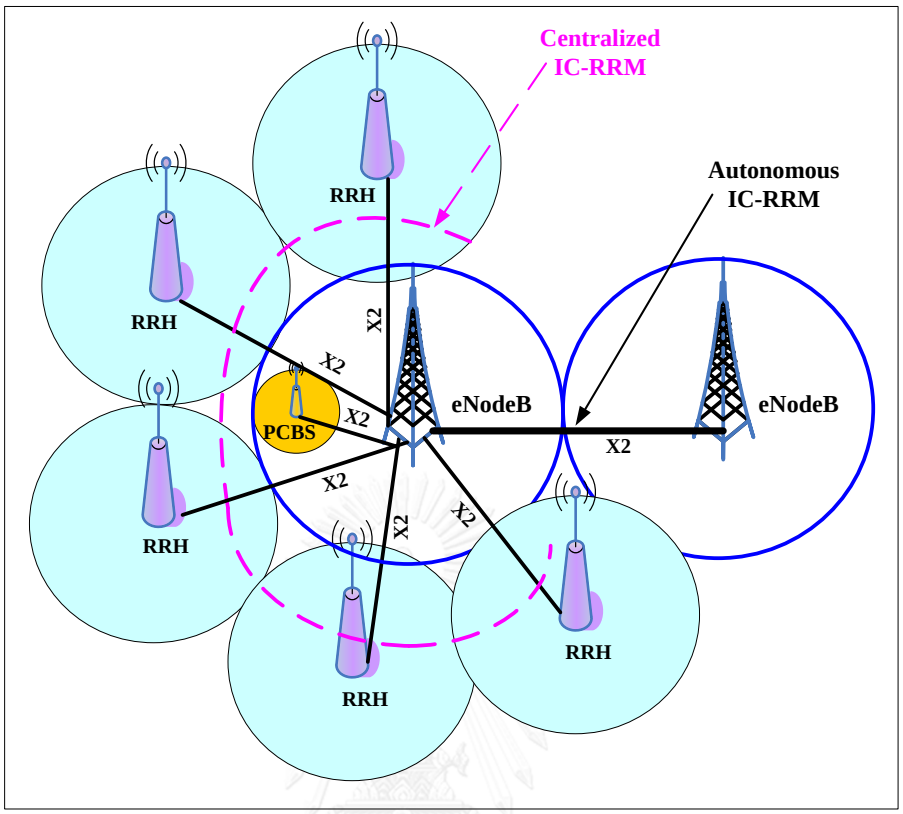

Figure 2.8: Network architecture for IC-RRM.

controlling wireless networks is based on programming networks in a distributed manner where control plane is distributed network wide both logically and physically in networking devices. Usually, wireless network control mechanisms are based on either a local or a global network view. In a distributed programmable network, typically a network control mechanism is based on a local network view. The local network view is usually centered on a network entity such as a cell and a UE where the former is termed as cell-centric, and the latter is termed as device-centric network control. On the other hand, in a centralized programmable network, a network control mechanism is usually based on a global network view where a centralized network entity controls the whole network with global information of the network. This centralized network entity is termed literally as controller which can be implemented physically in a distributed manner where physical controllers exchange information to one another, but logically they can act as a single control entity [52-53]. 5G networks can be evolved in either a logically centralized or a logically distributed programmable

control networks. Since the former is not the scope of this research, the later approach is considered. Note that logically distributed programmable control networks can be of cell-centric control or device-centric control as described below.

2.4.1 Cell-centric control networks

In traditional cell-centric architectures, a UE gets services from a network by making a connection establishment both in the UL and in the DL that carry user data traffic and control signals by using either a frequency division duplex or a time division duplex technique. All BSs (typically MCBSs) have usually the same transmission power for homogeneous networks. BSs are deployed and scaled on capacity demand, following a cell planning strategy, e.g., frequency resource reuse factor. A network is controlled in a distributed manner where each BS takes responsibilities of all UEs under its coverage and hands off to an adjacent BS with the assistance of a mobility management entity (MME). Functionalities of all layers (i.e., layer 1, layer 2 and layer 3) are performed at a MCBS. All UEs within MCBS coverage are under the sole control of BS. C-/U-plane functionalities of a UE are performed locally at a MCBS. A UE is controlled by the network employing both C-plane and U-plane connectivity which are governed by the same entity. For example, when a UE initiates a service request to a MCBS, from the network and cell selection procedures to an end of a service session, all control signaling and user data transferred between the MCBS and the UE over the whole session are governed by the same MCBS as long as the UE does not reselect or hand-off to a different MCBS. After successfully handing off, only a new MCBS governs the UE, and all functionalities regarding control and data planes are transferred to the new MCBS from the old MCBS. In short, a UE cannot be served for C-plane and U-plane functionalities by different BSs at a time. To boost capacity of homogeneous networks, SCs can be deployed in the coverage of a MC such that the same carrier can be reused in the SC tier.

2.4.2 Device-centric control networks

In device-centric control network architecture, a device should be able to communicate with a network through multiple nodes by exchanging multiple flows in a HetNet [3]. Hence, a set of nodes provide connectivity to a device, and functions of these nodes should be contextualized to a specific device during a session. To introduce a device specific architecture to 5G networks, many changes on existing cell-centric networks need to be addressed, e.g., decoupling C-plane and U-plane, serving UL/DL by separate nodes, decoupling baseband processing unit from processing hardware unit of a node, and beamforming with a high antenna directivity at mmWave spectrums. A model of device-centric network architecture for 5G networks is shown in Figure 2.9 [3]. Because 5G networks will encompass heterogeneous nodes, many of which will likely be unplanned by the network provider, flexible and reliable accesses of these nodes to the network will become crucial issues. Decoupling features have been proposed to address these issues. In the following, a number of proposed decoupling features are discussed briefly, and further detail on them can be found in Appendix A.

A. Decoupling C-plane and U-plane

In distributed HetNets, SCs can be deployed with a separation of C-plane and U-plane. In this configuration, U-plane of a UE is served by SCs, whereas C-plane is served by a MC. A SC simply provides U-plane traffic, and the MC provides C-plane traffic to a UE. SCs are not configured with cell-specific signals, e.g., synchronization signals, and all radio resource control (RRC) connection procedures are provided by the MC. Hence, these SCs are also termed as Phantom Cells [4]. SCs can be assigned with a high frequency band such as mmWave. However, to provide the mobility requirement, the MC is assigned with an existing microwave cellular spectrum. This can help address a high capacity need for 5G networks by SCs, and at the same time, reduce the number of hand-offs because of large coverage area by the MC. There are two scenarios for realization of C-plane and U-plane splitting, namely, SCs with baseband processing located at a MCBS and SCs with independent baseband processing. In scenario 1, all baseband processing of SCs and a MC are performed at the MCBS. SCs simply carry U-plane traffic to a UE. Though physically separated, the MCBS and a SCBS are logically seen as a single entity. Because of common U-plane

processing of all SCs, there is a limitation to the maximum number of SCs that can be deployed in a MC coverage. This scenario can be applied to the 3GPP LTE carrier aggregation deployments [54].

In scenario 2, each SC has its independent baseband processing system, and hence a SC appears as a separate entity from the MC. This configuration of C-plane and U-plane overcomes the limitation of scenario 1 because of a local baseband processing at a SC itself and helps scale network capacity. Based on scenario 2, a new RAN architecture that employs C-/U-plane separation has been proposed in [4] as shown in Figure 2.9(a). C-plane of a SC is managed by a MCBS, and U-plane is served by the SC itself that requires a new data path (S1-U) as a backhaul to connect to the core network. The MCBS is connected to the SC via a new interface X3. The MC first sends an RRC message to a UE to measure channel conditions between the UE and the SC for the connection establishment. After measuring channels, the UE then reports channel conditions to the MC. The MC then asks the SC via backhaul links for its preparation to serve the UE. Once the SC confirms with a positive response for its preparation to the MC, the MC then initiates to the UE an RRC connection set-up request from the SC to the UE. The UE then requests for a connection to the SC using the random access (RA) procedure with preamble. The SC then responds to the UE's RA request, and the UE then sends the RRC connection set-up (between the SC and the UE) confirmation message to the MC. User data are now sent directly via S1-U interface from the core network to the SC, and the SC then sends user data to the UE.

B. Decoupling downlink and uplink

In the DL of HetNets, different BSs have different transmission powers with a difference of more than 20 dB between a MCBS and a FCBS, and hence their coverages vary accordingly. However, in the UL, transmission powers from UEs are almost the same. In the DL, the maximum signal-to-interference-plus-noise ratio (SINR) region follows the transmission power of each BS, i.e., a MCBS with the largest, and a FCBS with the smallest. However, this is not the case in the UL where the maximum SINR region of a MCBS suffers the most, and the maximum SINR region of a FCBS can

surpass the coverage of a MCBS [55]. This is because UEs are comparatively much closer to a SCBS than a MCBS. Hence, a UE may have a good coverage for the UL from one BS and from another BS for DL. Further, when UEs are served by different BSs for the UL transmissions, they may cause interferences to one another if UEs are assigned the same resources in the UL. Hence, classical interference models considering symmetry in the UL/DL are not directly applicable for HetNets. So, the UL/DL should be considered as separate networks along with new interference models for HetNets with asymmetry in transmission power and irregularity in deployment. Figure 2.9(b) shows an example scenario of this type of network architectures.

C. Decoupling baseband processing unit and node

In this decoupling approach [56], by introducing virtualization concepts on BSs, baseband signal processing hardware unit, i.e. baseband unit, is decoupled from its node, i.e., BS [3], and all baseband units are aggregated centrally into a virtual BS pool. Centralized baseband unit, cooperative radio with distributed antenna based RRHs and real-time cloud radio access network (C-RAN) can address requirements of 5G networks. With a centralized baseband unit, a reduction in site costs and with RRHs, an increase in spectrum efficiency can be achieved. Further, with real-time cloud infrastructure and BS virtualization, dynamics in resource allocation, a reduction in power consumption, and an increase in infrastructure utilization can be achieved. C-RAN is an alternative approach to current networks and is targeting to the most typical HetNets scenario [56]. Based on a layer-wise (both control and data planes) functional splitting between a baseband unit and RRHs, full centralization and partial centralization of C-RAN can be realized. In full centralization of C-RAN, baseband (i.e., layer 1), layer 2 and layer 3 are incorporated in a baseband unit. However, in partial virtualization of C-RAN, layer 1 functionalities are left with RRHs. In either case, a C-RAN consists of three main components [56], namely, a baseband unit which is incorporated with a high-performance programmable processor and a real-time virtualization technology, distributed RRHs which are integrated with antennas, and high speed low latency optical fibers that connect all RRHs to the baseband unit. Figure 2.9(c) shows example C-RAN architecture [56].

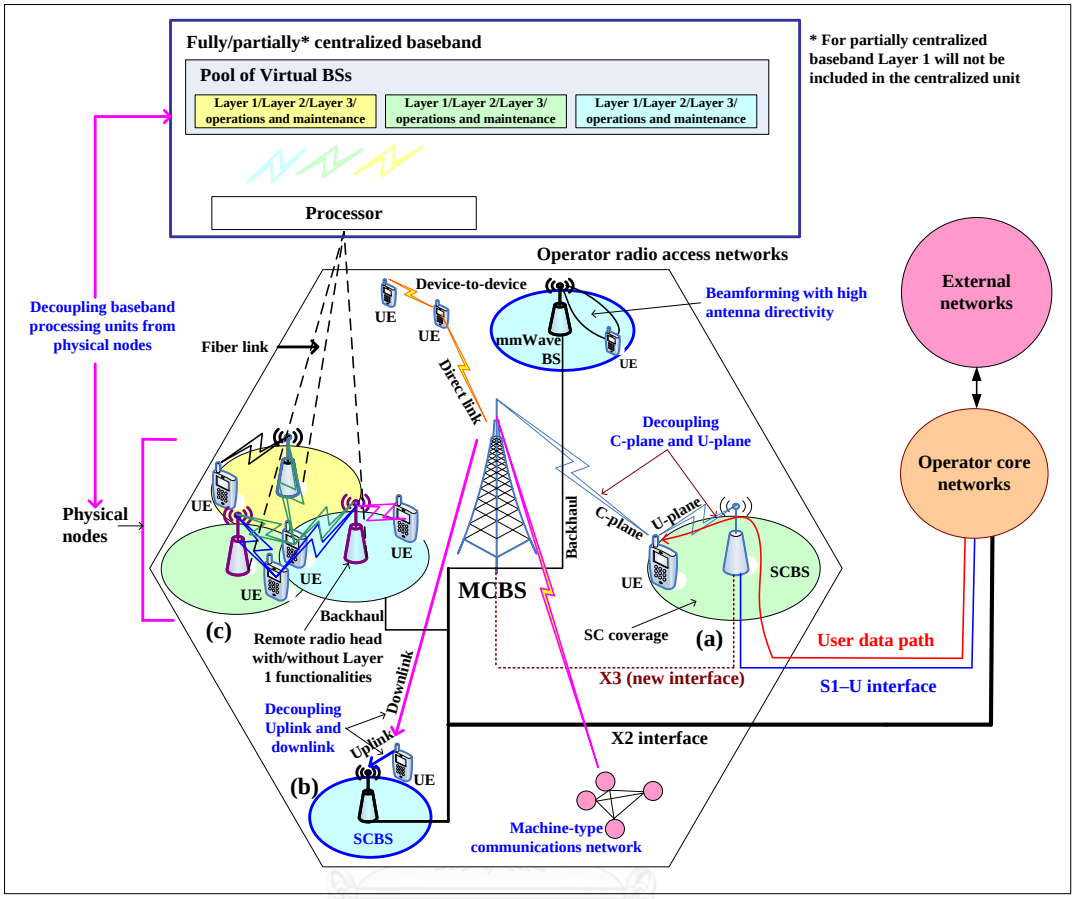

Figure 2.9: A device-centric network architectural model for 5G networks.

2.5 Backhaul networks

2.5.1 Deployment scenarios and solutions

5G networks will be denser than current HetNets in LTE-Advanced systems. In such a complex HetNet, a tight integration and a high level of cooperation between cells are crucial to address several significant and unavoidable issues such as interference management and load balancing. Backhaul networks will play a significant role on connecting BSs in a dense HetNet and providing a channel to communicate and to cooperate one BS to another. Backhaul networks take a considerable share of the total cost of ownership of the network. Hence, backhaul solutions should be cost-effective, easy to install, highly scalable and flexible, and not be a barrier to performances of

HetNets [57]. However, reusing the same spectrum between spatially separated cells puts much requirements on delay, delay variation, and synchronization, particularly between a MC and a SC.

There are a number of backhaul solutions such as microwave links using above 20 GHz frequency bands [58], microwave links using sub-6 GHz frequency bands, point-to-point optical fiber, point-to-multipoint optical fiber, category 5/6 LAN, and digital subscriber line. Backhaul solutions vary with requirements such as scalability, cost-effectiveness, and quality of experience. Scalability of a network can be achieved through a well-defined and carefully selected set of these backhaul technologies. By considering a common approach for traffic management by using single-vendor provided solutions, the total cost of ownership for the SC layer can be made one-half from, e.g., reduced infrastructures by the proper coordination [59] to address the cost issue. If a backhaul solution needs to address quality of experience, one way to do so is to ensure a proper coordination between radio nodes and layers which require a high performance end-to-end backhaul solution such as optical fiber or LOS microwave link, particularly for links from MCs whenever possible. If a fixed backhaul solution is not available, wireless links can be used as a default choice, and NLOS can also be considered for a greater degree of freedom.

For outdoor deployments, wireless and optical fiber backhauls are good choices and for indoor deployments, reuse of existing copper and optical fiber can be considered. Practical deployment scenarios, e.g., on city street, there are mainly two deployment scenarios, namely, an indoor environment (e.g., indoor hotspot) and an outdoor environment (e.g., bus stop). For an indoor hotspot, usually a PC is deployed, and can be connected to a MC over an existing digital subscriber line backhaul. However, based on capacity demands and environment profiles, optical fiber or LOS microwave can be considered. For almost all other indoor SCs, almost any backhaul can be used. For an in-building scenario, telephony cable and copper category 5/6 cable are seem to be the most used backhauls. For an outdoor microcell, it should be connected to the MC via a LOS or a high performing NLOS backhaul. Figure 2.10 [57] shows the capacity and delay characteristics of various backhaul transmission technologies.

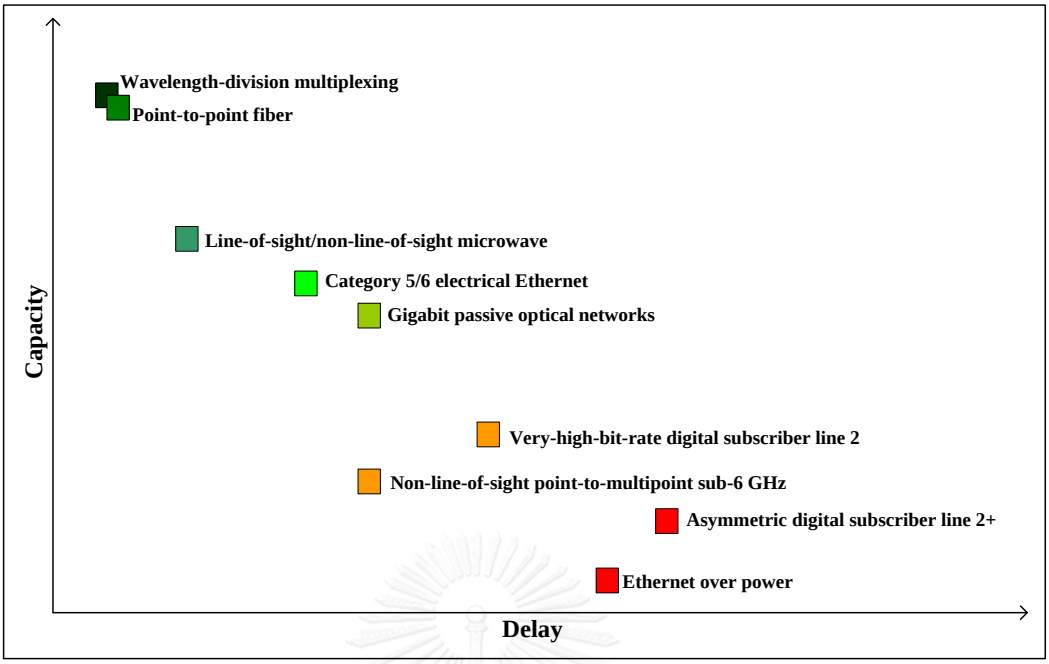

Figure 2.10: Capacity and delay characteristics of various backhaul transmission technologies.

2.5.2 Backhaul solutions for 5G networks

The backhaul solutions for SCs in Dense HetNets can be implemented either centralized or distributed manner as given in [60] for 5G networks. In a centralized backhaul solution, SCs are deployed in the coverage of a MC and are connected to the MC via mmWave wireless links. Each SC transmits data to the MC and the MC acts as the anchor or the central point for aggregating all data from SCs. The MC is connected to the core network via fiber to the cell backhaul as shown in Figure 2.11 (top). However, in distributed backhaul solution, a group of SCs form a cluster or a cooperating set, and one of the SCs act as an anchor that collects all the data from other SCs within the cluster. The anchor SC is connected to the core network via fiber to the cell backhaul (Figure 2.11 (bottom)) [60].

In 5G networks, the mmWave spectrum is considered as one of the major enabling technologies for high capacity. The low latency and high capacity fiber backhaul is expected to be complemented with NLOS microwave links and LOS mmWave wireless links with a peak capacity of about 10-25 Gbps [61]. According to

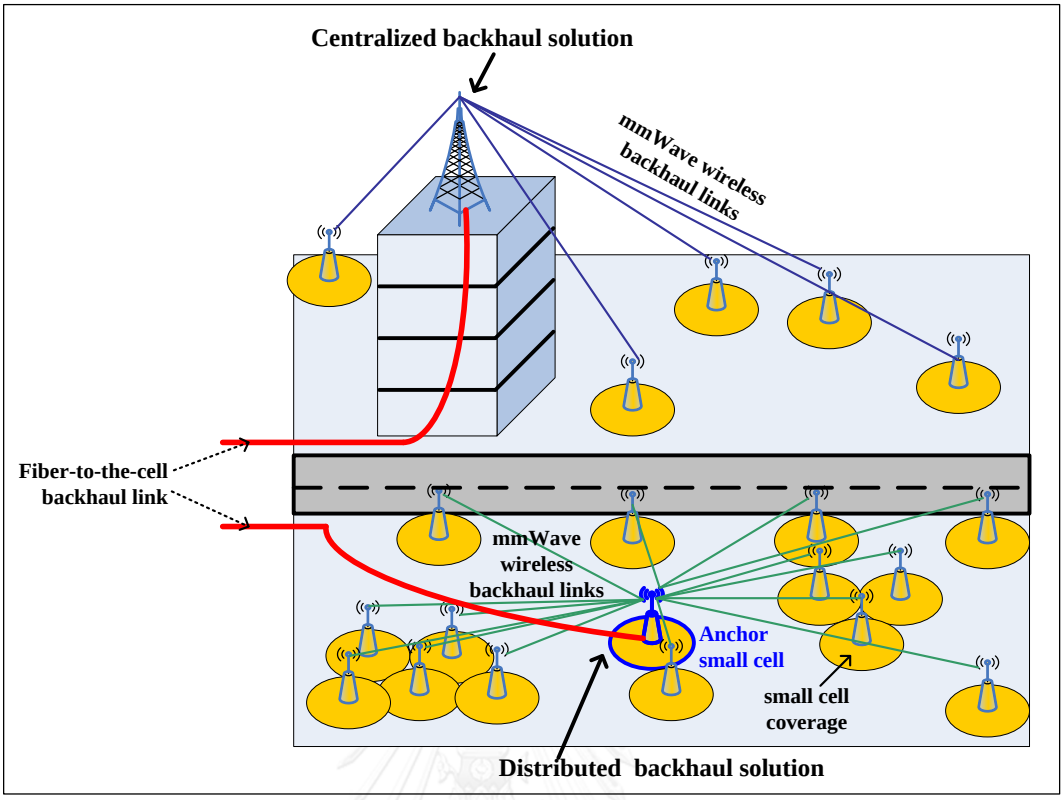

Figure 2.11: Backhaul solution scenarios: centralized (top) and distributed (bottom).

[61], the 60GHz band (between 57 GHz and 66 GHz) and E band (71-76 GHz and 81-86 GHz) are well suited for mmWave wireless because of large BW availability in these bands, e.g. 9 GHz and 10 GHz respectively, license free or light-licensed, and almost worldwide availability. For short links, 60 GHz band can be a good choice as compared to E band because of free of license fee to make the network more cost-effective. This high capacity mmWave wireless backhaul provides operators with an alternative solution to the traditional backhauling, by using multi-hop short distant links with each hop of 100-200 meters. With multi-hop mmWave wireless links, high capacity backhaul of up to 1 km can be viable [62].

2.6 Synchronization in HetNets

Synchronization in HetNets is very important because of an unplanned deployment of SCs. Time synchronizations mainly affect the cooperation mechanism

between cells for the coordinated transmissions among multiple BSs as well as for the alignment of these signals at a receiver. In addition, handovers between cells are time sensitive, and an accuracy of 1.5 micro seconds for time synchronization is required in a time division based LTE system [46]. There are mainly three links that may be utilized for time synchronization, namely, backbone, satellite, and cellular links [46]. Since SCs are typically connected to the core network via IP links, time synchronization could be possible to achieve by using IEEE 1588 protocol, i.e. precision time protocol, which employs time-stamped packets between a server and its clients. However, in the context of SCs, precision time protocol may face a lot of difficulties in terms of synchronization error and new investments from deploying precision time protocol enabled routers throughout the paths between clients and a server.

The use of satellite source such as global positioning system can provide a highly accurate time information over satellite links in both frequency and time. The global positioning system is commonly equipped with time division duplex based MCs. However, it requires a good global positioning system-enabled receiver. Since SCs such as FCs are expected to be deployed mainly to cover indoor environments, a satellite signal strength is not good enough in an indoor coverage with a resultant long time to synchronize or possibly no synchronization at all. The use of cellular networks for time synchronization can be performed by network listening to the synchronization signals from neighboring cells, which are possibly synchronized already, to perform timing adjustments.

Network listening synchronization for SCs is specified in the 3GPP [46]. SCs can listen to the primary synchronization signal or the secondary synchronization signal or the common reference signal from neighboring BSs to perform time synchronization. This approach is cost-effective since it does not impose any extra infrastructure requirement. However, if the link between a MC and a SC does not exist, then network listening cannot be done. In this case, SC networks can perform time synchronization in a distributive manner. Every SC at each iteration detects the synchronization signal and sets a new time based on its own time and the time from its neighboring SCs. Eventually, within a short time, all SCs converge to the same time value.

2.7 In-building cellular mobile communications

2.7.1 Signal propagations in in-building scenario

Propagation in indoor environments is a complex phenomenon and is difficult to model all the aspects such as reflection, diffraction, scattering, and building layout and construction effects that govern the propagation. Though in principle, both indoor and conventional mobile channels show similar basic features such as multipath dispersion from reflection and scattering phenomenon and can be described with the same mathematical model, however they do differ in a number of major aspects as given in Table 2.3 [63]. With a conventional mobile channel means a mobile channel observed when a BS antenna is elevated by, e.g. a tower or placed on a roof-top of a building, and a mobile antenna is at a low level.

Table 2.3: Indoor versus conventional outdoor cellular mobile propagation.

Aspect	**Mobile channel**	
	Conventional mobile channel	Indoor mobile channel
Time and space	Stationary in time (due to mainly the signal dispersion caused by large fixed objects such as buildings in comparison to the motion of people and vehicles) and non-stationary in space	Non-stationary both in time- (due to the motion of people and equipment around a mobile antenna) and-space
Path loss and variation in mean signal level	Lower as compared to the indoor channel	-
Applicability of negative-exponent distance-dependent path loss model	Well established	Not universally accepted
Doppler shift	High because of high velocity of mobile users	Negligible
Transmit power	High	Low

2.7.2 Indoor propagation mechanisms

According to [64], there are three categories of most dominant propagation paths of signal through floors in buildings, which are as follows:

- *Category 1*: Transmission paths through floors that may include multiple reflections between walls before or after going through the floors, which are significant when the transmitter and receiver are far from the windows.
- *Category 2*: Paths that include multiple diffraction at the window frames and involve successive diffractions at frames or edges of windows at different floors of the buildings and also subsequent scattering events, which carry significant power along diffracted paths when the transmitter and receiver are close to the windows.
- *Category 3*: Paths that involve reflections from scatters outside the building back into the measurement site which is mainly due to reflections from nearby buildings and is strong enough in dense urban environments, where nearby buildings are expected to be in close proximity and can potentially reflect strong signals back onto lower floors of the building under consideration [65].

As reported in [65], as more floors are penetrated, category 3 are considered to become more pronounced because of external paths that contribute more toward the received power as compared to the signal penetrated through floors (i.e., direct component) within the building caused because of a reduction in signal strength from penetrating through floors and an increase in strength of reflected signals. With an increase in the number of penetrated floors, the proportion of power arriving via external reflection paths increases significantly up to 93.2% after two floor separations. With both simulations and measurements, reflections from nearby buildings have been shown to increase the received signal by over 10 dB [65]. Hence, when reusing the same frequency within a building, reflections can cause to increase the co-channel interference. Since the reflected signals are external to the building and hence largely free space, the magnitude of reflected signals on lower floors remain the same. The

strength of the reflected signal is dependent on the distance to the nearby structure, and the majority of the reflected power arrives on single-bounce paths, with double-bounce reflections delivering at most 7.7% of the total power [65]. Further discussion on other aspects such as attenuation caused by multi-floors and floor materials, indoor propagation modeling, and types of buildings and their impact on signal propagation can be found in Appendix A.

2.8 Issues of small cell deployments

Density of BS and transmit power per tier play a significant role on the capacity and coverage of mobile networks. BS consumes about 60% of the total energy of cellular networks [23]. MCBSs are designed mainly for a large coverage rather than providing a high data rate. Because of an enormous increase in high data rate services mainly in indoor environments, a large portion of data traffic is expected to be offloaded to low power SC networks. Employing such HetNets in recent standards has been considered as a primary element [23]. A number of major issues related to the deployment of SCs are pointed out in the followings.

2.8.1 Randomness

SCs specifically FCs are mainly expected to be deployed by the customers in an ad-hoc manner and hence randomness in FC deployment is considered to be taken into account while designing SC networks [22]. If SCs are deployed as an overlaid non-cooperative network, a significant level of cross-tier interference between macro-tier and SC-tier causes to happen which results in limiting the coverage and capacity of the SC network. Cross-tier interference depends on factors such as BS density, transmit powers [22]. As mentioned in [22], it is infeasible to determine how dense and strong BSs are randomly located and currently activated, and is emphasized that densely located SCBSs are to be able to sense their neighbors and be self-configured and optimized to render the cross-tier interference. However, the implementation of the features of self-configuration and optimization in SCs results in additional complexities

and associated costs. Hence, relative BS densities per tier and the number of active BSs per tier in a HetNet is considered to be a primary design concern of SC networks [22]. Authors in [66] proposed a coverage coordination scheme for SC networks where each SC performs self-configuration and self-optimization of pilot transmit power aligned with the interference experienced at a SC.

2.8.2 Randomness modeling practice

For Intra-tier, the randomness of BS placements is frequently modelled as Poisson point process [67-69]. In Poisson Point Process, the average number of BSs per unit area, i.e. BS density, is probabilistically determined, and the aggregate interference experienced at a randomly selected UE is considered to be statistically identical. Several existing works have applied Poisson point process based randomness modeling. Authors in [70] developed a tractable framework of single-tier network by modeling BS distribution as Poisson point process and showed that BS density does not have any impact on SINR statistics, which means that the coverage probability is independent of the BS density. This is because of the fact that the excessive interference from the denser BS deployment is compensated owing to attaching a UE to a closer BS and ensure better connectivity network wide. In addition, the authors in [71] showed that adding more tiers, e.g. randomly adding different SCs have no impact on coverage probability since a UE gets attached to the best BS in the best tier. The major advantage of Poisson point process based randomness of SC modeling is analytical tractability such that closed form solution can be obtained with reasonable simplicity in assumptions. However, in complex scenarios, e.g. 3D network scenario, more realistic use cases are difficult to capture, and hence, no existing literature has been found.

Since the inter-tier interference varies with the BS density and the transmit power per tier, the coverage of each tier also varies accordingly. A number of existing works have addressed an optimal BS density issue. Authors in [72-73] showed an optimal relative BS density per tier to maximize transmission capacity under closed access of FCs for a two-tier HetNet. The BS distribution is modelled as Poisson point process in 2D HetNet scenario. Whereas, authors in [74-76] investigated under open

access FCs to optimize relative BS densities by controlling a fraction of open access FCs considering the BS distribution modelled as Poisson point process in 2D HetNet scenario. In [77], authors showed that the optimization of joint and dis-joint sub channel allocation depends on the relative BS densities and transmit powers.

2.8.3 Minimum separation distance between small cells

Authors in [22] proposed to use a BS location model with a minimum cell separation distance to ensure a minimum distance between any two cells in each tier using the Matern hardcore process such that no cells can lie within a predefined minimum distance from any other cell. Each BS simply checks whether or not if there has already been any activated cell with the predefined distance to determine an effective BS density. Larger the minimum distance, lesser the probability that a BS to be activated because of probabilistically presence of more neighboring BSs with the circle with radius equals to the minimum distance. Minimum separation distance was used to show that load balance per cell depends on relative BS densities and transmit powers. Minimum separation distance helps to adjust the number of BSs to be activated to reduce the area power consumption and to balance the load over cells effectively with changing user density [23] and can be implemented in a distributive manner by adopting self-organizing network (SON) [22]. Note that Matern hardcore process can be approximated as Poisson point process by introducing an exclusion region around each BS [22].

Authors in [23] proposed a strategy to find a minimum separation distance between SCs and derived an optimal minimum separation distance between SCs by adopting modified Matern hardcore process to analyze the effect of separation distance on the coverage of SC networks. Like [22], the authors in [23] also considered self-configuration of BS deployments. In addition, the authors showed numerically that a larger target user throughput necessitates a lower minimum separation distance (for a given user density), and so is required for a higher user density (for a given target user throughput). When the minimum separation distance approaches to zero, it requires

more SCs to deploy in order to support more users and achieve the required target user throughput.

All these aforementioned works addressed enforcing a minimum distance based on the interference statistics around SCBSs, i.e. by sensing the presence of neighboring SCBSs to avoid intra-and inter-tier interferences by modeling BS locations as Poisson Point Processes. However, a minimum distance can also be enforced by proper allocation of resources to SCBSs such that the interference is independent of the effect of randomness of BS locations. It means that, no matter how randomly BSs are distributed, as long as interference level at a UE is limited, there is no need to take into account of BS location. Hence, rather than enforcing a minimum distance which is the function of random BS distribution deployed by customers, a mechanism that can address interference issues to ensure an optimal distance between SCs would be more impactful because of controlling SCs from the network side and independent of BS randomness in distribution.

Further, stochastic geometric approaches are mainly applied so far in the existing literature for 2D BS location scenario with more simplistic homogenous Poisson point process or Matern hardcore process, whereas the study of 3D scenario existing in practical indoor buildings is not obvious because of complexity and intractability of analytical expressions. This necessitates a more realistic yet simple enough model to analyze such a 3D interference modeling and to enforce a minimum distance. Furthermore, modeling SCs using a random distribution of SCBSs is not a universal necessity. This is because of the fact that FCs are available in three modes, e.g. closed access, open access, and hybrid access of the first two. Since typically, open access FCs as well as most hybrid access FCs are deployed by the operators to provide high data rate coverage in indoor environment, regular grid based model such as square-grid based model can be applied for modeling. Hence, operators can use such simple square-grid based model for enforcing minimum distance between SCs and reusing resources in SCs to improve spectral efficiency as much as possible. Further, since employing stochastic geometric approach in 3D in-building scenario is typically complex and analytically intractable, CSG FCs can be also be modelled using square-grid based model considering that the average interference statistics over a cluster of FCs remain typically the same. This issue is addressed in Chapter 4.

2.8.4 3D versus 2D modeling and impacts on FC interference

Authors in [5] investigated the impact of three-dimensionality of FC deployments on cross-and co-tier interferences using realistic building data and showed that interference effects of urban FC deployments under 3D scenario is significantly higher than that when considering 2D case, and heterogeneity in building heights plays an important role on the aggregate interference effect in FC networks. Typically, the interference in HetNets has been studied considerably under 2D scenario, flat, and homogeneous networks structure for deployment heights [5]. Though 2D modeling is simple, it is not accurate enough since it cannot account the complex combination of deployments and propagation effects in realistic 3D buildings. This is raised by a number of facts as follows [5]:

- FCs in upper floors are more susceptible to interference from neighboring BSs when operating under the same frequency than those in lower floors, e.g. ground floor, due to the presence of low loss because of presence of more LOS components in a larger area than those FCs operating in lower floors. Hence, channel conditions are different in lower floors (e.g., ground floor) from that in upper floors. This implies that the height of a building has an important effect on overall interference in FC networks.
- The interference signal is the most from the nearest adjacent building, which degrades with an inclusion of additional adjacent buildings (with almost very low after the fourth adjacent building).
- An increase in the number of interferers and modification of interference pattern.

Hence, the authors in [5] proposed to consider modeling HetNets under 3D scenario to introduce more accurate interference effects than that in 2D scenario.

2.8.5 3D small cell networks modeling

Modeling of interference in FCs installed densely in 3D scenario is an important area of research to analyze interference, capacity, and coverage effects in indoor environments. Since in urban areas, most indoor environments are modeled as 3D building where a dense deployment of FCs in 3D buildings will be an obvious scenario in order to address high data rate demand of 5G networks, a number of existing works have already addressed this issue of modeling SC networks in such 3D scenarios, e.g. office buildings and residential areas. For example, the authors in [16] addressed the issue of interference coordination in 3D building scenario for an unplanned deployment of FCs by considering a system with multi-floor buildings having FCs installed densely in them within the coverage of MCs. They proposed a graph based interference coordination scheme consisting of three phases, namely FC interference graph establishment, FC clustering, and frequency resource allocation. The authors showed numerically that the intra-cell interference of FCs of the same building is the dominant source of interference as compared to the cross-tier interference from the MC as well as interferences from FCs of other surrounding buildings because of the presence of high external wall penetration loss of a building. FCs are clustered based on measurement reports from their associated UEs, and an interference graph is then formed depending on whether or not an interference between FCBSs exist. Each cluster is assigned with orthogonal frequency resources to avoid co-channel interference. With simulation results, the authors showed that their proposed interference coordination scheme performed better than other conventional schemes such as universal frequency reuse scheme where each FC is assigned with the whole system BW and frequency hopping scheme where each FC can choose ¼ of the total sub channels.

2.8.6 Self-configuration and self-optimization of FCBSs

With self-configuration mechanism, a FC initiates its' transmit power by sensing the interference from the neighboring FCs to ensure a constant coverage, and with self-optimization mechanism, a FC continually adjust its' transmit power using

transmit power control (based on surrounding radio environments) so that the coverage of FC does not make an interference with other outdoor cell such as MC. A FCBS first measure the average received pilot power (over multiple frame in time) from the neighboring FCBSs and MCBSs and configures its pilot power identical on average to that of neighboring FCBSs and MCBSs at an initial cell radius. Self-configuration provides only the initial coverage and is refined over time using self-optimized power control mechanism. The time average received power measured by UEs associated to a FCBS is feedback periodically to the FC BS. The FCBS also evaluates the received interference-plus-noise power and the pilot power of it is then updated based on whether or not the difference between the feedback power by UEs and the measured interference-plus-noise power is greater than the predefined threshold or not [66].

2.9 Resource allocation in HetNets

Dynamic resource allocation or packet scheduling is one of the most important functionalities of RRM. Almost all other functionalities are affected with the performance of packet scheduling. Packet scheduling allocates or de-allocates resources, including buffer and processing resources and RBs to both the C-/U-plane packets. Selection of radio bearers onto which packets are to be scheduled, management of necessary resources such as power, frequency, time, and space, consideration of quality-of-service associate with each radio bearer, channel state information (CSI) for UEs, buffer status, interference situation, and so on along with restriction or preference on a portion of RBs due to interference coordination are all parts of responsibilities of dynamic resource allocation or packet scheduling [54].

Packet scheduling policy can be developed based on a number of performance metrics, e.g. maximum SINR, maximum fairness, or a trade-off of these two, and the schedulers based on these metrics are respectively called as max-min, Round Robin and Proportional Fair. In LTE, max-min schedules a UE with the highest SINR at a RB in any transmission time interval (TTI), and hence it provides the best average throughput performance but at the least the fairness. This is because UEs with good channel conditions are always scheduled, and those with poor channel conditions such as the

cell-edge UEs are scheduled very less and sometimes never at all. Round Robin schedules UEs with an equal turn in a given period of time with an equal amount of RBs for each UE, and hence it provides the best fairness but usually at the worst average throughput performances since it does not consider a UE channel condition into account. Proportional Fair provides a good tradeoff between these two schedulers by considering all UEs' past average throughput into account such that a UE who has been scheduled very frequently in the past will be given less preference to scheduling even though its channel condition is far better than the other peer UEs. Proportional fair scheduler is usually preferable to other two schedulers because of its optimal average throughput and fairness performances. However, its algorithm development more is complex than that of max-min and Round Robin schedulers. There are many existing literatures that examine the performance of these schedulers in HetNets from various perspectives in order to improve performance metrics such as throughput, fairness, and other quality-of-service metrics.

The role of packet scheduling in HetNets is very significant. Packet scheduler is located at the MCBS. In HetNets, SCs such as FCs, PCs, and relay stations are all connected to the MCBS. The packet scheduler at MCBS takes the decision of which UE in what time at which RB (or a group of RBs) at what transmit power at which antenna port in which cell is to be scheduled based on several parameters such as CSI, precoding metric, mobility, quality-of-service requirement, UE location, UE serving cell, cell load, cell cooperation, interference mechanism, and so on. There is no specification from standardization bodies for packet scheduling principle and operation requirements, and network operators usually define packet scheduling strategy based on their respective network capacity, user demands and operators' goals.

2.10 Cooperative communications

In dense HetNets, an effective approach to address interferences from one cell to another is to ensure a very tight coordination among cells such that the same frequency can be reused among SCs with an appropriate cooperation. The use of

cooperative principles will play a significant role on the 5G network capacity achievement.

Cooperation can be defined as a process of working together [78]. In cellular wireless networking aspects, a number of BSs and UEs cooperate to address common network goals such as channel diversification, resource allocation, interference mitigation, and so on. The perspectives of cooperation are broad, and in this work, we particularly emphasize those perspectives that are highly relevant on current mobile networks, specifically the 3GPP LTE with a projection toward future 5G networks. The concept of cooperative communications was addressed first in [79], where the author proposed a three-terminal relay channel with a derivation of upper and lower limits of capacity. Later, the authors in [80] investigated the capacity of a cooperative relay channel and set a theoretical basis for the research on cooperative communications. Currently, in LTE release 10 (LTE-Advanced), cooperative communications has been standardized as one of the advanced technologies to address many crucial issues such as interference, capacity, diversity, cell-edge user throughput by including relay stations and CoMP communications. Relay stations are used to allow communication to a destination node by relaying signals from the network and vice versa. In CoMP, a group of network nodes (also termed a cooperating set) coordinate among each other, and this type of cooperation is termed as node cooperative systems.

Relay stations use three possible cooperative protocols, namely, amplify-and-forward, decode-and-forward, and compress-and-forward. If a backhaul link is poor, amplify-and-forward and compress-and-forward protocols are favorable. However, for a good relay backhaul link, decode-and-forward is more advantageous [81]. Since relays are deployed in the coverage of a MC, relay cooperative schemes are also called intra-cell CoMP where relay stations and a MCBS cooperate. Cooperation in node cooperative systems can be held by either joint processing or coordinating strategies among nodes in a cooperating set. In joint processing, data among all cooperating nodes are first exchanged via backhaul links, and transmissions and receptions of data take place jointly from all nodes at a time to improve mainly user throughputs. All cooperating nodes are connected to each other via high speed backhaul links, and are forming a DAS which can easily take advantage of spatial diversity, resulting in an improved overall network capacity. In the coordinated node cooperation, all

cooperating nodes in a set coordinate strategies, e.g., resource allocation, beamforming pattern via backhaul links to reduce interferences from adjacent nodes. Control information such as CSI is shared for coordination among all cooperating nodes.

The joint processing is further categorized into two, namely, joint transmission and dynamic point selection. Irrespective of CoMP scheme, control signals, e.g. physical downlink control channel (PDCCH), are only transmitted from the serving cell, i.e. the cell where the current physical location of a UE exists. In joint transmission, all points or partly in a cooperating set are associated with a UE specific demodulation reference signal (US-RS) and transmit user data simultaneously to a UE coherently or non-coherently in a time-frequency resource to improve received signal qualities and data throughputs of the UE. However, in dynamic point selection (muting), user data are transmitted from only one point of a cooperating set, while all other points are muted even though the user data is available at all points. Transmitting or muting a point may change simultaneously from one subframe to another following a specific scheduling strategy such as the minimum path loss between a point and a UE [51].

In coordinated scheduling/coordinated beamforming, user data are available only in the serving point; however scheduling or beamforming decisions are taken after coordinating with all other nodes in a cooperating set. With a combination of joint processing and coordinated scheduling/coordinated beamforming that results in a hybrid scheme, a few points can involve in joint transmission simultaneously, while other points can cooperate for coordinated scheduling/coordinated beamforming in a time-frequency resource. All these schemes are shown in Figure 2.12. CoMP communications have been considered for LTE Release 11 [82], and a number of scenarios of CoMP communications are considered for both the UL/DL in homogeneous networks as well as HetNets [83].

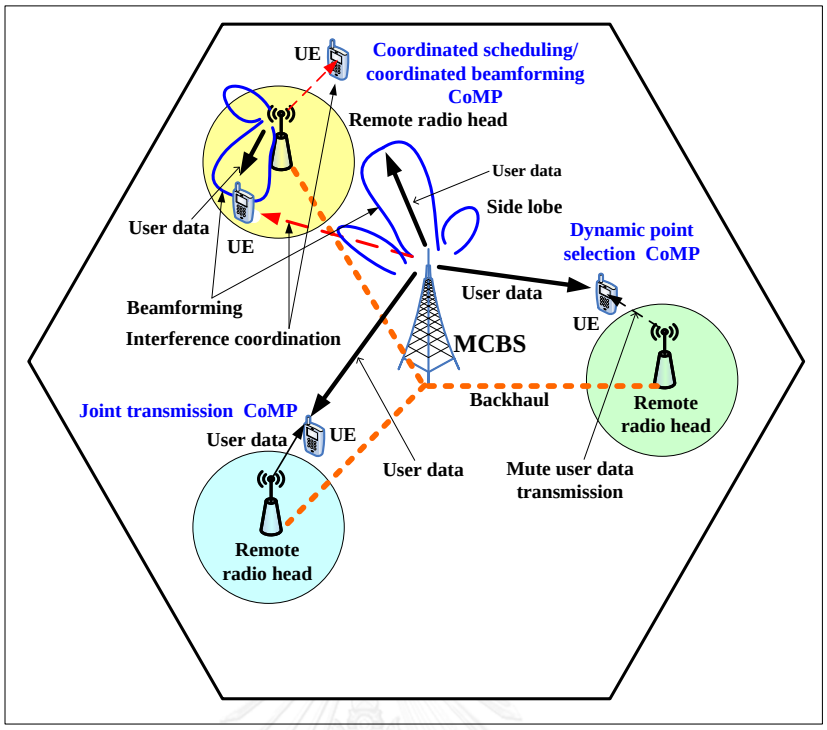

Figure 2.12: CoMP schemes in HetNets.

2.11 Summary

In this chapter, relevant reviews on necessary concepts, theories, techniques, and methods for the dissertation research are discussed. In sections 2.1 through 2.6, a brief review on 5G mobile networks is given, and a 5G network architectural evolution framework, consisting of three evolutionary directions, is developed. Though there are a number of enabling technologies in each evolutionary direction, the review is limited to those enabling technologies that mainly concern with meeting capacity demand of 5G networks, specifically MC, PC and, FC based dense HetNets and eICIC based interference management for resource reuse and allocation in 3D in-building scenario for RAN node and performance enabler, cell-centric and device-centric networks for network control programming platform, and deployment scenarios and solutions of backhaul networks and synchronization of HetNets for backhaul network platform and synchronization. However in Appendix A, additional enabling techniques along these directions are given. In section 2.7, a brief discussion on 3D in-building cellular mobile communications, including indoor signal propagations and mechanisms, is given.

Section 2.8 highlights a number of issues of SC deployments such as randomness and its modeling practice, minimum separation distance between SCs, 3D versus 2D modeling and impacts on FC interference, and 3D SC networks modeling. In section 2.9, radio resource allocation and its role on HetNets are discussed. Finally in section 2.10, cooperative communication mechanisms are discussed.

CHAPTER 3
RADIO RESOURCE REUSE TECHNIQUE FOR 3D IN-BUILDING DENSE SMALL CELL

In this chapter, a frequency reuse and scheduling algorithm (FRSA) using an adaptive ABS based eICIC technique to reuse frequency resources in FCs is proposed. FCs are deployed in 3D multi-floor buildings in dense urban environments of a multi-tier network, including FCs and PCs in a MC coverage. By exploiting the high external wall penetration loss and in-between distance of neighboring buildings, all FCs in a building are considered as a FCL. The impact of varying the number of ABSs on the throughput performance of FRSA is analyzed, and an OPNA for FRSA is derived. An adaptive OPNA scheme for FRSA is developed, and its outperformance over a static OPNA scheme is shown.

3.1 Introduction

Increase in capacity with an expensive and limited bandwidth is one of the major concerns of existing cellular mobile networks in order to address a continual increase in the number of mobile users and the demand for a high per user data rate. This results in initiating investigations on next generation mobile networks, i.e. 5G mobile networks, the capacity of which will most likely be driven by three major aspects, namely, network densification, spectrum extension, and spectral efficiency technique [4]. Based on recent researches, network densification is found to be the major driver [84] where SCs such as FCs are deployed in the large coverage of a MC. Because of smaller coverage and hence less transmission power than a MC, such type of networks are termed as HetNets. Since the capacity increases with the SC density, providing that the interference is within a limited range, it is desirable to deploy SCs as densely as possible that results in an extension of the so-called HetNets to dense HetNets. Dense

HetNets take advantages of a short distance between a SCBS and a UE and reusing MC spectrum in SCs by managing interference between cells using techniques, e.g. eICIC defined in 3GPP release 10 [1]. In indoor cFC deployment, clustering FCs and reusing resources with a proper interference management are the major challenges in urban environments that raise a number of issues discussed in the followings.

Firstly, FC clustering which is an effective technique to improve network capacity by disjointing a set of FCBSs over the whole or a part (e.g., a multi-floor building) of a MC coverage into a number of subsets or groups. A group of such FCBSs is called a FCL. Existing FC clustering approaches over a MC coverage are associated with a number of pitfalls, mainly as follows:

- The maximum resource reuse factor for FCLs per MC is difficult to define as the size of a FCL and the maximum amount of resources allocated in it are interdependent because of co-channel interference from neighboring FCLs [21].
- Since in practice indoor FCBSs are typically deployed by users and random in placement, prior knowledge of the number of FCLs in a MC coverage [21] is not immediate.
- An extreme level of network densification cannot be exploited fully since decreasing the size of one FCL necessitates increasing the distances from its neighboring FCLs to keep the co-tier interference limited.
- There is an additional computational complexity from estimating the number of FCLs per MC due to different size of FCLs [21].

Secondly, typical interference management and frequency reuse analysis in 2D scenario for regular HetNets where the density of serving SCs is less than that of served UEs [84] is not practical enough particularly in urban environments where the existence of a vast number of multi-storage buildings is obvious. Though 2D modeling for FCs is simple but not accurate enough since it cannot account complex combinations of deployment and propagation effects that exist in physical buildings [5]. The major issues that need to be considered when reusing resources in FCs in a structured 3D multi-floor building environment as compared to that in a 2D environment are as

follows. With 2D modeling of SCs, it is not possible to capture these issues that exist in physical 3D multi-floor buildings.

- The external wall penetration loss of any buildings
- The distance between neighboring buildings and co-channel interference effect from SCs of neighboring buildings
- The inter-floor and inter-wall penetration losses
- The complex signal propagation from effects such as diffraction alongside a building and reflection within a building

Thirdly, interference management using eICIC particularly in dense HetNets under 3D in-building scenario is not obvious. Hence, the proposed solutions in literature for regular HetNets in the 2D scenario [85-87] cannot be applied directly to the 3D in-building dense HetNets. Consequently, how to cluster FCs, manage interference using well established techniques such as eICIC, and reuse resources in FCs deployed in dense multi-floor buildings deployed in a large MC coverage in urban environments still remain open issues.

An effective solution for 3D in-building coverage is DAS where antennas of a BS are distributed within a building. Several works studied interference management and resource reuse aspects using DAS in 3D in-building scenarios [12-15]. However, one of the major difficulties with DAS is that each antenna covers typically a larger area than that by a FC, and hence resource reuse and correspondingly overall throughput gain by DAS are lower than that achieved by FC based HetNets [13]. A number of studies also addressed issues of interference management and resource reuse in FCs under 3D in-building scenario. In [5], authors investigated the impact of 3D FC deployments on cross-tier and co-tier interferences using realistic building data and showed that interference effects of urban FCs under 3D are significantly higher than that when considering 2D scenario. Authors in [16] proposed a graph based adaptive FC clustering scheme for inter-FC interference coordination within the same building. Also, authors in [17] proposed a dynamic clustering based cognitive sub-band allocation scheme to reduce inter-FC interference. FCLs are formed using inter-FC

interference graphs, and resources are reused in each disjoint FCL within a building. In [18], authors proposed a semi-static resource allocation scheme where the minimum number of subbands, one for each FC, is computed by solving a node-coloring heuristic algorithm in a multi-floor building over iBuildNet, an indoor network planning and optimization tool. In [19], authors proposed an adaptive soft frequency reuse scheme where groups of FCs are formed using the received signal strength indication from UEs, and different frequency reuse factors and transmission powers are adjusted to mitigate mutual interference. Authors in [20] exploited FFR using iBuildNet to propose a cooperative transmission and a semi-static interference mitigation scheme for in-building dense FCs.

Most of these existing works addressed FC clustering within the same building for reusing resources in FCLs rather than over a large MC coverage. Authors in [21] addressed FC clustering over a MC coverage, however the proposed approach is limited to 2D scenario. Though in reality, indoor MUs cannot get access to CSG FCBSs and interfere with FCBSs and FUs, the existence of indoor MUs within buildings has been overlooked. Hence, no cross-tier interference managements, mainly in the DL between indoor MUs and FUs and in the UL between indoor MUs and CSG FCBSs, have been addressed. Also, implications on interference from neighboring buildings because of reusing resources have not been emphasized which affect the maximum resource reuse factor per MC coverage.

Furthermore in practice, it is obvious to deploy PCs for hotspot coverages to offload outdoor MUs along with indoor FCs, investigations with a system considering both types of SCs have been mostly overlooked. A scheduling algorithm that can account of data rate demand of a system having multiple SC user categories, e.g. PC offloaded MUs and FUs, has not been reported either. Note also that, in HetNets FC clustering and reusing resources in 3D in-building scenario (mostly for two-tier networks) and eICIC for interference management have been studied separately in literature, and to the best of our knowledge, a combined scheme that can benefit from both eICIC techniques and multi-tier dense HetNets over a large MC coverage has not been addressed yet. We address these aforementioned issues of HetNets in this chapter.

To reuse resources in a structured 3D multi-floor building environment, as mentioned earlier we exploit issues 1 and 2, i.e. the external wall penetration loss of

any buildings and the distance between neighboring buildings, to show that the co-tier co-channel interference effect from SCs of neighboring buildings is negligible, and hence we propose a FC clustering approach by considering all FCs per building as a FCL. Issues 3 and 4 are addressed using TD and FD eICIC techniques by an orthogonal allocation of RBs, in the whole system bandwidth of the MC, to all SCs located within a building based on their channel conditions. We then propose a FRSA for an arbitrary value of ABS in a multi-tier network consisting both in-building FCs and outdoor PCs in the coverage of an urban MC. The FRSA is developed in two schemes, namely common resource pool and allocation (CRPA) and orthogonal resource pool and allocation (ORPA) where one differs from another in the way different MUs are prioritized during ABSs. Since indoor MUs within FCLs typically get less RB resources scheduled than other MUs irrespective of the number of ABSs, we propose a model for estimating an OPNA and derive an OPNA per FC cluster basis under two schemes, namely adaptive and non-adaptive OPNAs, in order to vary dynamically the number of ABSs imposed on FCs per building based on the presence of indoor MUs within the building to avoid cross-tier interference between indoor MUs and FCs. An optimization algorithm for OPNA schemes is developed, and its implementation aspects are discussed. We also develop a schematic of the scheduler implementation for FRSA and discuss the capacity outperformance of FRSA over a number of existing works. Further, a number of technical and business perspectives of the proposed FRSA are discussed. The proposed FC clustering and FRSA, using eICIC through modeling an OPNA per cluster basis, benefit from the following features:

- A FCL is formed by considering all FCs deployed in a building, and hence there is no computational complexity from estimating cluster size.
- The system model considers a more realistic multi-tier system with different types of SCs than a typical two-tier system.
- Interference effects from indoor MUs within buildings on CSG FCBSs and FUs are addressed.
- Because of an orthogonal frequency allocation to FCs per FCL, complex intra-cell interference in a FCL is avoided.

- The proposed FRSA is independent of the co-tier co-channel interference from neighboring FCLs, and hence a FCL size is independent from others.
- Because of its semi-centralized feature, the FRSA takes advantages of both the centralization feature through updating OPNAs per ABS pattern period to address network delays between the MCBS and FCLs, and the decentralization feature through updating frequency allocation per TTI to address fast fading effect on channels between FUs and FCBSs.

The chapter is organized as follows. The system model is presented in section 3.2 in terms of system architecture, FC clustering, interference management, problem formulation, and proposed FRSA. In section 3.3, we discuss OPNA for eICIC techniques in terms of proposing a model for an OPNA estimation and deriving an OPNA under two schemes, namely adaptive and non-adaptive schemes. We develop an optimization algorithm for both schemes and discuss its implementation aspects. In section 3.4, the simulation model is presented in terms of simulation parameters, assumptions and performance analysis for a number of simulation scenarios. We also report the outperformance of the adaptive OPNA scheme as compared to the non-adaptive one. In section 3.5, a number of scheduler implementation perspectives of FRSA are described, and a performance comparison of FRSA with a number of existing works are carried out. In section 3.6, we discuss a number of technical and business perspectives of FRSA, and summarize the chapter in section 3.7.

3.2 System model

3.2.1 System architecture, interference management and FC clustering

A. System architecture

We consider a square-grid based FC coverage area where each FCL consists of a number of 2D floors, and each floor consists of a number of square-grid apartments with side length *a* as shown in Figure 3.1(a). Each apartment has one FCBS with a

coverage area of $(a \times a)\ m^2$, which is placed in the center of the apartment and assumed static. A fixed free space around its building of a FCL and some free space between two neighboring FCLs are assumed. In general, a and the value of free space are random variables. A UE per FCBS is considered and placed at the farthest radial distance from the FCBS. The system architecture is illustrated in Figures 3.1(b) and 3.1(c). We consider a single MC of a corner excited 3-sectored MC site and a number of SCs,

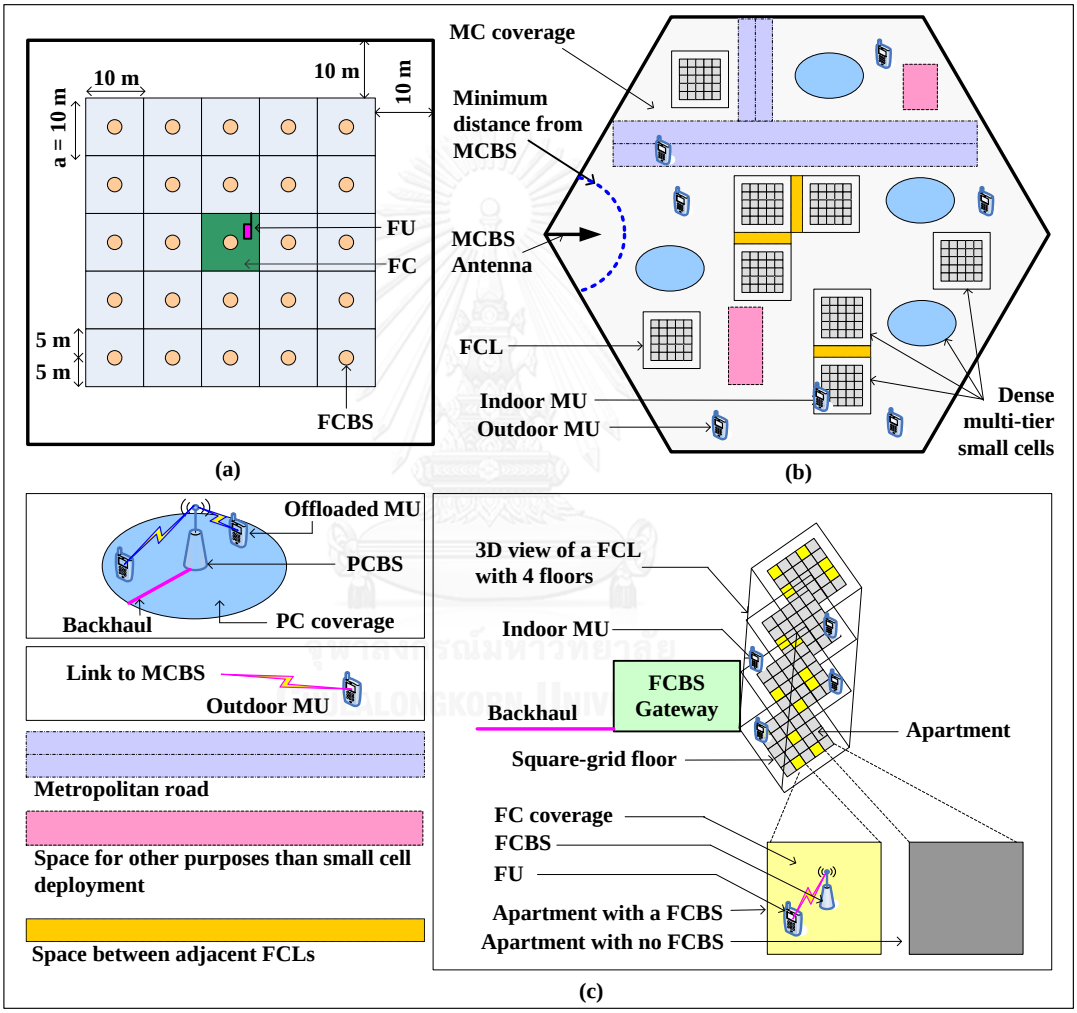

Figure 3.1: (a) Proposed 2D floor architecture of a FCL; system architecture: (b) dense deployment of SCs (c) links of SCBSs to UEs and MCBS, links of MCBS to MUs, and other used spaces in a MC.

including outdoor PCs and indoor FCs. A certain percentage of MUs are assumed within all FCLs. All indoor MUs are served by the MC. In addition, a certain percentage of outdoor MUs are offloaded to nearby PCs. FCs are dropped as clustered as shown in

Figure 3.1(a). In Figure 3.1(c), an apartment with yellow color represents that a FCBS is deployed in it, and the one with ash color represents an absence of a FCBS in it.

B. Interference management and FC clustering

In the system architecture shown in Figure 3.1 for the DL, when all BSs operate at the same frequency in any TTIs, the co-channel interferences that any offloaded MUs can experience are from the neighboring FCBSs and PCBSs as well as the MCBS. Any outdoor MUs can experience co-channel interference from the neighboring FCBSs and PCBSs. However, indoor MUs can experience co-channel interference from the neighboring FCBSs and PCBSs. Any FUs can experience co-channel interference from other FCBSs of the same building, FCBSs of the neighboring buildings, and the neighboring PCBSs. To form clusters of FCs deployed in a 3D building, both inter-cluster level and intra-cluster level interference effects need to be managed. In general, there are in total eleven sources of co-channel interference as shown in circles in Figure 3.2 that can be generated, of which four of them are experienced by FUs, two are by offloaded MUs, three are by outdoor MUs, and the remaining two of them are experienced by indoor MUs, when all types of BS operate at the same RB *i* in the same TTI *t* as given below. Note that implicitly, the co-channel interference from any serving BSs (any BSs to which any UEs is attached to for being served by the network) to any serving UEs has not been considered since typically a scheduler does not schedule the same RB *i* under the coverage of any BSs to multiple UEs in any TTIs *t* unless any special mechanisms is considered.

From the MCBS to a FU for the UE in any FCLs, $I_{t,i}^{FUMC}$

From a FCBS to a FU for the BS and UE located in different FCLs, $I_{t,i}^{FUdFC}$

From a FCBS to a FU for the BS and UE located in the same FCL, $I_{t,i}^{FUsFC}$

From a PCBS to a FU for the UE located in any FCLs, $I_{t,i}^{FUPC}$

From a PCBS to a MU for the UE located in MC, $I_{t,i}^{oMUPC}$

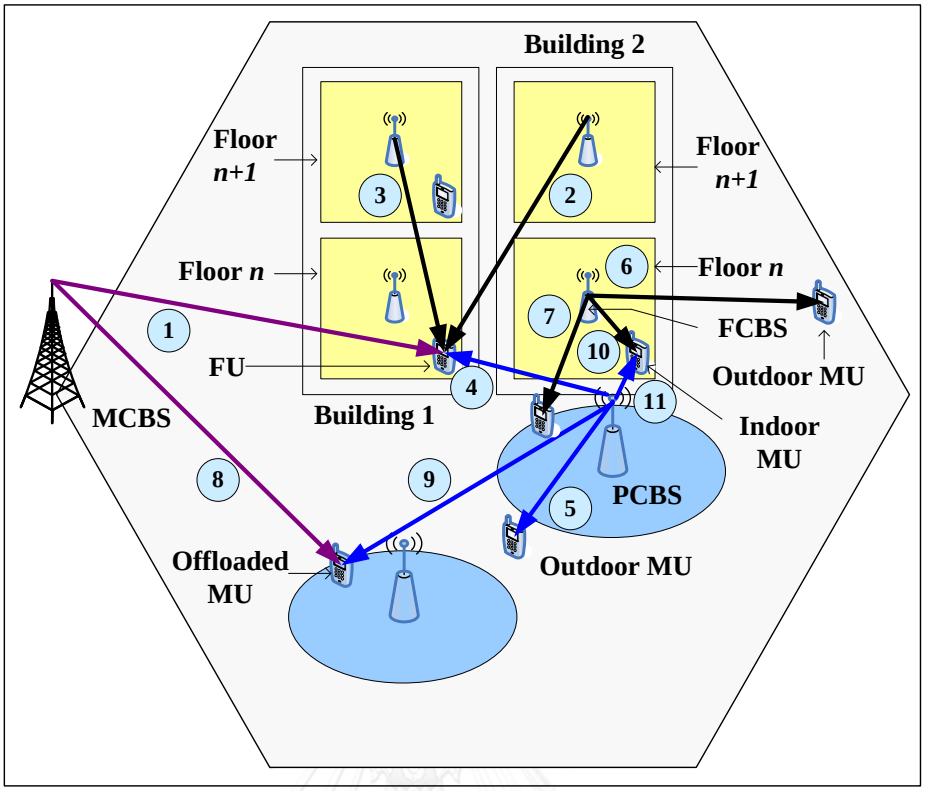

Figure 3.2: Sources of co-channel interference for the system shown in Figure 3.1(b) when all BSs operate at the same RB i in the same TTI t. A number in circle represents the corresponding source of interference.

From a FCBS to a MU for the UE located in MC, $I_{t,i}^{oMUFC}$

From a FCBS to a MU for the UE located in a PC, $I_{t,i}^{ofMUFC}$

From the MCBS to a MU for the UE located in a PC, $I_{t,i}^{ofMUMC}$

From a PCBS to a MU for the UE located in different PC, $I_{t,i}^{ofMUPC}$

From a FCBS to a MU for the BS and UE located in the same FCL, $I_{t,i}^{iMUFC}$

From a PCBS to a MU for the UE located in any FCLs, $I_{t,i}^{iMUPC}$

Hence with no interference management, when all BSs of multiple tiers operate at the same RB *i* in the same TTI *t*, an aggregate link level interference experienced by any UEs, of a total of four UE categories denoted as ζ, such that $\zeta = \{1, 2, ..., \zeta_{\max}\}$ where $\zeta_{\max} = 4$, can be expressed as follows:

For a FU, $I_{t,i}^{FU} = I_{t,i}^{FUMC} + I_{t,i}^{FUsFC} + I_{t,i}^{FUdFC} + I_{t,i}^{FUPC} = I_{t,i}^{UC_1}$

For an outdoor MU, $I_{t,i}^{oMU} = I_{t,i}^{oMUFC} + I_{t,i}^{oMUPC} = I_{t,i}^{UC_2}$

For an offloaded MU, $I_{t,i}^{ofMU} = I_{t,i}^{ofMUMC} + I_{t,i}^{ofMUPC} + I_{t,i}^{ofMUFC} = I_{t,i}^{UC_3}$

For an indoor MU, $I_{t,i}^{iMU} = I_{t,i}^{iMUPC} + I_{t,i}^{iMUFC} = I_{t,i}^{UC_4}$

Hence, the link level aggregate interference at RB i in TTI t, $I_{t,i}$ can be expressed as follows:

$$I_{t,i} = 1_{UC}\left(I_{t,i}^{UC_\zeta}\right) I_{t,i}^{UC_\zeta} \tag{3.1}$$

where $UC = \left\{ I_{t,i}^{UC_1}, ..., I_{t,i}^{UC_{\zeta_{\max}}} \right\}$. $1(\cdot)$ defines that $1(\cdot) = 1$ if $I_{t,i}^{UC_\zeta}$ exists in the set UC for any ζ, otherwise $1(\cdot) = 0$. The interference sources 2, 3, and 9 occur at the co-tier level, whereas others occur at the cross-tier level. In the following, we first analyze the co-channel interference effect from sources 1 and 2.

Proposition 3.1: *The co-tier co-channel interference from a neighboring FCL (Figure 3.3) and the cross-tier co-channel interference from the MCBS at a FU located in any FCLs are negligible.*

Proof 3.1: We assume that all FCBSs in all FCLs have the same transmission power. For simplicity, we assume that all channels experience the same fading effect such that the fading effect of the serving link cancels out that of the interfering link when their signal power difference at a FU is considered. Hence, no fading effects are considered in the following analysis. Further, since we use the 3GPP recommended simplified path loss model for indoor FCs and consider mostly Radio Access Networks - Group 4 assumptions (Table B.5 and Table B.7 in Appendix B), the small-scale fading effect modeling is not a necessity in general, and is not needed for simplistic interference scenarios and modeling [88].

Following [37], the path loss for a signal from a co-channel interfering FCBS of a neighboring FCL on a serving FU of the serving FCL is given by

$$\begin{aligned} \mathrm{PL}_{\mathrm{int}}^{FCBS} &= \mathrm{PL}_{ind} + \mathrm{PL}_{out} + \mathrm{L}_{\mathrm{tow}} \\ &= \left[127 + 30\log_{10}\left(R_{ind}/1000\right)\right] + \left[15.3 + 37.6\log_{10} R_{out}\right] + 2\,\mathrm{L}_{\mathrm{ow}} \end{aligned} \quad (3.2)$$

where $\mathrm{PL}_{ind} = 127 + 30\log_{10}\left(R_{ind}/1000\right)$ [37] is the path loss for an interfering signal for an indoor distance R_{ind}; $\mathrm{PL}_{out} = 15.3 + 37.6\log_{10} R_{out}$ [37] is the path loss for an outdoor distance $R_{out} \geq 20\,\mathrm{m}$ between two neighboring FCLs (see Figure 3.3); $\mathrm{L}_{\mathrm{tow}} = 2\,\mathrm{L}_{\mathrm{ow}}$ is the total external wall penetration loss for an interfering signal; and L_{ow} is an external wall penetration loss.

For a serving FU at a distance $R = R_{ref}$ from a sFCBS, the path loss is given by [37]

$$\mathrm{PL}_{ser}^{FCBS} = 127 + 30\log_{10}\left(R_{ref}/1000\right) \quad (3.3)$$

Since signals from the sFCBS and interfering FCBS travel approximately the same distance in their respective indoor coverage to reach a serving FU, assuming $R_{ref} = R_{ind}$, the difference in path losses experienced by the serving and interfering signals is given by

$$\mathrm{PL}_{dif}^{FCBS} = \mathrm{PL}_{\mathrm{int}}^{FCBS} - \mathrm{PL}_{ser}^{FCBS} = \left[15.3 + 37.6\log_{10} R_{out}\right] + 2\mathrm{L}_{\mathrm{ow}}$$

For $\mathrm{L}_{\mathrm{ow}} = 20\,\mathrm{dB}$ [37] and $R_{out} = 20\,\mathrm{m}$, $\mathrm{PL}_{dif}^{FCBS} = 104.21\,\mathrm{dB}$, i.e. the interfering signal strength is 104.21 dB less than that of the desired signal. Hence, the co-tier co-channel interfering signal is $10^{-10.421}$ times the desired signal and is negligible compared to the desired signal at FU.

Following the same procedure, the cross-tier co-channel interference power (in dBm) from the MCBS at a FU in any FCLs can be expressed as

$$\begin{aligned} P_{int}^{MCBS} &= P_{t}^{MCBS} - \mathrm{PL}_{int}^{MCBS} \\ &= 46 - \left(15.3 + 37.6\log_{10} R_{out}^{MCBS} + \mathrm{L}_{\mathrm{ow}}\right) \end{aligned}$$

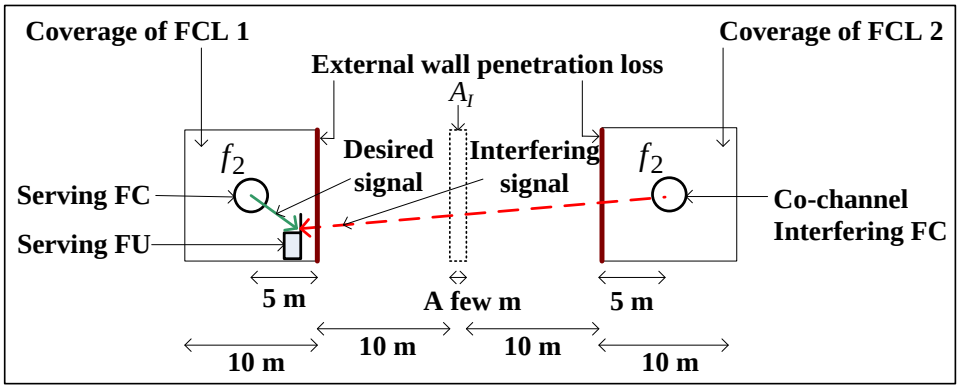

Figure 3.3: Signal propagation between FCs of two neighboring FCLs.

$$= 30.7 - 37.6 \log_{10} R_{out}^{MCBS} - \mathrm{L_{ow}} \tag{3.4}$$

where R_{out}^{MCBS} is the distance between the MCBS and a FU. $\mathrm{PL}_{\mathrm{int}}^{MCBS} = 15.3 + 37.6 \log_{10} R_{out}^{MCBS} + \mathrm{L_{ow}}$ is the path loss for an interfering signal from the MCBS, and $P_t^{MCBS} = 46$ dBm [37] is the transmission power of the MCBS.

If a serving FU is at a distance $R = R_{ref}$ from a sFCBS with a transmission power of 20 dBm, the desired signal power at the serving FU is given by

$$P_{ser}^{FCBS} = -\left(107 + 30 \log_{10}\left(R_{ref}/1000\right)\right) \tag{3.5}$$

In the worst case scenario, i.e. $R = R_{ref} = 5\sqrt{2}$ m and $R_{out}^{MCBS} = 85$ m (where 75 m is the minimum separation distance between a MCBS and a SC, and 10 m is the free space around the building for a FCL [37]), and for $\mathrm{L_{ow}} = 20$dB , the difference in power of received signals at the serving FU is given by $P_{dif} = P_{\mathrm{int}}^{MCBS} - P_{ser}^{FCBS} = -19.36$ dBm = $0.0115 \cong 10^{-2}$, i.e. the interfering signal strength is 100 times less than that of the desired signal, and can be considered negligible as compared to the desired signal.

As the distance of a FCL from the MCBS increases, the cross-tier co-channel interference power from the MCBS at a FU decreases and approaches to zero at the MC boundary. Hence, we can safely assume that the co-tier co-channel interference effect from any neighboring FCLs and the cross-tier co-channel interference effect from the MCBS at a FU in any FCLs are negligible even when we reuse the same frequency in each neighboring FCL. ■

In a similar manner, following the Proof 3.1 of Proposition 3.1, because of high external wall penetration loss and low SCBS transmit power, it can be shown that the cross-tier interference effects that exist between any other categories of indoor UEs and outdoor SCBSs and vice versa, i.e. the co-channel interference effect from sources 4, 6, and 7, are negligible. We address co-channel interferences from sources 3, 5, 8, 9, 10, and 11 through managing these co-channel interferences by avoiding the allocation of resources to UEs both in frequency and time simultaneously. More specifically, interferences from sources 3, 5, 8, 9, and 11 are managed by employing FD eICIC, whereas sources 10 and 11 (for ORPA scheme described below) by employing TD eICIC. All indoor MUs, offloaded MUs, and outdoor MUs in the MC coverage are allocated to RBs orthogonally. The system bandwidth of the MCBS is reused in each FCL, and RB allocations to all FUs in a FCL is considered orthogonal. If a MU is within a building, i.e. FCL, the TD ABS based eICIC is applied to FCs of that FCL to avoid co-channel interference between indoor MUs and FUs. Figures 3.4(a) and 3.4(b) show

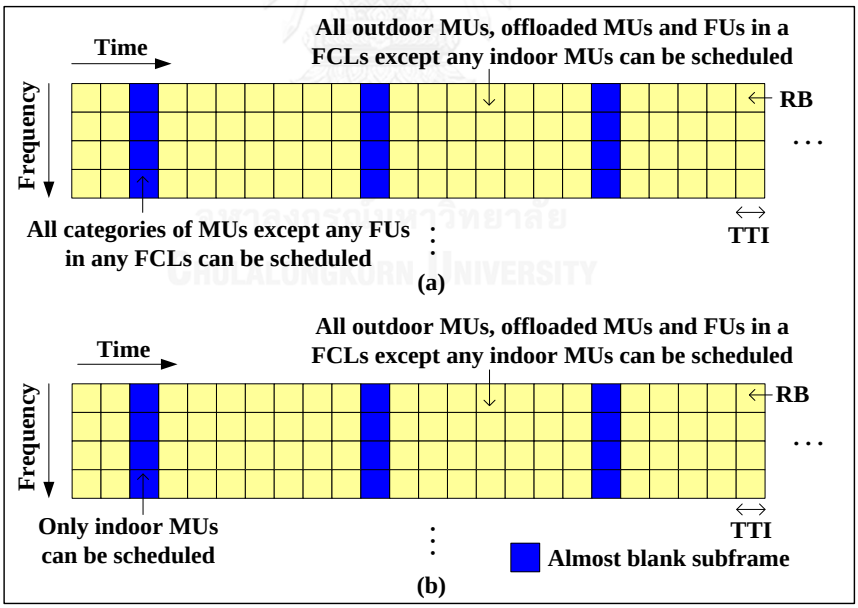

Figure 3.4: ABS based TD eICIC (a) CRPA, (b) ORPA.

respectively the application of ABS in CRPA and OPRA schemes. In ORPA, ABSs are kept reserved for scheduling only indoor MUs in FCLs. However in CRPA, all outdoor

MUs are allowed to transmit data during ABSs. In both CRPA and ORPA, FUs are scheduled only during non-ABSs.

Remark 3.1: The existence of a MU whether or not within any buildings can be determined by measuring the DL path loss of the MU at the MCBS, which is typically used for mobility management. This is because of the fact that once a MU enters a building, there is a sudden rise in path loss of the MU or equivalently a sudden fall in received signal strength at the MU within a short distance because of experiencing an additional external wall penetration loss of the building, typically about 20 dB. When a MU is found within a building, the MU is scheduled only during ABSs irrespective of whether or not the MU is within the coverage of any FCBSs in the building. This is because the proposed CRPA and ORPA are developed based on the existence of any MUs within any buildings, not within the coverage of any FCBSs in any buildings. Hence, whether or not an indoor MU is within or out of coverage of any FCBSs in any buildings does not have any effects on the proposed interference management schemes, CRPA and ORPA.

Therefore, using the Proof 3.1 of Proposition 3.1 and aforementioned interference management approach for the considered system architecture in Figure 3.1, all possible sources of interference both inter-cluster and intra-cluster levels are shown either negligible or managed, and hence we propose to consider all FCs within a multi-floor building as shown in Figure 3.1(c) as a cluster of FCs to reuse resources in them using eICIC techniques. Hence, the number of clusters of FCs is equal to the number of buildings in the coverage of the MC.

Remark 3.2: The proposed FC clustering approach is mainly based on the fact that it can take advantages of the high external wall penetration loss of 3D multi-floor buildings and the free space distance between adjacent buildings to address co-channel interferences from the MCBS and FCBSs of adjacent buildings, and hence it is not transportable to model 2D planar deployment of FCBSs. Further, the proposed FC clustering approach can address the 3D signal propagation issues in multi-floor buildings such as penetration losses from any floors and internal walls within any

floors, diffraction effect alongside a building, and reflection effect within a building by considering an orthogonal allocation of RBs to FCBSs using FD eICIC technique. In general, it may however not be the case when considering a non-orthogonal RB resource allocation to FCBSs within a 3D multi-floor building and may necessitate special attention, which is beyond the scope of this chapter and is addressed in the following chapter. Nevertheless, our aim in this chapter is to propose a simple yet reasonable approach using eICIC techniques for clustering FCs, which are deployed indoor within only 3D multi-floor buildings in a MC coverage so that additional computational complexities from the typical FC clustering approaches proposed in existing literature such as [21] can be avoided.

3.2.2 Problem formulation

A. Multi-tier network model

Denote P_M, P_P, and P_F as the transmission powers of a MC, a PC, and a FC respectively. Consider that there are M RBs in system bandwidth B_{sys}, and N MUs in the system. Let S_P denote the number of PCs in the MC coverage. Consider that the number of offloaded MUs is uniformly distributed in the interval [1, U_{OFL}]. Let U_P^q denote the number of MUs offloaded by a PC S_P^q such that $\forall q U_P^q \in \left[0,\ U_{P,\max}^q\right]$ where $\{U_{P,\max}^q = N^+ : U_{OFL} = \sum_{q=1}^{S_P} U_P^q \le N^+\}$. If all PCs have an equal number of offloaded MUs U_P, i.e. $\forall q U_P^q = U_P$ then the total number of offloaded MUs, $U_{OFL} = S_P \times U_P$. However, in general, U_P^q is a random variable which varies from one PC to another, and the realization of U_P^q for a PC is mutually independent from the others. If μ_{iM} denotes the ratio of the number of indoor MUs, then the total number of indoor MUs is $U_{MI} = \mu_{iM} \times N$, outdoor MUs is $U_{MO} = N\text{-}U_{OFL}\text{-}U_{MI}$, and MUs served by the MC is $U_M = U_{MO}+U_{MI}$.

Let $\boldsymbol{N_M}$ denote the set of indices of all MUs such that $\boldsymbol{N_M} = \{1, 2, 3, \ldots, N\}$. Denote $\boldsymbol{N_{MO}}$, $\boldsymbol{N_P}$, and $\boldsymbol{N_{MI}}$ respectively the set of indices of all outdoor MUs, offloaded

MUs, and indoor MUs. Note that $\boldsymbol{N_M}$ is partitioned randomly into three disjoint subsets $\boldsymbol{N_{MO}}$, $\boldsymbol{N_P}$, and $\boldsymbol{N_{MI}}$. Let $\boldsymbol{F_{CL}}$ = {1, 2, 3, …, L} denote the set of FCLs, L denote the maximum number of FCLs in a MC coverage, and S_F denote the number of active FCs in each FCL. Assuming that S_F is the same for all FCLs, the total number of active FCs in the system is $S_{FS} = L \times S_F$. Consider that the numbers of FUs in FCLs are independent and uniformly distributed in the interval [1, U_F]. In general, U_F is a random variable which varies from one FCL to another, and the realization of U_F for a FCL is mutually independent from the others where a realization is defined as a simulation run time.

Let U_F^w denote the number of FUs served by a FC S_F^w in a FCL such that $\forall w U_F^w \in \left[0,\ U_{F,\max}^w\right]$ where $\{U_{F,\max}^w = N^+ : U_F = \sum_{w=1}^{S_F} U_F^w \le N^+\}$. If all FCs have an equal number of FUs U_{FC}, i.e. $\forall w U_F^w = U_{FC}$, then the total number of FUs in any FCLs, U_F = $S_F \times U_{FC}$. However, in general, U_F^w is a random variable which varies from one FCBS to another, and the realization of U_F^w for a FCBS is mutually independent from the others. If each FC in a FCL serves one UE, i.e. $U_{FC} = 1$, the total number of FUs in a FCL is $U_F = S_F$, and in the system is $U_{FS} = L \times U_F$. Let $\boldsymbol{N_F}$ denote the set of all FU indices in a FCL such that $\boldsymbol{N_F}$ = {1, 2, 3, …, U_F}.

The realization of MUs served by the MC and PCs are not mutually independent since MUs served by PCs are MUs offloaded from the MCBS, and the schedulers have a complete knowledge when a MU is offloaded. However, an offloaded MU to any PCs is equally likely in a realization. FCLs and PCs are located randomly and uniformly in the MC area. The indoor MUs are distributed randomly and non-uniformly within FCLs such that $\sum_{l=1}^{L} u_{MI}^l = U_{MI}$ where $\{u_{MI}^1, u_{MI}^2, \ldots, u_{MI}^L\}$ denotes the set of numbers of indoor MUs in $\boldsymbol{F_{CL}}$. All outdoor MUs, offloaded MUs, and FUs are distributed randomly and uniformly within their respective BSs' coverage area. Let $\boldsymbol{T}$ denote simulation run time with the maximum time of Q (in time step each lasting 1 ms) such that $\boldsymbol{T}$ = {1, 2, 3, …, Q}. Let $\boldsymbol{T_{ABS}}$ denote the number of ABSs in every ABS pattern period of T_{APP} subframes, such that $\boldsymbol{T_{ABS}} \subseteq \boldsymbol{T}$ and $\boldsymbol{T_{ABS}}$ = {t: $t = v.T_{APP} + n_A$; v = 0, 1, 2, …, Q/T_{APP}; n_A = 1, …, T_{ABS}} where T_{ABS} = 1, 2, …, T_{APP} corresponds to ABS patterns

φ = $1/T_{APP}$, $2/T_{APP}$, ..., T_{APP}/T_{APP} respectively. Let t_{ABS} and $t_{non-ABS}$ denote respectively an ABS and a non-ABS such that $t_{ABS} \in \boldsymbol{T_{ABS}}$ and $t_{non-ABS} \in \boldsymbol{T \backslash T_{ABS}}$.

B. Estimation of system capacity

Let d_{MU}, d_{PC}, and d_{FCL} denote respectively the distances of any MU, PC, and FCL from the MCBS, and d_{FC} denote the distance between a FCBS and a FU. The distances of all UEs of each category in a realization are generated following the respective distribution functions as mentioned earlier. The path loss is calculated using path loss formulas given in Table B.5 in Appendix B). Consider a FCL in which *M* RBs are reused. Since during an ABS, no FC can transmit data signal, following (C.5) in Appendix C, the aggregate capacity of all FCLs for an arbitrary ABS pattern φ can be expressed as

$$\begin{aligned}\sigma_{FC}(\rho_{FC}) &= \sum_{t=1}^{Q}\sum_{i=1}^{M}(1-\varphi)\,\frac{S_{FS}}{S_F}\,\sigma_{t,i}(\rho_{t,i}) \\ &= (1-\varphi)\frac{S_{FS}}{S_F}\sum_{t=1}^{Q}\sum_{i=1}^{M}\sigma_{t,i}(\rho_{t,i}) \\ &= K\frac{S_{FS}}{S_F} \qquad (3.6)\end{aligned}$$

where $K = (1-\varphi)\sum_{t=1}^{Q}\sum_{i=1}^{M}\sigma_{t,i}(\rho_{t,i})$, and $\sigma_{t,i}(\rho_{t,i})$ denotes the throughput response of all FUs in $t \in \boldsymbol{T \backslash T_{ABS}}$ over *M* RBs.

Assume that all link characteristics between FUs and FCBSs in any FCLs are the same such that for a given φ, *K* which is the slope of (3.6) is a constant, and the steepness of *K* varies only with φ, i.e. a higher value of φ results in a smaller variation in capacity. Also the capacity of FCLs increases linearly with S_{FS}.

Remark 3.3: Since the same RB resources are reused in FCs of each FCL orthogonally, an RB in any FCLs is reused only once. This implies that the aggregate throughput per

FCL varies linearly with the number of reused RBs. Since the same number of RBs is reused in each FCL in any non-ABSs, the aggregate throughput supported by all FCLs varies also linearly with the FCL density, i.e. S_{FS}.

Assuming the same channel characteristic of all links between FUs and FCBSs in all FCLs, (3.6) can be rewritten as

$$\sigma_{FC}(\rho_{FC}) = K'(1-\varphi)\frac{S_{FS}}{S_F}$$

$$= K'\left(1-\frac{T_{ABS}}{T}\right)\frac{S_{FS}}{S_F} \tag{3.7}$$

where $K' = K/(1-\varphi) = \sum_{t=1}^{Q}\sum_{i=1}^{M}\sigma_{t,i}(\rho_{t,i})$.

Equation (3.7) implies that the capacity $\sigma_{FC}(\rho_{FC})$ varies linearly with φ and follows the response of a straight line equation that passes through the origin which steepness is mainly defined by the ABS pattern. Further, the capacity increases linearly with an increase in the number of FCLs, whereas decreases with an increase in the number of ABSs. However, the throughput per FU in a FCL decreases with an increase in the FCL size, i.e. $|S_F|$. Hence for a given ABS pattern, higher density of FCLs results in more achievable capacity per MC coverage.

The total system capacity over the whole system bandwidth for Q TTIs can be expressed as the sum throughput of all UEs as follows

$$\sigma(\rho) = \sum_{t=1}^{Q}\sum_{i=1}^{M}\sigma_{t,i}(\rho_{t,i}) \tag{3.8}$$

where for CRPA, σ and ρ are responses of all MUs in $t \in \boldsymbol{T_{ABS}}$ as well as outdoor MUs, offloaded MUs, and all FUs in $t \in \boldsymbol{T \backslash T_{ABS}}$, whereas for ORPA, σ and ρ are responses of only indoor MUs in $t \in \boldsymbol{T_{ABS}}$ and outdoor MUs, offloaded MUs, and all FUs in $t \in \boldsymbol{T \backslash T_{ABS}}$.

C. Utilization factor of reusable resources

The TD eICIC avoids interference at the cost of reusable resources since during an ABS, no FC can transmit because of reusing the same system bandwidth of MC in each FCL. The percentage wastage of reusable time resources T_w over an ABS pattern period T for L FCLs (i.e., resource reuse factor) can be expressed as

$$\%T_w = \varphi L \times 100 \tag{3.9}$$

Similarly, the percentage reusable time resource utilization factor over T for the resource reuse factor L can be expressed as follows

$$\% U_T = (1-\varphi) L \times 100 \tag{3.10}$$

As an example, for $\varphi = 0.25$ and $L = 10$, the corresponding $\% U_T = (1-0.25) \times 100 = 75$. Hence, the utilization of reusable resources is affected by the ABS pattern and resource reuse factor.

Remark 3.4: From (3.10), it can be found that with a decrease in φ, there is a corresponding increase in U_T, and so is the overall system capacity. However, this causes the throughput of indoor MUs to decrease accordingly. So, there should be a trade-off between the values of U_T and the overall throughput of indoor MUs.

D. Proportional fair scheduling

The proportional fair scheduling algorithm is described in Appendix C.

3.2.3 Proposed frequency reuse and scheduling algorithm

The proposed FRSA for an arbitrary number of ABSs is given in Algorithm 3.1. The algorithm works as follows. Given N, S_P, U_P, and μ_{iM} as inputs, N is first disjointed into three groups to estimate U_{OFL}, U_{MI}, and U_{MO} randomly. Following the co-channel

Algorithm 3.1: Frequency reuse and scheduling algorithm.

01: **Inputs**:

(i) Set: B_{sys}, P_M, P_P, P_F, μ_{iM}, S_P, S_F, N, U_P, U_F, M, Q, L, φ, t_c, β, G_t, G_r, L_F

(ii) Initialize: $t \in \{\boldsymbol{T_{ABS}}, \boldsymbol{T \backslash T_{ABS}}\} = \{1, \ldots, Q\}, \{u_{MI}^1, u_{MI}^2, \ldots, u_{MI}^L\}$,
$\forall t,i : \{P_{t,i}, N_{t,i}, NF_{t,i}\}$, $\boldsymbol{N_M}$, $\boldsymbol{N_{MO}}$, $\boldsymbol{N_P}$, $\boldsymbol{N_{MI}}$, $\boldsymbol{N_F}$, d_{FCL}, d_{PC},
d_{MU}, $\sigma_{hetnet}^{MCBS} \leftarrow 0$, $\sigma_{hetnet}^{FCBS} \leftarrow 0$, $V \in \{\text{CRPA, ORPA}\}$

(iii) Select: U_{OFL}, U_{MI}, U_{MO}

(iv) Estimate: $\forall t,i : \{\text{PL}_{t,i}, \text{LS}_{t,i}, \text{SS}_{t,i}, \rho_{t,i}, \sigma_{t,i}(\rho_{t,i})\}$

02: **for** t = 1 to Q
03: | **if** $t = t_{ABS}$
04: | | **if** V = CRPA
05: | | | $N := U_{MO} + U_{MI} + U_{OFL}$
06: | | **elseif** V = ORPA
07: | | | $N := U_{MI}$
08: | | **end if**
09: | | $U_{FS} := 0$; $U_S := N$
10: | **elseif** $t = t_{non-ABS}$
11: | | $U_{MI} := 0$; $N := U_{MO} + U_{OFL}$; $U_{FS} := L \times U_F$; $U_S := N + U_{FS}$
12: | **end if**
13: | **for** i = 1 to M
14: | | Estimate throughput of scheduled MU $\forall t,i,x \; \sigma_{t,i,x}(\rho_{t,i,x})$
15: | | Update throughput of MUs $\forall N \; \sigma_{hetnet}^{MCBS} \leftarrow \sigma_{t,i,x}(\rho_{t,i,x}) + \sigma_{hetnet}^{MCBS}$
16: | **end for**
17: | **for** l = 1 to L
18: | | **for** i = 1 to M
19: | | | Estimate throughput of scheduled FU $\forall t,i,x,l \; \sigma_{t,i,x,l}(\rho_{t,i,x,l})$
20: | | | Update throughput of FCLs $\forall U_F \; \sigma_{hetnet}^{FCBS} \leftarrow \sigma_{t,i,x,l}(\rho_{t,i,x,l}) + \sigma_{hetnet}^{FCBS}$
21: | | **end for**
22: | **end for**
23: | Update system level throughput $\forall U_s \; \sigma_{hetnet}^{BS} \leftarrow \sigma_{hetnet}^{MCBS} + \sigma_{hetnet}^{FCBS}$
24: **end for**
25: Estimate system level throughput (Mbps) $\sigma_{hetnet}^{sys} = (\sigma_{hetnet}^{BS} \times 180 \times 10^3) / 10^6$
26: **Outputs**: σ_{hetnet}^{sys}

interference avoidance scheme, U_{OFL}, U_{MI}, and U_{MO} are then scheduled by the FD proportional fair scheduler for MUs, and a FD proportional fair scheduler for each FCL to schedule FUs of the respective FCL in both CRPA and ORPA schemes. The same process repeats for all M RBs in each TTI and continues for all TTIs of the simulation run time. The aggregate throughput is then estimated and summed over all RBs for all TTIs for MUs as well as FUs of all FCLs over all reused M RBs for all non-ABSs. The overall system level throughputs for CRPA and ORPA schemes are then estimated by adding the aggregate throughput of MUs of the respective scheme to the aggregate throughput of all FUs in all FCLs. The shadow fading and small-scale fading of all UEs are estimated and updated in each TTI per realization for disjoint scheduler implementation of FRSA, which we will discuss in detail in a later section. We do not show explicitly the calculation of SINR and throughput in the algorithm, instead which we have explained in the problem formulation.

3.3 OPNA estimation model, scheme, algorithm and implementation

We consider the aggregate throughputs of all outdoor MUs and indoor MUs to propose a model for estimating an OPNA of TD eICIC technique which necessitates first to proof the following proposition.

Proposition 3.2: *The aggregate throughput response of each category of MUs, i.e. outdoor MUs, offloaded MUs, and indoor MUs, is a linear function of T_{ABS} and can be modeled as a straight-line equation when operating under ORPA scheme.*

Proof 3.2: Let $\sigma_{FU}(\rho_{FU}), \sigma_{oM}(\rho_{oM})$, and $\sigma_{oF}(\rho_{oF})$ denote respectively the throughput responses of all FUs, outdoor MUs, and offloaded MUs in $t \in \boldsymbol{T} \backslash \boldsymbol{T_{ABS}}$, and $\sigma_{iM}(\rho_{iM})$ denote the throughput of all indoor MUs in $t \in \boldsymbol{T_{ABS}}$. For the ORPA scheme and any arbitrary values of φ, following (3.6), we can express the followings

$$\sigma_{oF}(\rho_{oF}) = (1-\varphi)\sum_{t=1}^{Q}\sum_{i=1}^{M}\sigma_{t,i}(\rho_{t,i}) \tag{3.11}$$

$$\sigma_{oM}(\rho_{oM}) = (1-\varphi)\sum_{t=1}^{Q}\sum_{i=1}^{M}\sigma_{t,i}(\rho_{t,i}) \tag{3.12}$$

$$\sigma_{iM}(\rho_{iM}) = \varphi\sum_{t=1}^{Q}\sum_{i=1}^{M}\sigma_{t,i}(\rho_{t,i}) \tag{3.13}$$

such that using (3.7) and (3.8), the following holds

$$\sigma(\rho) = \sigma_{FU}(\rho_{FU}) + \sigma_{oM}(\rho_{oM}) + \sigma_{oF}(\rho_{oF}) + \sigma_{iM}(\rho_{iM}) \tag{3.14}$$

Equations (3.11)-(3.13) imply that the aggregate throughput of each UE category is a linear function of φ, i.e. T_{ABS}. Hence, their responses can be modeled as straight-line equations. This proof can also be found justified with the simulation results in the following sections. ■

3.3.1 Proposed model for an OPNA estimation

Let $\sigma_{iM}(T_{ABS})$ and $\sigma_{oM}(T_{ABS})$ denote respectively the aggregate throughput responses of all indoor MUs and outdoor MUs as functions of T_{ABS}. From (3.12) and (3.13), when $\varphi = 0$ (i.e., the minimum value), the value of $\sigma_{iM}(T_{ABS})$ is the minimum (i.e., zero), whereas the value of $\sigma_{oM}(T_{ABS})$ is the maximum. However, these values are flipped, when $\varphi = 1$ (i.e., the maximum value). Hence, $\sigma_{oM}(T_{ABS})$ and $\sigma_{iM}(T_{ABS})$ can be modeled mathematically as follows

$$\sigma_{oM}(T_{ABS}) = -m_o T_{ABS} + C_o^{\max} \tag{3.15}$$

$$\sigma_{iM}(T_{ABS}) = m_i T_{ABS} \tag{3.16}$$

where m_o and m_i are the slopes of the respective equations, and $C_o^{\max}$ is the maximum aggregate throughput of outdoor MUs at $T_{ABS} = 0$.

In Figure 3.5, the aggregate throughput responses of all outdoor MUs and indoor MUs of the proposed model under the ORPA scheme given by (3.15)-(3.16) are illustrated for estimating an OPNA. Since offloaded MUs experience relatively a higher

throughput than other categories of MUs, we consider to find out a value of T_{ABS} such that the aggregate throughputs of all outdoor MUs and indoor MUs are equal or at least close to the point of equality to allow experiencing a uniform throughput by both categories of MUs and a seamless transition of a MU between indoor and outdoor environments. Since an increase in T_{ABS} results in an increase in aggregate throughputs

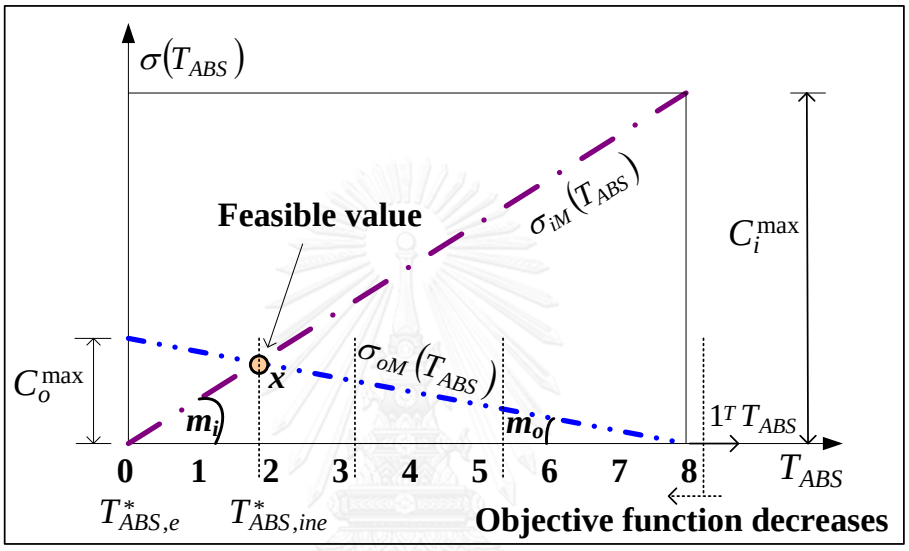

Figure 3.5: Aggregate throughput responses of all indoor MUs and outdoor MUs for ORPA scheme.

of indoor MUs and a decrease in aggregate throughputs of outdoor MUs, these throughput responses must intersect at a certain point. The value of T_{ABS} at which they intersect is the value of an OPNA (T^*_{ABS}) which can be any positive real numbers on T_{ABS} axis such that $0 \le T_{ABS} \le 8$. However, in practice T_{ABS} is strictly a positive integer such that $T_{ABS} \in Z^+ : 0 \le Z^+ \le 8$. Hence, T^*_{ABS} is rounded to the nearest maximum integer value of T_{ABS} to give a favor to indoor MUs so that $T^*_{ABS} = \lceil T_{ABS} \rceil$.

3.3.2 OPNA schemes

We estimate an OPNA in two schemes, namely non-adaptive and adaptive OPNAs, and describe in the following. For both schemes, we consider an aggregate

throughput of all indoor MUs to give a favor to FUs to increase the overall system level throughput because of poorer channel conditions of indoor MUs than FUs. Further, it reduces computational complexity of the OPNA optimizer since the optimizer needs only to compute an aggregate throughput. However, this does not affect the performance of indoor MUs since the number of indoor MUs per FCL is typically far less than that of FUs.

A. Non-adaptive OPNA

In this scheme, we assume that there exists at least one indoor MU per FCL such that the condition $\sigma_{iM}(T_{ABS}) > 0$ strictly holds, and an OPNA is the same for all FCLs in every ABS pattern period. Since minimizing the aggregate throughput of outdoor MUs and maximizing the aggregate throughput of indoor MUs should result in the same solution of an OPNA for an equal aggregate throughput of both indoor MUs and outdoor MUs (Figure 3.5), the optimization problem can be expressed in terms of outdoor MUs for objective function as follows

$$\begin{aligned} &\text{minimize} && \sigma_{oM}(T_{ABS}) \\ &\text{subject to} && \sigma_{iM}(T_{ABS}) - \sigma_{oM}(T_{ABS}) = 0 \end{aligned}$$

The above optimization problem can be solved as

$$\sigma_{iM}(T_{ABS}) - \sigma_{oM}(T_{ABS}) = 0$$

$$m_i T_{ABS} - \left(-m_o T_{ABS} + C_o^{\max}\right) = 0$$

$$T_{ABS}^{*} = C_o^{\max} / (m_o + m_i) \tag{3.17}$$

But $m_o = C_o^{\max}/T$ and $m_i = C_i^{\max}/T$ where $C_i^{\max}$ denotes the maximum aggregate throughput of indoor MUs at $T_{ABS} = 8$. Hence, an OPNA can be deduced as

$$\begin{aligned} T_{ABS,ine}^{*} = T_{ABS}^{*} &= C_o^{\max} / \left(C_o^{\max}/T + C_i^{\max}/T\right) \\ &= \left(C_o^{\max} / \left(C_o^{\max} + C_i^{\max}\right)\right) T \end{aligned} \tag{3.18}$$

The major advantage of this scheme is its simplicity in update mechanism for an OPNA per FCL since the same OPNA is applied to all FCLs. Moreover, the information about the OPNA for all FCLs can be sent by a broadcast signal by the

MCBS in every ABS pattern period rather than sending per FCL basis to reduce control signaling overheads. Furthermore, it guarantees a minimal throughput of indoor MUs because of $\sigma_{iM}(T_{ABS}) > 0$.

Remark 3.5: The non-adaptive OPNA scheme does not guarantee the maximization of overall system level throughput because of applying the same OPNA to all FCLs irrespective of the presence of an indoor MU in each FCL.

B. Adaptive OPNA

The assumption of at least one indoor MU per FCL in non-adaptive OPNA scheme may not be always the case in reality for a non-homogeneous distribution of indoor MUs in FCLs since there is a high possibility that no indoor MUs may present within some FCLs for a number of ABS pattern periods. This bottleneck can be resolved by adapting the application of OPNAs to FCLs such that an OPNA for the next ABS pattern period for a FCL is applied by estimating the exact throughput of indoor MUs in the current ABS pattern period, which could be either zero in the absence of any indoor MUs or the obtained throughput of indoor MUs in a FCL. Hence, a FCL should be considered to be applied with an OPNA for the next ABS pattern period only if at least one indoor MU is present in it during the current ABS pattern period such that the optimization problem can be formulated as follows

$$\begin{aligned} &\text{minimize} && \sigma_{oM}(T_{ABS}) \\ &\text{subject to} && \sigma_{iM}(T_{ABS}) \geq 0 \end{aligned}$$

For $\sigma_{iM}(T_{ABS}) > 0$, the solution of this optimization problem is the same as in non-homogeneous scheme, and hence

$$T^*_{ABS,ine} = \left(C_o^{\max} / \left(C_o^{\max} + C_i^{\max}\right)\right) T \tag{3.19}$$

For $\sigma_{iM}(T_{ABS}) = 0$, there is no indoor MU in a FCL such that

$$T^*_{ABS,e} = \left(C_o^{\max} / \left(C_o^{\max} + C_i^{\max}\right)\right) T = 0 \tag{3.20}$$

3.3.3 OPNA optimization algorithm and implementation

The optimization algorithm for both adaptive and non-adaptive OPNA schemes is described in Algorithm 3.2. The algorithm can be implemented by two offline FD proportional fair schedulers of which one is responsible for all indoor MUs and the other is for all outdoor MUs to schedule indoor MUs and outdoor MUs for estimating $C_i^{\max}$ and $C_o^{\max}$ respectively. The operating principle of these schedulers is similar

Algorithm 3.2: OPNA optimization algorithm.

01: **Inputs**:
  (i) Initialize: $L, C_o^{\max}, C_i^{\max}, T_{ABS}, U_{MI}^l, U_{MI}, U_{MO}, T \leftarrow 8$
  (ii) Compute: $\forall U_{MO}\ C_o^{\max}, \forall U_{MI}\ C_i^{\max}$
02: **if** $\forall l\ U_{MI}^l > 0$
03: $\quad \forall l\ T_{ABS} = \lceil T_{ABS,ine}^* \rceil$
04: **elseif** $\forall l\ U_{MI}^l \geq 0$
05: $\quad$ **for** l = 1 to L
06: $\quad\quad$ **if** $U_{MI}^l > 0$
07: $\quad\quad\quad T_{ABS,l} = \lceil T_{ABS,ine}^* \rceil$
08: $\quad\quad$ **elseif** $U_{MI}^l = 0$
09: $\quad\quad\quad T_{ABS,l} = T_{ABS,e}^* \leftarrow 0$
10: $\quad\quad$ **end if**
11: $\quad$ **end for**
12: **end if**
13: **Outputs**: $T_{ABS}, T_{ABS,l}$

to that of online FD proportional fair schedulers for MUs at the MCBS except that their scheduling decisions are not used for the real-time data transmission per TTI. Rather, their functions are to estimate throughputs of all indoor MUs and outdoor MUs separately in each TTI based on the CSI reported by the online FD scheduler and sum these throughputs to the throughputs estimated in the previous TTIs over an ABS pattern period.

These aggregate throughputs of indoor MUs and outdoor MUs over an ABS pattern period are inputs to an OPNA optimizer to execute optimization Algorithm 3.2. The throughputs of indoor MUs and outdoor MUs are compared until the condition $\sigma_{iM}(T_{ABS}) \geq \sigma_{oM}(T_{ABS})$ is satisfied. After rounding, i.e. $\lceil T_{ABS} \rceil$, the value of TTI at which the condition satisfies is the value of an OPNA, i.e. T^*_{ABS}, which is supplied to the TD scheduler at the MCBS in order to apply to FCLs over the next ABS pattern period. Both offline schedulers then reset their respective aggregate throughputs over the current ABS pattern period to zero. The same process repeats in every ABS pattern period. The OPNA optimization algorithm as well as the adaptive scheme can be implemented alongside the TD scheduler at the MCBS, and the duration of ABS pattern period can be chosen depending on the delay characteristic of X2 backhauls between the MCBS and FCLs.

Remark 3.6: The value of an OPNA irrespective of the types of scheme is estimated based on the condition $\sigma_{iM}(T_{ABS}) \geq \sigma_{oM}(T_{ABS})$. However, an OPNA scheme whether or not adaptive is defined by how the estimated value of an OPNA, i.e. T^*_{ABS}, over an ABS pattern period is applied to FCLs.

3.4 Simulation parameters, assumptions and results

3.4.1 Simulation parameters and assumptions

The default simulation parameters used for the system level simulation are listed in Table B.5 and Table B.7 in Appendix B. Unless stated explicitly, the default value for any parameters is used from Table B.5 and Table B.7 in Appendix B. The typical FC models used for evaluating the performance of FCs are dual-stripe model with multiple floors and 5×5 grid-based model with single floor [88] recommended by the 3GPP. Each of these models assumes a number of square apartments on a floor and is actually the variation of the proposed square-grid based system model in Figure 3.1 for FC clustering. Hence, we use the simplified path loss model and assume the similar

mechanisms recommended for the dual-stripe model in the proposed FC clustering model.

We consider proportional fair schedulers rather than simple Round Robin schedulers to address multi-user diversity gain from a random and uniform FU distribution, i.e., a highly spread distance distribution between a FU and a sFCBS, such that the path loss varies significantly at FUs from one to another and non-LOS components exist at frequencies below 3 GHz. Also, eICIC is considered to address mainly the cross-tier interferences between indoor MUs and femto-tier. Further, rather than choosing sophisticated but computationally complex theoretical models such as ray tracing, we consider simple empirical models recommended for evaluation by the 3GPP for modeling indoor FCs. Because we consider FCs in all FCLs to experience the similar signal propagation characteristics, there would not be any significant deviation in the performance results from using empirical models that do not necessarily guarantee the transportability between environments.

3.4.2 Performance results

Figure 3.6 shows that the system capacity increases with the FCL density regardless of the ABS pattern. The impact is also the same for an increase or a decrease in the system bandwidth on the overall system capacity since the same frequency resources is reused in each FCL. However, as the number of ABSs increases, the system capacity decreases correspondingly with the highest value achieved for the ABS pattern of 1/8 and the lowest for 8/8 (Figure 3.7).

From Figure 3.8, it can be found that indoor MUs under the CRPA scheme get almost always deprived of scheduling RB resources irrespective of the number of ABSs in comparison with offloaded MUs because of better channel conditions provided by PCs. This is because of why the ORPA is proposed as a special case of CRPA where indoor MUs are given with the sole priority for scheduling RB resources during ABSs such that the capacity of indoor MUs can be improved with an increase in the number of ABSs as shown in Figure 3.9. This does not however impact considerably on the overall capacity performance from employing ORPA in comparison with CRPA as

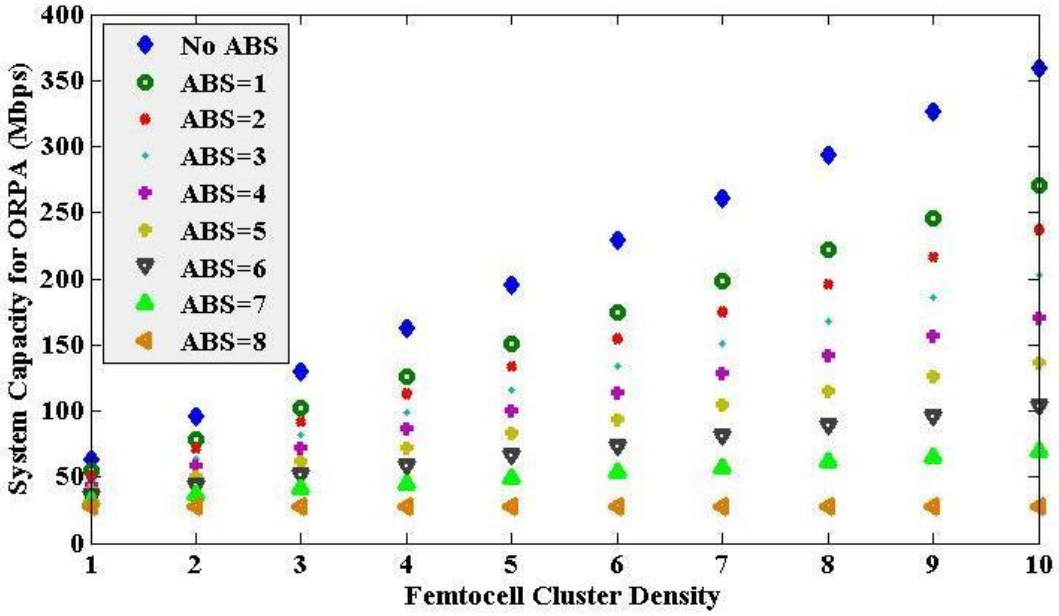

Figure 3.6: System capacity versus FCL density for ORPA HetNets.

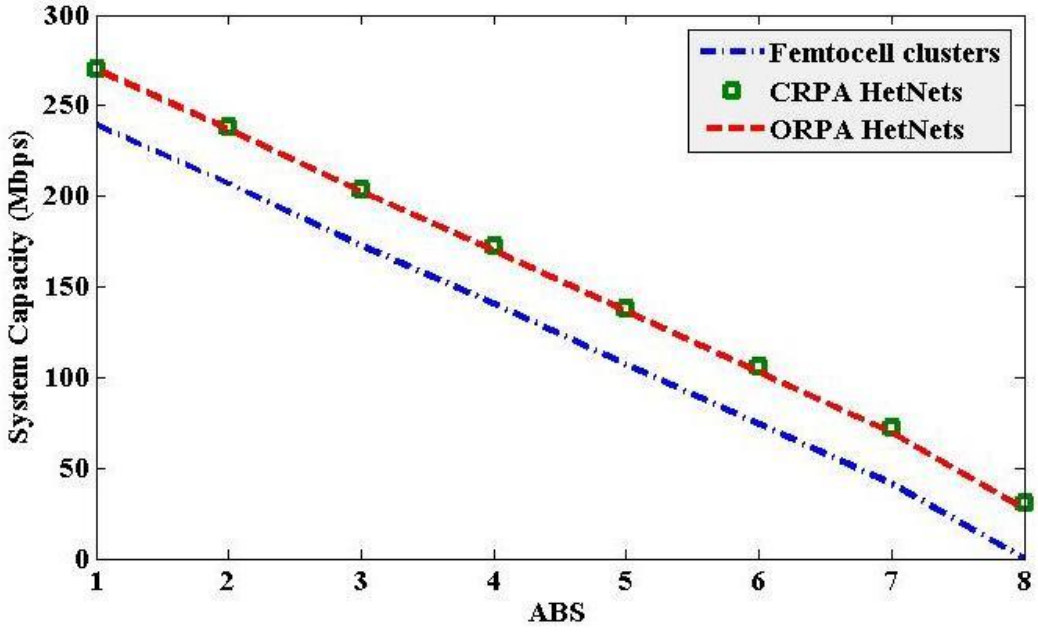

Figure 3.7: System capacity versus the number of ABSs ($L=10$).

shown in Figures 3.8 and 3.9. Though PCs are deployed mainly for providing with a high UE throughput in hotspots, in ORPA scheme, offloaded MUs and FUs cannot get

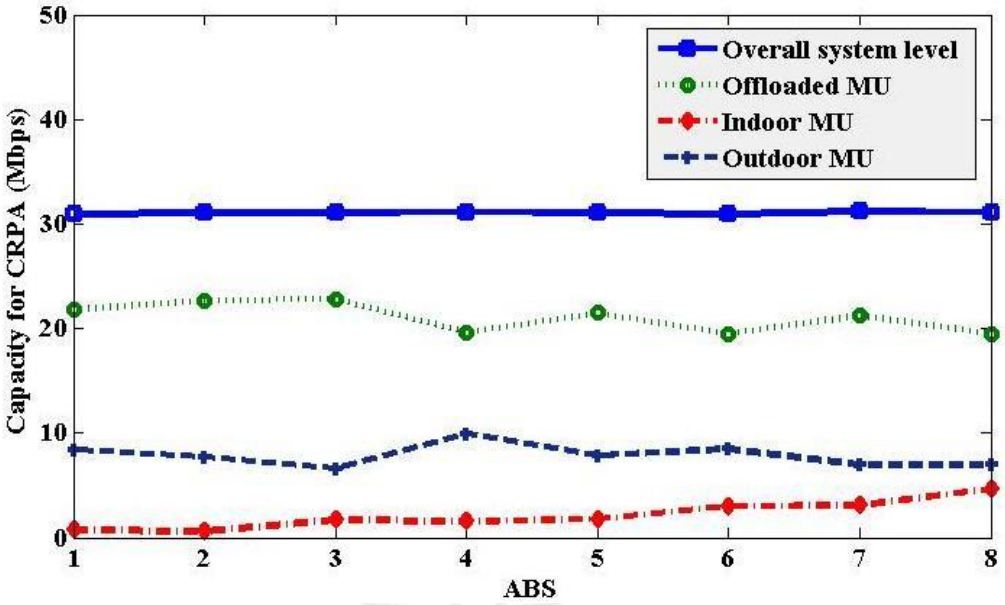

Figure 3.8: Capacity performance of different MUs with the number of ABSs for CRPA HetNets.

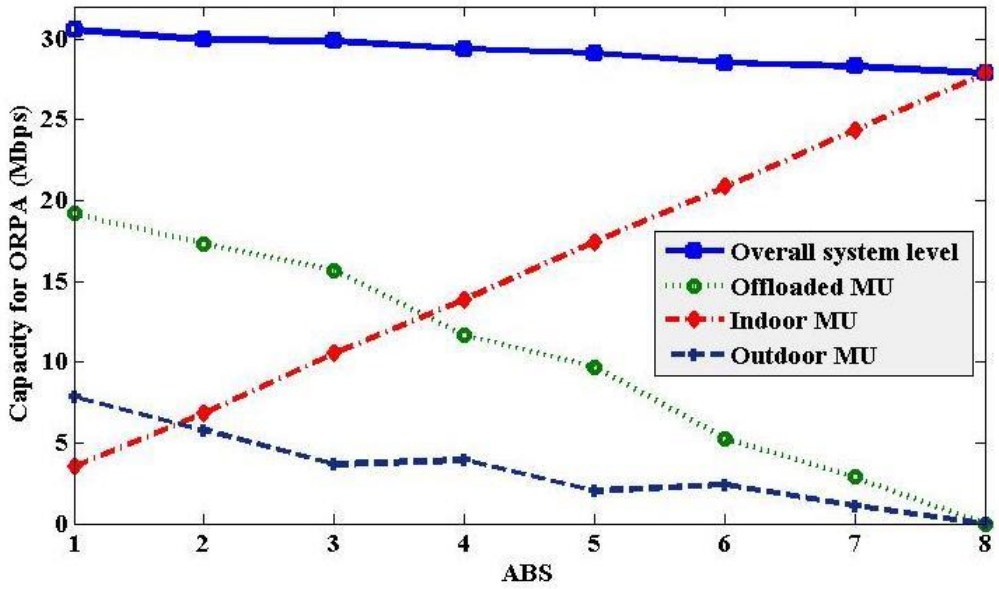

Figure 3.9: Capacity performance of different MUs with the number of ABSs for ORPA HetNets.

access to any resources during ABSs, and hence their capacity degrades considerably with an increase in the number of ABSs. Hence, there has to be a trade-off among these multiple goals such that all UEs are properly served system wide, which we have

already addressed by deriving an OPNA and the impact of which is shown in the following with the non-adaptive and adaptive OPNA schemes.

Remark 3.7: In ABS based TD eICIC, the system capacity performance gain from the co-channel FCLs is not straightforward and is a function of multiple factors, namely the ABS pattern, system bandwidth, and FCL density as given by (3.7).

Remark 3.8: The throughput response of each MU category shows near linear straight-line response which justifies our proposed model to derive an OPNA in section 3. Note that a slight variation in response for outdoor MUs as compared to the proposed model, given by (3.15) and (3.16), is caused because of the random channel characteristic of each outdoor MU link with the MCBS. However, the average trend in response over an ABS pattern period matches with the proposed model.

We compare the performance of the adaptive OPNA scheme with the non-adaptive, i.e. static, scheme as shown in Figure 3.10. The adaptive scheme is evaluated under two cases - one with 4 FCLs and the other with 8 FCLs (out of 10 FCLs) without the presence of any indoor MUs in them such that an OPNA is not applied to these FCLs. However in non-adaptive scheme, the same OPNA is applied and updated for all FCLs per ABS pattern period. It can be found that the adaptive OPNA scheme outperforms the non-adaptive scheme and approaches to the maximum throughput when no indoor MU is present in all 10 FCLs. Note that the adaptive OPNA scheme ensures a number of practical cases as follows:

- An OPNA is computed based on the con-current network statistics, e.g. CSI of indoor MUs and outdoor MUs in every TTI.
- It is highly adaptive with the user statistics, e.g. a FCL is refrained from applying with an OPNA in the next ABS pattern period if there is no indoor MU present in it over the current ABS pattern period.

- The maximal reuse of time resources in FCs can be performed, e.g. all subframes can be allocated to FCs of a FCL over the next ABS pattern period if no indoor MU is present in it over the current ABS pattern period.
- It can be implemented with a simple binary logic circuit since an OPNA has only two states 0 and T^*_{ABS} .

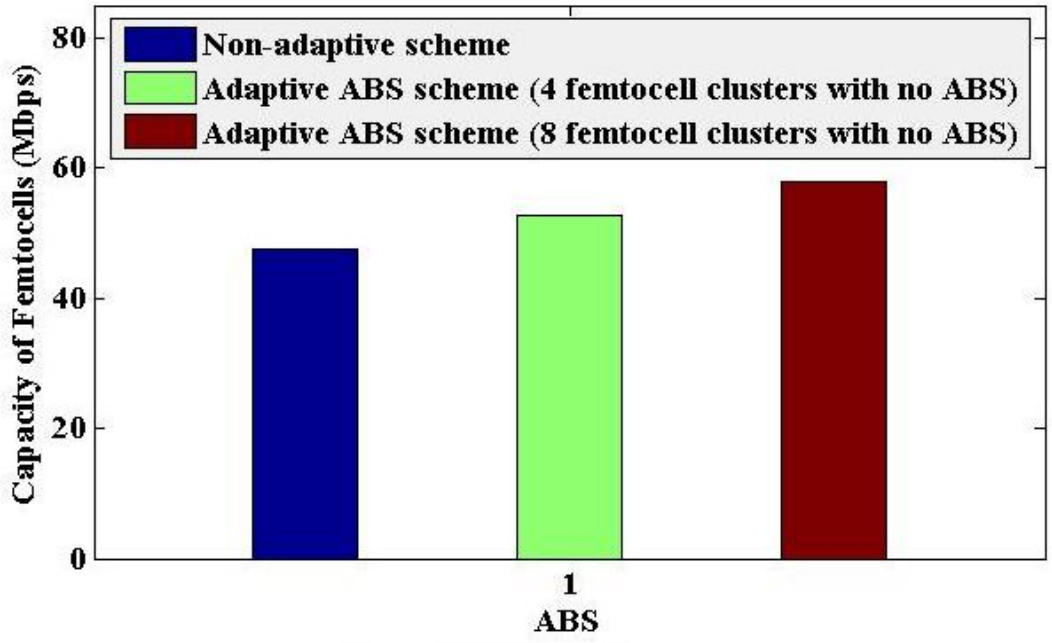

Figure 3.10: Capacity performances of adaptive and non-adaptive OPNA schemes.

Though the complexity of OPNA update mechanism per FCL basis in the adaptive OPNA scheme is higher than that in the non-adaptive OPNA scheme, we aim to reuse resources as much as possible, and hence we propose to employ the adaptive OPNA scheme.

3.5 FRSA scheduler implementation, operation and performance comparison

3.5.1 FRSA scheduler implementation and operation

The scheduler for FRSA can be implemented either jointly or dis-jointly depending on whether the FD schedulers for all FCLs are implemented jointly or dis-jointly with the TD scheduler, which is implemented at the MCBS. A FD scheduler for each FCL can be dedicated to schedule RB resources of the system bandwidth to its FCs, and hence in total, (L+1) schedulers are needed for the system - one for all MUs and L for all FCLs. A TD scheduler is needed to allocate subframes to all UEs in the system. In dis-joint implementation, to communicate with the MCBS, one cluster head per FCL that can be any FCBSs in a FCL is considered, and the FD scheduler of a FCL can be implemented at its cluster head. However, the FD scheduler for all MUs is implemented at the MCBS. All FUs in a FCL can directly report their channel conditions and traffic demands to their cluster heads, and the TD scheduler updates each cluster head about an OPNA per ABS pattern period. To adapt OPNAs per FCL basis, the existence of an indoor MU within a FCL during an ABS pattern period is informed by the indoor MU itself in the UL to the TD scheduler which in turn informs the corresponding cluster head of an OPNA over the X2 backhauls so that RBs should be scheduled by the cluster head to its FCs only during non-ABSs. Whereas for no presence of any indoor MUs over an ABS pattern period in a FCL, the TD scheduler informs the cluster head of that FCL to allocate RBs to its FCs in all TTIs over the next ABS pattern period.

In joint implementation, all FCBSs in a FCL inform the cluster head of their traffic demands, which in turn communicates to the respective v scheduler at the MCBS. The TD scheduler informs all the FD schedulers of OPNAs for all FCLs. Information regarding the allocation of RB resources from a FD scheduler of a FCL are then sent over the X2 backhauls to the respective cluster head to relay to FCs of that FCL. Since both schedulers are located at the MCBS, there is no need to exchange information over X2 backhauls for updating OPNAs. Nevertheless, numerous advantages of the dis-joint scheduler implementation over the joint one are that the small-scale fading effect per TTI level can be addressed easily and control overheads as well as network delays over X2 backhauls can be reduced significantly since the allocation of RB resources is performed locally at each FCL. However, for the joint implementation, small-scale fading effect per TTI level may not be possible to address because of the network delays over X2 backhauls from sending control overheads to

each cluster head. Hence, channel modeling for FCs may rely on accounting only the large-scale fading effect. Since we consider small-scale fading effect for all FCLs, the proposed algorithm can better be addressed with the dis-joint scheduler implementation. Figure 3.11 shows a schematic of the dis-joint FD scheduler implementation. The joint scheduler can be implemented straight-forward by moving all the FD schedulers from all FCLs to the MCBS.

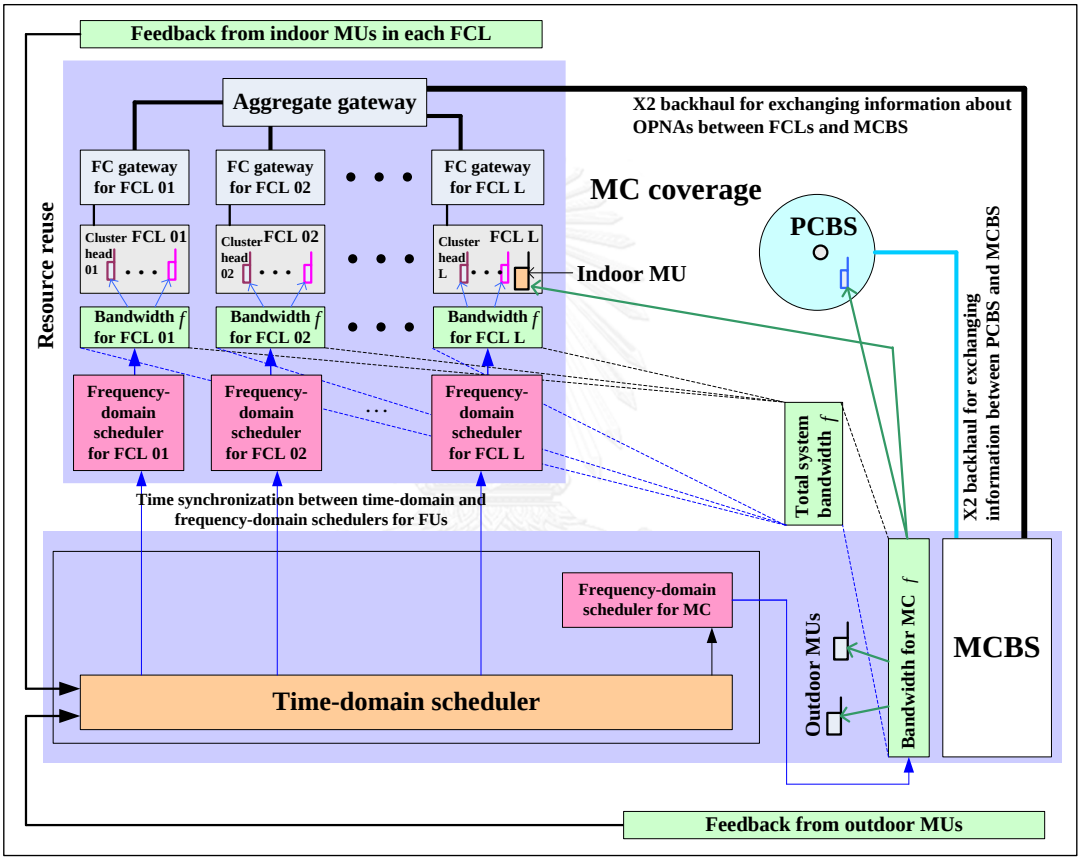

Figure 3.11: Dis-joint FD scheduler implementation for FRSA.

Remark 3.9: In Figure 3.11, only the online FD schedulers are shown, and two offline FD schedulers for the adaptive OPNA scheme are not shown explicitly to avoid ambiguity. However, as mentioned earlier, these offline FD schedulers can be implemented alongside the TD scheduler at the MCBS.

3.5.2 FRSA performance comparison

We evaluate the performance of the proposed FRSA against the generic FFR techniques [94], the FC clustering and frequency reuse scheme in [21], and the existing results in [6, 94] in the following.

A. Generic FFR techniques [94]

The FFR technique is an efficient approach for reusing resources and interference management in HetNets scenario. A good explanation of a number of FFR schemes such as strict FFR, soft FFR, and FFR-3 have been presented in [94] to compare the performance of the authors' proposed optimal static fractional frequency reuse (OSFFR) scheme for interference management and resource reuse in MC and FC based HetNets. In FFR, the resource reuse is considered by partitioning the coverage of a MC mainly into two, namely MC-center and MC-edge, each of which is then partitioned further into a number of sectors for schemes such as FFR-3. In contrast to our proposed schemes ORPA and CRPA where a FC in any FCLs can be allocated to any RBs of the system bandwidth, only a fraction of the total system bandwidth is allowed to assign to a FC in FFR schemes [94]. A detail discussion on these schemes can be found in [94].

We consider comparing our proposed resource reuse schemes with the FFR schemes in [94]. For brevity, instead of reproducing the same results, we use the performance results in [94] directly for FFR schemes to compare with our schemes. As shown in [94], the average network sum rate with OSFFR outperforms other FFR schemes, which can achieve the maximum 70 kbps (approximately) for 40 FCs per MC. Note that the average network sum rate is expressed as [94]

$$\sigma_{avg}^{nsr} = \frac{\sum_{x_m \in N_M} \sum_{i \in M_{RB}} \Gamma^i_{x_m, m_m} \, \sigma^i_{x_m, m_m}}{N} + \frac{\sum_{f \in N_{FS}} \sum_{x_f \in U_{FU}} \sum_{i \in M_{RB}} \Gamma^i_{x_f, f} \, \sigma^i_{x_f, f}}{U_{FS}} \qquad (3.21)$$

where N is the total number of MUs, and U_{FS} is the total number of FUs in the system. m_m denotes a MCBS, x_m denotes a MU, i denotes a subchannel or RB, x_f denotes a FU, f denotes a FCBS, and σ^i denotes the capacity of a UE on subchannel i. Further,

$\boldsymbol{N_M}$ = {1, 2, 3, …, N}, $\boldsymbol{N_{FS}}$ = {1, 2, 3, …, S_{FS}}, $\boldsymbol{U_{FU}}$ = {1, 2, 3, …, U_{FS}}, and $\boldsymbol{M_{RB}}$ = {1, 2, 3, …, M}. $\Gamma^i = 1$ when a subchannel i is allocated to a UE, otherwise it is set to 0.

Figure 3.12 shows the outperformance of our proposed ORPA scheme for σ_{avg}^{nsr} as compared to all the FFR schemes in [94] by manifold. Because of reusing the same system bandwidth of 1 MHz in each of the 8 FCLs, each with 5 FCs, such that a large amount of spectrum can be allocated to each FU, σ_{avg}^{nsr} for 1/8 ABS pattern is much higher than any FFR schemes [94]. Apparently, σ_{avg}^{nsr} is not affected by the total number of FUs per MC but per FCL such that the total system bandwidth can be distributed among only FUs per FCL, instead of per MC as is the case of FFR schemes [94]. This is because of why there is a gradual drop in σ_{avg}^{nsr} as the number of FCBSs increases per MC for FFR schemes [94]. Further, since the whole system bandwidth is reused in each FCL, σ_{avg}^{nsr} should vary with the number of FCLs in which a given set of FCs per MC are deployed. σ_{avg}^{nsr} is maximum of 5×10^6 kbps for 40 FCLs (for 1 FC per FCL) such that the whole system bandwidth can be allocated to a single FU, and minimum of 1.25×10^5 kbps for a single FCL (for 40 FCs per FCL) such that the same system bandwidth is allocated among all 40 FCs as in the case of FFR schemes [94], assuming that all FCs in all FCLs have the same channel conditions. This implies that the minimum value of $\sigma_{avg}^{nsr} = 1.25\times10^5$ kbps that can be achieved by the proposed ORPA scheme still exceeds substantially that of any FFR schemes as shown in Figure 3.12. Hence, in our proposed FCL model, because of reusing the whole system bandwidth and an orthogonal allocation of its RBs to all FCs per FCL, more users can be served which is not obvious for any FFR schemes in 2D scenario in [94] because of increased co-channel interference from neighboring FCs with an increase in the number of FCs per MC. Hence, our proposed ORPA scheme is not only outperforming the generic FFR techniques in terms of σ_{avg}^{nsr} but also allowing scalability with an increase in SC density per MC.

B. FC clustering and frequency reuse scheme [21]

We carry out a quantitative performance comparison of the proposed FRSA with the FC clustering and frequency reuse scheme in [21] for the average data rate per FU per FCL with the same setup of simulation parameters and assumptions as in *Table I* in [21]. The FC clustering in [21] has been proposed by disjointing a set of FCs

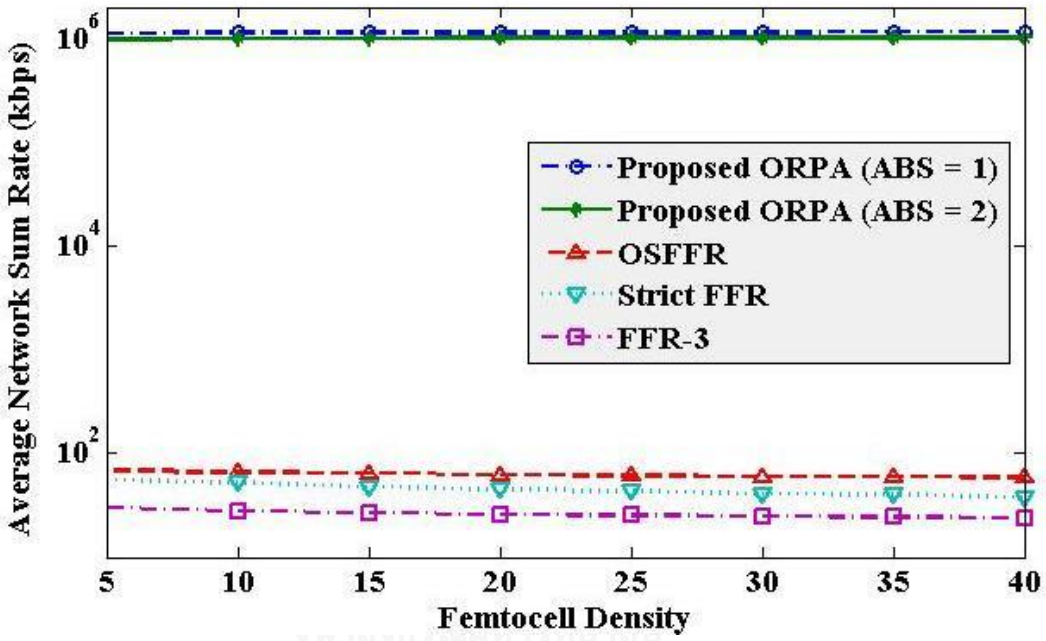

Figure 3.12: Average network sum rate of FFR schemes [94] and the proposed ORPA scheme of FRSA (for M = 5, L = 8, U_F = 5, φ = {1/8, 2/8}, T = 8 TTIs).

deployed within an indoor environment. Each disjoint set of FCs is called a FC cluster where clusters are formed by the FC gateway. All subbands of the system bandwidth are available to both MUs and FUs, and the entire system bandwidth is allocated orthogonally to FCs in each cluster. The simulation results of our proposed FRSA with an adaptive OPNA shows that the average data rate per FU varies from 4.3 Mbps (for ABS = 1) to 4.9 Mbps (for ABS = 0), which is within and even exceeding the best performance result of slightly less than 4.5 Mbps for 5 FCBSs in [21] obtained for semi-definite program. Further, for the smallest cluster size of 1 FCBS, the average data rate per FU varies from 21.5 Mbps (for ABS = 1) to 24.5 Mbps (for ABS = 0) in our proposed FRSA. As the number of FUs per FCL increases, there is a corresponding

decrease in the average data rate per FU which is also the case in [21]. As long as the number of subchannels is equal to or greater than the number of FCBSs per FCL, which is considered as the maximum cluster size in [21], our proposed FRSA performs better than the FC clustering and frequency reuse scheme in [21].

C. Consistency evaluation

In our proposed FRSA, to avoid co-channel interference using eICIC techniques, the average spectral efficiency varies linearly with the FC density as shown in Figure 3.13. The similar trend has been noted in [94]. This implies that the

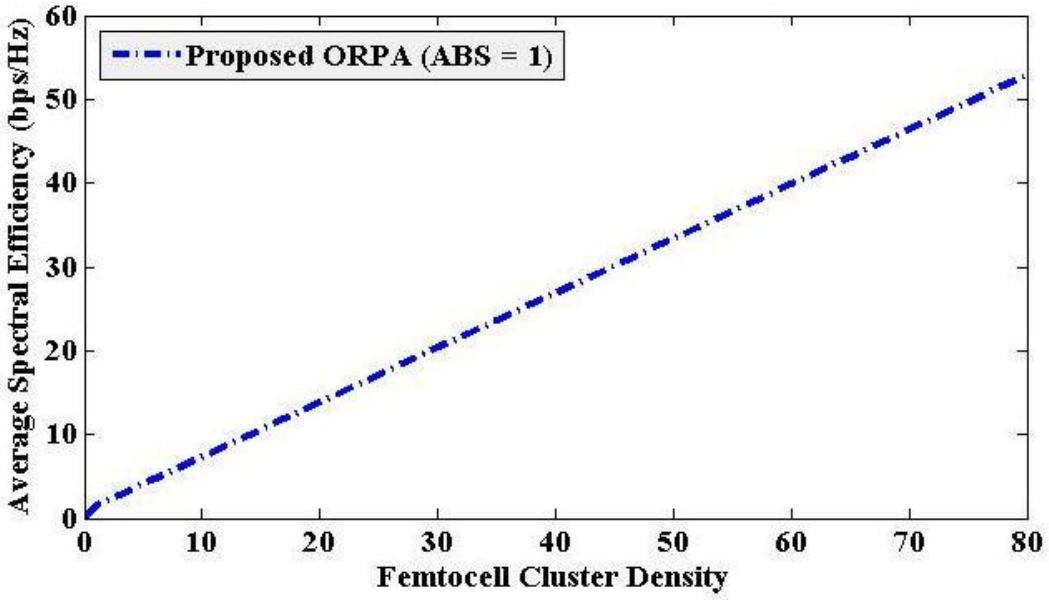

Figure 3.13: Average spectral efficiency of the proposed ORPA scheme of FRSA (for M = 5, L = 80, S_F = 5, φ = 1/8, $\boldsymbol{T}$ = 8 TTIs).

performance results of the proposed FRSA are consistent with the existing literature. Note that with the presence of interference, the capacity varies linearly with FCs up to a certain number as shown in [6] and is beyond the scope of this chapter since we consider the interference avoidance technique, eICIC, both at the co-tier and cross-tier levels.

3.6 FRSA technical and business perspectives and way forward

A number of business values from network operators' viewpoint to implement FRSA are pointed out as follows:

- One of the important issues of FC networks is randomness and plug-and-play feature of FC deployment within a building mainly by end users, and network operators do not typically have prior knowledge on it. Hence, the SON technique is typically considered in FCs to address interference because of random placement of FCs. However, by employing FRSA, SON enablement feature of FCs can be avoided since both time and frequency resources are allocated to all FCBSs orthogonally using eICIC irrespective of their placements. Hence, randomness of FCs can be easily catered, and an additional cost from SON feature of FCs can be avoided.
- The LTE-Advanced network has been deployed and evolved toward reaching a high capacity of NGMN. Because of high scalability from scheduler implementations with density of SCs over a large MC coverage, a gradual migration from regular HetNets of the existing LTE-Advanced network to ultra-dense HetNets of NGMN can be easily performed by FRSA. Hence, except upgradation of FRSA with a growing traffic demand, no cost from buying a new product for switching to NGMN is needed.
- FRSA addresses the problem of dense HetNets in a realistic in-building urban scenario rather than any hypothetical FCL shape, size and density. Hence, it can be applied without any prior modification to adapt with any real urban environment. Any urban map with specific details of buildings in terms of, e.g. density and height, along with statistics of FCBSs is sufficient to operate FRSA and hence can reduce efforts from FC networks planning in urban environments and save the associated costs.
- Since eICIC techniques have been in operation in existing networks, no additional implementation complexity from eICIC will raise. Only implementation of schedulers and necessary backhauls are to be needed in

place. Hence, operators can easily implement FRSA using existing techniques without a significant investment on current networks.

A noticeable characteristic of FRSA is that with an increase in FCs in a FCL, average data rate per FU of that FCL should be decreased because of reusing the same and fixed system bandwidth. This however does not affect overall system level capacity over MC coverage since proportional fair schedulers mainly check channel conditions of FUs in a FCL irrespective of their number and allocates RBs to them accordingly. Also effect of this issue can be minimized either by increasing system bandwidth or by considering reuse of system bandwidth more than once in a FCL. Because NGMN is expected to have more system bandwidth using, e.g. industrial, scientific and medical bands below 6 GHz than current networks, the first option can be easily addressed. Since in this chapter, our focus is to avoid computational complexity from FC clustering, we will explore the second option in our future work to make this effect minimal by adapting dynamically resource reuse factor per FCL basis with statistics of FCs per FCL.

3.7 Summary

In this chapter, we propose a FRSA for FCs deployed in dense multi-floor buildings in a multi-tier HetNet in a large urban MC coverage by employing ABS based eICIC techniques. The cross-tier interference between the FC-tier and MC-plus-PC-tier is managed by ABS based TD eICIC, and the co-tier interference of UEs in any tiers is managed by allocating RB resources orthogonally using FD eICIC. To reuse frequency in FCs in dense urban buildings using ABS based eICIC techniques, two major challenges, namely FC clustering and modeling an OPNA is addressed. An approach for FC clustering is proposed by considering all FCs per 3D multi-floor building as a cluster of FCs through exploiting the high external wall penetration loss and in-between distance of neighboring buildings. We propose a model for estimating an OPNA and derive an OPNA per cluster basis under two schemes, namely adaptive OPNA and non-adaptive OPNA, to avoid cross-tier interference between FUs and indoor MUs within

buildings. We develop an optimization algorithm for both OPNA schemes and discuss its implementation aspects.

The performance of FRSA is analyzed under two schemes, namely CRPA and ORPA where one differs from the other in the way MUs is prioritized during ABSs. The impact of varying the number of ABSs as well as FCs per 3D multi-floor building on the throughput performance of FRSA is analyzed through an extensive system level simulation. The overall system capacity for different ABS patterns is found to improve linearly with the FCL density, and the capacity outperformance of the adaptive OPNA scheme over the non-adaptive OPNA scheme is shown. Finally, the scheduler operation and implementation for FRSA is discussed, and the capacity outperformance of FRSA over a number of existing techniques in literature such as FFR techniques is shown. Unlike existing works, major distinctive features of the proposed FRSA are as follows:

- It does not need any computational efforts for estimating an appropriate FCL size.
- It considers the interference effect on CSG FCBSs and FUs because of the presence of indoor MUs within 3D multi-floor buildings.
- It studies a powerful eICIC techniques in a dense multi-tier HetNets with various types of SCs which adaptively updates an OPNA per FCL basis based on its actual traffic and user statistics per ABS pattern period.
- It is not susceptible to the complex intra-cell interference within a cluster of FCs.
- It acquires a semi-centralized feature to take advantages of both the centralization feature through updating OPNAs per ABS pattern period to reduce control overheads and address network delays between the MCBS and any FCLs, and the decentralization feature through updating the RB allocation per TTI basis to address small-scale fading between any sFCBSs and FUs.

CHAPTER 4
INTERFERENCE MODELING AND MINIMUM DISTANCE ENFORCEMENT TO REUSE RESOURCE IN 3D IN-BUILDING SMALL CELL

In this chapter, an analytical model using planar-Wyner model for intra-floor and linear-Wyner model for inter-floor interferences modeling in a 3D multi-floor building in order to derive a minimum distance between FCBSs for optimization constraints, namely link level interference, spectral efficiency, and capacity is proposed. Two strategies for reusing resources more than once within the building are proposed. An algorithm of the proposed model is developed by including its application to an ultra-dense deployment of buildings over a MC coverage. With an extensive numerical analysis and system level simulation, the capacity outperformance of NORRA over ORRA schemes by manifold is demonstrated. Further, it is shown that the expected spectral efficiency of 5G networks can be achieved by applying the proposed model to an ultra-dense deployment of FCBSs.

4.1 Introduction

Network densification is one of the key enablers to achieve an expected capacity and spectral efficiency of 5G mobile networks [4] through reusing resources in SCs, such as FCs. Reuse of resources in FCs relies on the inter-FC distance, which is a function of co-channel interference generated from neighboring FCs. In urban environments, where an existence of thousands of 3D multi-floor buildings is an obvious scenario, modeling co-channel interference and a minimum distance between FCs in 3D multi-floor scenario, e.g. office buildings and residential areas, to address a high data rate demand of 5G networks has become one of the major growing concerns.

Typically, interference in HetNets has been studied considerably in 2D scenario [5]. Modeling 2D interference is simple but not accurate enough for multi-floor buildings since it cannot capture complex combinations of deployment and propagation effect existing in realistic 3D multi-floor buildings. Authors in [5], investigated the impact of three-dimensionality of FC deployments on cross-and co-tier interferences using realistic building data, showed that the interference effect of FCs in urban 3D scenario is significantly higher than that when considering 2D case, and proposed to model HetNets in 3D scenario rather than 2D. Note that with 2D scenario, we infer that SCs, i.e. FCs, are located within either closed indoor coverages, e.g. a single floored building, a single floor of a multi-floor building, or open outdoor coverages, e.g. a MC area. Whereas, with 3D scenario, we infer that FCs are located within multi-floor buildings, and hence hereafter, we use 3D in-building to refer inside multi-floor buildings.

Theoretically, the maximum capacity of a SC can be achieved when it is allocated with the whole system bandwidth. However, in practice, it is difficult to achieve, and only a fraction of the system bandwidth is allocated to a SC to overcome co-channel interference. Since a SC, particularly FC, typically has a limited coverage, we can take this as an advantage through reusing as much system bandwidth as possible simultaneously in more than one FC within a FCL to boost the network capacity using a limited system bandwidth. However, reusing frequency resources in FCs simultaneously results in a significant amount of co-channel interference if a minimum distance between cFCs is not enforced. A denser FC network causes a higher co-channel interference effect at a UE. Hence, how to model co-channel interference and enforce a minimum distance between cFCs [6] for reusing resources in FCs, particularly in 3D in-building scenario, has been active research area.

Existing literatures addressed discreetly a number of such issues as modeling interference, enforcing a minimum distance, placing BS optimally, and reusing and allocating resources in SC networks in both 2D and 3D scenarios. In 3D in-building scenario, along with other approaches, several works considered resource allocation as an important technique to deal with indoor FC interference issues. For example, in [18], authors proposed a semi static resource allocation scheme based on FFR to avoid interference in 3D multi-floor buildings using indoor networking and optimization tool,

iBuildNet. Authors in [19] proposed a soft frequency reuse scheme for interference management in dense FC networks deployed in a multi-floor office building, based on the serving user's received signal strength indication, to classify all interfering FCs into several groups and select adaptively the soft FFR and transmit power for each group. In [96], a distributed power resource self-optimization scheme for the DL operation of dense and self-organized FC network, deployed in a 3D six-floor building overlaid by the existing MC in an urban environment, to address inter-FC interference was proposed.

Furthermore, a number of existing works addressed the issue of indoor FCBS placement. Authors in [97] developed a linear programming problem model for an optimal placement of FCBSs inside an enterprise multi-floor building. The problem of jointly optimizing FCBS placement and power control in commercial multi-floor building environments was addressed by authors in [98] to enhance the battery life for mobile handsets by proposing a mathematical model. However, none of these aforementioned works addressed the problem of enforcing a minimum distance between FCBSs in 3D in-building scenario.

Like 3D, several works addressed a number of issues of FCBS in 2D scenario, e.g. [99-101] for an optimal placement of FCBSs, [94, 102-105] for the interference management and resource reuse and allocation in FC networks, and [22-23] for enforcing a minimum distance between FCBSs, as follows. In [99], a FCBS placement scheme was proposed by authors based on forming as well as updating subregions of the total area of interest such that BSs in subregions, one for each subregion, could satisfy the coverage requirement of all UEs within the total area. Authors in [100], investigated an optimal placement of a FC by considering a single rectangular room without internal walls, and proposed a simulation and theoretical optimization framework to find an optimal placement within the room. In [101], authors also investigated an optimal placement of a FC within a room, and derived a closed form FC placement expression to improve throughput by considering a single FCBS in a single-floored building.

In [102], to mitigate interference of FC networks in residential or enterprise environments, a game-theoretic approach was presented by authors in cooperative FC orthogonal frequency division multiple access networks. Whereas, authors in [94]

evaluated three state-of-the-art FFR deployment schemes, namely strict FFR, soft FFR, and FFR-3 schemes in addition to their proposed optimal static FFR scheme for orthogonal frequency division multiple access-based two-tier HetNets comprised of MCs overlaid with FCs. Further, in [103], a dynamic frequency resource management was proposed by using a graph coloring approach to mitigate the DL interference of indoor FCs and increase frequency channel utilization under co-channel deployment in a two-tier MC and FC network. Additionally, authors in [104] proposed a mechanism to determine allocation of resources among subscribed and non-subscribed users through hybrid access FCs by coordinating their transmission powers to get rid of additional interference experienced by FCs. Nevertheless, in [105], authors proposed a price-based UL interference management scheme under co-channel deployment for dense FC systems where the MCBS was considered to control the received interference through pricing the interference from FUs subject to a maximum tolerable interference power constraint.

In [22], with a minimum cell separation distance, authors proposed to use a BS location model to ensure a minimum distance between any two cells in each tier using the Matern hardcore process such that no cells could lie within a predefined minimum distance from any other cells. They investigated the randomness in placement of SCs, derived an optimal (lower bound) minimum separation distance between BSs, and showed that the cell coverage could be improved by introducing a minimum separation distance between BSs per tier. Authors in [23], proposed a repulsive cell activation strategy, and derived an optimal minimum separation distance between SCs by adopting modified Matern hardcore process to analyze the impact of a minimum separation distance on the coverage of SC networks using a numerical search. Both [22] and [23] addressed to enforce a minimum distance based on the interference statistics around SCBSs by modeling BS locations as Poisson point processes in 2D scenario.

However, addressing all these aforementioned indoor SC issues, particularly interference modeling, enforcing a minimum distance, and reusing and allocating resources in SCs, under 2D scenario is not practical mostly in urban environments because of an existence of dense 3D multi-floor buildings. In urban environments, SCs are expected to deploy densely per floor level in each building to address high indoor data rate and spectral efficiency for future mobile networks which demands these SC

network issues to explore by considering the third dimension, i.e. the height of buildings, to capture 3D effects on indoor signal propagations, e.g. floor attenuation loss, diffraction effects through edges of any buildings, and neighboring buildings' signal propagation effects, through developing a closed form analytical model.

Stochastic geometric approaches have been mainly applied so far in the existing literatures under 2D random BS location scenario with a simple homogenous Poisson point process or Matern hardcore process. However, because of complexity and intractability of stochastic analytical closed form expressions, the study under 3D in-building scenario of BS locations is not obvious. An effective way to develop a closed form yet simple enough analytical model, which can capture most of these 3D effects, for characterizing interference between FCs located on different floors in a multi-floor building is to consider a regular pattern of FCBS locations both intra-and inter-floor levels. A minimum distance between FCBSs can then be enforced such that certain constraints are satisfied. A proper reuse and allocation of resources in FCBSs within a building can be performed based on an estimated minimum distance between FCBSs. To our best knowledge, a study of this kind is not obvious in the existing literatures which we aim to address in this chapter by proposing a novel and tractable analytical model for characterizing co-channel interference and enforcing a minimum distance between FCBSs deployed densely within a 3D multi-floor building to reuse resources in FCBSs with the purpose of achieving prospective high capacity and spectral efficiency demands of 5G networks as our contribution.

In addressing the contribution, we consider a multi-tier network comprising a MC, a number of PCs and a set of FCs located within a 3D multi-storage building. The building consists of a number of floors, and each floor is modelled as square-grid based apartments, each with a FCBS located in it. We consider to reuse RBs in FCBSs more than once following the estimated minimum distance. Because RBs are reused more than once, they remain no longer orthogonal, and hence the term NORRA. However, in ORRA scheme, the whole system bandwidth is reused orthogonally once in FCBSs within the building in every TTI. The ABS based eICIC techniques are considered to manage interference between MC-plus-PC tier and FC tier both for NORRA and ORRA schemes.

We divide the whole contribution into numerous subsequent issues and solve consecutively in a number of phases as listed below:

- *Phase 1*: We first propose and develop an analytical model for intra-floor interference using planar-Wyner model and inter-floor interference using linear-Wyner model of FCBSs deployed within a 3D multi-floor building.
- *Phase 2*: We then derive mathematical expressions for a minimum distance to enforce between FCBSs both intra-and inter-floor levels for a number of optimization constraints such as link level interference power, spectral efficiency, and capacity.
- *Phase 3*: By enforcing the derived minimum distances (in phase 2) to FCBSs for any constraints, we propose two resource reuse strategies for reusing frequency resources in those FCBSs which are apart from one another by at least the required minimum distance, and show the capacity outperformance of NORRA scheme over ORRA by employing one of the resource reuse strategies for the link capacity constraint.
- *Phase 4*: We develop an algorithm of the proposed model (in phases 1 and 2) for both single and multiple buildings scenarios using the considered resource reuse strategy for the capacity analysis in phase 3.
- *Phase 5*: The application of the proposed model from a single to multiple buildings deployed within the coverage of a MC to address an ultra-dense deployment of FCBSs for 5G networks is then discussed. With a rough estimation under an example scenario of an ultra-dense deployment of FCBSs, by employing the proposed model, we show that the prospective spectral efficiency of 5G networks can be achieved.
- *Phase 6*: Finally, we discuss several technical and business perspectives of the proposed model for a number of key aspects.

We organize the chapter as follows. In section 4.2, FC interference modeling both intra-and inter-floor levels is discussed. We show derivations of a minimum distance between cFCBSs for a number of approaches based namely on link level

interference power, spectral efficiency, and capacity constraints both intra-and inter-floor levels in section 4.3. The numerical results of a minimum distance derived under each approach in section 4.3 are shown and analyzed in section 4.4. We propose two strategies for reusing resources in FCBSs, discuss system models, compare the performances of ORRA and NORRA schemes with a resource reuse strategy, and detail an algorithm for developing the proposed model under a multi-tier network for both cases of single and multiple number of 3D multi-floor buildings over a MC coverage in section 4.5. In section 4.6, several technical and business perspectives of the proposed model are discussed. Finally, we summarize the chapter in section 4.7.

4.2 Interference modeling of femtocell networks in 3D in-building scenario

4.2.1 Interference modeling architecture

A. Intra-floor interference modeling architecture

We consider a 3D multi-floor building that consists of a number of 2D floors, and each floor consists of a number of square-grid apartments with each side length a as shown in Figure 4.1. A cluster of FCBSs is deployed in apartments of the building such that each apartment has one FCBS. We define nominal cell coverage of each FCBS as the coverage equivalent to the area of an apartment $(a \times a)$ m^2. Each FCBS is placed in the center of ceiling of apartment and assumed static. A fixed amount of free space around the building is considered. We consider typical values of a = 10 m and free space of 10 m [88, 106]. However, in general, a and the amount of free space are random variables. A FU per FCBS is considered and placed at the farthest radial distance from its sFCBS if resources are reused in it, i.e. cFCBS. However, for non-cFCBSs, a FU is distributed randomly and uniformly in its FCBSs' nominal coverage.

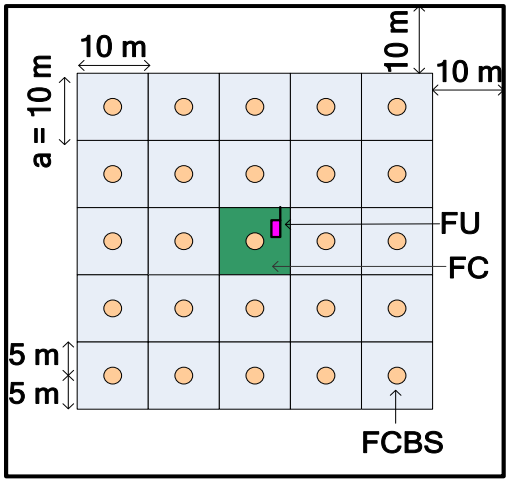

Figure 4.1: 2D intra-floor architecture.

Figure 4.2 shows the proposed intra-floor co-channel interference modeling where a link between a cFCBS and serving FU (sFU) is termed as co-channel interference link, and the one between sFU and its sFCBS is termed as desired link. We consider planar-Wyner model [107] for modeling 2D intra-floor interference among

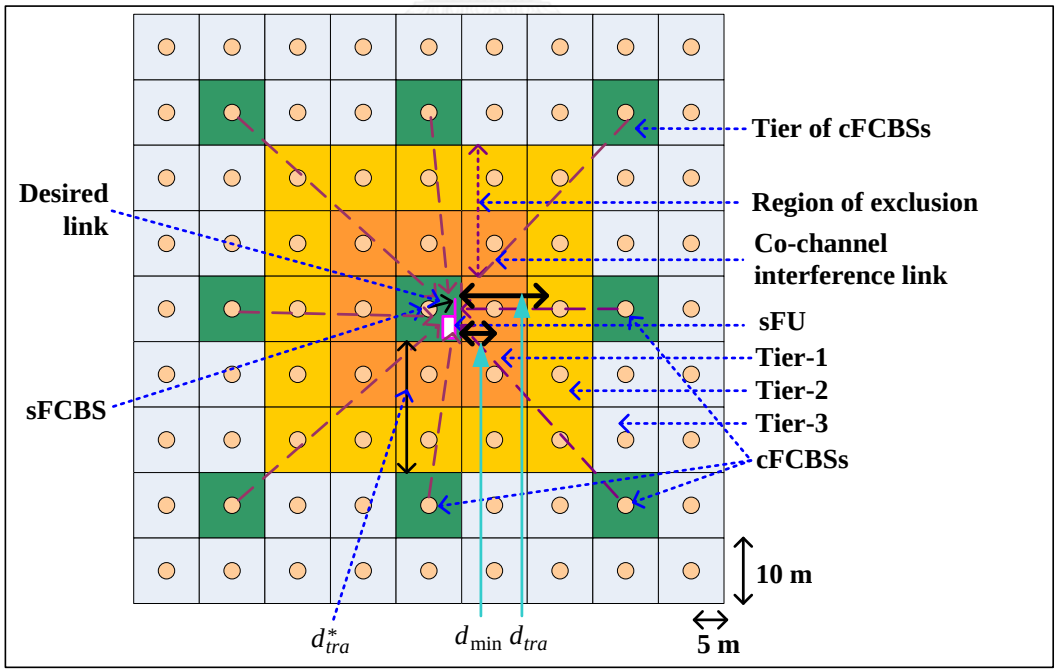

Figure 4.2: Intra-floor co-channel interference and RoE modeling.

FCBSs located on any floors. An illustration of an example aggregate interference effect of all cFCBSs at sFU of a sFCBS is shown in Figure 4.2. The region up to which the aggregate interference is significant enough so that it exceeds a maximum allowable aggregate interference at sFU is termed as the region of exclusion (RoE) for reusing the same resources of sFCBS in any FCBSs within RoE. Hence, RoE in Figure 4.2 is up to tier-2 and is shown in yellow color. Irrespective of tier indices, the maximum number of cFCBSs for any sFCBSs is 8. Though the distances of all cFCBSs in any tiers from a sFCBS and its associated sFU are not the same, for mathematical simplicity, we assume that co-channel interference effect at sFU of each cFCBS of the same tier is the same. Note that we use the subscript *tra* to mean intra-floor level and *ter* to mean inter-floor level in the following.

B. Inter-floor interference modeling architecture

We assume that all FCBSs are located on the ceilings and centers of all apartments. Recall that a sFU is located at the farthest radial distance $d_{\min}$ from its sFCBS if sFCBS is a cFCBS and for simplicity, at the same height as that of its sFCBS. Note that the location of sFU vertically at distance $d_{\min}$ does not affect considerably the overall inter-floor interference power received at sFU. This is because of the fact that moving a sFU towards the ceiling of apartment of sFCBS causes co-channel interference power at sFU from a cFCBS located on a floor up from that of sFCBS to increase and from the one located down on a floor from that of sFCBS to decrease such that the overall co-channel interference power effect does not vary considerably. The reverse phenomenon is happened when moving a sFU towards the floor of apartment of sFCBS.

Since intra-floor interference modeling addresses co-channel interference effect within a floor, and there exists an additional high floor attenuation loss between sFU and a cFCBS, it is not necessary to take into account of co-channel interference effect from all cFCBSs on co-channel interferer floors except those two cFCBSs located on either a vertically straight up or down floors from the serving floor of sFCBS. We define a serving floor as the one where sFCBS is located, and an interferer floor as the one

where any cFCBSs of sFCBS is located. With this concern, inter-floor interference modeling can be performed by using linear-Wyner model [107] such that each of the two cFCBSs is at distance d_{ter}^{*} away from sFCBS as shown in Figure 4.3.

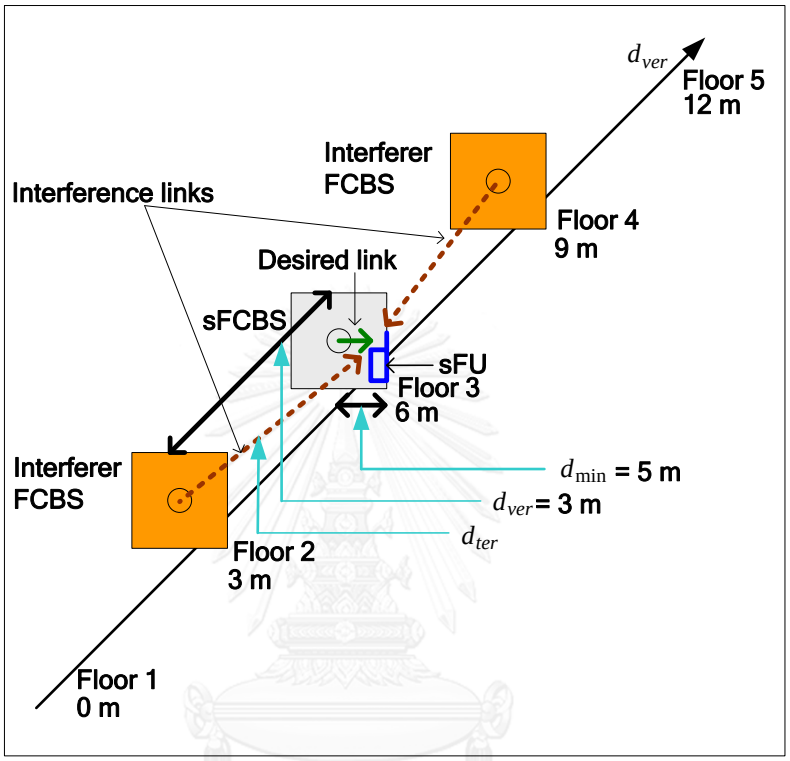

Figure 4.3: Inter-floor interference modeling and architecture.

C. 3D in-building interference modeling architecture

Figure 4.4 shows a detail diagram of 3D in-building FC interference modeling combining the effects of intra-floor and inter-floor co-channel interference. If the reuse of resources is performed on an intermediate floor, two cFCBSs need to be considered of which one is located on a bottom floor, and the other is on an up floor from the serving floor so long as both cFCBSs exist on both sides of the serving floor. However, if the serving floor is either the top or bottom most of all floors, the number of cFCBSs is only one since there is at most one cFCBS located respectively on either a bottom or an up floor from the serving floor.

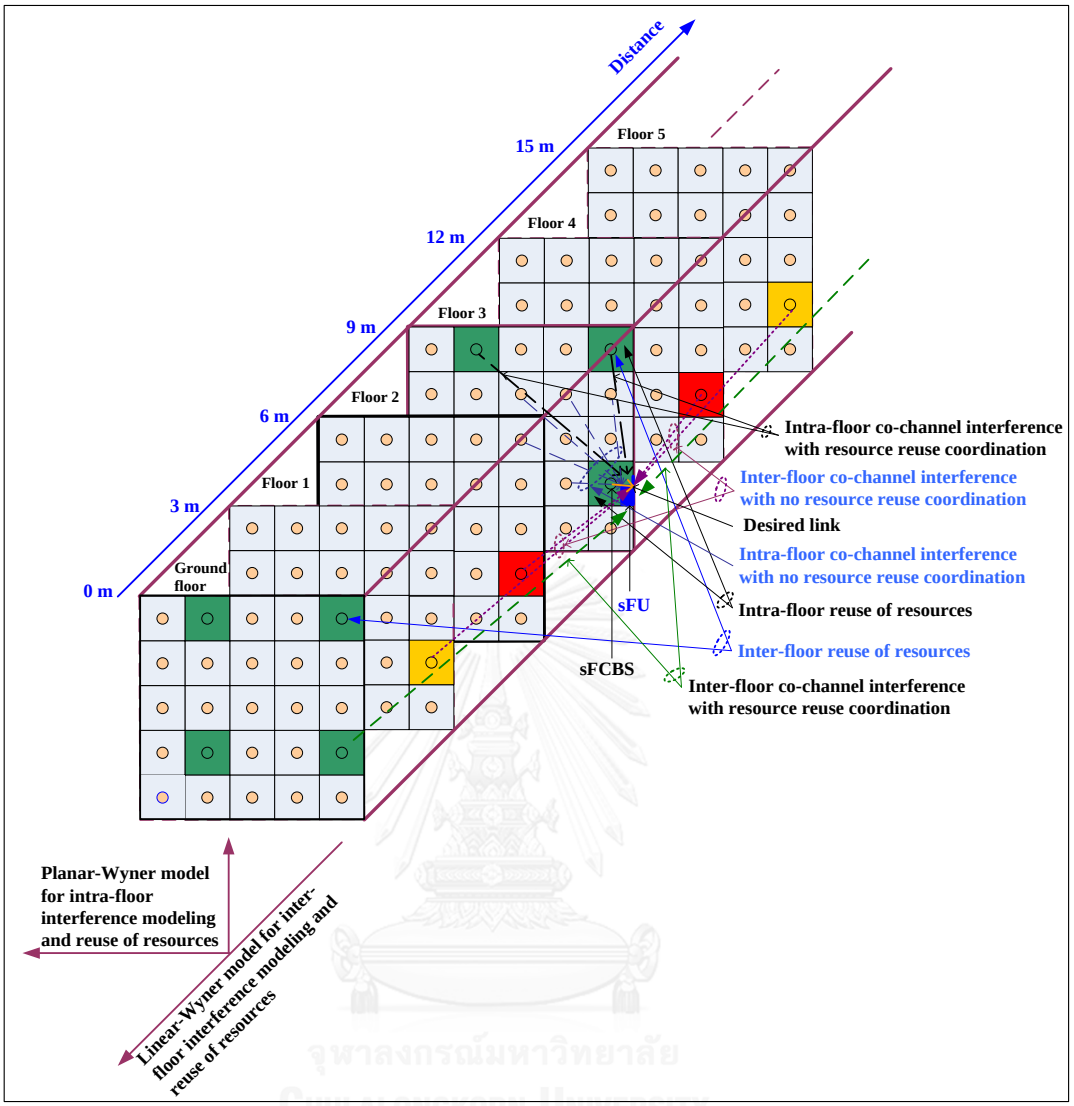

Figure 4.4: A detail 3D in-building intra-and inter-floor interferences model and architecture for reusing resources in FCBSs.

4.2.2 Interference modeling consideration and assumption

A. Indoor propagation

There are mainly two approaches that can be considered for modeling signal propagation in-building scenario: (i) one approach is to consider nearby buildings' reflection effects, particularly in urban environments where buildings are very close in distance to one another; (ii) the other approach is not to consider nearby buildings' reflection effects such that an isolated building is concerned, and only in-building

propagation of signals through floors, reflected signals from walls, ceilings, and floors, and diffracted signals from the edges of building through windows are to be considered. This is, to a great extent, a valid assumption when both the transmitter and receiver are located inside a building such that there is sufficient building attenuation to make the effect of surroundings insignificant [108]. Certainly, considering the second approach will make the modeling simpler but less accurate particularly for dense urban environments. However, simplification of indoor propagation modeling is worthy enough since we aim to address the issue of enforcing a minimum distance for reusing resources within a building where both the transmitter and receiver are located in close proximity. Though we consider approach 2, we also show the applicability of proposed model for an ultra-dense deployment of FCBSs' buildings, given that the co-channel interference effect from neighboring buildings is insignificant, and in either case, the validity of the proposed resource reuse strategies within a building will not be affected.

B. Path loss

We consider using the empirical model recommended by 3GPP for indoor FC path loss for LTE-Advanced system evaluation methodology that avoids modeling any internal walls explicitly [88, 106] to model indoor signal propagation and interference effects because of simplicity of empirical models. Note that considering either empirical or theoretical model will not affect the validity of the proposed resource reuse strategies since resource reuse pattern varies with the propagation model, i.e. a minimum distance between cFCBSs, within a building and hence will not have any effects on the generalization and originality of the proposed resource reuse strategies. In order to avoid modeling internal walls, the simplified 3GPP indoor path loss model for FCs takes into account more of shadowing effect, e.g. standard deviation of 10 dB for a link between a UE and its sFCBS and 8 dB between a UE and all other interferer links, than any other models which consider an explicit modeling of internal wall penetration losses and a shadowing standard deviation of 4 dB. This simplified 3GPP indoor path loss model for FCs has been applied considerably in the existing literature, e.g. [90, 109-112].

C. Fading effect

We do not consider any fading effect components in modeling interferences which is reasoned in the following. In indoor environments, there is a high possibility of the existence of LOS components between a UE and a BS. The indoor channel within the same local area is grossly similar as the channel's structure does not change considerably over short distances [63]. Since we consider similar structure for all apartments within a multi-floor building, all indoor channels can be assumed to experience the similar shadowing effect. Further, the small-scale channel fading occurs due to Doppler spread and delay spread effects on the channel. However, due to relatively low mobility of UEs and objects between a UE and BS, an indoor channel between a UE and BS experiences a less Doppler spread as compared to an outdoor channel which results in a large channel coherence time. Further, an indoor channel observes a less delay spread, mostly less than 100 ns, [63, 113] which results in a large channel coherence bandwidth. Since the bandwidth of most indoor devices is relatively small, indoor channels can be assumed to experience frequency flat fading [114]. Because of less delay and Doppler spreads of indoor channels, indoor channel characteristics are less susceptible to small-scale fading effects and do not change significantly within the same location area. Hence, expectantly indoor channels between FUs and cFCBSs within a building can be considered to experience approximately the same overall large-and small-scale fading effects.

By considering normalized interference power of any cFCBSs at any distances from sFU with respect to the nearest cFCBS at the minimum distance from sFU as the reference maximum interference power, the common fading effect components, i.e. small-and large-scale fading, of the links exist between sFU and a cFCBS and between sFU and the reference cFCBS cancels one another such that there is no fading component present in the normalized interference power expression of a cFCBS. Hence, considering fading effect components in the proposed model is not a necessity so that simplified expressions in the proposed model for both intra-and inter-floor interferences and a minimum distance between cFCBSs under a set of constraints can

be derived. A proof (Proof 4.3) for justification of this statement is given in Proposition 4.3.

D. Grid-based non-random placement of FCBSs

We model both intra-floor and inter-floor interferences by considering non-random placement of FCBSs at the center of square-grid based apartments. This however does not necessarily infer that the proposed model is susceptible to the random placement of FCBSs. The reason is underpinned in the followings:

1. RoE modeling

The RoE is modelled not by considering a minimum distance to enforce based on the actual physical location of cFCBSs, but by considering a minimum distance between the position of a sFU and the cell-edge boundaries (facing towards the direction of sFU) of all cFCBSs' nominal coverages of any tiers. In intra-floor modeling, these cell-edge boundaries of all cFCBSs of tier-*s*, where *s* is any arbitrary number, are the external walls with the smallest distances from sFU that separate the apartment of any cFCBSs of tier-*s* from that of its neighboring cFCBSs of tier-(*s*-1), for any optimization constraints to satisfy. The RoE is then defined by all cFCBSs of the tier-*s* such that no matter wherever any cFCBSs within its apartment is located, all cFCBSs of tier-*s* cannot be considered for reusing resources. Hence, under any optimization constraints, if the required minimum distance to enforce is found to fall within the separation distance between the external walls (i.e., walls that separate any cFCBSs of tier-*s* from that of tier-(*s*-1) and tier-(*s*+1)) of any cFCBSs' apartment, e.g. 0 m and 10 m for tier-1 cFCBSs and 10 m and 20 m for tier-2 cFCBSs (see Figure 4.2), no resource can be considered to reuse in cFCBSs of that tier, i.e. tier-1 and tier-2 respectively for the above example. This implies that irrespective of the placement of any cFCBSs within its apartment, the proposed model is not affected because of defining RoE based on a span of distance of 10 m width rather than a single point of any cFCBS's locations.

This explanation is equally applicable for inter-floor modeling where external walls by floors and tiers by floor heights, e.g. 0 m to 3 m for tier-1, 3 m to 6 m for tier-2, and tier width of 3 m are considered. Hence, the randomness in placement of FCBSs has apparently no effects on modeling a minimum distance to enforce between cFCBSs and defining the corresponding RoE. In addition, the resource reuse strategies take into account of the RoE of FCBSs as input to reuse resources in cFCBSs. Hence, the resource reuse strategies are not the function of and have nothing directly to concern with the randomness in physical placement of FCBSs. In particular, the resource scheduler schedules resources for reusing in cFCBSs only by knowing the RoE of cFCBSs. Since defining RoE is independent of the physical locations of cFCBSs, so are the resource reuse strategies.

Note that the center of an apartment is considered as the default location for a FCBS for modeling purposes, particularly to take advantages from the normalized interference expressions so that by avoiding fading effect components, simple closed form expressions for interferences can be derived. In addition, with this consideration, both the dominant cFCBSs, i.e. cFCBSs in tier-1, and the sFCBS are located at the same distance from the worst location of sFU such that the weakest desired signal and the strongest interference signal powers received at sFU can be considered to carry out the worst case scenario modeling and analysis for interferences, minimum distance enforcements, and resource reuse strategies. Certainly, the default location of any FCBSs can be considered at any other locations within an apartment than the center one. However, this will cause interference expressions to be complex because of appearing more variables in the expressions, e.g. the distance between the sFCBS and sFU and the distances between each cFCBS and sFU of any tiers.

2. Average interference statistics

Considering that the average interference statistics over all FCBSs in the building remain the same, random placements of CSG FCBSs can also be analyzed using the proposed model. The reason can be underpinned by the fact that given a total number of FCBSs per building, moving a FCBS towards neighboring FCBSs cause an

increase in interference between them, however that also results in a corresponding decrease in interference between the FCBS and other FCBSs located opposite to the direction of movement such that the aggregate interference from all neighboring FCBSs do not change considerably. Since in the proposed model, a minimum distance is enforced based on an optimization constraint, setting an appropriate constraint value and making it adaptive over time based on interference statistics, the proposed model can easily address any variations in interference statistics.

3. FC access modes and deployment strategies of operators

FCs are available in three modes, namely CSG, open access mode, and hybrid mode of the first two. Typically, CSG FCBSs are deployed randomly by end users, whereas open access FCs are deployed following a regular pattern by network operators. Usually, network operators do open access FCs a favor to provide access to as many users as possible, whereas end users do CSG FCs a favor to restrict access to a set of subscribed users. However, as mentioned in [115], in addition to residential environments, open access FCs can be deployed in public places such as markets, hotspots, and stations to replace PCs because of low cost and ease of implementation of FCBSs. Operators such as SoftBank Mobile [115] decided to use open access FCs to serve indoor users. Further in developing countries, users may not be willing to deploy FCs on their own expenses, and network operators are expected to deploy open access FCs in indoor environments to provide high indoor data rate. Additionally, in urban environments, to reduce gap in quality-of-service between cell-edge cellular users and FC users at the cell edge boundary of a large cell and provide a high capacity uniformly network wide, network operators can deploy open access FCs within buildings. Hence, network operators can use our proposed model to improve network spectral efficiency and capacity as much as possible.

4. Guidelines by operators

Given a set of guidelines by operators, including location and transmit power of a FCBS within an apartment, CSG FCBSs can also be deployed by end users following the square-grid pattern.

5. Compliance with assumptions and existing works

We assume that all FCBSs have the same transmit power with an omnidirectional radiation pattern which is compliant with the physical placement of all FCBSs at the center of their apartments in the proposed square-grid model. Further, a number of existing works such as [99], [116] also considered grid based modeling of BSs where BSs are considered to place at the center of its coverage. All receivers are partitioned in inner receiver grids into a number of disjoint cells as evenly as possible such that each cell approximates the coverage area served by its BS.

4.2.3 Interference modeling

We consider normalization of the interference power for modeling both intra-floor and inter-floor interferences to simplify interference power expressions for deriving their closed form solutions and easy of analyses such that in line with [117-118], the normalized interference power is defined as the ratio of the interference power received from any cFCBSs of any tiers at sFU to the interference power received from a cFCBS closest to the sFU, i.e. at the minimum distance, $d_{\min} = 5\,\text{m}$ for intra-floor and at the minimum vertical distance $d_{ver} = 3\,\text{m}$ for inter-floor interferences as shown in Figures 4.2 and 4.3 respectively. The interference power from each cFCBS is normalized such that $\forall \psi\ \alpha_{\psi} \in [0,1] : \alpha_1 = \alpha_2 =, \ldots, = \alpha_{\psi_m} = \alpha_{tra}$ for intra-floor and $\forall \psi\ \alpha_{\psi} \in [0,1] : \alpha_1 = \alpha_2 =, \ldots, = \alpha_{\psi_m} = \alpha_{ter}$ for inter-floor interference power received from any cFCBSs ψ of any tiers, where ψ_m denotes the maximum number of cFCBSs per tier.

A. Intra-floor interference modeling

Based on the above explanation for the normalized interference power, the normalized aggregate intra-floor interference power at sFU can be expressed as

$$\alpha_{agg,tra} = \sum_{\psi=1}^{\psi_m} 1_{r_\psi}(\alpha_\psi)\,\alpha_\psi \tag{4.1}$$

where $r_\psi \in \{\alpha_1, \alpha_2, \alpha_3, ..., \alpha_{\psi_m}\}$, and $1(\cdot)$ defines that $1(\cdot)=1$ if α_ψ exists in the set r_ψ for any ψ, otherwise $1(\cdot)=0$.

Proposition 4.1: *Using the 3GPP indoor path loss model of FCBSs [88, 106] and considering the interference effect of first-tier cFCBSs and a maximum transmit power of 20 dBm of any FCBSs, the normalized value of intra-floor interference power at an arbitrary distance d_{tra} from a cFCBS at sFU is given by*

$$\alpha_{tra}(d_{tra}) = (d_{\min}/d_{tra})^3 \tag{4.2}$$

Proof 4.1: We consider to model co-channel interference power of a cFCBS at an arbitrary distance d_{tra} as the power received by sFU using the 3GPP indoor path loss model of FCBSs for LTE-Advanced system evaluation methodology that avoids modeling any internal walls explicitly [88, 106]. For a transmit power P_t of a FCBS in dBm and path loss $\mathrm{PL}(d_{tra})$ in dB at distance d_{tra} in m, co-channel interference power from a cFCBS at sFU is given by (dBm)

$$\alpha_{c,tra}(d_{tra}) = P_t - \mathrm{PL}(d_{tra}) = 20 - (127 + 30\log_{10}(d_{tra}/1000))$$

$$\alpha_{c,tra}(d_{tra}) = -(107 + 30\log_{10}(d_{tra}/1000))$$

$$\alpha_{c,tra}(d_{tra}) = 10^{-(107+30\log_{10}(d_{tra}/1000)/10)}$$

$$\alpha_{c,tra}(d_{tra}) = 10^{-(10.7+3\log_{10}(d_{tra}/1000))}$$

We consider only the first tier of cFCBSs with respect to a sFCBS. The maximum value of co-channel interference $\alpha_{\max,tra}(d_{tra})$ from a cFCBS attains when

the distance between sFU and a cFCBS $d_{tra} = d_{\min}$ such that $\alpha_{\max,tra}(d_{\min}) = 10^{-(10.7+3\log_{10}(d_{\min}/1000))}$ where $d_{\min}$ is the distance between sFCBS and sFU, which is also the minimum (reference) distance of any cFCBSs and sFU. Hence, the normalized value of intra-floor interference from a cFCBS at sFU $\alpha_{tra}(d_{tra})$ can be expressed as

$$\alpha_{tra}(d_{tra}) = \alpha_{c,tra}(d_{tra}) / \alpha_{\max,tra}(d_{tra})$$

$$\alpha_{tra}(d_{tra}) = 10^{(-10.7-3\log_{10}(d_{tra}/1000)+10.7+3\log_{10}(d_{\min}/1000))}$$

$$\alpha_{tra}(d_{tra}) = 10^{(3\log_{10}(d_{\min}/d_{tra}))}$$

$$\alpha_{tra}(d_{tra}) = 10^{\log_{10}(d_{\min}/d_{tra})^3}$$

$$\alpha_{tra}(d_{tra}) = (d_{\min}/d_{tra})^3$$

$$\alpha_{tra,dB}(d_{tra}) = 3\log_{10}(d_{\min}/d_{tra}) \quad \blacksquare$$

Figure 4.5 shows $\alpha_{tra}(d_{tra})$ as a function of d_{tra}. Let $P_{r,tra} = 1$ denote the normalized desired received signal power at a sFU and $n_p \in [0, 1]$ denote normalized noise power. The signal-to-interference-plus-noise-ratio at sFU can be expressed as

$$\rho_{tra} = P_{r,tra} \Big/ \left(\sum_{\psi=1}^{\psi_m} 1_{r_\psi}(\alpha_\psi)\alpha_\psi + n_p \right)$$

In the worst case, $\psi_m = 8$ such that

$$\rho_{tra} = P_{r,tra} \Big/ \left(\sum_{\psi=1}^{8} \alpha_\psi + n_p \right) = P_{r,tra} / (8\alpha_{tra} + n_p)$$

Hence, spectral efficiency at sFU can be expressed as

$$\sigma_{tra} = \log_2(1 + \rho_{tra}) \tag{4.3}$$

For a bandwidth $= \Xi_{tra}$, a link capacity at sFU is given by

$$\sigma_{tra} = \Xi_{tra} \log_2(1 + \rho_{tra}) \tag{4.4}$$

B. Inter-floor interference modeling

Modeling in-building signal propagation characteristics between floors is difficult [119]. According to [119], based on measurements, floor attenuation is not a linear function (in dB) of the number of floors separating a BS from a UE. This can be caused due to diffraction of signal energy along sides of the building itself and scattered energy from neighboring buildings received at different floors of the building [120]. The greatest attenuation occurs when a BS and a UE are at a single floor apart. The overall attenuation with an increase in the number of floors increases at a smaller rate. Hence, we capture this variation of signal attenuation with distance d_{ter} from one floor to another (i.e., inter-floor) by an additional adjustable attenuation factor (in dB) $\alpha_f(d_{ter})$ to the intra-floor interference model. d_{ter} of a cFCBS from sFU can be expressed as $d_{ter} = \sqrt{d_{\min}{}^2 + d_{ver}{}^2}$ where d_{ver} is the vertical distance between sFCBS and any cFCBSs on a floor other than that of sFCBS. To be consistent with the intra-floor interference modeling, we consider all other parameters the same as in the case of intra-floor modeling, however with an addition of $\alpha_f(d_{ter})$ such that inter-floor interference power is given by

$$\alpha_{c,ter}(d_{ter}) = -\left(107 + \log_{10}\left(d_{ter}/1000\right)\right) + \alpha_f(d_{ter}) \tag{4.5}$$

Since we consider an isolated building, $\alpha_f(d_{ter})$ is modeled following the second approach of indoor propagation modeling as mentioned earlier, i.e. without considering effects of nearby buildings. In [120], authors also did not consider effects of nearby buildings except signals through-floor and diffraction for a building. Measurements were made for up to 11 floors separating the transmitter and the receiver. As reported in [120], the measured signal decreases by about 12 dB per floor for the first 6 floors, i.e. n_{fl} = 1 to 6, of separation and an average of 1.35 dB per floor for n_{fl} = 7 to 12. The effect of diffracted signal components was found insignificant as compared to the component through floors, which was also reported by [65]. Since the overall response of these component signals is not linear with the number of floors, the variation in $\alpha_f(d_{ter})$ is modeled by using the measured penetration losses as reported by [120] for

up to the number of floors n_{fl} = 12 in this chapter and is given in Table 4.1 where for n_{fl} = 13 and beyond, a random value [0, 1] in dB is considered. The model is consistent with the measurement or empirical models in [121] where the average floor attenuation factor was reported as non-linear function of the number of floors between the transmitter and receiver.

Table 4.1: Adjustable attenuation factor for inter-floor penetration loss.

Number of floors (n_{fl})	1 - 6	6 - 12	13 - beyond
$\alpha_f(d_{ter})$ (dB/floor)	12	1.35	[0, 1]

Proposition 4.2: *Using the same conditions as in Proposition 4.1 and a floor attenuation factor* $\alpha_f(d_{ter})$*, the normalized value of inter-floor interference power for an arbitrary distance* d_{ter} *from a cFCBS located on a floor other than that of sFCBS at sFU is given by*

$$\alpha_{ter}(d_{ter}) = 10^{-(0.1\alpha_f(d_{ter}))}\left(d_{\min}/d_{ter}\right)^3 \tag{4.6}$$

Proof 4.2: From (4.5), $\alpha_{c,ter}(d_{ter})$ in absolute value can be expressed as

$$\alpha_{c,ter}(d_{ter}) = 10^{-\left(10.7+3\log_{10}\left(d_{ter}/1000\right)+\alpha_f(d_{ter})/10\right)}$$

The normalized received power at sFU can be expressed as

$$P_{r,ter}(d_{ter} = d_{\min}) = 10^{-\left(10.7+3\log_{10}\left(d_{\min}/1000\right)\right)}$$

Hence, the normalized co-channel interference power $\alpha_{ter}(d_{ter})$ from any cFCBSs on any floors other than the floor of sFU can be expressed as

$$\alpha_{ter}(d_{ter}) = \alpha_{c,ter}(d_{ter})/P_{r,ter}(d_{ter})$$

$$\alpha_{ter}(d_{ter}) = 10^{\left(-10.7-3\log_{10}(d_{ter}/1000)-\alpha_f(d_{ter})/10+10.7+3\log_{10}(d_{\min}/1000)\right)}$$

$$\alpha_{ter}(d_{ter}) = 10^{\left(3\log_{10}(d_{\min}/d_{ter})-\alpha_f(d_{ter})/10\right)}$$

$$\alpha_{ter}(d_{ter}) = 10^{\left(\log_{10}(d_{\min}/d_{ter})\right)^3} \times 10^{-(\alpha_f(d_{ter})/10)}$$

$$\alpha_{ter}(d_{ter}) = 10^{-(0.1\alpha_f(d_{ter}))} (d_{\min}/d_{ter})^3$$

$$\alpha_{ter,dB}(d_{ter}) = -0.1\alpha_f(d_{ter}) + 3\log_{10}(d_{\min}/d_{ter}) \quad \blacksquare$$

In (4.6), an additional factor $10^{-(0.1\alpha_f(d_{ter}))}$ appears in comparison with (4.2). The inter-floor interference power given by (4.6) in dB $\alpha_{ter,dB}(d_{ter})$ is evaluated numerically in comparison with the intra-floor interference power given by (4.2) in dB $\alpha_{tra,dB}(d_{tra})$ and is shown in Figure 4.5. From Figure 4.5, it can be found that the normalized interference powers of intra-floor as well as inter-floor (with no floor attenuation effect) vary linearly with distance. The inter-floor interference power decays considerably faster with distance as compared to the intra-floor interference power because of an additional floor attenuation effect. Note that the characteristic responses of the normalized interference powers in absolute values show an exponential decay with distance, which is obvious from either (4.2) for $\alpha_{tra}(d_{tra})$ or (4.6) for $\alpha_{ter}(d_{ter})$. Further, for inter-floor interference modeling, the distance on *x* axis in Figure 4.5 represents d_{ver}. However, the response of inter-floor interference is shown for the corresponding value of $d_{ter} = \sqrt{d_{\min}{}^2 + d_{ver}{}^2}$ to each value of d_{ver}. Hence, for low values of d_{ver} in comparison with $d_{\min} = 5$, d_{ter} is dominated by $d_{\min}$. However, as the value of d_{ver} increases substantially, d_{ter} is mainly dominated by d_{ver}. This can be found in Figure 4.5 where for low values of d_{ver}, the inter-floor interference power response (without floor attenuation effect) shows slightly sloppy, and becomes almost straight line for high values of d_{ver}.

Since the minimum distance between a sFU and a cFCBS in intra-floor level is $d_{\min} = 5\,\text{m}$ and in inter-floor level is $d_{ver} = 3\,\text{m}$, and the maximum values of both interference powers occur at these minimum distances as shown in Figure 4.5. Note also that the floor attenuation loss $\alpha_f(d_{ter})$ for a received signal is not fixed and is non-uniform which varies based on the number of floors between a transmitter and a

receiver. $\alpha_f(d_{ter})$ has typically a burst effect on the propagating signals while penetrating through any floors and is absent between any two consecutive floors. This can be observed in Figure 4.5 where between any two consecutive floors, the floor attenuation effect remains fixed, and the distance dependent path loss exists. However, the floor attenuation effect is substantial across each floor width, particularly for the first 6 floors of separation between a transmitter and a receiver (Table 4.1).

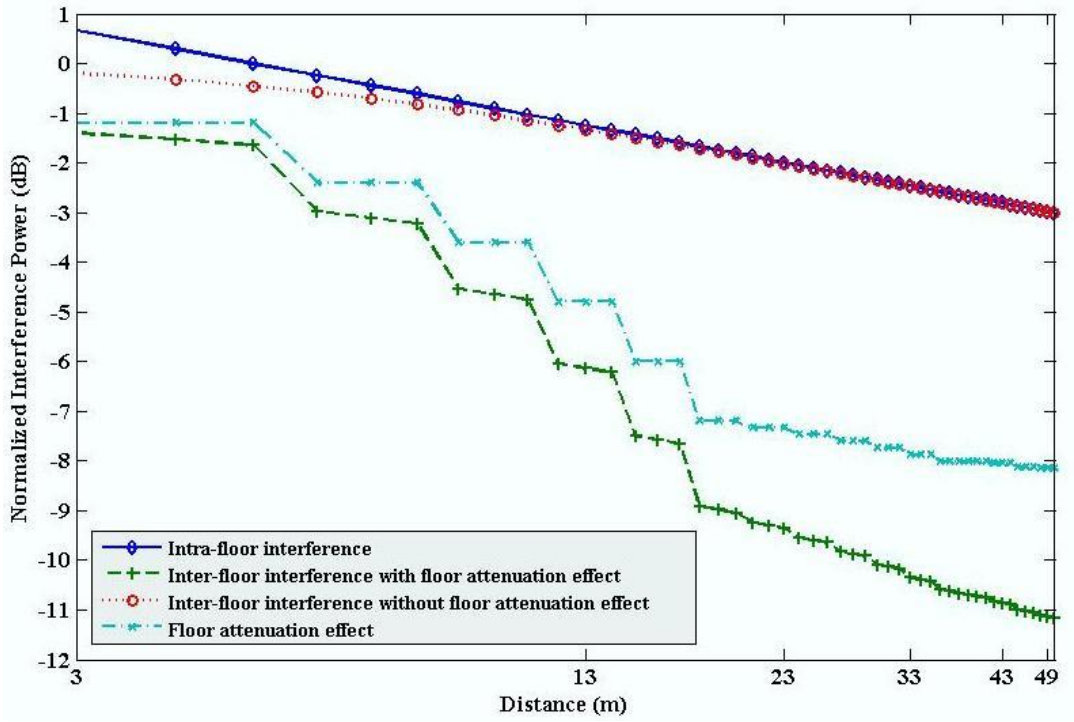

Figure 4.5: Normalized intra-floor and inter-floor interference powers (in dB) with distance for a single cFCBS at a sFU.

Proposition 4.3: *Considering fading effect components in the proposed model is not a necessity so that simplified expressions in the proposed model for both intra-and inter-floor interferences and a minimum distance between cFCBSs under a set of constraints can be derived.*

Proof 4.3: To justify this concern, we study the Proposition 4.1 by considering the small-scale fading $\gamma_{s,i}$ and large-scale shadowing effect $\gamma_{l,i}$ per co-channel interference link. Using the 3GPP indoor path loss model of FCBSs for LTE-Advanced

system evaluation methodology that avoids modeling any internal wall explicitly [88, 106], and following the same conditions as in Proof 4.1, the co-channel interference power from a cFCBS at sFU is given by (dBm)

$$\begin{aligned}\alpha_{c,tra}(d_{tra}) &= P_t - \mathrm{PL}(d_{tra}) + \gamma_{s,i} + \gamma_{l,i} \\ &= 20 - (127 + 30\log_{10}(d_{tra}/1000)) + \gamma_{s,i} + \gamma_{l,i}\end{aligned}$$

Following Proof 4.1, the above expression can be written as

$$\alpha_{c,tra}(d_{tra}) = 10^{-(10.7+3\log_{10}(d_{tra}/1000)-0.1(\gamma_{s,i}+\gamma_{l,i}))}$$

Considering that indoor channels between sFU and any cFCBSs experience approximately the same fading effects, the maximum value of co-channel interference $\alpha_{\max,tra}(d_{tra})$ from a cFCBS attains when the distance between sFU and a cFCBS $d_{tra} = d_{\min}$ such that

$$\alpha_{\max,tra}(d_{\min}) = 10^{-(10.7+3\log_{10}(d_{\min}/1000)-0.1(\gamma_{s,i}+\gamma_{l,i}))}$$

where $d_{\min}$ is the distance between a sFCBS and its sFU, which is also the minimum (reference) distance of any cFCBSs and sFU. Hence, the normalized value of intra-floor interference from a cFCBS at sFU $\alpha_{tra}(d_{tra})$ can be expressed as

$$\alpha_{tra}(d_{tra}) = \alpha_{c,tra}(d_{tra}) / \alpha_{\max,tra}(d_{\min})$$

$$\alpha_{tra}(d_{tra}) = 10^{(-10.7-3\log_{10}(d_{tra}/1000)+0.1(\gamma_{s,i}+\gamma_{l,i})+10.7+3\log_{10}(d_{\min}/1000)-(\gamma_{s,i}+\gamma_{l,i}))}$$

$$\alpha_{tra}(d_{tra}) = 10^{(3\log_{10}(d_{\min}/d_{tra}))}$$

$$\alpha_{tra}(d_{tra}) = 10^{\log_{10}(d_{\min}/d_{tra})^3}$$

$$\alpha_{tra}(d_{tra}) = (d_{\min}/d_{tra})^3$$

which is the same as in Proof 4.1. Hence, the model is independent of the small-scale and large-scale fading effects. ■

4.3 Approaches for enforcing a minimum distance

In a 3D multi-floor building, since cFCBSs are present in both intra-floor and inter-floor levels as shown in Figure 4.4, the total aggregate interference power at sFU is given by

$$\alpha_{agg,tot} = \alpha_{agg,ter} + \alpha_{agg,tra} \tag{4.7}$$

$$\alpha_{agg,tot} = 10^{-(\alpha_f(d_{ter})/10)} y_{\max,ter} \left(d_{\min}/d_{ter}\right)^3 + y_{\max,tra} \left(d_{\min}/d_{tra}\right)^3$$

where $\alpha_{agg,tra}$ and $\alpha_{agg,ter}$ denote respectively an aggregate interference power of intra-floor and inter-floor cFCBSs received at sFU.

Proposition 4.4: *Let* $\alpha_{thr,tra}, \alpha_{thr,ter}$, *and* $\alpha_{thr,tot}$ *respectively denote intra-floor interference, inter-floor interference, and total interference power constraints at sFU. If* $\alpha_{agg,ter} \le \alpha_{thr,ter}$ *and* $\alpha_{agg,tra} \le \alpha_{thr,tra}$, *then* $\alpha_{agg,ter} + \alpha_{agg,tra} \le \alpha_{thr,ter} + \alpha_{thr,tra}$.

Proof 4.4: Consider that $\alpha_{agg,tot}$ is constrained such that at sFU $\alpha_{agg,tot} \le \alpha_{thr,tot}$, and hence $\alpha_{agg,ter} + \alpha_{agg,tra} \le \alpha_{thr,tot}$.

Since $\alpha_{thr,ter} + \alpha_{thr,tra} = \alpha_{thr,tot}$

$\alpha_{agg,ter} + \alpha_{agg,tra} \le \alpha_{thr,ter} + \alpha_{thr,tra}$

Hence, for $\alpha_{agg,ter} \le \alpha_{thr,ter}$ and $\alpha_{agg,tra} \le \alpha_{thr,tra}$, the above condition must satisfy. ■

To find a minimum value of d_{tra} and d_{ter}, we separate the problem into two sub-problems where sub-problem 1 is for finding a solution of d_{tra} intra-floor level and sub-problem 2 is for finding a solution of d_{ter} inter-floor level.

Sub-problem 1:

minimize d_{tra}

subject to $\alpha_{agg,tra} \le \alpha_{thr,tra}$

$P_t \le P_{t,\max}$

Sub-problem 2:

minimize d_{ter}

subject to $\alpha_{agg,ter} \le \alpha_{thr,ter}$

$P_t \le P_{t,\max}$

To ensure that solutions from sub-problems 1 and 2 will be satisfied by the total interference requirement that must not exceed a tolerable value $\alpha_{thr,tot}$, we set $\alpha_{thr,ter} + \alpha_{thr,tra} \leq \alpha_{thr,tot}$.

Since spectral efficiency and link capacity are also functions of interference, sub-problems 1 and 2 for these constraints can also be formed following the above-mentioned approach. Hence, we propose three approaches to find a minimum distance between cFCBSs for both intra-floor and inter-floor interference scenarios based on how constraint sets are developed, namely interference, spectral efficiency, and link capacity constraints. The first two approaches are generic and independent of the number of reused RBs in a cFCBS, whereas the third approach considers the impact of varying the number of reused RBs in a cFCBS which we show in the following. Derivations of optimal minimum distances d^*_{tra} and d^*_{ter} respectively for intra-floor and inter-floor levels under each approach are performed in the following. For each approach, we assume that all FCBSs operate at the same maximum transmit power $P_t = P_{t,\max}$.

4.3.1 Approach 1: interference constraint

A. Intra-floor level

In this approach, an optimal solution for a minimum distance d^*_{tra} to reuse resources in cFCBSs intra-floor level is derived by constraining sub-problem 1 with an aggregate interference power constraint $\alpha_{thr,tra}$. An increase in $\alpha_{thr,tra}$ results in the more reuse of the same set of RBs Ξ_{tra} of system bandwidth and vice versa. Although more reuse of resources causes overall capacity to increase proportionally, an increase in $\alpha_{thr,tra}$ causes at the same time to decrease overall capacity logarithmically as given by Shannon's capacity formula. Hence, a trade-off between Ξ_{tra} and $\alpha_{thr,tra}$ is to be considered such that $\alpha_{thr,tra}$ can provide an optimal maximum capacity at a minimal

separation distance d_{tra}^{*} which can be found by solving the following optimization problem.

$$\begin{aligned} &\text{minimize} && d_{tra} \\ &\text{subject to} && \alpha_{agg,tra} \le \alpha_{thr,tra} \\ & && P_t \le P_{t,\max} \end{aligned}$$

The solution of the above optimization problem d_{tra}^{*} is given by

$$d_{tra}^{*} \ge d_{\min}\left(y_{\max,tra}/\alpha_{thr,tra}\right)^{1/3} \tag{4.8}$$

Proof 4.5: Since we are interested in the worst case scenario, we consider the maximum number of intra-floor cFCBSs, i.e. $y_{tra} = y_{\max,tra} = 8$. Hence using (4.2), the maximum aggregate interference power at sFU can be expressed as

$$\alpha_{\max,tra} = y_{\max,tra}\left(d_{\min}/d_{tra}\right)^{3}$$

However, $\alpha_{\max,tra} \le \alpha_{thr,tra}$ such that $\alpha_{\max,tra} = y_{\max,tra}\left(d_{\min}/d_{tra}\right)^{3} \le \alpha_{thr,tra}$

The above condition is satisfied when $d_{tra} = d_{tra}^{*}$ such that

$$y_{\max,tra}/\alpha_{thr,tra} \le \left(d_{tra}^{*}/d_{\min}\right)^{3}$$

Solving for d_{tra}^{*} yields, $d_{tra}^{*} \ge d_{\min}\left(y_{\max,tra}/\alpha_{thr,tra}\right)^{1/3}$ ■

From (4.8), it can be found that d_{tra}^{*} is independent of Ξ_{tra}, and so is aggregate interference at sFU (see (4.2)). Any numbers of RB can be reused in cFCBSs which are located at distances at least $d_{tra} = d_{tra}^{*}$ from one another.

B. Inter-floor level

Following the same procedure as that applied for intra-floor level, a minimum distance d_{ter}^{*} is derived for an inter-floor interference power constraint $\alpha_{thr,ter}$ at sFU. Hence, applying the inter-floor interference modeling, a minimum distance between

cFCBSs d_{ter}^{*} for reusing resources in cFCBSs inter-floor level can be found by solving the following optimization problem.

$$\begin{aligned} &\text{minimize} && d_{ter} \\ &\text{subject to} && \alpha_{agg,ter} \le \alpha_{thr,ter} \\ & && P_t \le P_{t,\max} \end{aligned}$$

The solution for d_{ter}^{*} of the above optimization problem is given by

$$d_{ter}^{*} \ge d_{\min} \left(10^{-\left(\alpha_f\left(d_{ter}^{*}\right)/10\right)} \left(y_{\max,ter} \,/\, \alpha_{thr,ter}\right)\right)^{1/3} \tag{4.9}$$

where $y_{\max,ter} = 1$ for single-sided cFCBSs, and $y_{\max,ter} = 2$ for double-sided cFCBSs.

Proof 4.6: With double-sided cFCBSs, sFU experiences co-channel interference from cFCBSs on its both sides, one on top and the other on bottom floors from the serving floor such that for a given interference constraint, each cFCBS contributes $1/y_{\max,ter} = 1/2$ of the total interference constraint. The inter-floor interference power from a cFCBS can be given by

$$\alpha_{agg,ter} = 10^{-\left(\alpha_f(d_{ter})/10\right)} \left(d_{\min}/d_{ter}\right)^3$$

According to the constraint, $\alpha_{agg,ter} \le \alpha_{thr,ter}$ such that

$$\alpha_{agg,ter} = 10^{-\left(\alpha_f(d_{ter})/10\right)} \left(d_{\min}/d_{ter}\right)^3 \le \alpha_{thr,ter}/y_{\max,ter}$$

The above condition is satisfied when $d_{ter} = d_{ter}^{*}$ such that

$$10^{-\left(\alpha_f\left(d_{ter}^{*}\right)/10\right)} \left(y_{\max,ter}/\alpha_{thr,ter}\right) \le \left(d_{ter}^{*}/d_{\min}\right)^3$$

Solving for d_{ter}^{*}, $d_{ter}^{*} \ge d_{\min} \left(10^{-\left(\alpha_f\left(d_{ter}^{*}\right)/10\right)} \left(y_{\max,ter} \,/\, \alpha_{thr,ter}\right)\right)^{1/3}$ ■

Hence, RB resources can be reused in a cFCBS for both single-and double-sided cFCBSs located at distance $d_{ter} \ge d_{ter}^{*}$ from the location of sFU. Since interference power constraint per cFCBS is decreased for double-sided cFCBSs, d_{ter}^{*} requirement is increased accordingly as can be found from (4.9).

4.3.2 Approach 02: spectral efficiency constraint

A. Intra-floor level

Rather than solving an indirect optimization problem by considering an interference constraint as in approach 1, in this approach, a link level spectral efficiency constraint is considered. This is because of the fact that a link capacity is directly proportional to its link spectral efficiency, which is a logarithmic function of the aggregate interference that the link experiences. Hence, a direct optimization problem for a minimum distance can be solved by a spectral efficiency constraint such that the optimization problem can be expressed as

$$\begin{aligned} &\text{minimize} && d_{tra} \\ &\text{subject to} && \sigma_{tra,se} \geq \sigma_{thr,se} \\ & && P_t \leq P_{t,\max} \end{aligned}$$

where $\sigma_{thr,se}$ denotes spectral efficiency constraint which is upper limited by 4.4 bps/Hz for a link signal-to-interference-plus-noise-ratio $\rho_{tra} \geq 22\,\text{dB}$. The value of $\sigma_{thr,se} = 0$ to 4.4 bps/Hz depends on network performance requirements. The solution of the above problem for an interference limited scenario, i.e. $\alpha_{agg,tra} >> n_p$, is given by

$$d_{tra}^{*} \geq d_{\min}\left(y_{\max,tra}\left(2^{\sigma_{thr,se}} - 1\right)\right)^{1/3} \tag{4.10}$$

Proof 4.7: Intra-floor link capacity σ_{tra} can be expressed as

$$\sigma_{tra} = \Xi_{tra}\log_2\left(1 + 1/\left(\alpha_{agg,tra} + n_p\right)\right) \text{ bps}$$

$$\sigma_{tra,se} = \sigma_{tra}/\Xi_{tra} = \log_2\left(1 + 1/\left(\alpha_{agg,tra} + n_p\right)\right) \text{ bps/Hz}$$

where $\alpha_{agg,tra} = \alpha_{\max,tra} = y_{\max,tra}\left(d_{\min}/d_{tra}\right)^3$.

However, $\sigma_{tra,se} \geq \sigma_{thr,se}$ which is satisfied when $d_{tra} \geq d_{tra}^{*}$.

Hence, $\log_2\left(1 + 1/\left(\alpha_{agg,tra} + n_p\right)\right) \geq \sigma_{thr,se}$

$$\log_2\left(1+1/\left(y_{\max,tra}\left(d_{\min}/d^*_{tra}\right)^3+n_p\right)\right)\geq \sigma_{thr,se}$$

$$1+1/\left(y_{\max,tra}\left(d_{\min}/d^*_{tra}\right)^3+n_p\right)\geq 2^{\sigma_{thr,se}}$$

$$y_{\max,tra}\left(d_{\min}/d^*_{tra}\right)^3 \leq 1/\left(2^{\sigma_{thr,se}}-1\right)-n_p$$

$$\left(d^*_{tra}/d_{\min}\right)^3 \geq \left[y_{\max,tra}\left(2^{\sigma_{thr,se}}-1\right)\right]/\left[1-n_p\left(2^{\sigma_{thr,se}}-1\right)\right]$$

$$d^*_{tra}\geq d_{\min}\left[y_{\max,tra}\left(2^{\sigma_{thr,se}}-1\right)/\left(1-n_p\left(2^{\sigma_{thr,se}}-1\right)\right)\right]^{1/3}$$

For $\alpha_{agg,tra} >> n_p$, the above expression can be rewritten as

$$d^*_{tra}\geq d_{\min}\left(y_{\max,tra}\left(2^{\sigma_{thr,se}}-1\right)\right)^{1/3}$$ ■

B. Inter-floor level

Similar to intra-floor level, the optimization problem for inter-floor interference can be expressed as follows

$$\begin{aligned} &\text{minimize} && d_{ter} \\ &\text{subject to} && \sigma_{ter,se}\geq\sigma_{thr,se} \\ & && P_t\leq P_{t,\max} \end{aligned}$$

The solution of the problem for $\alpha_{agg,ter} >> n_p$ is given by

$$d^*_{ter}\geq d_{\min}\left(10^{-\left(0.1\alpha_f\left(d^*_{ter}\right)\right)}y_{\max,ter}\left(2^{\sigma_{thr,se}}-1\right)\right)^{1/3} \tag{4.11}$$

where $y_{\max,ter}=1$ for single-sided cFCBSs, and $y_{\max,ter}=2$ for double-sided cFCBSs.

Proof 4.8: Inter-floor link capacity σ_{ter} can be expressed as

$$\sigma_{ter}=\Xi_{ter}\log_2\left(1+1/\left(\alpha_{agg,ter}+n_p\right)\right)\text{ bps}$$

$$\sigma_{ter,se}=\sigma_{ter}/\Xi_{ter}=\log_2\left(1+1/\left(\alpha_{agg,ter}+n_p\right)\right)\text{ bps/Hz}$$

where $\alpha_{agg,ter}=\alpha_{\max,ter}=10^{-\left(0.1\alpha_f\left(d_{ter}\right)\right)}\,y_{\max,ter}\left(d_{\min}/d_{ter}\right)^3$

The condition $\sigma_{ter,se} \geq \sigma_{thr,se}$ is satisfied when $d_{ter} \geq d_{ter}^{*}$ .Hence,

$$\log_2\left(1+1/\left(\alpha_{agg,ter}+n_p\right)\right) \geq \sigma_{thr,se}$$

$$\log_2\left(1+1/\left(10^{-\left(0.1\alpha_f\left(d_{ter}\right)\right)} y_{\max,ter}\left(d_{\min}/d_{ter}^{*}\right)^3+n_p\right)\right) \geq \sigma_{thr,se}$$

$$10^{-\left(0.1\alpha_f\left(d_{ter}\right)\right)} y_{\max,ter}\left(d_{\min}/d_{ter}^{*}\right)^3 \leq 1/\left(2^{\sigma_{thr,se}}-1\right)-n_p$$

Solving for d_{ter}^{*}, $d_{ter}^{*} \geq d_{\min}\left[10^{-\left(0.1\alpha_f\left(d_{ter}^{*}\right)\right)} y_{\max,ter}\left(2^{\sigma_{thr,se}}-1\right)/\left(1-n_p\left(2^{\sigma_{thr,se}}-1\right)\right)\right]^{1/3}$

For $\alpha_{agg,ter} >> n_p$, $d_{ter}^{*} \geq d_{\min}\left(10^{-\left(0.1\alpha_f\left(d_{ter}^{*}\right)\right)} y_{\max,ter}\left(2^{\sigma_{thr,se}}-1\right)\right)^{1/3}$ ■

4.3.3 Approach 03: link capacity constraint

A. Intra-floor level

Approaches 1 and 2 use link quality in terms of link signal-to-interference-plus-noise-ratio and link spectral efficiency and are independent of reused RBs in cFCBSs. However, capacity is a product of two terms, bandwidth and link quality and is varied linearly with the former and logarithmically with the later. Hence, we can exploit the effect of reused RBs to find a minimum distance. The main feature of this approach is that a minimum distance and hence the number of times of reusing resources for a set of cFCBSs can be made adaptive by varying the number of reused RBs in each cFCBS on top of varying either signal-to-interference-plus-noise-ratio or link spectral efficiency. We use Shannon's capacity formula directly to address a direct optimization problem to be solved such that bandwidth resources in terms of RBs can be considered to reuse in each cFCBS so long as the product of the link quality and the number of reused RBs at least equals to a predefined link capacity constraint. Note that the effect of reusing an RB in a cFCBS causes to create the maximum of 8 co-channel interferers per tier.

We consider only the effect of tier-1 co-channel interference since the interference effects from tier-2 and above are negligible because of considerably a long enough distance of any cFCBSs of those tiers from sFU. Let Ξ_{tra}^{wr} denote the number of

RBs to be reused in a cFCBS. Since there are at most $y_{\max,tra}$ cFCBSs in any tiers with respect to sFCBS, any reuses of Ξ_{tra}^{wr} causes an additional aggregate interference power $\alpha_{\max,tra}$ from $y_{\max,tra}$ cFCBSs. Note that a sFCBS is also a cFCBS when a minimum distance between cFCBSs is enforced. Hence, a minimum distance between cFCBSs is to be derived such that a decrease in capacity of a cFCBS because of $\alpha_{\max,tra}$ and an increase in capacity because of reusing Ξ_{tra}^{wr} number of RBs in it satisfy the link capacity constraint denoted by $\sigma_{thr,tra}$. A minimum distance can be obtained by solving the following optimization problem

$$\begin{aligned} &\text{minimize} && d_{tra} \\ &\text{subject to} && \sigma_{tra} \geq \sigma_{thr,tra} \\ & && P_t \leq P_{t,\max} \end{aligned}$$

By solving the above optimization problem for $\alpha_{agg,tra} >> n_p$, an optimal solution for d_{tra}^* is given by

$$d_{tra}^* \geq d_{\min}\left(y_{\max,tra}\left(2^{\sigma_{thr,tra}/\Xi_{tra}^{wr}}-1\right)\right)^{1/3} \tag{4.12}$$

Proof 4.9: The capacity from reusing Ξ_{tra}^{wr} RBs in a cFCBS is given by

$$\sigma_{tra} = \Xi_{tra}^{wr}\log_2\left(1+\left(1/\left(\alpha_{agg,tra}+n_p\right)\right)\right)$$

$$\sigma_{tra} = \Xi_{tra}^{wr}\log_2\left(1+\left(1/\left(y_{\max,tra}\left(d_{\min}/d_{tra}\right)^3+n_p\right)\right)\right)$$

According to the constraint, which satisfies when $d_{tra} \geq d_{tra}^*$, such that

$$\sigma_{tra} = \Xi_{tra}^{wr}\log_2\left(1+\left(1/\left(y_{\max,tra}\left(d_{\min}/d_{tra}^*\right)^3+n_p\right)\right)\right) \geq \sigma_{thr,tra}$$

$$\log_2\left(1+\left(1/\left(y_{\max,tra}\left(d_{\min}/d_{tra}^*\right)^3+n_p\right)\right)\right) \geq \sigma_{thr,tra}/\Xi_{tra}^{wr}$$

$$1/\left(y_{\max,tra}\left(d_{\min}/d_{tra}^*\right)^3+n_p\right) \geq 2^{\left(\sigma_{thr,tra}/\Xi_{tra}^{wr}\right)}-1$$

$$y_{\max,tra}\left(d_{\min}/d_{tra}^*\right)^3 \leq 1/\left(2^{\sigma_{thr,tra}/\Xi_{tra}^{wr}}-1\right)-n_p$$

$$\left(d_{tra}^*/d_{\min}\right)^3 \geq \left\lfloor y_{\max,tra}\left(2^{\sigma_{thr,tra}/\Xi_{tra}^{wr}}-1\right)\right\rfloor / \left[1-n_p\left(2^{\sigma_{thr,tra}/\Xi_{tra}^{wr}}-1\right)\right]$$

$$d_{tra}^{*} \geq d_{\min}\left[y_{\max,tra}\left(2^{\sigma_{thr,tra}/\Xi_{tra}^{wr}}-1\right)\Big/\left(1-n_p\left(2^{\sigma_{thr,tra}/\Xi_{tra}^{wr}}-1\right)\right)\right]^{1/3}$$

For $\alpha_{agg,tra} >> n_p$, $d_{tra}^{*} \geq d_{\min}\left(y_{\max,tra}\left(2^{\sigma_{thr,tra}/\Xi_{tra}^{wr}}-1\right)\right)^{1/3}$ ■

In the above equation, the minimum distance considers both the effects of co-channel interference in terms of $y_{\max,tra}$ and resource reuse in terms of the number of RBs Ξ_{tra}^{wr}. The main advantage of this approach is that resource reuse does not depend much on co-channel interference statistics, rather on the availability of Ξ_{tra}^{wr}. Even with a significant presence of the aggregate co-channel interference, by considering more RBs Ξ_{tra}^{wr} to reuse, we can boost the overall FC network capacity which in not obvious from approaches 1 and 2, e.g. what should be an appropriate value of Ξ_{tra}^{wr} for a given interference or spectral efficiency constraint. However with approach 3, a minimum distance can be easily found for a given value of Ξ_{tra}^{wr} . Note that the number of reused RBs must be able to achieve a given capacity constraint where 1 RB is equal to 180 kHz for LTE-Advanced systems. For example, for a capacity constraint $\sigma_{thr,tra} = 5 \times 4.4$ bps, we need at least 5 RBs to be reused since the link quality is limited by 4.4 bps/Hz. So, the value of Ξ_{tra}^{wr} must be chosen according to the value of capacity constraint.

B. Inter-floor level

Similar to intra-floor level for link capacity constraint, we use Shannon's capacity formula and consider the effect of tier-1 cFCBSs' from sFU. Let Ξ_{ter}^{wr} denote the number of RBs to be reused in an inter-floor cFCBS. d_{ter}^{*} can be obtained by solving the following optimization problem such that the link capacity σ_{ter} at sFU satisfies a link capacity constraint $\sigma_{thr,ter}$.

$$\begin{aligned} &\text{minimize} && d_{ter} \\ &\text{subject to} && \sigma_{ter} \geq \sigma_{thr,ter} \\ & && P_t \leq P_{t,\max} \end{aligned}$$

Solving the above problem, an optimal solution d_{ter}^{*} inter-floor level for $\alpha_{agg,ter} >> n_p$ yields

$$d_{ter}^{*} \geq d_{\min}\left(10^{-\left(0.1\alpha_f\left(d_{ter}^{*}\right)\right)} y_{\max,ter}\left(2^{\sigma_{thr,ter}/\Xi_{ter}^{wr}}-1\right)\right)^{1/3} \tag{4.13}$$

where $y_{\max,ter}=1$ for single-sided cFCBSs, and $y_{\max,ter}=2$ for double-sided cFCBSs.

Proof 4.10: Following the similar procedure as that in intra-floor level such that the capacity from reusing Ξ_{ter}^{wr} RBs in a cFCBS inter-floor level is given by

$$\sigma_{ter}=\Xi_{ter}^{wr}\log_2\left(1+\left(1/\left(10^{-\left(0.1\alpha_f\left(d_{ter}\right)\right)} y_{\max,ter}\left(d_{\min}/d_{ter}\right)^3+n_p\right)\right)\right)$$

Hence, following the constraint such that it satisfies when $d_{ter} \geq d_{ter}^{*}$ and similar steps as in intra-floor level yields

$$\sigma_{ter}=\Xi_{ter}^{wr}\log_2\left(1+\left(1/\left(10^{-\left(0.1\alpha_f\left(d_{ter}^{*}\right)\right)} y_{\max,ter}\left(d_{\min}/d_{ter}^{*}\right)^3+n_p\right)\right)\right)\geq \sigma_{thr,ter}$$

$$\left(d_{ter}^{*}/d_{\min}\right)^3 \geq \left[10^{-\left(0.1\alpha_f\left(d_{ter}^{*}\right)\right)} y_{\max,ter}\left(2^{\sigma_{thr,ter}/\Xi_{ter}^{wr}}-1\right)\right] \Big/ \left[1-n_p\left(2^{\sigma_{thr,ter}/\Xi_{ter}^{wr}}-1\right)\right]$$

$$d_{ter}^{*} \geq d_{\min}\left[10^{-\left(0.1\alpha_f\left(d_{ter}^{*}\right)\right)} y_{\max,ter}\left(2^{\sigma_{thr,ter}/\Xi_{ter}^{wr}}-1\right)\Big/\left(1-n_p\left(2^{\sigma_{thr,ter}/\Xi_{ter}^{wr}}-1\right)\right)\right]^{1/3}$$

For $\alpha_{agg,ter} >> n_p$, $d_{ter}^{*} \geq d_{\min}\left(10^{-\left(0.1\alpha_f\left(d_{ter}^{*}\right)\right)} y_{\max,ter}\left(2^{\sigma_{thr,ter}/\Xi_{ter}^{wr}}-1\right)\right)^{1/3}$ ■

4.4 Numerical result and analysis for minimum distance enforcement

4.4.1 Interference constraint

Since $y_{\max,tra}$ is a scalar quantity, the responses of normalized intra-floor interference power with distance given by (4.2) and (4.8) are similar as shown in Figure 4.5 for intra-floor scenario. Using (4.8), for an interference constraint $\alpha_{thr,tra}=0.11$ and $y_{\max,tra}=8$, the minimum distance $d_{tra}^{*} \geq 21$ m is required. In order to enforce d_{tra}^{*}, up to tier-2 from sFCBS is to be considered as RoE such that no resource can be reused in any FCBSs located up to tier-2 around sFCBS (see Figure 4.2). A key observation from

(4.8) is that the aggregate interference at sFU is inversely related to d^*_{tra} such that by allowing an increase in interference constraint, the minimum distance between cFCBSs can be reduced, and hence more reuse of the same resources can be achieved.

In inter-floor level, since the value of $\alpha_f\left(d^*_{ter}\right)$ is not known in prior to computing d^*_{ter}, we consider to use the constraint $\alpha_{agg,ter} \le \alpha_{thr,ter}$ directly to find the value of d^*_{ter} and hence d^*_{ver} as shown in Figure 4.6. In practice, any values of $\alpha_f\left(d^*_{ter}\right)$ can be known in prior from the number of floors between sFU and cFCBSs such that d_{ver} requirement can be found from the derived expressions directly. Figure 4.6 shows d^*_{ver} versus $\alpha_{thr,ter}$ for a set of ranges of $\alpha_{thr,ter}$ = 0.001 to 0.01, 0.01 to 0.1, and 0.1 to 1.0. From the figure, it can be found that d^*_{ver} requirement decreases with an increase in the value of $\alpha_{thr,ter}$.

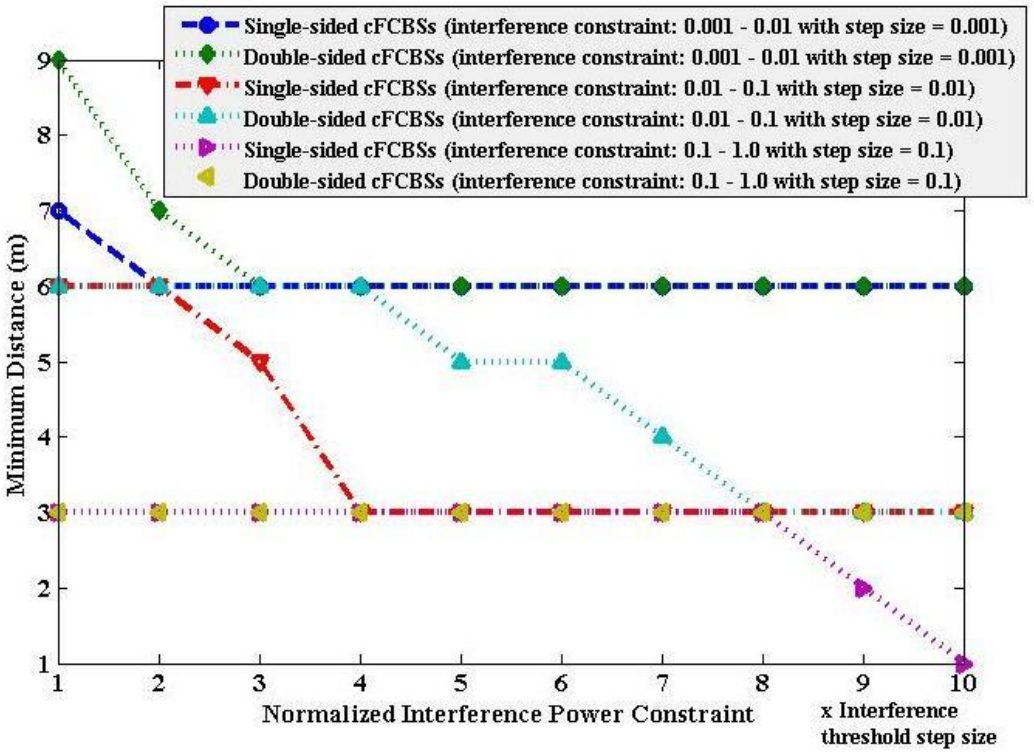

Figure 4.6: d^*_{ver} versus $\alpha_{thr,ter}$ inter-floor level.

Further, d^*_{ver} requirement for single-sided cFCBSs is less than or at least equal to that for double-sided cFCBSs because of the fact that $\alpha_{thr,ter}$ requirement per cFCBS becomes half for double-sided cFCBSs as compared to that of single-sided cFCBSs. The deviation in d^*_{ver} requirement between single-sided cFCBSs and double-sided cFCBSs is relatively high with a decrease in $\alpha_{thr,ter}$. For double-sided cFCBSs, d^*_{ver} requirement is the most of 9 m, i.e. 3 floors apart from the serving floor, for $\alpha_{thr,ter} = 0.001$ and the least of 3 m, i.e. 1 floor apart from the serving floor for $\alpha_{thr,ter} = 1.0$; whereas these values are respectively 7 m (i.e., 3 floors apart) and 1 m (i.e., no floors apart) for single-sided cFCBSs. Overall, a minimum separation distance between cFCBSs, is the maximum for cFCBSs located about the mid-floor of the building, decreases gradually as moving toward extreme floors for cFCBSs located on an intermediate floor between the mid and any extreme floors such that there exists double-sided cBCBSs, and the minimum for cFCBSs located at the extreme floors, i.e. ground and top most floors, such that there exists only single-sided cBCBSs.

Remark 4.1: The aggregate intra-floor interference at sFU is inversely related to the distance between a cFCBS and sFU, and hence reuse of resources intra-floor level can be increased by increasing intra-floor interference constraint. Further, for a multi-floor building, reuse of resources is the least for floors about the mid-floor of the building and increases to its maximum value for floors about the extreme floors. Hence, in comparison with intra-floor interference, floor penetration losses play a significant role on inter-floor interference effect at sFU to constrain the reuse of resources in cFCBSs.

4.4.2 Spectral efficiency constraint

Figure 4.7 shows the requirement of d^*_{tra} with the variation of $\sigma_{thr,se}$. From the figure, it can be found that d^*_{tra} increases almost linearly with an increase in $\sigma_{thr,se}$ from 0.5 to 4.5 bps/Hz. For example, d^*_{tra} of more than 27 m is required for a typical

maximum value of $\sigma_{thr,se}$ = 4.4 bps/Hz for the serving link, and hence resources can be reused in FCBSs located in tiers at least 3 tiers away from that of sFCBS.

Figure 4.8 shows inter-floor minimum distance requirement with inter-floor spectral efficiency constraint. The same procedure as in the case of interference

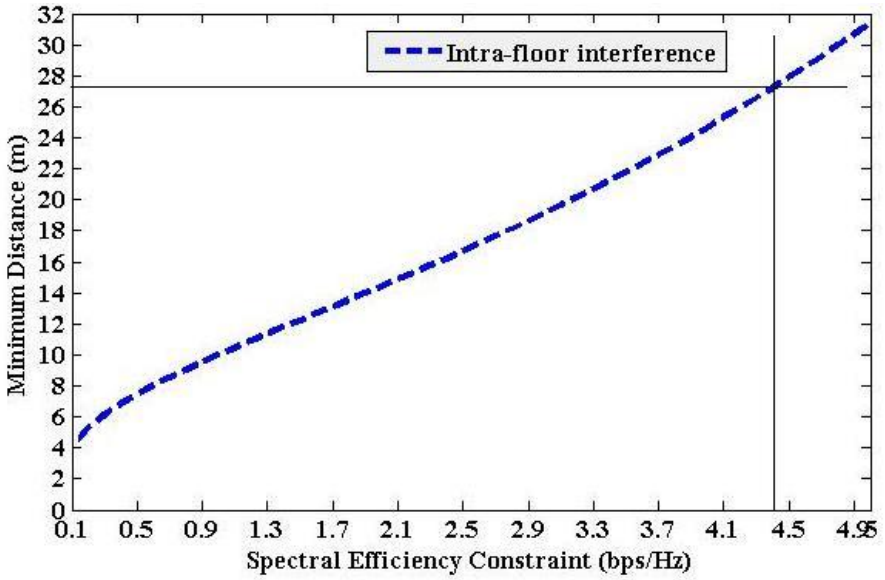

Figure 4.7: d_{tra}^{*} versus $\sigma_{thr,se}$ intra-floor level.

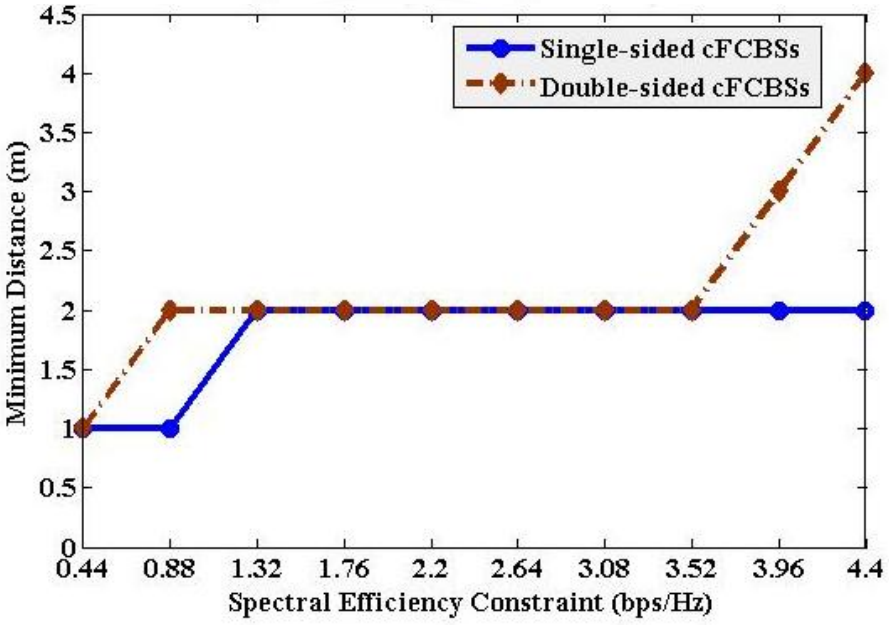

Figure 4.8: d_{ter}^{*} versus $\sigma_{thr,se}$ inter-floor level.

constraint is used, i.e. $\sigma_{ter,se} \geq \sigma_{thr,se}$, in order to find the value of d^*_{ter}, and hence d^*_{ver}. In contrast to inter-floor interference constraint, d^*_{ver} requirement decreases with a decrease in the value of $\alpha_{thr,ter}$. However, similar to interference constraint, d^*_{ver} requirement for the single-sided cFCBSs is at least equal or less than that for double-sided cFCBSs. The deviation in d^*_{ver} requirement between single-sided cFCBSs and double-sided cFCBSs is not significant enough as in the case of interference constraint since spectral efficiency requirement varies logarithmically with distance. The maximum deviation in d^*_{ver} requirement occurs when $\sigma_{thr,se}$ requirement reaches the typical maximum link quality of 4.4 bps/Hz. As shown in Figure 4.8, resources can be reused in every alternate floor for single-sided cFCBSs to achieve the maximum link quality, whereas for double-sided cFCBSs, resources can be reused in floors apart from each other by at least 2 intermediate floors.

Remark 4.2: With spectral efficiency constraint, d^*_{tra} requirement in intra-floor level increases linearly with the constraint. Further, estimating d^*_{ver} based on $\sigma_{thr,se}$ allows more reuse of resources because of logarithmic variation with distance than considering interference constraint which varies exponentially (see Figure 4.5). Since link quality is the prime concern for a given bandwidth to improve link capacity, it is preferable to consider spectral efficiency constraint because of allowing an estimation of d^*_{ver} by employing capacity formula directly.

4.4.3 Link capacity constraint

Figure 4.9 shows d^*_{tra} with capacity constraint $\sigma_{thr,tra}$ for varying the number of reused RBs Ξ^{wr}_{tra} and link spectral efficiency $\sigma_{tra,se}$ for reusing resources in cFCBSs intra-floor level. From the figure, it can be found that both Ξ^{wr}_{tra} and $\sigma_{tra,se}$ have significant impact on d^*_{tra} when optimization problem is constrained by $\sigma_{thr,tra}$. More specifically, the requirement of d^*_{tra} increases with an increase in $\sigma_{thr,tra}$ irrespective of

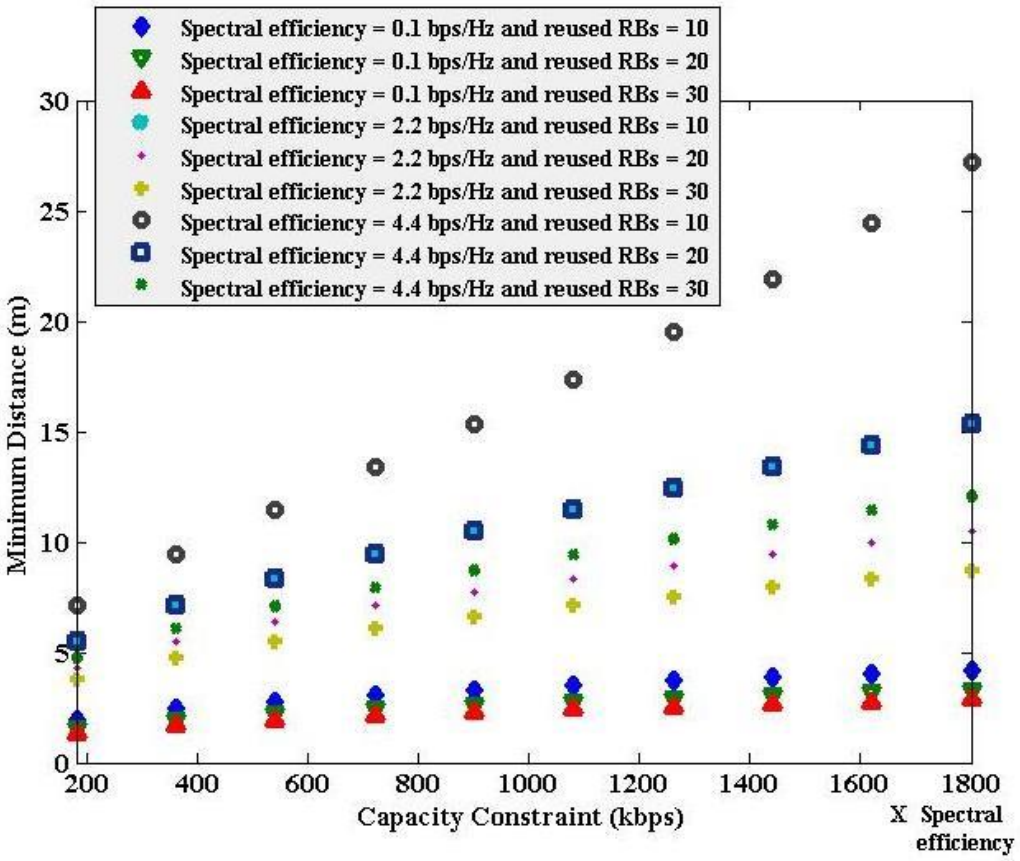

Figure 4.9: d^{*}_{tra} versus $\sigma_{thr,tra}$ for variable Ξ^{wr}_{tra} and $\sigma_{tra,se}$ intra-floor level.

the values of Ξ^{wr}_{tra} and $\sigma_{tra,se}$. Irrespective of the number of reused RBs, the requirement of d^{*}_{tra} increases with the better channel quality requirement of the serving link. Further, irrespective of the link quality, an increase in Ξ^{wr}_{tra} results in a decrease in the value of d^{*}_{tra}. Hence, a minimum value of d^{*}_{tra} can be achieved for a maximum value of Ξ^{wr}_{tra} and a minimum value of $\sigma_{tra,se}$ for a given $\sigma_{thr,tra}$. Note that the values of $\sigma_{thr,tra}$ on x-axis in Figure 4.9 are to be multiplied by the respective spectral efficiency values, i.e. 0.1 bps/Hz, 2.2 bps/Hz, and 4.4 bps/Hz.

Figure 4.10 shows d^{*}_{ter} with capacity constraint $\sigma_{thr,ter}$ for the variation of Ξ^{wr}_{ter} and $\sigma_{ter,se}$ inter-floor level. In general, the requirement of d^{*}_{ter} increases with an increase in $\sigma_{thr,ter}$, and decreases with an increase in Ξ^{wr}_{ter} for a given $\sigma_{thr,ter}$. The requirement of d^{*}_{ter} does not change significantly with a change in the value of Ξ^{wr}_{ter} as was the case in

intra-floor scenario, perhaps because of high floor penetration losses. As mentioned earlier, the value of Ξ_{ter}^{wr} should be carefully chosen particularly when a high link quality is expected as can be found from Figure 4.11 where it is shown that for Ξ_{ter}^{wr} less than the value of required RBs of 10 to achieve $\sigma_{thr,ter}$, with an increase in link quality requirement, the requirement for d_{ter}^{*} also increases significantly as compared to responses when Ξ_{ter}^{wr} is at least equal to 10. Also, like intra-floor scenario, a minimum value of d_{ter}^{*} can be achieved for a maximum value of Ξ_{ter}^{wr} for a given capacity constraint.

Remark 4.3: With capacity constraint, densification of FCBSs can be increased by keeping the value of $\sigma_{tra,se}$ as least as possible and increasing the value of Ξ_{tra}^{wr} in cFCBSs irrespective of the value of $\sigma_{thr,tra}$ intra-floor level, whereas by increasing value of Ξ_{ter}^{wr} in cFCBSs irrespective of the values of $\sigma_{thr,ter}$ and $\sigma_{ter,se}$ inter-floor level. Further, as a design consideration, it is recommended that Ξ_{ter}^{wr} should be chosen at least equal to the required RBs to achieve $\sigma_{thr,ter}$ with a high link quality.

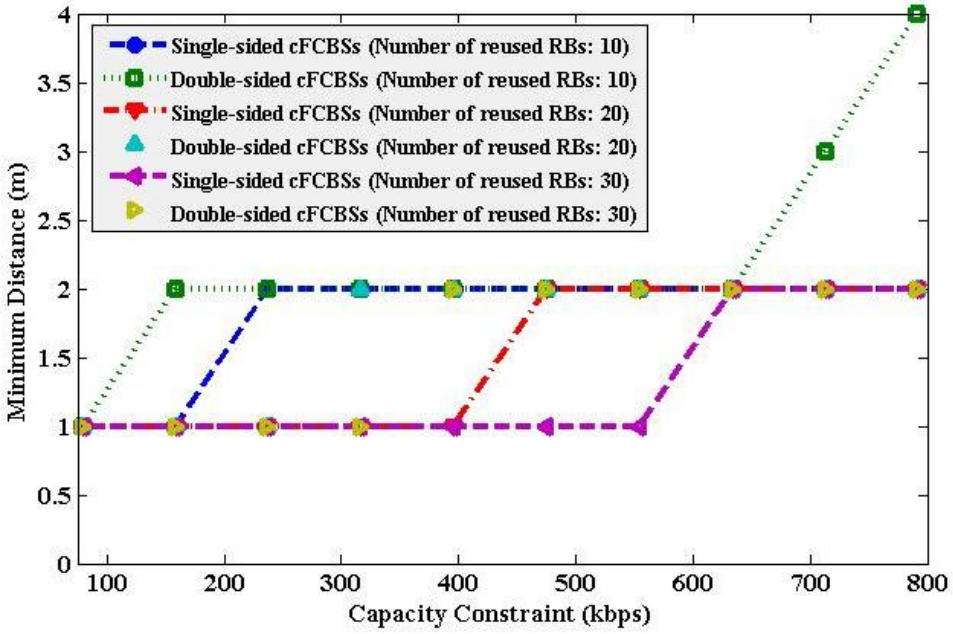

Figure 4.10: d_{ter}^{*} versus $\sigma_{thr,ter}$ for Ξ_{ter}^{wr} = 10, 20, and 30 inter-floor level.

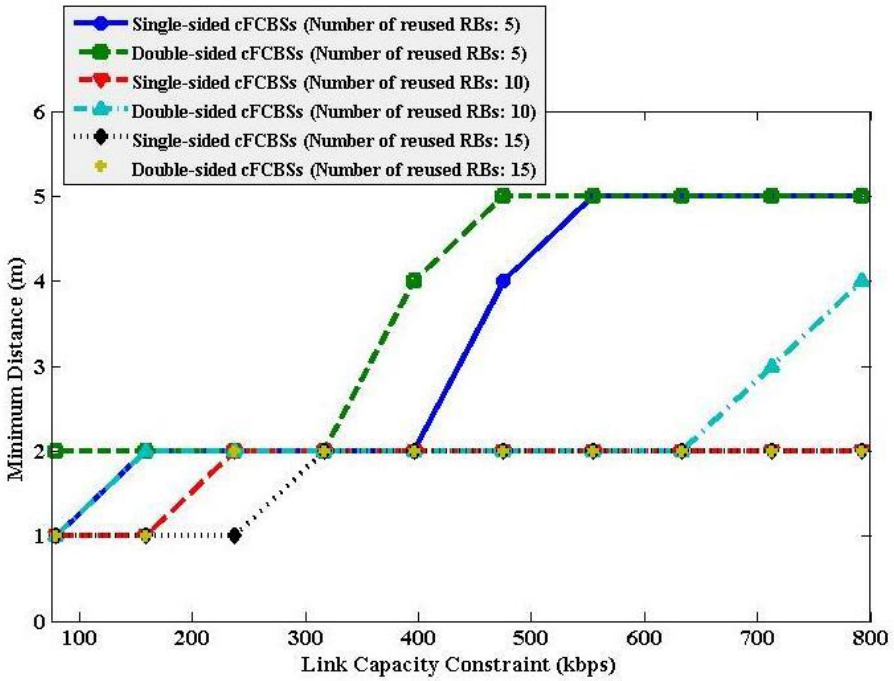

Figure 4.11: d_{ter}^{*} versus $\sigma_{thr,ter}$ for Ξ_{ter}^{wr} = 5, 10, and 15 inter-floor level.

4.5 Resource reuse architecture, strategy and gain in multi-tier networks

4.5.1 System architecture and interference management of multi-tier networks

System architecture of a multi-tier network is illustrated in Figure 4.12. We consider a single MC of a corner excited 3-sectored MC site and a number of SCs of various categories, including outdoor PCs and indoor FCs in an urban environment. All FCs are deployed in a 3D multi-floor building, i.e. L = 1, where L denotes the number of 3D buildings in a MC coverage. A certain percentage of MUs are considered within the building. All indoor MUs are served by the MC. In addition, a certain percentage of outdoor MUs are offloaded to nearby PCBSs.

We consider interference management for co-channel deployed FCBSs by avoiding allocation of the same radio resources mainly time and frequency to UEs such that co-channel interference can be avoided as shown in Figure 4.13. All indoor MUs

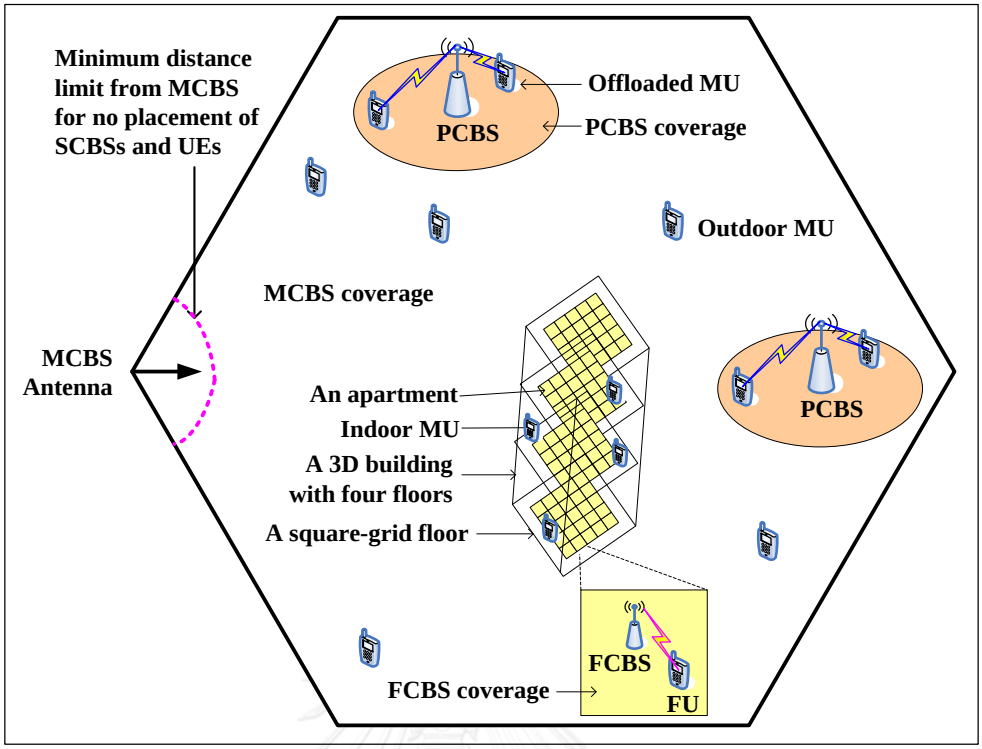

Figure 4.12: System architecture of a multi-tier network for $L = 1$.

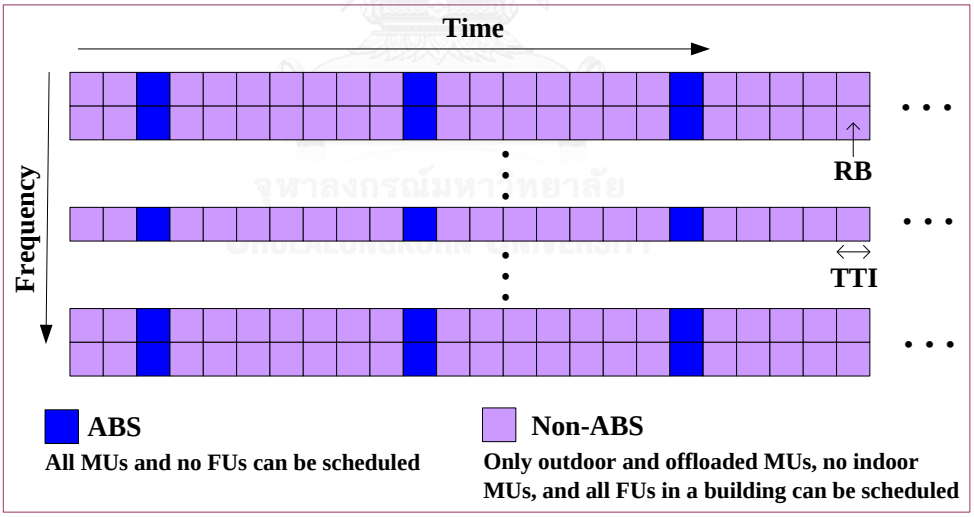

Figure 4.13: ABS based eICIC for interference management.

and outdoor MUs are allocated orthogonally to RBs. The same system bandwidth is reused in only FCBSs. If an indoor MU is within the building, TD ABS based eICIC is applied to avoid co-channel interference between the indoor MU and any FUs. All indoor MUs can transmit only during ABSs while all FCBSs mute transmission of control and data information except synchronization and broadcast channels. However,

indoor MUs are not served during non-ABSs by MCBS to avoid co-channel interference with FUs since FCBSs can transmit only during non-ABSs. All offloaded MUs and outdoor MUs can transmit in all TTIs.

4.5.2 Problem formulation

A. Multi-tier network model

Denote P_M, P_P, and P_F as the transmit powers of a MC, a PC, and a FC respectively. Consider that there are M RBs in system bandwidth and N MUs in the system. Let S_P denote the number of PCs in the MC coverage. If U_P denotes the number of MUs offloaded by a PC, the total number of offloaded MUs is $U_{OFL} = S_P \times U_P$. If μ_{iM} denotes the ratio of the number of indoor MUs, then the total number of indoor MUs is $U_{MI} = \mu_{iM} \times N$, outdoor MUs is $U_{MO} = N\text{-}U_{OFL}\text{-}U_{MI}$, and MUs served by MCBS is $U_M = U_{MO}+U_{MI}$.

Let $\boldsymbol{N_M}$ denote the set of indices of all MUs such that $\boldsymbol{N_M} = \{1, 2, 3, \ldots, N\}$. Denote $\boldsymbol{N_{MO}}$, $\boldsymbol{N_P}$, and $\boldsymbol{N_{MI}}$ respectively the set of indices of all outdoor MUs, offloaded MUs, and indoor MUs. Note that $\boldsymbol{N_M}$ is partitioned randomly into three disjoint subsets $\boldsymbol{N_{MO}}$, $\boldsymbol{N_P}$, and $\boldsymbol{N_{MI}}$. Let S_F denote the number of active FCBSs in the building. If each FC serves one FU, the total number of FUs is $U_F = S_F$. Let $\boldsymbol{N_F}$ denote the set of all FU indices such that $\boldsymbol{N_F} = \{1, 2, 3, \ldots, U_F\}$. Consider that the number of FUs is uniformly distributed in the interval $[1, U_F]$ where $U_F = 250$ in our simulation set up. The realization of MUs served by MCBS and PCBSs are not mutually independent since MUs served by PCBSs are MUs offloaded from MCBS, and the schedulers have a complete knowledge when a MU is offloaded. However, an offloaded MU to any PCBS is equally likely in a realization. Note that a realization is defined as a simulation run time.

The FC building and PCs are located randomly and uniformly within MC's area. All outdoor MUs, offloaded MUs, and FUs served by non-cFCBSs are distributed randomly and uniformly within their respective BSs' coverage areas. However, FUs served by cFCBSs are considered to locate at the farthest radial distances from their

respective cFCBSs. Let $\boldsymbol{T}$ denote simulation run time with the maximum time of Q (in time step each lasting 1 ms) such that $\boldsymbol{T}$ = {1, 2, 3, …, Q}. Let $\boldsymbol{T_{ABS}}$ denote the number of ABSs in every ABS pattern period (APP) of 8 subframes for our simulation set up, such that $\boldsymbol{T_{ABS}} \subseteq \boldsymbol{T}$ and $\boldsymbol{T_{ABS}}$ = {t: $t = 8v+z$; v = 0, 1, 2, …, Q/8; z = 1, …, T_{ABS}} where T_{ABS} = 1, 2, …, 8 corresponds to ABS patterns φ = 1/8, 2/8, …, 8/8 respectively. Let t_{ABS} and $t_{non-ABS}$ denote respectively an ABS and a non-ABS such that $t_{ABS} \in \boldsymbol{T_{ABS}}$ and $t_{non-ABS} \in \boldsymbol{T} \backslash \boldsymbol{T_{ABS}}$.

B. System capacity

Let d_{MU}, d_{PC}, and d_{BL} denote respectively the distances of any MUs, PCs, and FC buildings from the MCBS, and d_{FC} denote the distance between a FCBS and a FU. The distances of all UEs of each category in a realization are generated following the respective distribution functions as mentioned earlier. The path loss is calculated using path loss formulas given in Table B.5 in Appendix B.

Let U_{cFC} and U_{ncFC} denote respectively the number of cFCBSs and non-cFCBSs such that $U_F = U_{cFC} + U_{ncFC}$. Let M_{cFC} and M_{ncFC} denote respectively the number of reused RBs per cFCBS and the number of RBs for all non-cFCBSs such that $M = M_{cFC} + M_{ncFC}$. Let $\sigma_{thr,se}$ denote the required link spectral efficiency between sFU and sFCBS both intra-and inter-floor levels such that the required capacity constraint for each cFCBS can be given by $\sigma_{thr,ca} = \boldsymbol{M}_{cFC} \times \sigma_{thr,se}$. Hence, the aggregate capacity from reusing M_{cFC} RBs per cFCBS in the building can be given by

$$\sigma_{cFC} = \boldsymbol{U}_{cFC} \times \sigma_{thr,ca} = \boldsymbol{U}_{cFC} \times \left(\boldsymbol{M}_{cFC} \times \sigma_{thr,se}\right) \tag{4.14}$$

Since during an ABS, no FCBSs can transmit data signal, and the whole system bandwidth is reused in FCBSs of the building during non-ABSs, following (C.5) in Appendix C, the aggregate capacity of all FUs for any φ can be expressed as

$$\sigma_{FC} = \sum_{t=1}^{Q} \sum_{i=1}^{M_{ncFC}} (1-\varphi)\ \sigma_{t,i}\left(\rho_{t,i}\right) + (1-\varphi) \times \sigma_{cFC} \tag{4.15}$$

Similarly, the aggregate capacity of all MUs over *M* RBs for *Q* TTIs can be expressed as the sum throughput of all MUs as

$$\sigma_{MC} = \sum_{t=1}^{Q} \sum_{i=1}^{M} \sigma_{t,i}\left(\rho_{t,i}\right) \tag{4.16}$$

where σ and ρ are responses over *M* RBs of only indoor MUs in $t \in \boldsymbol{T_{ABS}}$ and all outdoor MUs and offloaded MUs in $t \in \boldsymbol{T}$.

Hence, the total capacity of the multi-tier network over *M* RBs for *Q* TTIs can be expressed as the sum throughput of all UEs in the network as

$$\sigma_{SYS} = \sigma_{MC} + \sigma_{FC} \tag{4.17}$$

C. Proportional fair scheduling

The proportional fair scheduling algorithm is described in Appendix C.

D. Jain's fairness index

Jain's fairness index is used to evaluate fairness performance of users served by all non-cFCBSs with a change in reused RBs per cFCBS and can be expressed as follows [92, 122]

$$F_J = \left(\sum_{x=1}^{U_{ncFC}} X_x \right)^2 \Bigg/ \left(U_{ncFC} \sum_{x=1}^{U_{ncFC}} X_x^{\,2} \right) \tag{4.18}$$

where X_x represents the total number of RBs allocated to user *x* over the simulation runtime.

4.5.3 Simulation parameters and assumptions

The default simulation parameters and assumptions used for system level simulation are listed in Table B.5 and Table B.6 in Appendix B. Hence, unless stated otherwise, the default value for any parameters is used from Table B.5 and Table B.6 in Appendix B. Further, eICIC is considered to address mainly the cross-tier

interference between indoor MUs and femto-tier that has been yet mostly overlooked in literature.

4.5.4 Resource reuse architecture modeling

We consider using graph coloring problem [123] to estimate the number of orthogonal set of sub-bands for reusing resources in cFCBSs for the given intra-and inter-floor constraints. In intra-floor level, the number of FCBSs in RoE of a cFCBS including the cFCBS is the chromatic number χ_{tra} , i.e. the minimum number of colors or orthogonal set of RBs scheduled by the scheduler. Note that the set of RBs allocated to any non-cFCBSs in any TTIs is decided by the scheduler based on certain metrics, e.g. performance metric in Proportional Fair scheduler. However for cFCBS, the resource allocation depends on the resource reuse strategy that we discuss in the following subsection. Each edge can be associated with any constraints, e.g. interference, spectral efficiency, or capacity constraints, to find a minimum distance between FCBSs. An edge between two FCBSs exists when a minimum distance for the corresponding constraint is satisfied. Note that any two FCBSs become cFCBSs only when a given constraint is satisfied so that a minimum distance, i.e. an edge, between them exists both intra-and inter-floor levels.

Similarly, in inter-floor level, each edge represents a minimum distance corresponds to an inter-floor constraint between floors holding cFCBSs. The chromatic number for inter-floor level χ_{ter} is the number of floors in RoE including the floor of cFCBS itself. Hence, the chromatic number (i.e., the total number of orthogonal bands) for both intra-and inter-floor levels (i.e., the building) is given by

$$\chi_{buil} = \chi_{ter} \times \chi_{tra} \tag{4.19}$$

Hence, we can now model the resource reuse graph for minimum distances and hence chromatic numbers both intra-and inter-floor levels. Figure 4.14 shows an example minimum distance constraint based resource reuse graph with respect to floor n+1 where each node represents a cFCBS, and each edge represents the constraint that is to be satisfied to reuse resources in cFCBSs. Note that RoEs for both intra-and inter-floor levels are shown with red color lines; edges in blue color represent that the

constraint is satisfied for a minimum distance; and green color circles represent cFCBSs, and ash color circles represent non-cFCBSs. Hence, resources can be reused in every 3 FCBSs intra-floor level and every alternate floors inter-floor level.

The conventional FFR strategies are primarily developed for homogeneous mobile networks and later on extended to HetNets to improve capacity of 4G mobile networks. The FFR strategies exploit outdoor MC coverage by partitioning and then reusing frequency in those partitions to improve capacity and spectral efficiency performances. Mainly outdoor MC based, FFR strategies cannot be transported to indoor 3D in-building SC networks where both horizontal and vertical placements of FCBS need to exploit. Hence, novel frequency reuse strategies need to develop by taking into account of indoor 3D in-building propagation characteristics such as short distance co-channel interference effect, floor effect, external wall effect, and 3D structural geometrical effect. Hence, unlike conventional FFR strategies, we propose two strategies to reuse RB resources in cFCBSs in this chapter, particularly for 3D in-building FC networks, for an aggressive reuse of the whole system bandwidth in FCBSs

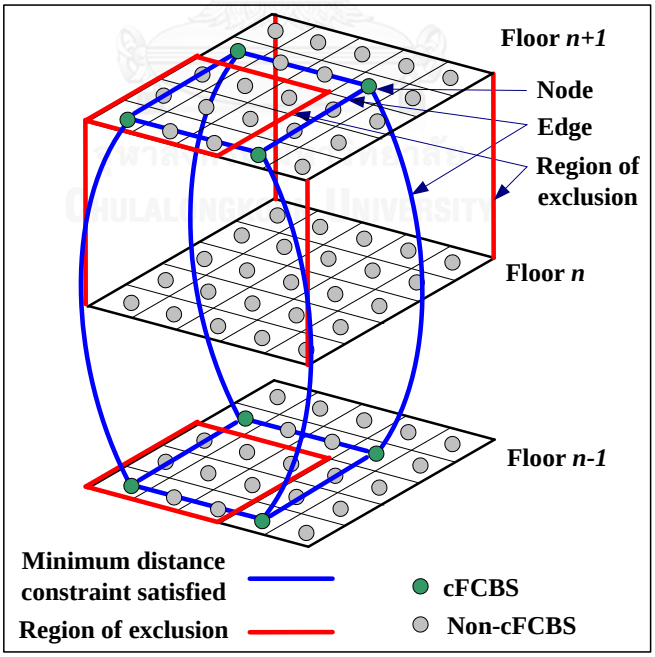

Figure 4.14: A minimum distance constraint based intra-and inter-floor resource reuse graph for 3D in-building scenario.

to address high capacity and spectral efficiency demands of the next generation mobile networks, i.e. 5G mobile networks.

4.5.5 Resource reuse strategies and gain

A. Resource reuse strategies

In strategy 1, FCBSs' clusters are formed based on RoE in both intra-and inter-floor levels, and the whole system bandwidth is reused in each cluster following a static frequency allocation scheme to avoid co-channel interference, e.g. each FCBS is allocated to the same amount of frequency, such that all FCBSs in RoE are cFCBSs with respect to neighboring clusters. In strategy 2, a fraction of system bandwidth is kept reserved for reusing RBs in each cFCBS such that a RoE is formed with respect to each cFCBS, and the remaining RBs of system bandwidth are allocated to all intra-floor level non-cFCBSs of the building dynamically, based on their channel characteristics in each TTI orthogonally following FD eICIC for co-channel interference avoidance between non-cFCBSs, as shown in Figure 4.15. Since a fixed portion of system bandwidth is reused to only the cFCBS of any RoEs, a FD scheduler is sufficient to schedule all FCBSs within the building. However, in strategy 1, scheduler can be

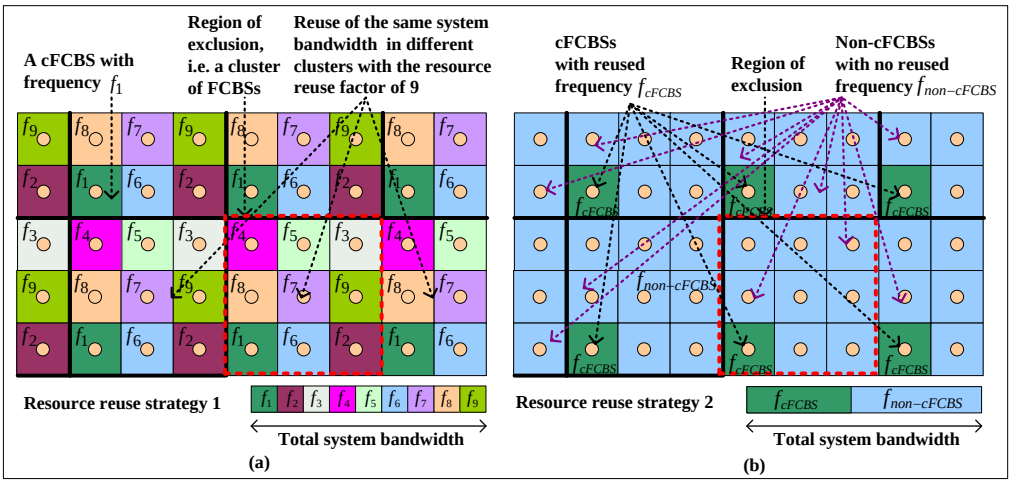

Figure 4.15: Proposed resource reuse strategies: (a) resource reuse strategy 1 and (b) resource reuse strategy 2.

implemented either jointly where all FCBSs in the building can be scheduled by a single scheduler or disjointly where FCBSs in each RoE are scheduled by a separate FD scheduler.

In strategy 1, since all FCBSs in all RoEs gain advantage from the link capacity constraint enforced by an optimizer, the overall capacity gain from resource reuse strategy 1 is expected to be higher than that of resource reuse strategy 2. However, complexities in computation for implementation of strategy 1 are higher than that of strategy 2 because of computing the cluster size, i.e. RoE, number of clusters, and RB allocation planning for FCBSs cluster wide. Further, because of a static RB allocation, reuse of RBs becomes dependent on the deployment of FCBSs within any RoEs since reused RBs may be wasted because of an absence of any FCBSs within a RoE, which is a realistic scenario in which certain RBs have already been defined and cannot be reallocated to other FCBSs because of causing co-channel interference with FCBSs of neighboring RoEs. Furthermore, dynamic allocation of RBs based on the activation of a FCBS cannot also be exploited in strategy 1. However, in strategy 2, a scheduler simply looks at the requests of active FCBSs in any TTIs and allocates them dynamically. Further, reuse of RBs in cFCBSs is also flexible since the amount of reused RBs can be varied dynamically based on network requirements, e.g. for less cFCBSs being active, more RBs can be allocated to non-cFCBSs in a RoE. In addition, the pattern of cFCBSs can be easily changed by changing cFCBSs' indices and the value of optimization constraint. Furthermore, network operators can also provide selective quality-of-service, e.g. a high data rate user can be served by a cFCBS, and a low data rate user by a non-cFCBS by flexibly changing the amount of RBs to be reused in cFCBSs. Hence, we consider strategy 2 to carry out performance comparison between ORRA and NORRA schemes.

In Algorithm 4.1 for an arbitrary value of L, all the steps from intra-and inter-floor interference characterization, through a minimum distance enforcement to finally proposing resource reuse strategy 2 to develop the proposed model for 3D in-building scenario are captured. 20% and 40% of system bandwidth are considered to reuse in each cFCBS and kept reserved. The remaining RBs of system bandwidth are allocated to all non-cFCBSs within the building following eICIC techniques. Hence, for 5 MHz, i.e. 25 RBs, 5 and 10 RBs are reused in each cFCBS, and 20 and 15 RBs are allocated

to non-cFCBSs respectively. Approach 3 with two capacity constraints, one for 5 RBs and the other for 10 RBs, with a link spectral efficiency of 3.4594 bps/Hz are used to estimate a minimum distance between cFCBSs both intra-and inter-floor levels and hence the number of cFCBSs in the building. Since our goal is to show the performance of NORRA over ORRA scheme, for simplicity of inter-floor minimum distance estimation, we consider the worst case scenario such that only double-sided cFCBSs exist in the building. However in practical scenario, both single-sided and double-sided cFCBSs exist, and hence the capacity performance should be improved because of the presence of single-sided cFCBSs that allow overall more reuse of resources in cFCBSs on floors about the extreme floors. For TD eICIC, ABS = 1 is considered. For a given link spectral efficiency and the number of reused RBs per cFCBS, we can estimate the capacity of all cFCBSs. Hence, the overall capacity under NORRA scheme for all FCBSs within the building can be found by summing the capacities of all non-cFCBSs and all cFCBSs.

B. Resource reuse gain for $L = 1$

Recall that with ORRA scheme the whole system bandwidth is reused only once in all FCBSs within the building using FD eICIC technique. For the system level simulation parameters and assumptions as given in Table B.5 and Table B.6 in Appendix B, the capacity performances with ORRA scheme can be found by setting the number of reused RBs per cFCBS to zero and using (4.15)-(4.17), which are σ_{FC} = 4.348 Mbps for the FC network and σ_{SYS} = 9.716 Mbps for the multi-tier network. However, for NORRA scheme, an increase in the number of reused RBs per cFCBS causes the capacity of cFCBSs and hence the FC network to increase proportionately by manifold as compared to ORRA scheme. Meanwhile, the capacity of non-FCBSs decreases because of less RBs available for allocation to them. On an average, with the resource reuse strategy 2 under the same scenario as that of ORRA, the system capacity

Algorithm 4.1: Interferences characterization, minimum distance enforcement, and resource reuse strategy for 3D in-building FC Networks.

01: **Inputs**:

02: (i) Set: B_{sys}, P_M, P_P, P_F, μ, S_P, S_F, n_p, U_P, U_F, M, Q, L, φ, t_c, β, G_t, G_r, L_F, M_{cFC},

M_{ncFC}, $P_{t,\max}$, $d_{\min}$, $d_{tra,\min}$, $d_{tra,\max}$, $d_{ter,\min}$, $d_{ter,\max}$, $\alpha_f(d_{ter})$, d_{ver}, n,

$d_{tra} = [d_{tra,\min}, d_{tra,\max}]$, $d_{ter} = [d_{ter,\min}, d_{ter,\max}]$, $y_{\max,tra}$, $y_{\max,ter}$, $\sigma_{thr,se} = [0, 4.4]$,

$\alpha_{thr,tra} = [\alpha_{thr,tra,\min}, \alpha_{thr,tra,\max}]$, $\alpha_{thr,ter} = [\alpha_{thr,ter,\min}, \alpha_{thr,ter,\max}]$,

$\sigma_{thr,tra} = [\sigma_{thr,tra,\min}, \sigma_{thr,tra,\max}]$, $\sigma_{thr,ter} = [\sigma_{thr,ter,\min}, \sigma_{thr,ter,\max}]$, $\Xi_{tra} = [\Xi_{tra,\min}, \Xi_{tra,\max}]$,

$\Xi_{ter} = [\Xi_{ter,\min}, \Xi_{ter,\max}]$, $O_{thr,tra} = [\alpha_{thr,tra}, \sigma_{thr,se}, \sigma_{thr,tra}]$, $O_{thr,ter} = [\alpha_{thr,ter}, \sigma_{thr,se}, \sigma_{thr,ter}]$

03: (ii) Initialize: $t \in \{\boldsymbol{T_{ABS}}, \boldsymbol{T} \backslash \boldsymbol{T_{ABS}}\} = \{1, \ldots, Q\}$

04: (iii) Estimate: $\forall t,i : \{\mathrm{PL}_{t,i}, \mathrm{LS}_{t,i}, \mathrm{SS}_{t,i}, \rho_{t,i}, \sigma_{t,i}(\rho_{t,i})\}$, U_{cFC}, U_{ncFC}

05: Estimate: $\forall d_{tra}\ \alpha_{tra}(d_{tra}) = (d_{\min}/d_{tra})^3$; $\forall d_{ter}\ \alpha_{ter}(d_{ter}) = 10^{-(0.1\alpha_f(d_{ter}))}(d_{\min}/d_{ter})^3$

06: *// Minimum distance enforcement*

07: Estimate: $\forall \alpha_{thr,tra}\ d^*_{tra} \geq d_{\min}(y_{\max,tra}/\alpha_{thr,tra})^{1/3}$ // interference constraint

08: $\forall \alpha_{thr,ter}\ d^*_{ter} \geq d_{\min}\left(10^{-(\alpha_f(d^*_{ter})/10)}(y_{\max,ter}/\alpha_{thr,ter})\right)^{1/3}$

09: $\forall \sigma_{thr,se}\ d^*_{tra} \geq d_{\min}\left(y_{\max,tra}(2^{\sigma_{thr,se}} - 1)\right)^{1/3}$ // spectral efficiency constraint

10: $\forall \sigma_{thr,se}\ d^*_{ter} \geq d_{\min}\left(10^{-(0.1\alpha_f(d^*_{ter}))} y_{\max,ter}(2^{\sigma_{thr,se}} - 1)\right)^{1/3}$

11: $\forall \Xi_{tra} \forall \sigma_{thr,tra}\ d^*_{tra} \geq d_{\min}\left(y_{\max,tra}(2^{\sigma_{thr,tra}/\Xi^{wr}_{tra}} - 1)\right)^{1/3}$ // link capacity constraint

12: $\forall \Xi_{ter} \forall \sigma_{thr,ter}\ d^*_{ter} \geq d_{\min}\left(10^{-(0.1\alpha_f(d^*_{ter}))} y_{\max,ter}(2^{\sigma_{thr,ter}/\Xi^{wr}_{ter}} - 1)\right)^{1/3}$

13: Find: χ_{tra} using d^*_{tra} for $O_{thr,tra}$, χ_{ter} using d^*_{ter} for $O_{thr,ter}$, $\chi_{buil} = \chi_{ter} \times \chi_{tra}$

14: Estimate: (i) $\forall t\, \forall i\ \sigma_{MC} = \sum_{t=1}^{Q} \sum_{i=1}^{M} \sigma_{t,i}(\rho_{t,i})$ *// resource reuse strategy 2*

15: (ii) $\sigma_{cFC} = U_{cFC} \times (M_{cFC} \times \sigma_{thr,se})$

16: (iii) $\forall t \forall i\ \sigma_{FC} = \sum_{t=1}^{Q} \sum_{i=1}^{M_{ncFC}} (1-\varphi)\ \sigma_{t,i}(\rho_{t,i}) + (1-\varphi) \times \sigma_{cFC} : U_F = S_F$ for $L = 1$

17: $= L \times \left(\sum_{t=1}^{Q} \sum_{i=1}^{M_{ncFC}} ((1-\varphi) \times \sigma_{t,i}(\rho_{t,i})) + ((1-\varphi) \times \sigma_{cFC}) : U_F = S_F \right)$ for $L > 1$

18: (iv) $\sigma_{SYS} = \sigma_{MC} + \sigma_{FC}$, $\sigma_{SE} = \sigma_{SYS}/M.Q$

19: (v) $F_J = \left(\sum_{x=1}^{U_{ncFC}} X_x \right)^2 \Big/ \left(U_{ncFC} \sum_{x=1}^{U_{ncFC}} X_x^{\,2} \right)$

(*continued*)

(*continued*)
20: **Outputs**:
21: Plot: $\alpha_{tra}(d_{tra})$ versus d_{tra}, $\alpha_{ter}(d_{ter})$ versus d_{ter}, d^*_{tra} versus $O_{thr,tra}$, and d^*_{ter} versus $O_{thr,ter}$
22: Display: $L, \sigma_{SYS}, \sigma_{SE}, \sigma_{FC}, F_J$

σ_{SYS} of 135 Mbps and 257.13 Mbps can be achieved for the number of reused RBs M_{cFC} of 5 and 10 respectively using (4.14)-(4.17). Hence, the reuse of an RB per cFCBS can improve the system capacity by more than 2.6 (e.g., $257.133/(9.716\times10)\cong 2.64$ for the number of reused RBs = 10) times. Note that an increase in the number of RBs allocated to non-FCBSs results also in an improved aggregate capacity of all non-cFCBSs. However, the overall FC network capacity performance degrades significantly because of scheduling RBs only once in non-cFCBSs as opposed to reusing them in all cFCBSs in a building.

Remark 4.4: Irrespective of the number of reused RBs per cFCBS, NORRA outperforms ORRA scheme by manifold. The outperformance factor depends on the type and value of constraint and the number of reused RBs allocated per cFCBS, which directly affect a minimum distance to enforce between cFCBSs and hence the number of cFCBSs.

Though an increase in the number of reused RBs per cFCBS causes to increase the overall FC network capacity significantly, it degrades the fairness performance of non-cFCBSs accordingly since non-cFCBSs then need to compete relatively more with a reduced number of RBs allocated for them. Hence, there should be a trade-off in RB allocation between the overall fairness of non-cFCBSs and capacity gain from reusing RBs in cFCBSs. Since a link capacity requirement varies with time and the number of FCBSs per building, the number of reused RBs can be made adaptive with the number of non-cFCBSs, e.g. the more the number of non-cFCBSs in a building, the less the number of reused RBs per cFCBS would be considered such that reasonable overall FC

network capacity and fairness of non-cFCBSs in RB allocation can be achieved. Since we consider the maximum number of RBs that can be allocated to FCBSs is 25 which is much less than the maximum number of FCBSs in the building, i.e. 250, and allow the system to run for one APP to show the capacity and fairness performances, the value of fairness factor using (4.18) is relatively low, e.g. 0.103, 0.087, and 0.062 respectively for the number of reused RBs equals to 0, 5, and 10. With an increase in system bandwidth, e.g. 20 MHz or 100 RBs, and running the system for a long enough time, the value of fairness factor can be improved, however the capacity and fairness performances' trend would not be affected with such changes.

Remark 4.5: Reusing the whole system bandwidth in each cFCBS is not practically feasible since a cFCBS is always located within its RoE such that any RBs allocated to a non-cFCBS within the RoE of a cFCBS causes to create co-channel interference with that cFCBS.

C. Resource reuse gain for $L > 1$

The proposed model for a single 3D multi-floor building deployed in the coverage of a MC in Figure 4.12 can be applied to cover an extended multi-tier network consisting a large number of multi-floor buildings, i.e. $L > 1$, deployed ultra-densely over a MC coverage in urban environments. By knowing any urban profile and ensuring that co-channel interference from neighboring buildings is insignificant, the proposed model can be applied in each building by adapting the type and value of constraint and the number of reused RBs per cFCBS to reuse resources in an ultra-dense FC network in order to achieve high capacity and spectral efficiency requirements of 5G networks. A rough estimation with an example scenario, to find an upper bound on the number of buildings, i.e. the value of L, that can be deployed to reuse the same system bandwidth over a large MC coverage, and hence to estimate the capacity and spectral efficiency of the extended multi-tier network, is given in the following.

The multi-tier network in Figure 4.12 for a single building is extended in Figure 4.16 for an ultra-dense deployment of FCBSs and reusing resources in them by employing the proposed model. Since the whole system bandwidth is reused in each

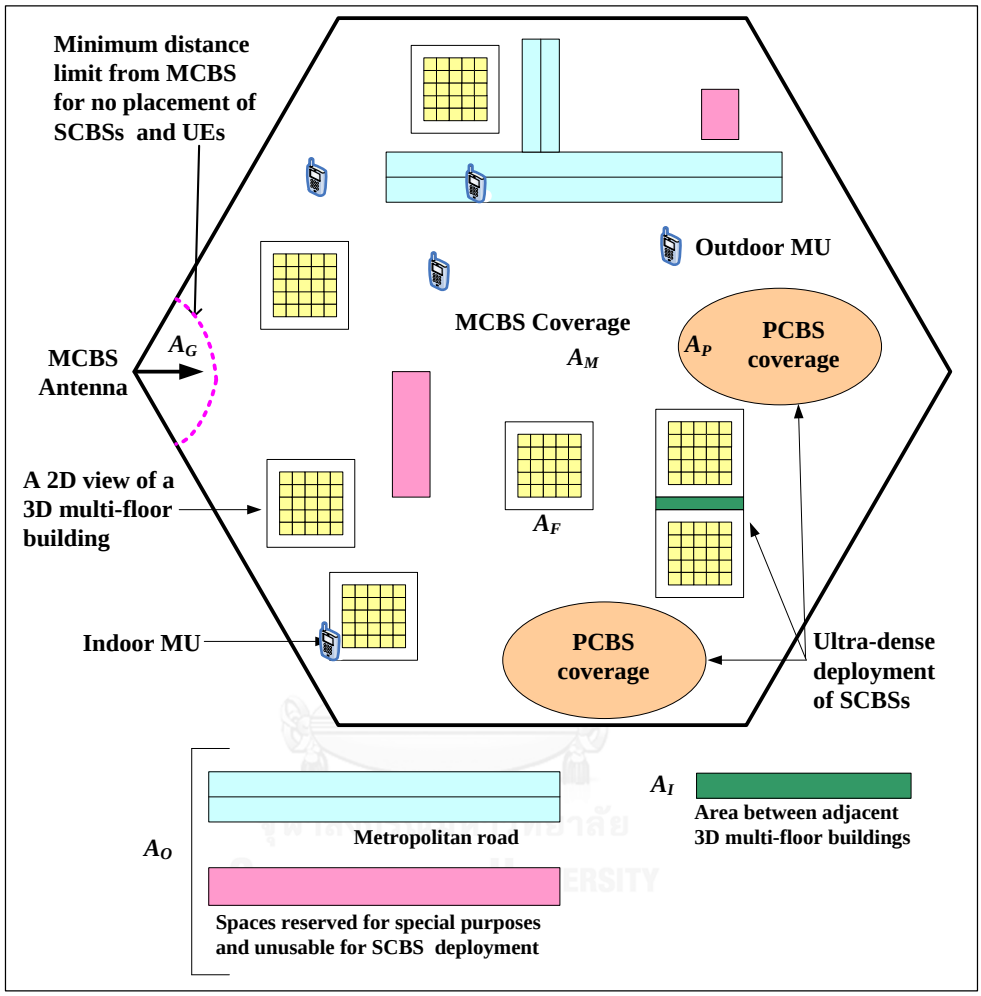

Figure 4.16: Extended multi-tier network architecture for an ultra-dense deployment of FCBSs over a large MC coverage for $L > 1$.

building, the upper bound of the number of buildings L in which the same system bandwidth can be reused over the MC coverage can be found roughly for a given φ as follows.

$$A_M = S_P \varepsilon_P A_M + L \varepsilon_F A_M + \varepsilon_A A_M$$

$$A_M = S_P \varepsilon_P A_M + L \varepsilon_F A_M + (\varepsilon_G + \varepsilon_O + \varepsilon_I) A_M$$

$$1 = S_P \varepsilon_P + L \varepsilon_F + \varepsilon_G + \varepsilon_O + \varepsilon_I$$

$$L = 1/\varepsilon_F \left(1 - S_P\varepsilon_P - \varepsilon_G - \varepsilon_O - \varepsilon_I\right) \tag{4.20}$$

where $\varepsilon_F = A_F/A_M$, $\varepsilon_P = A_P/A_M$, $\varepsilon_O = A_O/A_M$, $\varepsilon_I = A_I/A_M$, $\varepsilon_G = A_G/A_M$, $\varepsilon_A = \varepsilon_G + \varepsilon_O + \varepsilon_I$. $A_M = (3\sqrt{3}/2)R^2$ is the area of a regular hexagonal MC, and *R* is the radius of the MC. $A_F = l_F \cdot w_F$ is the area of a building. l_F and w_F are respectively the length and width of a building. $A_P = \Pi R_P^{\,2}$ is the area, and R_P is the radius of a circular PC. A_O is the area in a MC which is considered to be used for other purposes such as roads, parks, and playgrounds. A_I is the area of a MC which is considered to be left as free space between the external boundaries of two adjacent buildings. $A_G = \Pi R_G^{\,2}/6$ is the minimum separation area from the MCBS for no existence of any SCs. Hence, (4.15) for the total capacity of FC networks over a MC coverage for any φ is modified as follows

$$\sigma_{FC} = L \times \left(\sum_{t=1}^{Q} \sum_{i=1}^{M_{ncFC}} \left((1-\varphi) \times \sigma_{t,i}\left(\rho_{t,i}\right)\right) + \left((1-\varphi) \times \sigma_{cFC}\right) \right) \tag{4.21}$$

The total capacity of the multi-tier network over *M* RBs for *Q* TTIs over a MC coverage can be found by (4.17). Following [124], the average spectral efficiency over the whole system bandwidth for *Q* numbers of TTIs can be expressed as

$$\sigma_{SE} = \sigma_{SYS}/M.Q \tag{4.22}$$

In (4.22), the values of *M* and *Q* are in hertz and TTI respectively since σ_{SYS} is estimated per TTI basis. To clarify the applicability of the proposed model through (4.20)-(4.22) for an ultra-dense HetNet, we consider the 3GPP case 3 as an example scenario, for which the inter-site distance = 1732 m [37, 88]. Note that a regular hexagon has the same length of its each side, which is equal to its radius such that $\text{ISD} = R + R + R = 3R$, and $R = 1732/3 = 577.3\,\text{m}$. So, $A_M = (3\sqrt{3}/2)R^2$ $= 2.6 \times (577.3)^2 = 8665157\,\text{m}^2$. Assume that the radius of a circular PC is 40 m such that the area of a PC, $A_P = \Pi(40)^2 = 5024\text{m}^2$. However, the area of a $50 \times 50\ \text{m}^2$ square-grid based building, $A_F = 70 \times 70 = 4900\ \text{m}^2$ (see Figure 4.1). For a minimum separation of 75 m from MCBS, the area of this space, $A_G = \Pi(75)^2/6 = 2944.8\,\text{m}^2$. Assume that 2 PCs are deployed within the coverage of MC, and *L* buildings are deployed contiguously with $A_I = 0.05A_M$. Assume that $A_O = 0.1A_M$. Then

$\varepsilon_F = 0.005654, \varepsilon_P = 0.00579, \varepsilon_O = 0.1$, $\varepsilon_I = 0.05$, and $\varepsilon_G = 0.00339$. Hence, roughly the maximum number of 3D buildings that can be deployed with no overlapping with other objects and SCs within the MC coverage can be found by (4.20)

$$L = (1/0.005654) \times (1 - 0.01158 - 0.00339 - 0.1 - 0.05) \cong 147$$

For simplicity, considering the similar propagation characteristics and FCBS locations in all L buildings, the total capacity that can be achieved for 5 and 10 reused RBs per cFCBS per building using (4.17) are respectively $\sigma_{SYS} \cong 147 \times 135 \text{ Mbps} = 19845 \text{ Mbps}$ and $\sigma_{SYS} \cong 147 \times 250 \text{ Mbps} = 36750 \text{ Mbps}$. The average system level spectral efficiency using (4.22) are $19845 \text{ Mbps} / (8 \text{ TTI} \times 5 \text{MHz}) = 496.12 \text{ bps/Hz}$ and $36750 \text{ Mbps} / (8 \text{TTI} \times 5 \text{MHz}) = 918.75 \text{ bps/Hz}$ respectively, which are $496.12/30 \cong 16.5$ and $918.75/30 \cong 30.6$ times respectively that of 4G LTE-Advanced systems, i.e. 30 bps/Hz, [125] and greater than the expected spectral efficiency, i.e. 10 times that of 4G networks [34, 95], to be achieved for 5G networks.

Remark 4.6: Although we consider performing a rough estimation under a simplistic scenario, it gives us an understanding that the expected spectral efficiency requirement of 5G networks can be achieved by employing the proposed model to an ultra-dense deployment of FCBSs in 3D multi-floor buildings.

4.6 Technical and business perspectives

A number of technical and business values from network operators' viewpoint to implement the proposed model are pointed out in the following.

- *Viability*: Typical interference avoidance and resource reuse analysis per FC basis, and FC clustering with an amorphous and a variable size of 2D FC clusters are not practical enough, particularly in urban environments, where the existence of a vast number of multi-floor buildings is an obvious scenario.

Hence, performance evaluations with a realistic indoor scenario, e.g. dense and clustered FC deployment within a 3D structure are required so that a FU of FCBS, e.g. cFCBS, can be scheduled with a large bandwidth for data transmission to boost the network capacity significantly.

- *Complexity*: Based on a minimum distance and hence location of cFCBSs within a building, clustering of FCBSs can be performed without any further computational effort. Moreover, in strategy 2, there is no need for FC clustering to allocate RBs orthogonally to non-cFCBSs which further reduces computational complexity.
- *Scalability*: The LTE-Advanced network has been deployed and evolved toward reaching a high capacity of 5G networks. Because of independence of the density of FCBSs in a building, the proposed model is highly scalable. Hence, a gradual migration from regular HetNets of the existing 4G LTE-Advanced network to an ultra-dense 5G HetNets can be easily performed.
- *Flexibility*: The proposed model addresses the problem of dense HetNets in a realistic in-building urban scenario, and hence can be applied without any prior modifications on it to adapt with any real urban environments. Any urban maps with specific detail of buildings in terms of, e.g. density and height, along with statistics of FCBSs in each building is sufficient for implementation of the proposed model that results in reducing efforts from planning FC networks in urban environments and saving associated costs.
- *Accessibility*: By employing the proposed model, SON enablement feature of FCBSs can be avoided since both time and frequency resources are allocated to all non-FCBSs orthogonally using eICIC within a cluster in resource reuse strategy 1 and the whole building itself in strategy 2. Hence, an additional cost from SON feature to avoid co-channel interference among FCBSs can be avoided.
- *Readiness*: Since eICIC techniques have been in operation in existing networks, no additional implementation complexity from eICIC will raise. Only implementation of schedulers for a large coverage and necessary backhauls are to be needed in place. Hence, operators can easily implement the proposed

model using existing techniques without any significant investments on current networks.

4.7 Summary

In this chapter, we propose a tractable analytical model for characterizing co-channel interference and enforcing a minimum distance between FCs to reuse resources in FCBSs deployed in a 3D multi-floor building. A multi-tier network comprising a MC, a number of PCs, and a 3D building which consists of a number of floors where each floor is modelled as a group of square-grid based apartments, and each apartment is installed with a FCBS is considered. Intra-floor interference using planar-Wyner model and inter-floor interference using linear-Wyner model [107] are modelled for modeling interference and enforcing a minimum distance between FCBSs in a 3D building for a number of optimization constraints, namely interference, spectral efficiency, and link capacity both intra-and inter-floor levels. Note that each of these constraints is a function of one another. Hence, performance results using one approach are still valid for another constraint. However, analysis using each constraint individually gives us a direct insight on the effect of a constraint on any performance measures.

Using the proposed model, resources are reused to certain FCBSs such that resource allocations remain no longer orthogonal, which we term it as NORRA scheme. However, in ORRA scheme, the whole system bandwidth of the MC is reused once among all the FCBSs in the building. The ABS based eICIC techniques are considered to avoid co-channel interference between MC-plus-PC tier and FC tier and schedule resources orthogonally. We develop two strategies to reuse RBs in cFCBSs, where in strategy 1, clusters of FCBSs are formed based on the RoEs of cFCBSs for reusing the whole system bandwidth in each cluster. In strategy 2, a fraction of RBs of system bandwidth kept reserved for reusing in each cFCBS, and the remaining RBs of system bandwidth are allocated to all non-cFCBSs of the building using FD eICIC technique. An algorithm for the proposed model including resource reuse strategy 2 is developed for both single and multiple 3D multi-floor building scenarios.

A comprehensive numerical analysis is carried out on enforcing a minimum distance between cFCBSs, and the capacity outperformance of NORRA scheme over ORRA in FC network by employing strategy 2 for capacity constraint is shown. The numerical analysis for enforcing a minimum distance reveals that, for a multi-floor building, the reuse of resources is not uniform which is the least for floors about the mid-floor of the building and increases to its maximum value for floors about the extreme floors, i.e. the ground or the top most floor. This can be reasoned by the fact that about the extreme floors, single-sided cFCBSs are more likely to be present than double-sided cFCBSs, which allow more reuse of resources in cFCBSs on floors about the extreme floors. Hence, floor penetration losses play a significant role on inter-floor interference effect at sFU to constrain the reuse of resources in cFCBSs. Further, resource reuse depends on the cFCBSs' floor location within a building.

The application of the proposed model from a single to multiple number of 3D multi-floor buildings deployed over a large MC coverage to address an ultra-dense deployment of FCBSs for 5G networks is discussed. With a rough estimation under an example scenario, it is shown that the prospective desired spectral efficiency of 5G networks can achieved with the proposed model. Finally, several technical and business perspectives of the proposed model, including viability, complexity, scalability, flexibility, accessibility, and readiness are pointed out. In addition to CSG FCBSs which are typically deployed by end users, operators can be benefitted the most by applying the proposed model to open or hybrid access FCBSs in order to enhance indoor user capacity.

CHAPTER 5
MULTI-BAND ENABLED SMALL CELL AND UE ARCHITECTURE FOR SPLITTING UP-/DOWN-LINK AND CONTROL-/USER-PLANE

In this chapter, a multi-band enabled FCBS and UE architecture is proposed in a multi-tier network for splitting the UL/DL as well as the C-/U-plane for 5G mobile networks. For multiple bands, co-channel microwave and different frequency 60 GHz mmWave bands for FCBSs with respect to the microwave band used by their over-laid MCBS are considered. The co-existence of co-channel microwave and different frequency mmWave bands on the same FCBS and UE is first studied to show their performance disparities in terms of system capacity and spectral efficiency in order to provide incentives for employing multiple bands at the same FCBS and UE and identify a suitable band for routing decoupled UL/DL or C-/U-plane traffic. A number of disruptive architectural design alternatives for 5G mobile networks, including a complete UL/DL splitting as well as a combined UL/DL and C-/U-plane splitting architectures are presented. The outperformances of the proposed architecture as compared to existing split architectures are shown.

5.1 Introduction

Rethinking traditional networking approaches whether or not to be applied for future mobile networks, i.e. 5G mobile networks, is caused by a number of facts, including (i) a high end-user data rate demand for a continual growing number of mobile users; (ii) asymmetric traffic volume in the UL/DL such that the traffic ratio of the UL to the DL vary considerably because of diversity in application usage by users, e.g. from 1:3 to 1:9 [126], an average of 1:6 [127], and globally 1:3.29 [128]. According to [129], the ratio of the UL to the DL traffic was around 1:6 in 2010, and was predicted

to rise up to 1:10 over the next five years as video traffic grows; (iii) different traffic characteristics of the C-/U-plane such that the backhaul traffic consists of a number of traffic, most of which are user generated data traffic in addition to C-plane overhead backhaul traffic from S1 signaling (14%), handover traffic (4%) on X2 backhaul between cells, and other management and synchronization traffic from wireless traffic [60]; (iv) diversity in transmit power of dense heterogeneous BSs; and (v) high traffic differentiation with certain flows being provided with dedicated resources for ensuring quality-of-service. Conventional mobile network standards require the UL/DL associated with the same BS. However, such an approach raises a number of issues, including (i) a huge gap in transmit power between UE and BS, (ii) diverse channel responses of the DL and the UL, (iii) different BSs for the strongest signals in the UL/DL for a UE, and (iv) near-and-far distance effect causing a UE's transmit power to be distance dependent [130]. Hence, a splitting of the UL/DL has been proposed in the literature [130] such that different BSs can serve the UL/DL separately.

Splitting of the UL/DL can benefit from a number of issues such as (i) splitting can allow new device-centric network design for 5G [3]; (ii) the UL/DL transmit powers' disparity can be made scalable with SCBS density; (iii) association of the UL/DL can be made based on different parameters, e.g. received power for the DL and path loss for the UL [131]; and (iv) an optimal UL/DL association can be performed. Further, C-plane traffic is bursty and discontinuous and typically more active during establishing connections. However, U-plane traffic is typically continuous [26-27]. To address these issues, authors in [4] proposed splitting of the C-/U-plane such that C-plane is to operate on low microwave and U-plane on high mmWave frequencies. Since splitting of the UL/DL is seen as one of the major changes in 5G [28], dual connectivity feature of a UE to communicate with two nodes operating at different frequencies has been proposed in [29]. Hence, an additional spectrum is expected to lead the co-existence of frequencies with diverse propagation characteristics within the same system to address the demand for high data rate services [3]. So far, existing literatures addressed splitting of the UL/DL or the C-/U-plane using two separate BSs operating at different frequencies.

However, rather than considering separate BSs operating at different bands for splitting the UL/DL or the C-/U-plane, also termed as different BSs based split

architecture (DBSA), splitting via the same BS, e.g. FCBS, enabled with multi-band, also termed as single BS based split architecture (SBSA), benefits from a number of such issues as follows:

- By decoupling the UL/DL or the C-/U-plane with a single FCBS on different frequency bands, there is no need for exchanging coordination control signaling [131] between BSs as opposed to the case when splitting via different BSs.
- Since C-plane signaling is performed at the same FCBS, there is no need for an additional X3 interface between any FCBSs and the MCBS as proposed in [4].
- By serving the C-/U-plane completely by different transceivers at the same FCBS, flexibility in switching power of U-plane transceiver between on and off states can be obtained because of no C-plane signaling for coordination between the MCBS and FCBSs is needed for initiating such activities as U-plane cell discovery, wake up, and sleep mode mechanisms as in the case of DBSA [7]. Since C-plane and U-plane transceivers are co-located at the same FCBS, based on a UE connection request in the UL, the C-plane transceiver can promptly inform the U-plane transceiver to change states from power off to power on, which greatly simplifies network management, reduces network wide response delay and overhead, and improves network wide energy efficiency.
- A UE association to any U-plane FCBSs can be performed in a simple way by the UE itself following the conventional cell association procedure, which is based on the reference signal received power strength, without taking any assistance from the MCBS. This can help avoid complex cell discovery mechanism for selection of an optimal U-plane cell for the UE as in the case of DBSA since the MCBS does not have any prior knowledge of sleeping U-plane BSs around the UE as in the case of serving the C-/U-plane via different BSs [7].
- Since both U-plane and C-plane are co-located at the same FCBS, prospective C-RAN feature can be adopted easily into multi-band enabled FCBS in SBSA because of no coordination is needed between the MCBS and the centralized baseband processing unit pools, which are connected to each other via common

public radio interface. The MCBS manages mobility and assists UEs for cell discovery via baseband processing unit pools [132].

Further, as in the case of splitting via different BSs in DBSA, the UL/DL can be scheduled at the same FCBS on different radio access technologies such as 3G wideband code division multiple access and LTE where one radio access technology, e.g. wideband code division multiple access, may operate on co-channel microwave band, and LTE may operate on mmWave band [131]. Furthermore, decentralized C-plane processing can release MCBS to process an enormous C-plane signaling overhead as proposed in [4] from an ultra-dense SC and improve scalability such that more FCBSs with traffic demand can be easily added. Though the co-existence of co-channel microwave and different frequency mmWave bands at the same FCBS has manifold benefits as aforementioned, in our best knowledge, no existing literature has addressed the issue of the UL/DL splitting and/or the C-/U-plane splitting with multi-band deployed at the same FCBS in SBSA for routing such decoupled traffic for 5G networks.

In this chapter, we address this issue by proposing a multi-band, i.e. co-channel microwave and different frequency mmWave bands, enabled FCBS and UE architecture for the UL/DL and the C-/U-plane splitting for 5G networks. A group of FCBSs, also termed as FC cluster, are deployed in a 3D multi-storage building. Each FCBS is deployed with two transceivers operating at these bands having a diverse propagation characteristic. The FD scheduler for allocating RBs of both bands is implemented at a cluster head, which can be any FCBS within the building. All FCBSs within the building communicate with CH via X2 interfaces. We first show the performances of microwave and mmWave bands enabled FCBSs under the same scenario to provide incentives on co-existing multiple bands at the same FCBS and UE and understand how and underpin why the decoupled UL/DL and the C-/U-plane traffic is to be routed on which of these two bands. Based on system level performances of both bands, we then propose a generic multi-band enabled FCBS and UE architecture for SBSA and develop a number of disruptive SBSA architectural design alternatives, including a complete UL/DL and C-/U-plane splitting as well as a combined UL/DL and C-/U-plane splitting for 5G networks. Performance evaluations of SBSA are carried

out, and the outperformances of a number of proposed SBSAs in comparison with DBSA in terms of system level capacity, average spectral efficiency, energy efficiency, and C-plane overhead backhaul traffic capacity are shown. Finally, we point out a number of business and technical perspectives and key research issues of SBSA to underpin its implementation.

The chapter is organized as follows. The system model of a multi-tier network is described in section 5.2 where we present system architecture, co-channel interference management, and multi-band resource scheduling algorithm for SBSA. In section 5.3, simulation scenarios, parameters, and results on performances of microwave and mmWave bands are described to give incentives for employing SBSA. A multi-band enabled FCBS and UE architecture for SBSA is proposed, and its connection establishment procedure, scheduler implementation, and traffic transport mechanism are discussed in section 5.4. In section 5.5, a number of SBSAs for the C-/U-plane and the UL/DL splitting are presented. Performance evaluations of SBSA are carried out in comparison with DBSA in section 5.6 in terms of system level capacity, average spectral efficiency, energy efficiency, and C-plane overhead backhaul traffic capacity. The business and technical perspectives of SBSA are discussed in section 5.7, and a number of open research issues regarding SBSA are pointed out in section 5.8. Finally, we summarize the chapter in section 5.9.

5.2 System model

5.2.1 System architecture and interference management

System architecture of a multi-tier network is illustrated in Figure 5.1. We consider a single MC of a corner excited 3-sectored MC site and a number of SCs of various categories, including outdoor PCs and indoor FCs in an urban environment. All FCs are deployed in a 3D multi-storage building modelled as 3GPP dual strip FC model. A certain percentage of the total MUs are considered inside the building. All indoor MUs are served by the MC. In addition, a certain percentage of outdoor MUs are offloaded to nearby PCBSs. An apartment in the building with yellow color represents

that a FCBS is deployed in it, and the one with ash color represents the absence of a FCBS in it. The architecture is used for both co-channel microwave and different frequency mmWave deployed FCBSs.

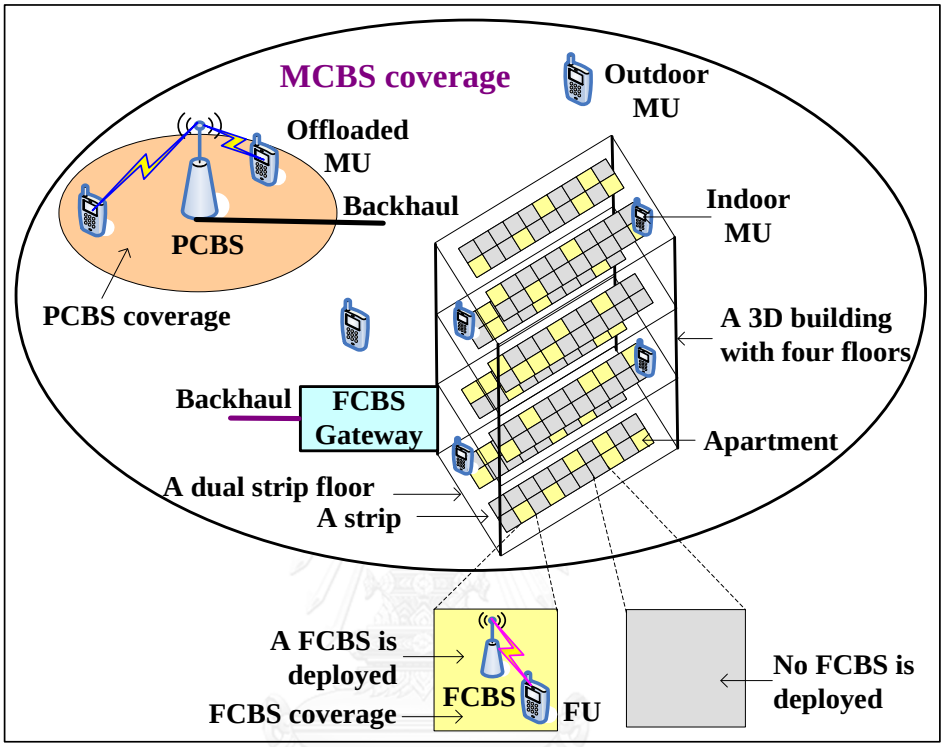

Figure 5.1: System architecture of a multi-tier network.

We consider interference management for co-channel deployed FCBSs by avoiding allocation of the same radio resources mainly time and frequency to UEs such that co-channel interference can be avoided. All indoor MUs and outdoor MUs are allocated orthogonally to RBs. The same system bandwidth is reused to all active FCs, and RB distribution among all indoor MUs is considered orthogonal. If a MU is within the building, TD ABS based eICIC is applied to avoid co-channel interference between indoor MUs and FUs as shown in Figure 5.2. ABSs are reserved for all MUs during which all FCBSs mute transmission of control and data information except synchronization and broadcast channels. However, indoor MUs are not served during non-ABSs by MCBS to avoid co-channel interference with FUs. For different frequency deployed FCBSs, we consider 60-GHz mmWave LOS band for all FCBSs and 2-GHz microwave band for MCBS and all PCBSs. MmWave RBs are also

allocated to FUs orthogonally both in TD and FD so that no co-tier interference management for FCBSs is needed. Since FCBSs are deployed at a different frequency from that of MCBS and PCBSs, there is no need for cross-tier interference management between MC-plus-PC tier and FC tier.

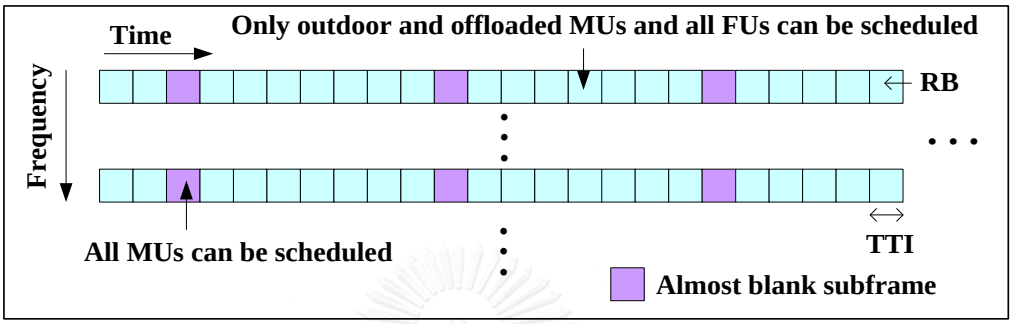

Figure 5.2: ABS based TD eICIC for co-channel interference avoidance in microwave band.

5.2.2 Problem formulation

A. Network model

Denote P_M, P_P, and P_F as the transmit powers of a MC, a PC, and a FC respectively. Consider that there are M RBs in microwave bandwidth B_1 and m RBs in mmWave bandwidth B_2 such that $B \in \{B_1, B_2\}$, and N MUs in the system. Let S_P denote the number of PCs in the MC coverage. Consider that the number of offloaded MUs is uniformly distributed in the interval [1, U_{OFL}]. Let U_P^q denote the number of MUs offloaded by the PC S_P^q such that $\forall q U_P^q \in [0,\ U_{P,\max}^q]$, where $\{U_{P,\max}^q = N^+ : U_{OFL} = \sum_{q=1}^{S_P} U_P^q \le N^+\}$. If all PCs have an equal number of offloaded MUs U_P, i.e. $\forall q U_P^q = U_P$ then the total number of offloaded MUs, $U_{OFL} = S_P \times U_P$. However, in general, U_P^q is a random variable which varies from one PC to another, and the realization of U_P^q for a PC is mutually independent from the others. We consider U_{OFL} = 4 in our simulation set up. If μ_{iM} denotes the ratio of the number of indoor MUs, then

the total number of indoor MUs is $U_{MI} = \mu_{iM} \times N$, outdoor MUs is $U_{MO} = N\text{-}U_{OFL}\text{-}U_{MI}$, and MUs served by the MC is $U_M = U_{MO}+U_{MI}$.

Let N_M denote the set of indices of all MUs such that $\boldsymbol{N_M} = \{1, 2, 3, \ldots, N\}$. Denote $\boldsymbol{N_{MO}}$, $\boldsymbol{N_P}$, and $\boldsymbol{N_{MI}}$ respectively the set of indices of all outdoor MUs, offloaded MUs, and indoor MUs. Note that $\boldsymbol{N_M}$ is partitioned randomly into three disjoint subsets $\boldsymbol{N_{MO}}$, $\boldsymbol{N_P}$, and $\boldsymbol{N_{MI}}$. Let S_F denote the number of active FCs in the building. Consider that the number of FUs is uniformly distributed in the interval [1, U_F] where U_F =10 in our simulation set up. Also let U_F^w denote the number of FUs served by the FC S_F^w such that $\forall w U_F^w \in \left[0,\ U_{F,\max}^w\right]$, where $\{U_{F,\max}^w = N^+ : U_F = \sum_{w=1}^{S_F} U_F^w \le N^+\}$. If all FCs have an equal number of FUs, U_{FC} i.e. $\forall w U_F^w = U_{FC}$ then the total number of FUs in the building, $U_F = S_F \times U_{FC}$. However, in general, U_F^w is a random variable which varies from one FCBS to another, and the realization of U_F^w for a FCBS is mutually independent from the others. Let $\boldsymbol{N_F}$ denote the set of all FU indices such that $\boldsymbol{N_F} = \{1, 2, 3, \ldots, U_F\}$. The realization of MUs served by MC and PCs are not mutually independent since MUs served by PCs are MUs offloaded from MC, and the schedulers have a complete knowledge when a MU is offloaded. However, an offloaded MU to any PC is equally likely in a realization. Note that a realization is defined as a simulation run time.

The FC building and PCs are located randomly and uniformly within MC's area. All outdoor MUs, offloaded MUs, and FUs are distributed randomly and uniformly within their respective BSs' coverage areas. Let $\boldsymbol{T}$ denote simulation run time with the maximum time of Q (in time step each lasting 1 ms) such that $\boldsymbol{T} = \{1, 2, 3, \ldots, Q\}$. Let $\boldsymbol{T_{ABS}}$ denote the number of ABSs in every ABS pattern period of 8 subframes for our simulation set up, such that $\boldsymbol{T_{ABS}} \subseteq \boldsymbol{T}$ and $\boldsymbol{T_{ABS}} = \{t: t = 8v+n_A;\ v = 0, 1, 2, \ldots, Q/8;\ n_A = 1, \ldots, T_{ABS}\}$ where $T_{ABS} = 1, 2, \ldots, 8$ corresponds to ABS patterns $\varphi = 1/8, 2/8, \ldots, 8/8$ respectively. Let t_{ABS} and $t_{non-ABS}$ denote respectively an ABS and a non-ABS such that $t_{ABS} \in \boldsymbol{T_{ABS}}$ and $t_{non-ABS} \in \boldsymbol{T} \backslash \boldsymbol{T_{ABS}}$.

B. System capacity and spectral efficiency

Let d_{MU}, d_{PC}, and d_{BL} denote respectively the distances of any MU, PC, and FC building from the MCBS, and d_{FC} denotes the distance between a FCBS and a FU. The distances of all UEs of each category in a realization are generated following the respective distribution functions as mentioned earlier. The path loss is calculated using the path loss formulas given in Table B.1 in Appendix B. For co-channel microwave enabled only FCBSs, since the whole system bandwidth is reused in FCBSs, and during an ABS, no FCBS can transmit data signal, the aggregate capacity of all FCBSs for any φ (following (C.5) in Appendix C) can be expressed as

$$\sigma_{cc}^{FC}\left(\rho_{cc}^{FC}\right)=\sum_{t=1}^{Q}\sum_{i=1}^{M}(1-\varphi)\ \sigma_{t,i}\left(\rho_{t,i}\right) \tag{5.1}$$

Hence, the total system capacity over *M* RBs for *Q* TTIs can be expressed as the sum throughput of all UEs as follows

$$\sigma_{cc}^{sys}\left(\rho\right)=\sum_{t=1}^{Q}\sum_{i=1}^{M}\sigma_{t,i}\left(\rho_{t,i}\right) \tag{5.2}$$

where σ and ρ are responses over *M* RBs of only indoor MUs in $t\in \boldsymbol{T_{ABS}}$, all FUs in $t\in \boldsymbol{T}\backslash\boldsymbol{T_{ABS}}$, and all outdoor MUs and offloaded MUs in $t\in \boldsymbol{T}$.

For different frequency mmWave enabled only FCBSs, since FCBSs operate at a different frequency from that of MCBS, $\varphi=0$ such that the aggregate capacity of all FCBSs is given by

$$\sigma_{df}^{FC}\left(\rho_{df}^{FC}\right)=\sum_{t=1}^{Q}\sum_{i=1}^{m}\sigma_{t,i}\left(\rho_{t,i}\right) \tag{5.3}$$

Hence, the total system capacity for *Q* TTIs can be expressed similarly as the sum throughput of all UEs as follows

$$\sigma_{df}^{sys}\left(\rho\right)=\sum_{t=1}^{Q}\sum_{i=1}^{M}\sigma_{t,i}\left(\rho_{t,i}\right)+\sigma_{df}^{FC}\left(\rho_{df}^{FC}\right) \tag{5.4}$$

where σ and ρ are responses of all MUs over microwave spectrum of *M* RBs and all FUs over mmWave spectrum of *m* RBs for all TTIs.

Following [93, 124], the average spectral efficiency over the whole system bandwidth for *Q* numbers of TTIs of co-channel microwave and different frequency mmWave enabled FCBSs can be expressed respectively as follows

$$\sigma_{cc}^{avg}(\rho) = \sigma_{cc}^{sys}(\rho)/M.Q \tag{5.5}$$

$$\sigma_{df}^{avg}(\rho) = \sigma_{df}^{sys}(\rho)/m.Q \tag{5.6}$$

Using average throughput and by inverse mapping, the system level effective signal-to-interference-plus-noise ratio $\rho^{eff}(\mathrm{dB})$ per RB per TTI of co-channel microwave only or different frequency mmWave only enabled FCBSs can be obtained. The inverse mapping function is represented by

$$\rho^{eff} = 10\log_{10}\left(2^{\sigma^{avg}(\rho)/\beta} - 1\right), \quad \text{for} -10\,\mathrm{dB} \le \rho^{eff} \le 22\,\mathrm{dB} \tag{5.7}$$

where $\sigma^{avg}(\rho)$ denotes respective average spectral efficiency of co-channel microwave only and different frequency mmWave only enabled FCBSs. The system level average spectral efficiency (bps/Hz) per RB per TTI of any scenario can be expressed as

$$\sigma^{sys}\left(\rho^{eff}\right) = \beta\log_2\left(1+10^{\rho^{eff}/10}\right), \quad \text{for} -10\mathrm{dB} \le \rho^{eff} \le 22\mathrm{dB} \tag{5.8}$$

C. Proportional fair scheduling

The proportional fair scheduling algorithm is described in Appendix C.

5.2.3 Multi-band resource scheduling algorithm

We develop a multi-band resource scheduling algorithm for SBSA as shown in Algorithm 5.1 where proportional fair scheduler is employed for scheduling radio resources to all UEs. Default simulation input and variable definitions are given in Table B.1 and Table B.2 in Appendix B. The algorithm works as follows. *N* is first disjointed into three groups to estimate U_{OFL}, U_{MI}, and U_{MO} randomly. For co-channel microwave enabled FCBSs, co-channel interference avoidance scheme, U_{OFL}, U_{MI}, and U_{MO} are then scheduled by separate FD proportional fair schedulers, one for all MUs and the other for all FUs. The same process repeats for all *M* RBs in each TTI and continues for all TTIs of the simulation run time. The aggregate throughput is then estimated and summed over all RBs and all TTIs of respective categories of MUs as

Algorithm 5.1: Multi-band resource scheduling algorithm for SBSA.

01: **Inputs**: (i) Set: P_M, P_P, P_F, μ_{iM}, S_P, S_F, N, U_P, U_F, M, m, Q, φ, t_c, β, G_t, G_r, L_F;
(ii) Initialize: $t \in \{\boldsymbol{T_{ABS}}, \boldsymbol{T \backslash T_{ABS}}\} = \{1,\ldots,Q\}, B \in \{B_1, B_2\}$, $\boldsymbol{N_M}$, $\boldsymbol{N_{MO}}$, $\boldsymbol{N_P}$, $\boldsymbol{N_{MI}}$, $\boldsymbol{N_F}$, $d_{BL}, d_{PC}, d_{MU}, \forall t,i: \{P_{t,i}, N_{t,i}, NF_{t,i}\}, \sigma_{mcwcc}^{MBS} \leftarrow 0, \sigma_{mcwdf}^{MBS} \leftarrow 0$, $\sigma_{mcw}^{FBS} \leftarrow 0$, $\sigma_{mmw}^{FBS} \leftarrow 0$, $\sigma_{cc}^{BS} \leftarrow 0, \sigma_{df}^{BS} \leftarrow 0$;
(iii) Select: U_{OFL}, U_{MI}, U_{MO};
(iv) Estimate: $\forall t,i: \{\mathrm{PL}_{t,i}, \mathrm{LS}_{t,i}, \mathrm{SS}_{t,i}, \rho_{t,i}, \sigma_{t,i}(\rho_{t,i})\}$;

02: **for** t = 1 to Q
03: **if** $B = B_1$
04: **if** $t = t_{ABS}$ $N := U_{MO} + U_{MI} + U_{OFL}$; $U_F := 0$; $U_S := N$;
05: **elseif** $t = t_{non-ABS}$ $U_{MI} := 0$; $N := U_{MO} + U_{OFL}$; $U_S := N + U_F$;
06: **end if**
07: **for** i = 1 to M Estimate throughput of the scheduled MU: $\forall t,i,x\ \sigma_{t,i,x}(\rho_{t,i,x})$
08: Estimate throughput of the scheduled FU: $\forall t,i,x\ \sigma_{t,i,x}(\rho_{t,i,x})$
09: Update throughput of MUs: $\forall N\ \sigma_{mcwcc}^{MBS} \leftarrow \sigma_{t,i,x}(\rho_{t,i,x}) + \sigma_{mcwcc}^{MBS}$
10 Update throughput of FCs: $\forall U_F\ \sigma_{mcw}^{FBS} \leftarrow \sigma_{t,i,x}(\rho_{t,i,x}) + \sigma_{mcw}^{FBS}$
11: **end for**
12: Update aggregate throughput: $\forall U_s\ \sigma_{cc}^{BS} \leftarrow \sigma_{mcwcc}^{MBS} + \sigma_{mcwcc}^{FBS} + \sigma_{cc}^{BS}$
13: Estimate system level throughput (Mbps): $\sigma_{cc}^{sys} = (\sigma_{cc}^{BS} \times 180 \times 10^3)/10^6$
14: Estimate spectral efficiency (bps/Hz): $\sigma_{cc}^{sys}(\rho_{cc}^{eff})$ using (5.5) and (5.7)-(5.8)
15: **elseif** $B = B_2$ $N := U_{MO} + U_{MI} + U_{OFL}$; $U_S := N + U_F$;
16: **for** i = 1 to M Estimate throughput of the scheduled MU: $\forall t,i,x\ \sigma_{t,i,x}(\rho_{t,i,x})$
17: Update throughput of MUs: $\forall N\ \sigma_{mcwdf}^{MBS} \leftarrow \sigma_{t,i,x}(\rho_{t,i,x}) + \sigma_{mcwdf}^{MBS}$
18: **end for**
19: **for** i = 1 to m Estimate throughput of the scheduled FU: $\forall t,i,x\ \sigma_{t,i,x}(\rho_{t,i,x})$
20: Update throughput of FCs: $\forall U_F\ \sigma_{mmw}^{FBS} \leftarrow \sigma_{t,i,x}(\rho_{t,i,x}) + \sigma_{mmw}^{FBS}$
21: **end for**
22: Update aggregate throughput: $\forall U_s\ \sigma_{df}^{BS} \leftarrow \sigma_{mcwdf}^{MBS} + \sigma_{mmw}^{FBS} + \sigma_{df}^{BS}$
23: Estimate system level throughput (Mbps): $\sigma_{df}^{sys} = (\sigma_{df}^{BS} \times 180 \times 10^3)/10^6$
24: Estimate spectral efficiency (bps/Hz): $\sigma_{df}^{sys}(\rho_{df}^{eff})$ using (5.6)-(5.8)
25: **Outputs**: $\sigma_{cc}^{sys}, \sigma_{df}^{sys}, \sigma_{cc}^{sys}(\rho_{cc}^{eff}), \sigma_{df}^{sys}(\rho_{df}^{eff})$;
26: **end if**
27: **end for**

well as all FUs over all reused *M* RBs for all non-ABSs.

For different frequency mmWave enabled FCBSs, both FD schedulers for MUs and FUs can schedule over all RBs of their respective system bandwidths for all TTIs. The overall system level throughput and spectral efficiency are then estimated by adding the aggregate throughput of all MUs to the aggregate throughput of all FUs. Note that for co-channel microwave, the same ABS pattern for all UEs is repeated in every ABS pattern period *T*. The shadow fading and small scale fading effects of all UEs are estimated and updated in each TTI per realization. We do not show explicitly calculations of signal-to-interference-plus-noise ratio and throughput in the algorithm, instead which we have explained in the mathematical model.

5.3 Simulation scenarios, parameters, assumptions and results

We consider two simulation scenarios, including FCBSs operating at co-channel microwave band and different frequency mmWave band. In the former case, all FCBSs operate at the same frequency as that of MCBS and PCBSs, and ABS based eICIC is used for co-channel operation of FCBSs. In the latter case, all FCBSs operate at mmWave band. Resources are allocated orthogonally both in time and frequency among all MUs on microwave band and all FUs on mmWave band. Default simulation parameters and assumptions used for system level simulation are listed in Table B.1 and Table B.2 in Appendix B. Note that though the typical maximum system bandwidths available in microwave and 60 GHz mmWave bands are respectively 100 MHz (for LTE-Advanced systems) and nearly 9 GHz starting at 57.24 GHz and ending at 65.88 GHz [135], we consider for performance evaluation only a fraction and an equal amount of 5 MHz as system bandwidth from both bands. However, since the capacity and spectral efficiency are directly proportional to the system bandwidth, the fundamental trends of performance metrics such as capacity and spectral efficiency with the change of an allocated system bandwidth will not be affected.

Figure 5.3 shows the effect of the number of ABSs on achievable capacity from FC networks when FCBSs are operated on co-channel microwave band. It can be found that FC networks' capacity decreases with an increase in the number of ABSs. This is

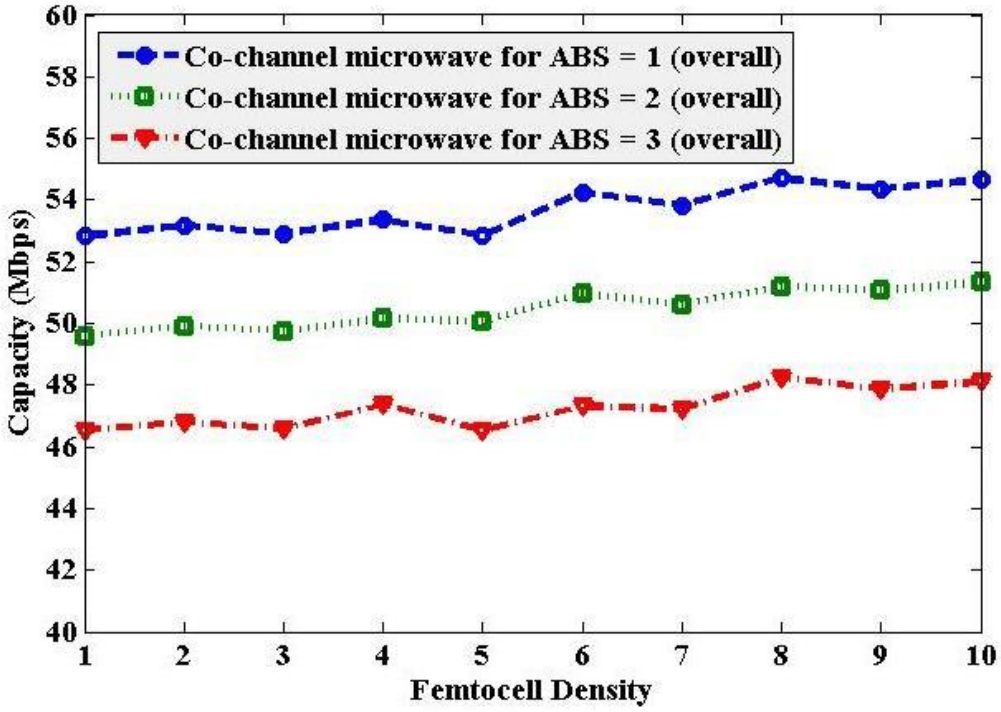

Figure 5.3: Effect of variation in the number of ABSs of TD eICIC on capacity of FC networks when all FCBSs operating on co-channel microwave band with FC density.

because of the fact that FC networks' capacity is inversely related to the number of ABSs as given by (5.1). Further, the capacity increases slightly with an increase in FC density irrespective of the number of ABSs due to multi-user diversity gain, i.e. the probability of better channel conditions for a given system bandwidth, particularly in microwave bands with non-LOS signal components, increases with an increase in the number of FUs and hence FCs. Since the best capacity performance of FC networks is achieved for ABS = 1 when all FCBSs operate on CC microwave band, we consider ABS = 1 as the default case for comparing the performances of co-channel microwave band with that of different frequency mmWave band in what follows.

As shown in Figure 5.4 and Figure 5.5, with mmWave deployed FCBSs, capacity and spectral efficiency performances improve by manifold as compared to the performances achieved by co-channel microwave deployed FCBSs. This is because, in co-channel microwave deployed FCBSs, channels between FCBSs and FUs suffer from non-LOS components originated by, e.g. reflection and scattering effects of intermediate objects and walls. In addition, FCBSs are not allowed to transmit during

ABSs for co-channel interference avoidance because of reusing the same microwave frequency in FCBSs. However, when operating on mmWave band, because of the presence of LOS components, channel conditions between FCBSs and FUs are far better than that when operating on co-channel microwave band, which in turn improves capacity performance. Further, from Figure 5.4, overall system capacity is mostly contributed by FUs as compared to other MUs. By operating both bands simultaneously, capacity performance can be improved further. Note that the number of RBs of system bandwidth is fixed and is allocated to FCBSs by proportional fair scheduler, which simply takes into account of channel conditions for the given past RB allocation statistics of each FCBS at any RB in any TTI.

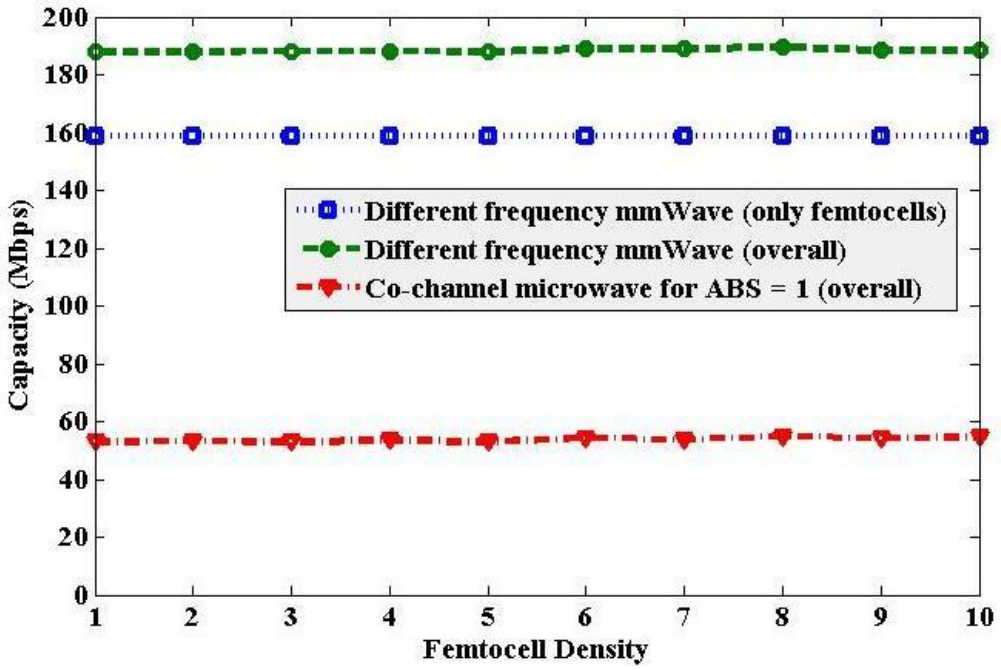

Figure 5.4: Capacity responses of different frequency mmWave and co-channel microwave enabled FCBSs with FC density.

The system level spectral efficiency response (Figure 5.5) follows the same as system capacity. With mmWave, system level spectral efficiency per FCBS - FU link can be improved by manifolds, e.g. about 3 times (Figure 5.5) as compared to what can be achieved by co-channel microwave. Since the channel conditions of FCBSs in indoor environments do not vary considerably, irrespective of the number of FCBSs, overall capacity and spectral efficiency for a given system bandwidth remains almost the same

(Figure 5.4 and Figure 5.5). However from Figure 5.6, it can be found that as system bandwidth increases, capacity of FC networks and the system as a whole also improve, which is an obvious case since an achievable capacity is directly proportional to the available system bandwidth. A noticeable difference in responses of different frequency mmWave and co-channel microwave is that an increase in system bandwidth by the same amount of respective band, mmWave improves capacity by almost four times as that of co-channel microwave due to its better channel conditions, i.e. signal-to-interference-plus-noise ratio responses as shown in Figure 5.4 such that more bits can be transmitted or received per hertz (Hz) on the mmWave band than that on the

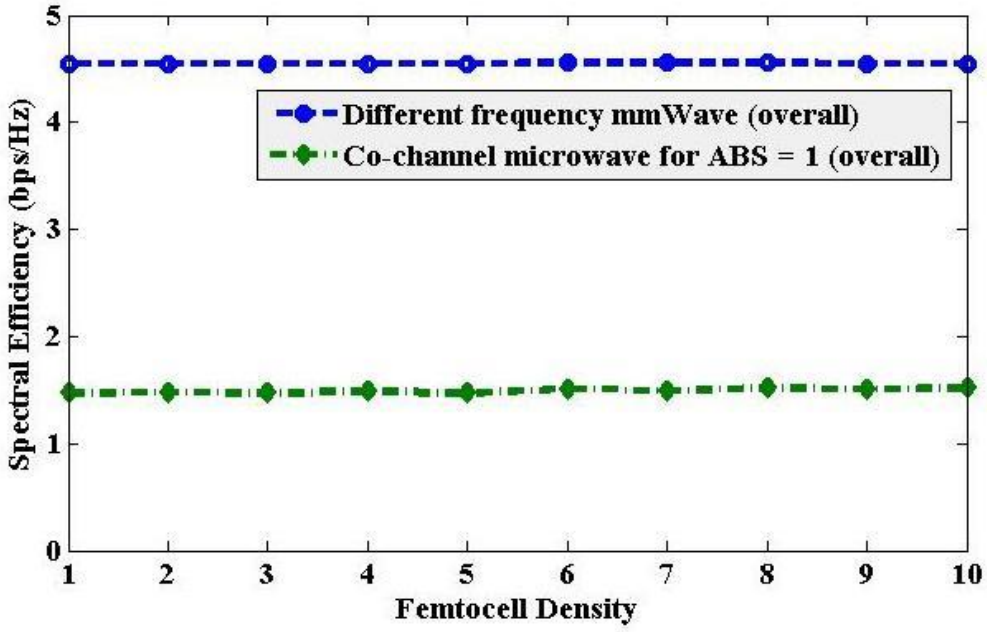

Figure 5.5: Spectral efficiency responses of different frequency mmWave and co-channel microwave enabled FCBSs with FC density.

microwave band. Overall, the frequency band on which FCBSs operate has a significant impact on overall system level capacity and spectral efficiency performances. This frequency band dependency of FCBSs can be explored such that depending on traffic demand and characteristic on the UL/DL and the C-/U-plane, an appropriate band either microwave, mmWave or both of multi-band enabled FCBSs can be operated adaptively to serve the generated traffic.

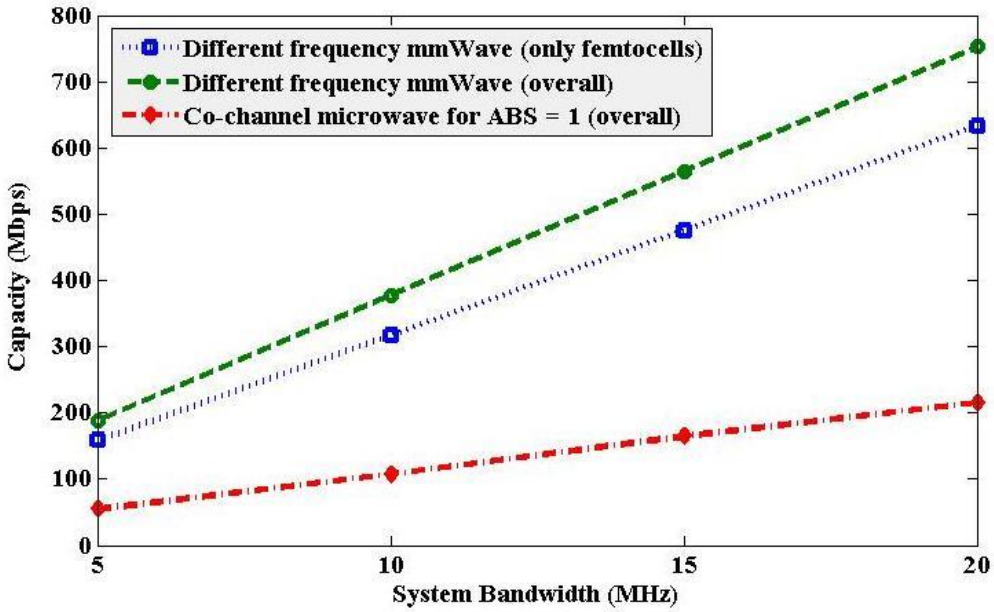

Figure 5.6: Capacity responses of different frequency mmWave and co-channel microwave enabled FCBSs with system bandwidth.

5.4 Multi-band enabled FCBS and UE architecture for SBSA

5.4.1 FCBS and UE architecture and connection establishment

The proposed multi-band enabled FCBS architecture for SBSA is shown in Figure 5.7(a) where a FU is communicating with its associated CSG FCBS on co-channel microwave for the UL and/or C-plane information and on different frequency mmWave for the DL and/or U-plane information by making dual connectivity with the same FCBS. Note that the architecture for cluster head is the same as in Figure 5.7(a) except that it additionally possesses medium access control layer scheduling functionalities for its own FUs as well as all FUs within the building. Based on traffic demand and characteristic served by a FCBS, FD scheduler at cluster head decides whether or not the traffic is to be served by either different frequency mmWave, co-channel microwave or both bands taking into account of FCBS's idle mode mechanism and notifies the corresponding FCBS by control signaling via X2 backhaul using its physical cell identity. The idle mode capability of a FCBS can help mute transmission on either one or both bands depending on traffic availability, characteristic, and

demand. Further, a FCBS can inform its served FU to mute its corresponding transceiver, which we discuss in the following. Hence, both system level energy efficiency and active-mode time of UE's battery can be increased. The architecture in Figure 5.7(a) is generic, and a number of variations of it can be obtained depending on how the UL/DL and the C-/U-plane traffic are configured for routing through mmWave and microwave bands, which we discuss with examples in section 5.5.

For UE architecture, since the propagation characteristic on mmWave bands differs considerably from microwave bands, we propose to use a separate transceiver with a separate baseband unit for each band of multi-band enabled UE architecture as shown in Figure 5.7(b). Modes operated on the microwave band, e.g. 3G and 4G, can use the microwave transceiver, whereas modes operated on the mmWave band, e.g. 60GHz, can use the mmWave transceiver [136]. An application processor can co-operate with baseband unit of each band. Considering separate transceivers for mmWave and microwave bands necessitates more space and associated cost for a UE design. However, since propagation characteristics on these bands are diverse, and majority of the current 4G smartphones particularly in the united states of America are dual stand-by design based (i.e., operating two modes on two transceivers simultaneously) [136], multiple transceivers for coexistence of microwave and mmWave bands at a UE are expected to be promising to address expected requirements of 5G mobile networks.

It is to be noted that since a FU has to be able to operate on both bands when it is within the coverage and only microwave band when out of coverage of its associated CSG FCBS, this will result in additional complexities and associated costs in UE hardware design. Further, if FCBSs are operated on licensed mmWave bands, an additional cost from licensing mmWave bands is needed. However, because of scarcity of available spectrums in microwave bands and a growing demand of high data rate applications leave least options but operating on high frequency mmWave bands. Further, a significant improvement in system capacity and spectral efficiency can be achieved as shown in Figure 5.4 and Figure 5.5 which will compensate these excess costs and complexities.

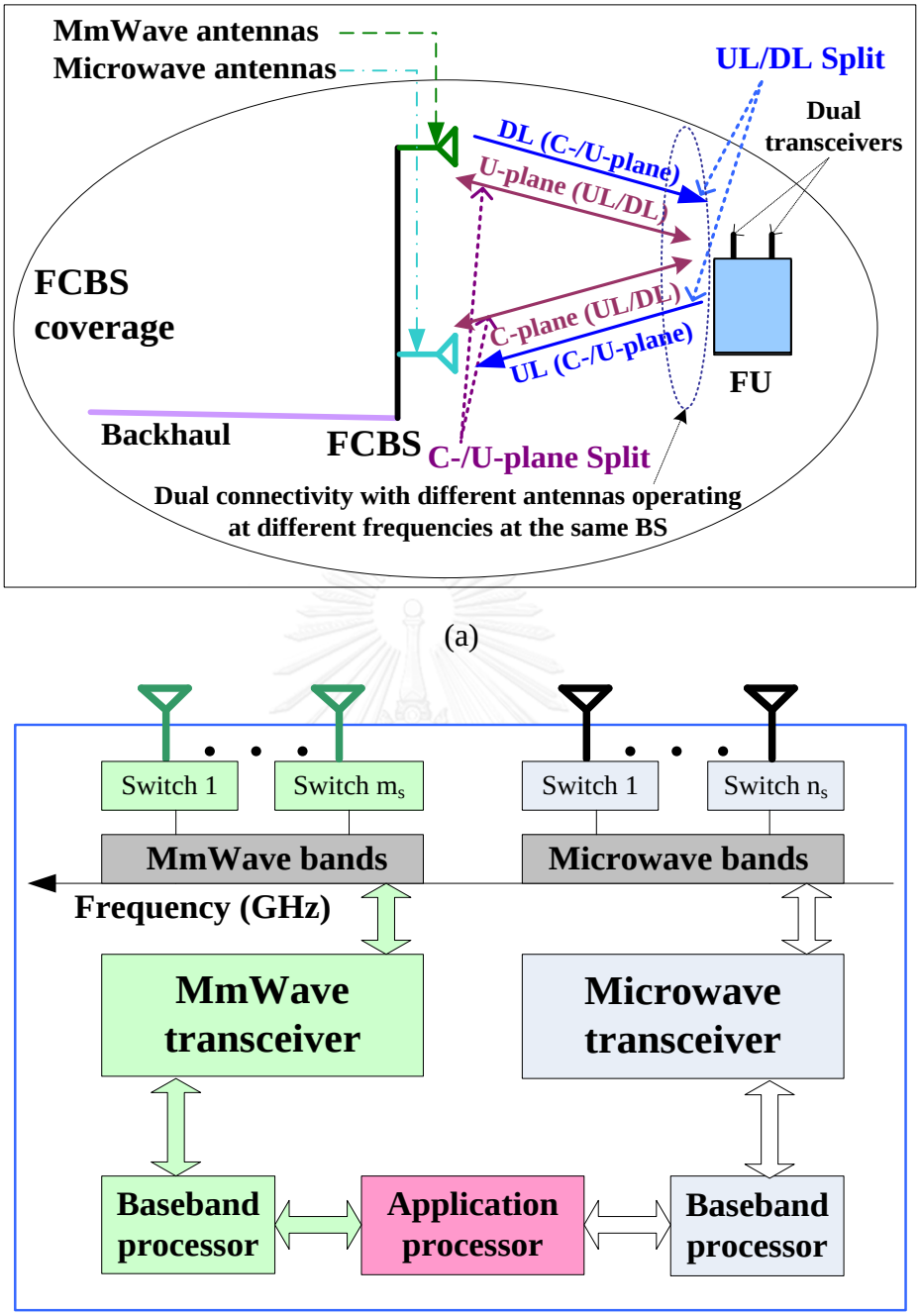

Figure 5.7: Proposed generic multi-band multi-transceiver enabled (a) FCBS and (b) UE architectures for the UL/DL splitting and the C-/U-plane splitting with dual connectivity at the same FCBS in SBSA.

An example connection establishment procedure of multi-band enabled FCBSs for LTE-Advanced systems is shown in Figure 5.8 which works as follows. A FU sends

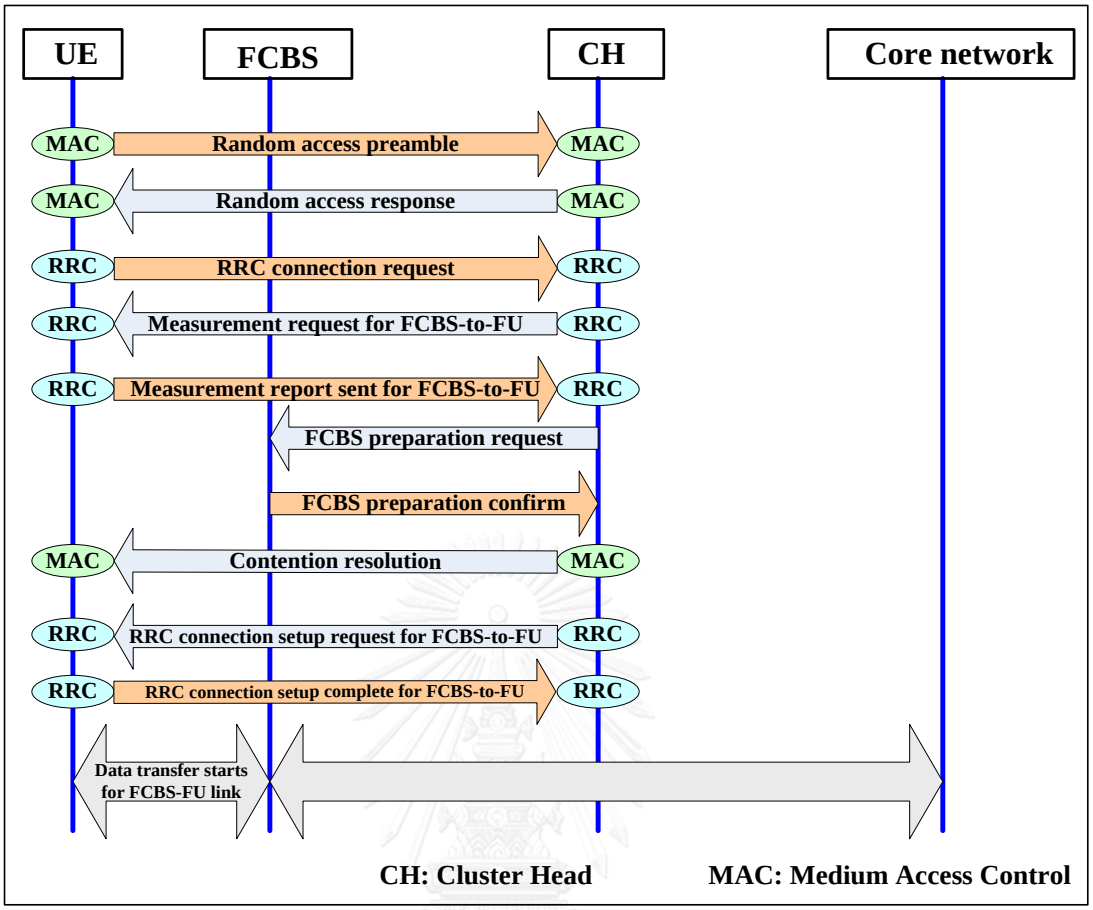

Figure 5.8: An illustration of connection establishment of multi-band enabled FCBS for LTE-Advanced systems.

a request for contention based random access procedure to obtain physical resources for the UL transmission, timing advancement, and cell radio network temporary identifier. The cluster head then replies with a positive response, and following so, FU initiates a radio resource control radio resource control request. The cluster head informs the associated sFCBS of the FU for its preparation. Once acknowledged by the FCBS, the cluster head sends FU a radio resource control connection setup request to set up connection with the FCBS. After configuring protocols as informed by the cluster head, FU then sends a radio resource control connection complete message to the cluster head, and data transfer then can take place between FCBS and FU.

5.4.2 Scheduler implementation and traffic transport mechanism

To schedule radio resources of multiple bands, we propose a disjoint FD scheduler implementation for multi-band FCBSs described as follows. A FD scheduler is implemented at the cluster head for all FUs dis-jointly with the TD scheduler located at MCBS. TD scheduler allocates subframes to all UEs in the system. However, a separate FD scheduler for all MUs is implemented at MCBS. When operating on co-channel microwave band, FUs can directly report their channel status and traffic demand through their CSG FCBSs to the cluster head, and TD scheduler updates the cluster head about ABS pattern per ABS pattern period. To adapt ABS patterns, an indoor MU in the building during an ABS pattern period informs its existence within the building in the UL to TD scheduler. TD scheduler in turn informs the cluster head of ABS patterns to be applied for the next ABS pattern period via X2 backhauls to schedule RBs to FCBSs only during non-ABSs of the ABS pattern, which is sent during the current ABS pattern period. Whereas in case of no presence of an indoor MU over a current ABS pattern period, TD scheduler informs the cluster head to allocate RBs to FCBSs for all TTIs in the next ABS pattern period (Figure 5.9). For different frequency mmWave band, since MCBS and PCBSs operate on a different frequency from FCBSs, there is no need for coordination between MC-plus-PC tier and FC tier. The FD scheduler at the cluster head can directly allocate mmWave RBs to FCBSs without taking any concern of the FD scheduler at MCBS irrespective of the presence of any indoor MUs within the building.

In general, for transporting traffic between a UE and an external packet data network, classifiers or filters, located at both PGW and UE, first classify traffic based on certain traffic criterion (e.g., data rate and delay). The classified traffic is then sent to FD scheduler at the cluster head to schedule them to either mmWave or microwave bands to send or receive traffic to/from FUs. For example in LTE-Advanced systems, classifiers may operate based on quality-of-service class identifier values such that guaranteed bit rate traffic class, e.g. conversational and non-conversational videos, real time gaming, can be allowed to serve by mmWave and non-guaranteed bit rate traffic class, e.g. transmission control protocol based world wide web and electronic-mail, by microwave as default bands. Further, delay in-tolerant traffic, e.g. IP multimedia subsystem signaling and a high maximum bit rate non-guaranteed bit rate traffic, e.g.

live video streaming, can be served by mmWave if allocation and retention priority can be satisfied.

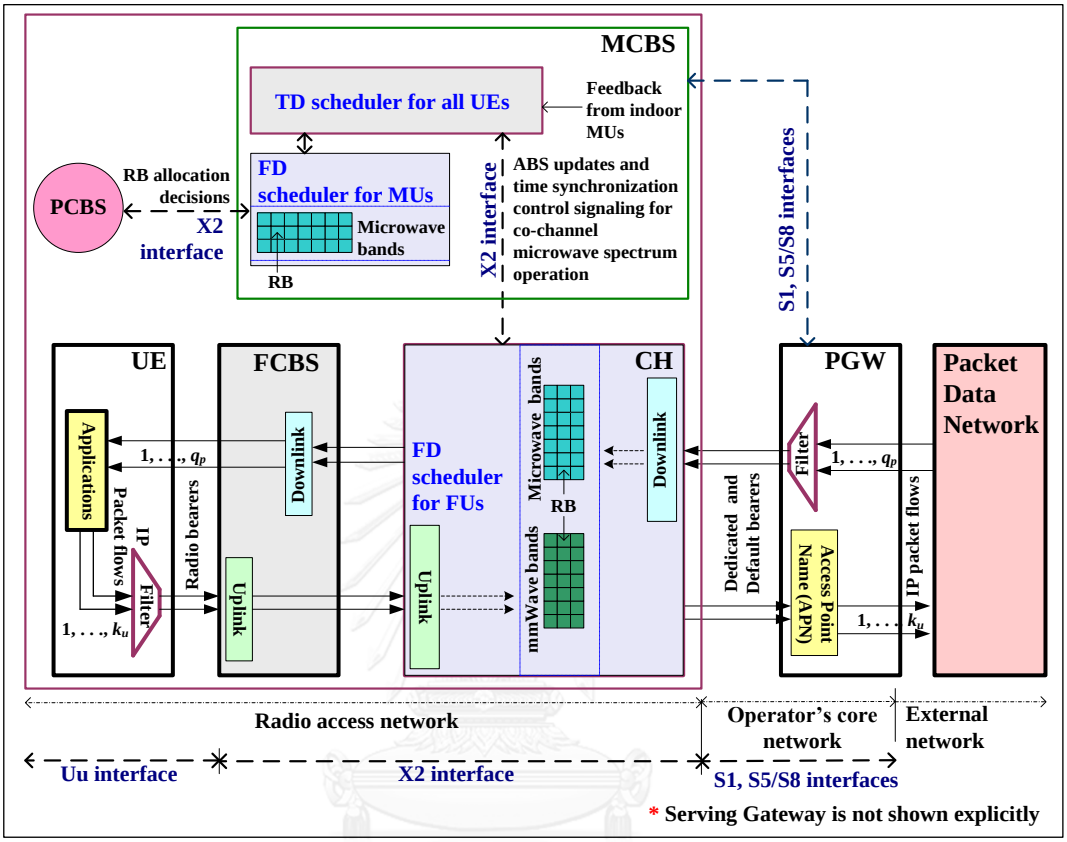

Figure 5.9: UL/DL traffic transport mechanism of LTE-Advanced systems using multi-band enabled single FCBS.

The UL/DL traffic transport mechanism of multi-band enabled FCBSs for LTE-Advanced systems is shown in Figure 5.9. In the DL, after filtering IP traffic, packet filters at PGWs create respective dedicated bearers from PGWs through SGWs, located between the cluster head and PGW and not shown explicitly in Figure 5.9, to FD scheduler at the cluster head. The FD scheduler can then schedule RBs of respective bands to classified traffic and informs via X2 backhauls to all FCBSs in the building to transmit traffic to their associated FUs by creating radio bearers. In the UL, filtering of generated IP traffic is performed at FUs, as opposed to PGW in the DL, and sent by creating radio bearers to respective FCBSs. All FCBSs then send the UL traffic via X2 backhauls to the cluster head, which then sends these traffic by creating necessary dedicated bearers based on traffic criterion via S1 interface through SGW to PGW. At

PGWs, a reverse operation to what was performed at FUs is executed to send the UL traffic to respective packet data networks through their access point networks.

5.5 UL/DL and C-/U-plane splitting architectures with multi-band enabled FCBS and UE

Since there is no specific standard for 5G networks, and the fundamental decision for 5G considers heavily on how to combine and leverage investments on existing 4G LTE networks with capabilities provided by 5G [137] along with a continual effort on LTE evolution through a number of releases by 3GPP beyond release 10 towards 5G, we consider to demonstrate all the proposed splitting architectures in this section using LTE-Advanced systems as default scenario. However, the idea and implementation will not be affected with such consideration.

5.5.1 Complete UL/DL splitting architecture

A complete splitting of the UL/DL at the cluster head using multiple bands in SBSA for 5G mobile networks is shown in Figure 5.10. A similar architecture was proposed by [138] where the MCBS was considered as the anchor point at which the UL/DL flow splitting and reassembling take place. In contrast to that, we consider splitting and reassembling to be performed at a SCBS, i.e. the cluster head of a FC cluster, where multiple bands, i.e. microwave and mmWave bands, are dedicated completely for the UL/DL traffic as default scenario, and all FCBS traffic in FC cluster is routed directly to the core network. Since FCBSs are in a FC cluster within a building and very close in distance from the cluster head, the minimal delay requirement between the cluster head and FCBSs for sending access stratum for layer 1 (L1), layer 2 and radio resource control signaling and non-access stratum for mobility and session management over X2 interface can be easily addressed.

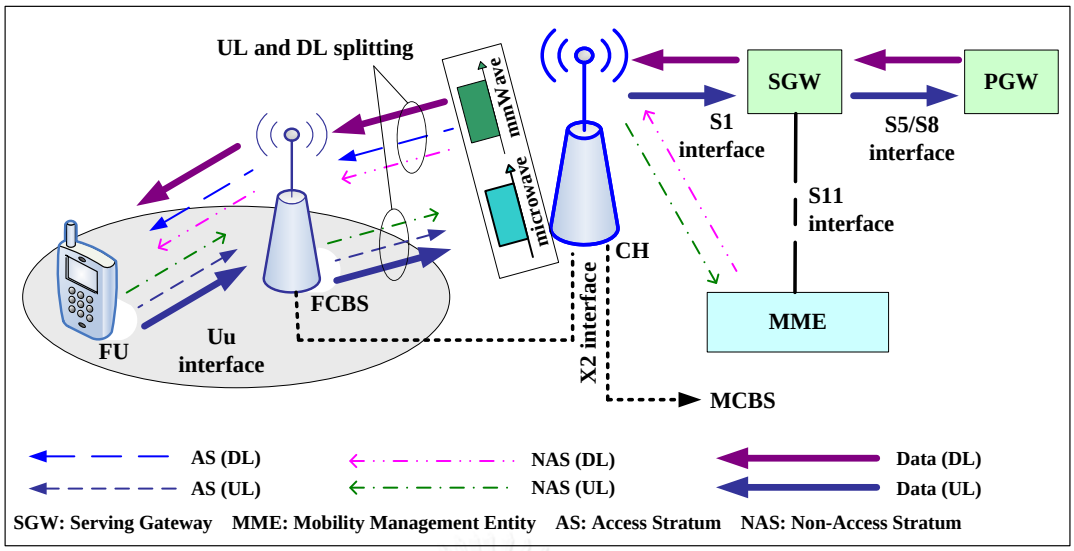

Figure 5.10: A complete UL/DL splitting architecture with multi-band enabled FCBS and UE in SBSA.

L1 functionality can be processed either at a FCBS or the cluster head depending on limitations of backhaul between the cluster head and a FCBS. If non-ideal backhauls such as digital subscriber line, copper cable are used, L1 functionally may be shifted to FCBSs to compensate delay. However, if ideal backhauls such as optical fiber are used, then L1 functionality can be processed at the cluster head for all FCBSs within a FC cluster. Further, since medium access control layer functionalities are considered to be performed by the cluster head only, this type of scheduling is termed as centralized scheduling mechanism where all FCBSs act as a simple transceiver except the cluster head with or without L1 functionality depending on backhaul characteristics between the cluster head and FCBSs.

With a complete separation of the UL/DL using different bands, a number of benefits can be achieved as follows:

- The capacity of the UL is independent of that of DL.
- Because of operating at different bands, there is no interference between the UL/DL signals.
- The UL or the DL transceiver can be switched on or off based on availability of traffic on either link such that network wide energy efficiency improves.

- High spectral utilization can be achieved since typically more traffic in the DL is served by mmWave band than that in the UL, which is served by microwave band.
- The cluster head can directly communicate to the core network without taking much concern of MCBS except for ABS pattern updates for co-channel microwave band.
- Since certain applications require guaranteed bit rate and are provided by establishing dedicated bearers, the establishment of dedicated bearers can be easily addressed by operating the UL/DL on different bands.
- Predicted excessive asymmetric traffic consumption in 5G networks requires link specific resources such that high data rate traffic can be easily served by mmWave band, regardless of the availability of the UL microwave resources.

5.5.2 Complete C-/U-plane splitting architecture

Another variation of a complete splitting mechanism in SBSA is to consider a complete C-/U-plane separation at the cluster head as shown in Figure 5.11. Since most

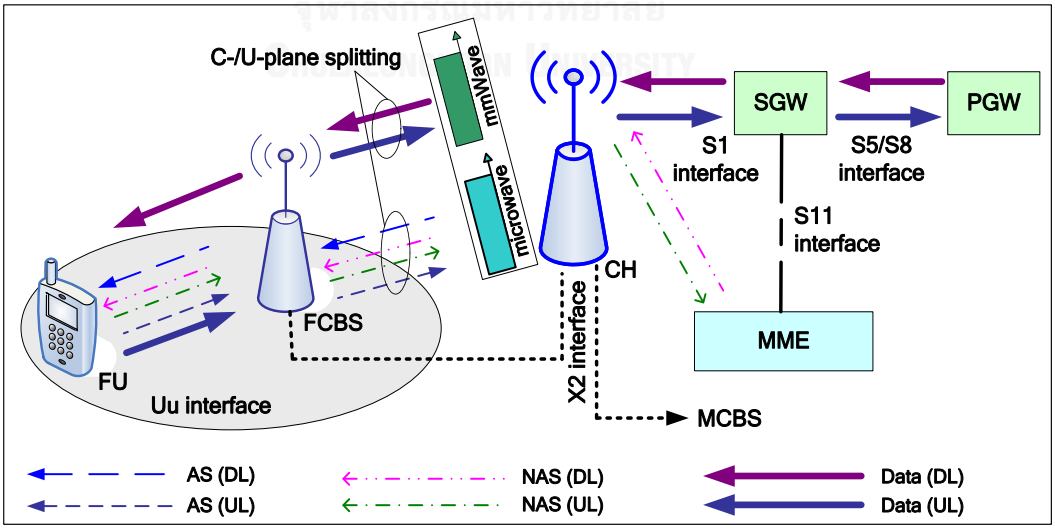

Figure 5.11: A complete C-/U-plane splitting architecture with multi-band enabled FCBS and UE in SBSA.

of the traffic is generated from the U-plane, the mmWave spectrum is solely dedicated to serve U-plane data traffic of both the UL and the DL, whereas the co-channel microwave band is dedicated solely for the low rate C-plane traffic of both the UL and the DL. The cluster head acts as the anchor point to split the C-plane and the U-plane traffic in both the UL and the DL. The L1 and the medium access control layer functionalities can be performed similarly as described in the case of a complete UL/DL splitting architecture shown in Figure 5.10.

5.5.3 Combined UL/DL and C-/U-plane splitting architecture

Because of considerably greater amount of traffic generated in the DL than the UL as well as in the U-plane than the C-plane, we propose a combined UL/DL and C-/U-plane splitting architecture in SBSA for 5G networks as shown in Figure 5.12 where the mmWave band is dedicated solely for the DL U-plane data traffic to achieve a high throughput per FU, and microwave band is dedicated for all control signaling traffic (i.e., the UL/DL and C-plane) and the UL U-plane data traffic. In addition, any low rate data traffic on C-plane for both the DL and the UL is considered to be served by the microwave band.

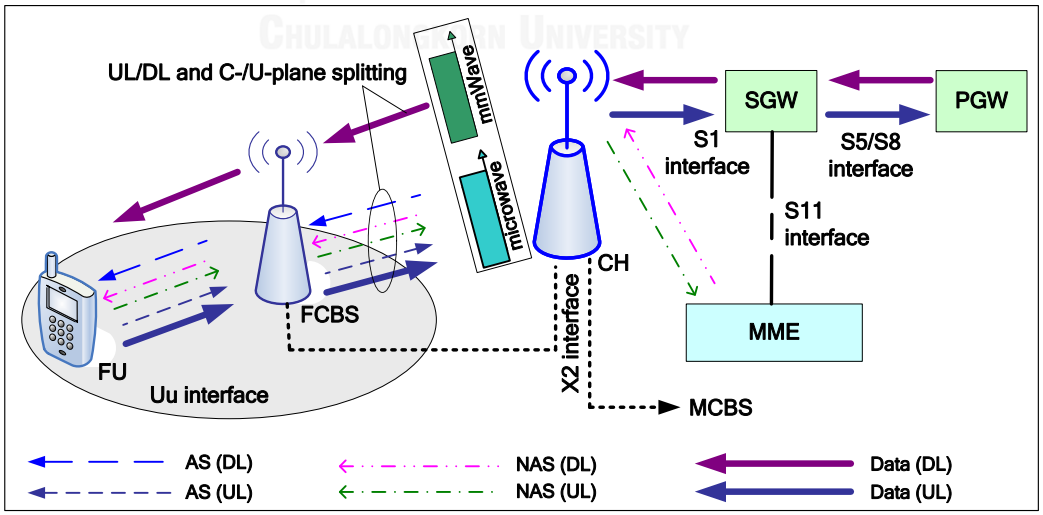

Figure 5.12: A combined UL/DL and C-/U-plane splitting architecture with multi-band enabled FCBS and UE in SBSA.

5.6 Performance evaluation

We consider both qualitative and quantitative performance evaluations of a number of proposed architectures in section 5.5 as follows.

5.6.1 Qualitative performance analysis

The major drawback of conventional C-/U-plane coupled mobile networks is that all BSs need to be always powered on irrespective of any UE's operating modes, i.e. idle or active mode, and data traffic demands in order to ensure a ubiquitous coverage because of the coupled C-/U-plane. This results in an under-utilization of radio resources mainly for U-plane traffic and a low network energy efficiency [7], which can be overcome by splitting the C-/U-plane traffic of UEs. The splitting of the C-/U-plane can be performed by employing either a single band transceiver or dual transceivers operating at different frequency bands at each SCBS as shown in Figure 5.13.

In a single band enabled SCBS, the C-/U-plane can be decoupled by operating a SCBS either at the same co-channel spectrum as that of the MCBS as shown in Figure 5.13(c) or at a different spectrum from that of the MCBS as shown in Figure 5.13(a). In this architecture, the C-plane is served by the MCBS, and the U-plane is served by SCBSs [7, 9, 24-25]. As mentioned earlier, since the splitting of a UE traffic is done by two different BSs, this split architecture is termed as DBSA. If SCBSs are operating at the co-channel spectrum as that of the MCBS, a proper cooperative interference management between the macro-tier and the SC-tier is needed to avoid co-channel cross-and co-tier interferences. However, if SCBSs are operation at a different spectrum from that of the MCBS, there is no need for the cross-tier interference management. The major drawback of DBSA is that the C-plane signaling network is very complex and challenging to design [7]. The complexity comes from the fact that the MCBS, i.e. the C-plane BS, does not have any prior information of instantaneous channel conditions between the in-active U-plane SCBSs and any UEs. Hence, selecting an

optimal U-plane SCBS and performing an initiation of wake up mechanism for an in-active SCBS are difficult [7].

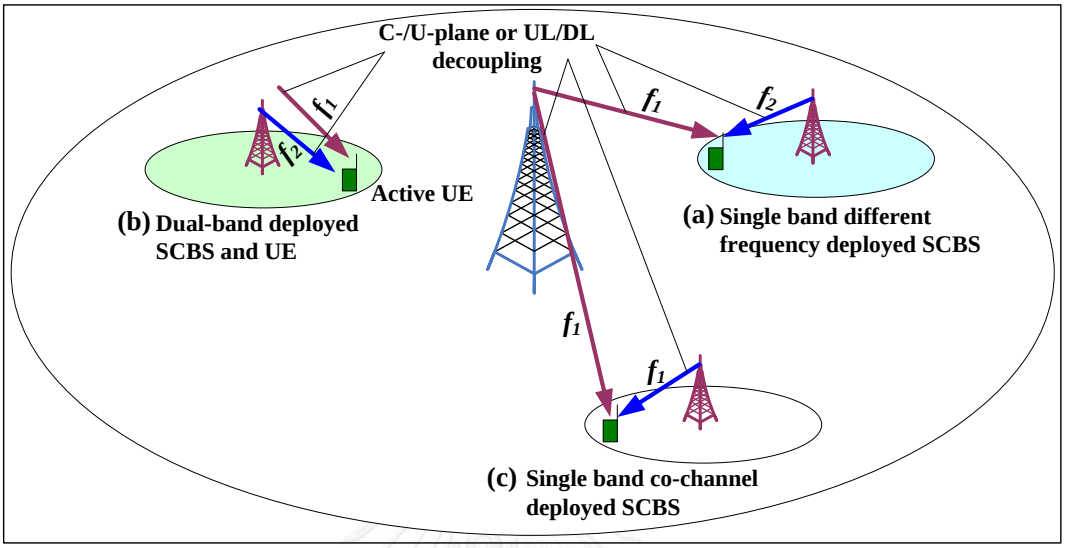

Figure 5.13: Different approaches to decoupling the C-plane and the U-plane traffic of a UE.

The other way to address the C-/U-plane splitting is to employ dual-band for dual transceivers in each SCBS, such that a SCBS operates at both the co-channel microwave band as that of the MCBS and different frequency mmWave band from that of the MCBS as shown in Figure 5.13(b). Since the splitting of a UE's traffic is done by the same SCBS, we refer this split architecture to SBSA. In SBSA, the C-/U-plane are decoupled by allowing a UE's C-plane traffic served by a transceiver operating at the co-channel microwave spectrum and U-plane traffic served by another transceiver operating at the mmWave spectrum at any SCBSs. The C-plane transceiver needs to be always on in order to ensure a ubiquitous coverage and the handover mechanism. However, the U-plane transceiver needs to be active only when there is an active data service request from any UEs and can be switched off if there is no data service request. This on-demand switching on and off the U-plane transceiver can result in a huge saving of SCBS power and improve the overall network energy efficiency. Further, since both the C-plane and the U-plane are served by the same SCBS, switching power on and off the U-plane transceiver depending on a UE's U-plane service request can be performed easily because of being the C-plane transceiver always in powered on mode

at the same FCBS. Hence, no coordination signaling is required between the C-plane and the U-plane BSs which overcomes the drawback of DBSA. Furthermore, because of serving both the C-plane and the U-plane by the same SCBS, the synchronization of both the U-plane and the C-plane handovers can be easily performed. Note that in SBSA, the single band operation for dual transceivers is not applicable since technically it does not make any sense. Table 5.1 shows a comparative performance evaluation of DBSA and SBSA.

5.6.2 Quantitative performance analysis

The control signaling overhead affects mainly two major performance metrics, namely capacity and energy efficiency [139]. This is because of the fact that an increase in control signaling overhead results in a corresponding decrease in radio resources available for user data transmission and additional energy consumption from transmitting these signaling traffic. Hence, we consider evaluating the performance of the proposed SBSA for these two metrics in comparison with the DBSA. In addition, we also evaluate the system level capacity and average spectral efficiency performances of SBSA in comparison with the DBSA. The proposed system model in section 5.2 is used for system level capacity, average spectral efficiency, and energy efficiency performances, while the model in [60, 140-142] is adopted to evaluate the backhaul control overhead traffic capacity performance in both SBSA and DBSA.

A. Backhaul control overhead traffic capacity

There are two backhaul interfaces in LTE systems, including S1 and X2. S1 conveys user data from the aggregate gateway, which is the entrance to the evolved packet core networks [141] to each BS, and X2 is responsible for exchanging mutual information between cells. Moreover, as the data demand increases, the demand for control signaling on S1 backhaul interface increases consequently. The backhaul traffic consists of a number of traffic, mostly the user generated U-plane traffic in addition to the overhead traffic from S1 signaling, handover between cells, and other management

Table 5.1: A comparative performance evaluation of DBSA and SBSA.

Aspect	DBSA	SBSA
Control signaling network	Complex	Simple
SCBS power on and off	C-plane BS always on, U-plane BS switches on based on data traffic request	C-plane transceiver always on, U-plane transceiver switches on based on data traffic request
MCBS and SCBS cooperation is needed	Yes	No
Multi-band enabled UE energy consumption for the C-plane in the UL traffic	Moderate (high transmit power of the transceiver for the C-plane in the UL because of a long distance between a UE and the MCBS)	Low (low transmit power of the transceiver for the C-plane in the UL because of a short distance between a UE and the SCBS)
Feedback delay	High (because of an additional latency during an idle to an active mode transition of a SCBS)	Less (because both the C-plane and the U-plane reside at the same SCBS)
U-plane cell discovery mechanism is needed	Yes (the MCBS performs the U-plane SCBS discovery mechanism for a UE)	No (UE driven based on reference signal received power strength)
Synchronization accuracy level needed for the U-plane and the C-plane traffic between the MCBS and any SCBSs	Very high (since the C-plane and the U-plane are served by different BSs)	Moderate (applicable only if the UE association to any U-plane SCBSs is performed via the MCBS)
Overall U-plane traffic capacity for a given bandwidth over a certain duration of time	Moderate (because of allocating additional resources for the C-plane signaling between the C-plane BS and the U-plane BS for cooperation)	High (because of no cooperation between the C-plane BS and the U-plane BS is needed and reusing the same microwave spectrum in SCBSs)
Complexity to introduce C-RAN	High (because of cooperation for the C-plane signaling between the MCBS and the baseband processing unit pools of the U-plane SCBSs)	Less (because of no cooperation for the C-plane signaling between the MCBS and the baseband processing unit pools of the U-plane SCBSs is needed)

and synchronization related activities. The overhead traffic is expressed as a proportion of the U-plane traffic which varies typically with the type of traffic (e.g., a large number of low data rate connections have more overhead signaling traffic than its counterpart, a small number of high data rate ones) [142].

The S1 signaling is related to the user data traffic. Since both the MCBS and FCBSs serve their own UEs' U-plane traffic in SBSA, which is routed directly to the core network separately by the respective BS category, the C-plane overhead from S1 signaling is the same in both DBSA and SBSA. Further in SBSA, a UE whenever is out of coverage of any FCBSs, it must be handed over either to any nearest FCBSs (if available) or the MCBS for both the U-plane and C-plane traffic. Since in DBSA, U-plane is typically served by small coverage of FCBSs, and the MCBS can serve some low data rate U-plane traffic, we assume that the handover signaling traffic in DBSA is the same as in SBSA. Note that, typically handover signaling overhead is very small as compared to the overall U-plane data traffic and is smaller than that of S1 signaling as well. Hence, in both DBSA and SBSA, the C-plane overhead from S1 signaling and handover mechanisms on the backhaul is present and is considered the same.

1. DBSA and SBSA

In typical DBSA, SCBSs are connected to a host MCBS. The C-plane low data rate traffic is served by a large coverage based MCBS to provide seamless and always-on connectivity, and U-plane high data rate traffic is served by the small coverage based SCBSs to provide high data rate services [7, 9, 24-25]. In line with [60], considering ideal backhaul links between the MCBS and SCBSs or between the SCBSs themselves and ignoring overhead from synchronization and management for wireless traffic, the U-plane data traffic is assumed to be related only with the bandwidth and average spectral efficiency in each BS. Assume that all SCBSs have the same bandwidth and average spectral efficiency such that the backhaul throughput can be expressed as the product of the bandwidth and average spectral efficiency in a SCBS [60, 142].

Assuming 10% overhead from S1 signaling and 4% overhead from handover traffic [60, 141], we can find the total throughput requirement.

Let γ_{sc} and γ_{mc} denote the average spectral efficiency of a SCBS and a MCBS respectively, and B_{sc} and B_{mc} denote the bandwidth of a SCBS and a MCBS respectively. Let x_c be the amount in percentage, expressed in proportion of U-plane traffic [142], for control signaling traffic over backhauls for cooperation between all FCBSs and the MCBS. Each FCBS is controlled directly by the MCBS individually. We assume that the UL control signaling traffic for any FCBSs at the MCBS is negligible in comparison with the DL control signaling traffic such that x_c is considered only in the DL of the MCBS. We describe in detail the modeling of x_c in a later section. Hence, the UL/DL throughputs of the MCBS can be expressed as [60, 140-142] follows:

$$\delta_{mc,d} = \begin{cases} 0.04.B_{mc}.\gamma_{mc,d} = \delta_{mc-UL,d} & \text{for UL} \\ (1+0.1+0.04+x_c).B_{mc}.\gamma_{mc,d} = \delta_{mc-DL,d} & \text{for DL} \end{cases} \tag{5.9}$$

Similarly, the UL/DL throughputs of a FCBS can be expressed as follows:

$$\delta_{sc,d} = \begin{cases} 0.04.B_{sc}.\gamma_{sc,d} = \delta_{sc-UL,d} & \text{for UL} \\ (1+0.1+0.04).B_{sc}.\gamma_{sc,d} = \delta_{sc-DL,d} & \text{for DL} \end{cases} \tag{5.10}$$

Since there are S_F FCBSs in the coverage of the MCBS, the total UL/DL throughputs of the backhaul can be expressed as follows:

$$\delta_{tot-UP/DL,d} = \begin{cases} S_F.\delta_{sc-UL,d} + \delta_{mc-UL,d} = \delta_{tot-UL,d} & \text{for UL} \\ S_F.\delta_{sc-DL,d} + \delta_{mc-DL,d} = \delta_{tot-DL,d} & \text{for DL} \end{cases} \tag{5.11}$$

Hence, the total backhaul throughput for DBSA can be expressed as follows [60]:

$$\delta_{tot-back,d} = \delta_{tot-UL,d} + \delta_{tot-DL,d} \tag{5.12}$$

Conversely, in SBSA, since both U-plane and C-plane are served by the same FCBS without taking any assistance from the MCBS except for ABS pattern period updates, there is no need for any additional C-plane control signaling overhead to be exchanged for cooperation between the MCBS and any FCBSs because of splitting the C-/U-plane. Hence, the value of x_c can be considered zero for SBSA such that (5.9) can be modified as follows:

$$\delta_{mc,s} = \begin{cases} 0.04.B_{mc}.\gamma_{mc,s} = \delta_{mc-UL,s} & \text{for UL} \\ (1+0.1+0.04).B_{mc}.\gamma_{mc,s} = \delta_{mc-DL,s} & \text{for DL} \end{cases} \quad (5.13)$$

Following (5.10)-(5.11), the UL/DL throughputs of any FCBSs and the total UL/DL throughput of the backhaul can be expressed as follows:

$$\delta_{sc,s} = \begin{cases} 0.04.B_{sc}.\gamma_{sc,s} = \delta_{sc-UL,s} & \text{for UL} \\ (1+0.1+0.04).B_{sc}.\gamma_{sc,s} = \delta_{sc-DL,s} & \text{for DL} \end{cases} \quad (5.14)$$

$$\delta_{tot-UP/DL,s} = \begin{cases} S_F.\delta_{sc-UL,s} + \delta_{mc-UL,s} = \delta_{tot-UL,s} & \text{for UL} \\ S_F.\delta_{sc-DL,s} + \delta_{mc-DL,s} = \delta_{tot-DL,s} & \text{for DL} \end{cases} \quad (5.15)$$

Hence, the total backhaul throughput of the proposed SBSA for the UL/DL splitting (Figure 5.10) can be found as follows:

$$\delta_{tot-back,s} = \delta_{tot-UL,s} + \delta_{tot-DL,s} \quad (5.16)$$

Note that though the (5.10)-(5.12) and (5.14)-(5.16) look similar in expressions except the subscripts, the values of $\gamma_{sc,d}$ and $\gamma_{sc,s}$ differ based on the type of frequency band used for serving the UL/DL of DBSA and SBSA as given in Table 5.2. The subscripts *d* in (5.9)-(5.12) and *s* in (5.13)-(5.16) denote respectively the perspectives of DBSA and SBSA.

Table 5.2: Frequency bands for serving the UL/DL of DBSA and SBSA.

	DBSA		**SBSA**	
UL/DL	**MCBS**	**FCBS**	**MCBS**	**FCBS**
UL	microwave	mmWave	microwave	microwave
DL	microwave	mmWave	microwave	mmWave

2. Modeling x_c of DBSA

In DBSA, a tight coordination of the C-/U-plane traffic to serve a UE simultaneously by the MCBS and FCBSs is needed to perform such activities as synchronization of U-plane traffic served by FCBSs and C-plane traffic served by the MCBS, idle and active mode switching of FCBSs, and cell discovery mechanism for an optimum FCBS selection by the MCBS. The arrivals of C-plane signaling traffic per FCBS because of this coordination of the C-/U-plane traffic can be modeled as

random and independent events. Let $A_1, ..., A_{S_F}$ denote respectively the mean number of arrivals of C-plane signaling traffic for FCBSs $1, ..., S_F$ during a certain period of time T_d such that the mean total number of arrivals A in time duration T_d for S_F FCBSs can be expressed as follows:

$$A = A_1 +, ..., + A_{S_F} \tag{5.17}$$

For simplicity, we assume that $\{\forall i\, A_i \in \mathrm{N} : A > 0, \text{for } i = 1, ..., S_F\}$, and each arrival for C-plane signaling contains an equal amount of traffic c irrespective of the number of arrivals per FCBS in T_d and the value of S_F. Hence in T_d, the total C-plane signaling traffic x_c exchanged over the backhaul for the C-/U-plane coordination of S_F FCBSs can be expressed as follows:

$$x_c = c \times A \tag{5.18}$$

To simplify further, assume that each FCBS has the same number of arrivals for coordination in T_d such that $\{\forall i\, A_i = A_s\}$, then (5.17)-(5.18) can be rewritten as follows:

$$A = A_1 +, ..., + A_{S_F} = S_F \times A_s$$

$$x_c = c \times (S_F \times A_s)$$

$$x_c = S_F \times (c \times A_s)$$

$$x_c = S_F \times c_s \tag{5.19}$$

where c_s is the total amount of C-plane signaling traffic per FCBS in T_d.

Equation (5.19) reveals that for a given c_s, the additional C-plane signaling traffic x_c is directly proportional to the number of FCBSs S_F and grows linearly with S_F. For numerical analysis, the default values are given in Table 5.3. Figure 5.14 shows the total backhaul capacity requirement for both DBSA and SBSA with the variation of the number of FCBSs S_F from 1 to 10 for c_s = 2%, 5%, and 10% of the U-plane data traffic per FCBS and is consistent with the results shown in [60, 141]. Note that typically the traffic demand in FCBSs varies significantly as compared to the MCBS

because of more context specific service demand and traffic usage pattern over time. From Figure 5.14, it can be found that there is an additional C-plane signaling traffic requirement for coordination between all FCBSs and the MCBS for DBSA as compared to the proposed SBSA. For instance, for c_s = 10%, there is an additional C-plane signaling traffic of 10 Mbps for 10 FCBSs (Figure 5.9), which is equivalent to approximately 4.76% ($10\text{Mbps}/210\text{Mbps}$) of the total backhaul U-plane data traffic of 210 Mbps (not shown explicitly in Figure 5.14), required for DBSA as compared to SBSA under the same scenario. Hence, the proposed SBSA outperforms the DBSA, which has been extensively considered for the 5G mobile network architecture in terms of the reduction in C-plane signaling overhead because of no coordination signaling required between FCBSs and the MCBS for serving the C-/U-plane traffic. This allows the allocation of more resources to U-plane data traffic transmission with SBSA than that with DBSA, which results in increasing the network capacity.

Table 5.3: Default parameters for backhaul traffic estimation.

Parameter	Value
Average spectral efficiency of the MCBS for microwave band in DBSA ($\gamma_{mc,d}$) in bps/Hz	2
Average spectral efficiency of a FCBS for mmWave band in DBSA ($\gamma_{sc,d}$) in bps/Hz	4
Average spectral efficiency of the MCBS for microwave band in SBSA ($\gamma_{mc,s}$) in bps/Hz	2
Average spectral efficiency of a FCBS for co-channel microwave band in SBSA ($\gamma_{sc,s}$) in bps/Hz	2
Average spectral efficiency of a FCBS for mmWave band in in SBSA ($\gamma_{sc,s}$) in bps/Hz	4
Bandwidth for the MCBS in both DBSA and SBSA (B_{mc}) in MHz	5
Bandwidth for a FCBS for mmWave band in both DBSA and SBSA (B_{sc}) in MHz	5
Bandwidth for a FCBS for co-channel microwave band in SBSA (B_{sc}) in MHz	5

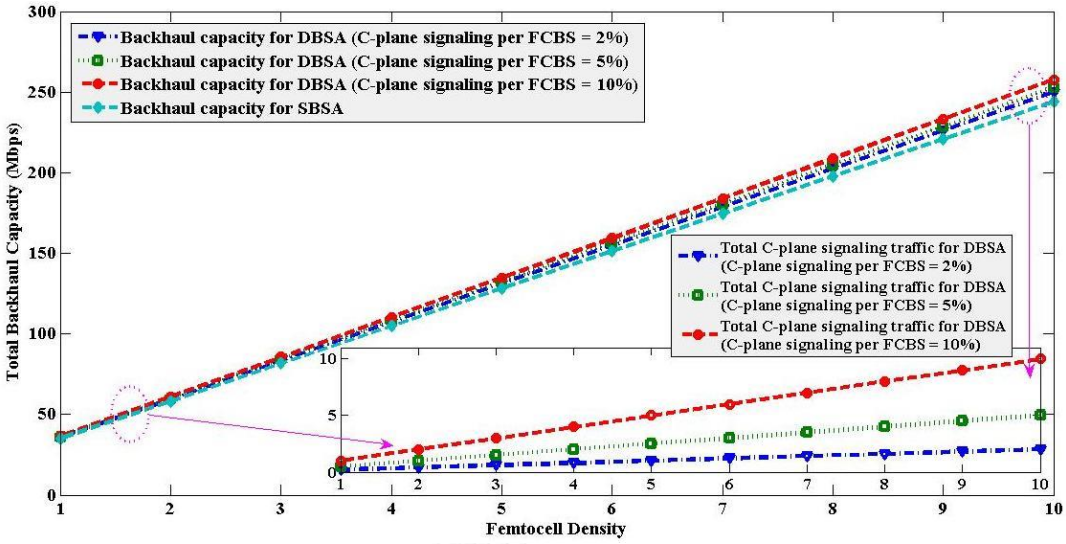

Figure 5.14: Total backhaul capacity requirement in DBSA and SBSA.

B. Energy efficiency performance

We use the models given in in Table B.1 and Table B.2 in Appendix B for evaluating the energy consumption of the proposed model for the C-/U-plane splitting architecture (Figure 5.11) in SBSA and DBSA. Since in the DL a UE under the coverage of a FCBS receives U-plane data traffic from the FCBS, and in the UL it transmits U-plane data traffic using the mmWave transceiver in both SBSA and DBSA, we consider evaluating the energy consumption of the C-plane in the UL in both SBSA and DBSA.

For the worst case scenario of the proposed system architecture, we consider a FU is located at the edge of the nominal coverage of a CSG FCBS within the building. In the proposed architecture, the C-plane traffic transmission in the DL and the UL of a FU is served by the co-channel microwave transceiver of the FCBS. However, in DBSA, the C-plane traffic transmission in the DL and the UL of a FU is served by the MCBS at co-channel microwave frequency. Figure 5.15 shows the C-/U-plane splitting under SBSA and DBSA for the energy consumption performance evaluation.

For simplicity we do not consider any fading effects for both indoor and outdoor cases so that the transmit power requirement can be solely expressed by the path loss. Note that each of the FCBSs shown in Figure 5.15 is located within a building. Hence,

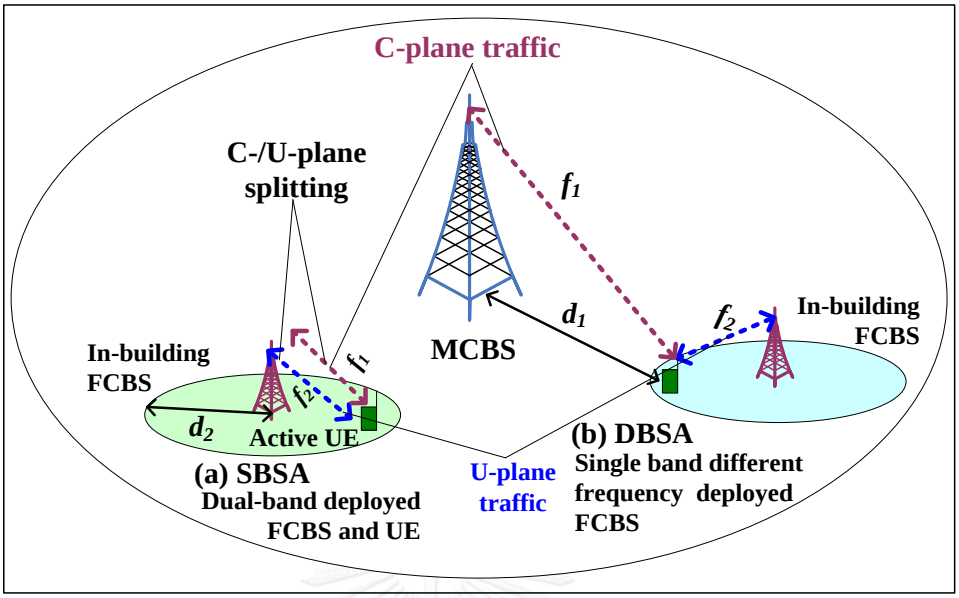

Figure 5.15: C-/U-plane splitting under SBSA and DBSA for the energy consumption performance evaluation: (a) SBSA and (b) DBSA.

for the above scenario in Figure 5.15 and the proposed C-/U-plane splitting architecture, using Table B.1 and Table B.2 in Appendix B, the path loss for C-plane traffic transmission between a FCBS and a FU in SBSA is given by

$$\mathrm{PL}\,(\mathrm{dB}) = 127 + 30\log_{10}(d_2/1000) \tag{5.20}$$

where d_2 is in m for 2 GHz.

Similarly, the path loss for C-plane traffic transmission between a MCBS and a FU in DBSA is given by

$$\mathrm{PL}(\mathrm{dB}) = 15.3 + 37.6\log_{10} d_1 + \mathrm{L}_{\mathrm{ow}} \tag{5.21}$$

where d_1 is in m, and $\mathrm{L}_{\mathrm{ow}} = 20$ dB.

Consider the worst case scenario such that the building is located at the MC edge boundary. Under this condition, we can find the maximum path loss that a link between the MCBS and a FU can experience. For an inter-site distance of 1732 m, the radius of a MC is $d_1 = 1732/3 \cong 577$ m. Then, path loss at this radial distance can be found using (5.21) as follows:

$$\mathrm{PL}\,(\mathrm{dB}) = 15.3 + 37.6\log_{10}(577) + 20 = 139.12\ \mathrm{dB}\ \text{(maximum)}$$

Since the minimum seperation distance between a MCBS and any SCBSs is 75 m, the minimum path loss can be calculated for d_1 = 75 m, which is 105.80 dB (minimum). Assume that the nominal coverage of a FCBS, d_2 = 5 m for a 10×10 m^2 apartment, using (5.20), the path loss for the proposed C-/U-plane splitting architecture can be found as follows:

$$\mathrm{PL}\,(\mathrm{dB}) = 127 + 30\log_{10}(5/1000) = 57.96\,\mathrm{dB}$$

From the above calculation, it can be found that the maximum and minimum path losses in DBSA incurs approximately 81.16 dB and 47.94 dB more path losses for the C-plane traffic in the DL and the UL respectively between a MCBS and a FU as compared to the proposed C-/U-plane splitting architecture in SBSA between a FCBS and a FU. Hence, to overcome such a huge deviation in path losses in DBSA and SBSA, both the MCBS in the DL and a UE in the UL in DBSA need to transmit C-plane traffic at a high power to achieve the receivers' sensitivity levels at both the MCBS and a UE. The C-plane signaling is considerable with respect to the U-plane traffic, e.g. 10% S1 signaling, 4% handover signaling, and other synchronization and UE specific traffic signaling overhead [60, 141] which in total constitutes a great portion of the total traffic carried by the network. Hence, in DBSA, the C-plane traffic transmission at high power results in a considerable amount of additional energy consumption in comparison with the SBSA. Further, since a UE's transmit power is much lower than that of a MCBS, this will affect greatly UE's battery operating time. Furthermore, the above result also implies the fact that the C-/U-plane splitting using different BSs are not able to address the transmit power disparity in the UL and the DL particularly for C-plane traffic, which is a very crucial need to improve UE's battery operating time and reduce interference effects. Hence, the proposed SBSA consumes less energy, i.e. more energy efficient, than the DBSA proposed in the literature for 5G networks.

C. System level capacity and spectral efficiency performances

We evaluate the relative system level capacity and spectral efficiency performances of SBSA and DBSA by employing them into the proposed system model in section 5.2. In SBSA, each FCBS is enabled with both the co-channel microwave

and different frequency mmWave bands. The total system capacity for *Q* TTIs for the multi-band enabled FCBS in SBSA can be expressed by the sum throughput of (5.2)-(5.3) as follows:

$$\sigma_{mb}^{sys}(\rho) = \sigma_{cc}^{sys}(\rho) + \sigma_{df}^{FC}\left(\rho_{df}^{FC}\right) \tag{5.22}$$

From Figure 5.4 and using (5.4) and (5.22), it can be found that the overall system level capacity in DBSA for different frequency mmWave, $\sigma_{df}^{sys}(\rho) \cong 188\,\text{Mbps}$, whereas the overall system level capacity in SBSA, $\sigma_{mb}^{sys}(\rho) \cong \sigma_{cc}^{sys}(\rho) + \sigma_{df}^{FC}(\rho) \cong (53+160)\,\text{Mbps} \cong 213\text{Mbps}$ such that $\sigma_{mb}^{sys}(\rho) > \sigma_{df}^{sys}(\rho)$. Hence, the system level capacity in SBSA is higher than that in DBSA.

Following [93, 124], the average spectral efficiency over the whole system bandwidth for *Q* numbers of TTIs in SBSA and DBSA can be expressed respectively as follows:

$$\sigma_{mb}^{avg}(\rho) = \sigma_{mb}^{sys}(\rho)/(M+m).Q \tag{5.23}$$

$$\sigma_{sb}^{avg}(\rho) = \sigma_{df}^{sys}(\rho)/(M+m).Q \tag{5.24}$$

Since $\sigma_{mb}^{sys}(\rho) > \sigma_{df}^{sys}(\rho)$, then $\sigma_{mb}^{avg}(\rho) > \sigma_{sb}^{avg}$ for the same values of *M*, *m*, and *Q* in both DBSA and SBSA. Hence, the average spectral efficiency in SBSA is also higher than that in DBSA.

5.7 Technical and business perspectives

A number of technical and business values from network operators' viewpoint to implement multi-band enabled FCBSs and UEs in SBSA are pointed out as follows:

5.7.1 Technical perspectives

- Since mmWave deployed FCBSs can achieve more capacity than that of microwave deployed ones because of various favorable features of mmWave bands, e.g. LOS propagation and full radio resource availability for FCBSs, it

is desirable to enable FCBSs with multiple bands in locations where the traffic fluctuation is very high such that based on traffic characteristics, a FCBS can switch to an mmWave band during a high traffic demand and to a microwave band during a low traffic demand. Whenever necessary, both bands can operate concurrently to increase the data rate further. With such an adaptive scheme for spectrum availability in FCBSs, network operators can provide on-demand data rate services, optimize location specific resource allocation, and maximize profit margin.

- The C-plane signaling overhead from the coordination between C-plane BSs and U-plane BSs for such mechanisms as cell discovery for selection of an optimal U-plane cell, initiation of wake up and sleeping modes for U-plane BSs, and synchronization of U-plane and C-plane traffic can be avoided because of co-location of the C-plane and the U-plane transceivers at the same FCBS.
- Due to a low transmit power and an omnidirectional antenna radiation pattern, a UE can transmit the UL traffic at low transmit power to a FCBS on the co-channel microwave spectrum because of shorter distance between a UE and a FCBS in SBSA than that between a UE and a MCBS in DBSA, which can help increase the UE's battery operating time. In addition, because of a relatively lower path loss, transmitting a C-plane traffic to a UE by the FCBS in the DL consumes less power in SBSA than transmitting by the MCBS in DBSA, which results in improving the network energy efficiency.
- Introducing C-RAN capability into the SBSA is less complex than that into the DBSA owing to no need for coordination over common public radio interface between the baseband processing unit pools and the MCBS.
- Transmit power disparity in the UL/DL in the DBSA can be overcome by allowing a UE to communicate for both the UL and the DL only via a FCBS such that more UL data rate can be achieved using SBSA at the same transmit power than that using DBSA.

5.7.2 Business perspectives

- In SBSA, since one of the transceivers is operating at the co-channel microwave frequency of the MCBS, there is no need for an additional investment on licensing any new spectrums for multiple bands at the same FCBS.
- Unlike DBSA, there is no need for an additional X3 interface for the coordination between the MCBS and FCBSs in SBSA which helps save the cost from implementing necessary backhauls for the X3 interface.
- To introduce C-RAN feature in SBSA, no fronthaul for the coordination over common public radio interface is needed between the MCBS and the baseband processing unit pools as compared to DBSA, and hence the cost from necessary fronthaul implementation can be avoided.
- Because of overcoming the additional C-plane signaling overhead for the coordination between the MCBS and FCBSs in SBSA, the cost of transmission in terms of b/s/Hz/J is less in SBSA than that when using DBSA.

5.8 Open research issues in SBSA

In the following a number of generic research issues under both device level and network level for multi-band enabled FCBSs in SBSA are discussed.

5.8.1 Multi-band device level

A. Integration of multiple bands

Though the concept of multi-band co-existence at the UE is straightforward, however their integration is not obvious since the exact answer to where this integration should take place in the protocol stack, i.e. at the radio frequency front end, baseband, medium access control or above medium access control layers, has not been well evaluated [143]. This is partly because of the fact that below 3 GHz microwave and 60 GHz mmWave bands have different propagation characteristics, e.g. the radiation pattern of the former is typically omnidirectional whereas the latter is highly directional.

Hence, an in-depth understanding on the multi-band integration in a device is a crucial need.

B. Concurrent operation of multiple bands

Though the simultaneous operation of both microwave and mmWave bands can contribute to improving the system capacity, it may have the negative impact on the power consumption. A UE may or may not be able to operate concurrently in different bands depending on the degree of tightness in their integration, which calls for researches on how and when to switch from one band to another [143], and how the split mechanisms for both the UL/DL and the C-/U-plane during switching either of the two bands off could be served.

C. Self-interference

With an increase in the number of simultaneously operating bands in a UE, the mixture of these different frequencies increases exponentially [144]. This effect is termed as self-interference which can be minimized by coordinating at a higher layer. However, it comes at the cost of affecting network performance metrics, e.g. throughput and maximum data rate, because of switching any bands off for a certain period of time [144]. Though in the proposed architecture, we consider the minimum value of two for a multi-band architecture, finding an optimal number of bands in a multi-band architecture are an important area of research for a balance trade-off between the reduction in self-interference and network performance.

D. Multi-band transceiver design

A multi-band transceiver consists of a number of parallel transceivers, one for each spectrum band, which meet at a common point of digital signal processing equipment. Each branch for a transceiver consists of a radio frequency bandpass filter for the corresponding spectrum band, a radio frequency frontend, and an analog-to-

digital converter. Overall, the closer this union point of these transceivers to the antenna, the less the number of required elements that causes a decline in the size and the cost of the device [145]. Hence, a comprehensive research on the development of such kind of multi-band transceiver with the point of their union as close as possible to the antenna is a crucial need.

E. System bandwidth of multiple bands

The sampling rate, which varies directly with the system bandwidth, of the microwave band is much less than that of the 60 GHz mmWave band. The size of the fast Fourier transform increases with an increase in the system bandwidth, and hence the size of fast Fourier transform for mmWave signal processing is also significantly greater than that for microwave signal processing. Since the size of fast Fourier transform affects directly the memory size and baseband processing power requirement, an optimal value of the system bandwidth for the microwave as well as the mmWave bands by taking into account of other network performance metrics is necessary [145].

5.8.2 Multi-band network level

A. FCBS cell discovery, UE association and handover mechanisms

One of the major distinctive features of SBSA over DBSA is that splitting of the UL/DL and the C-plane/U-plane are performed at the same FCBS to avoid coordination between the MCBS and FCBSs. This feature raises then how a number of mechanisms, particularly cell discovery, UE association, and handover, can be performed in SBSA. Because of serving both the C-/U-plane traffic of UEs in the UL/DL by the same FCBS, unlike DBSA, cell discovery needs to be performed by the UE itself like conventional mobile networks for all modes of FCBSs. Since a UE within the coverage of the MCBS is by default served only by the MCBS, and the transceiver for C-plane signaling of a FCBS is always active regardless of its U-plane states (because of power on and off mechanism for U-plane traffic), a UE can discover the

best FCBS based on the measurement of the strength of reference signal received powers of its neighbor FCBSs. The UE association and handover mechanisms of a UE can be performed either by the MCBS or a FCBS based on whether or not the UE has an access to the FCBS. For a non CSG (i.e., open or hybrid access mode) UE, since a UE is not enlisted to the CSG FCBS, it cannot place a request to the FCBS in the UL because of no access to that FCBS. However, a non CSG UE can proceed with a request in the UL to the MCBS with the physical cell identity of its discovered FCBS. The MCBS over the X2 backhaul then informs the corresponding FCBS and hands over both U-plane and C-plane bearers of the UE to the FCBS to set up connections for communication between the FCBS and the UE. However, for a CSG UE, since the UE is enlisted to the FCBS, the UE can proceed with a request in the UL to either the FCBS or the MCBS. If the UE proceeds with a request in the UL to the FCBS, the FCBS over the X2 backhaul then informs with its physical cell identity to the MCBS to hand over both U-plane and C-plane bearers of the UE to it. The procedure for placing request to the MCBS is the same as for a non CSG UE. Hence, development of techniques to perform effectively these mechanisms for CSG, open, and hybrid access FCBSs under a number scenarios as aforementioned are needed to be investigated carefully for SBSA and remain an open research issue.

B. Co-channel interference management in SBSA

If one of the transceiver is operated at the same frequency as that of the MCBS, which we propose in this chapter to improve spectral efficiency and to reduce additional spectrum licensing cost, co-channel interference must occur if a proper interference management is not performed. The ABS based eICIC is an effective solution to overcome this co-channel interference. However, as can be seen from Figure 5.3, with an increase in the number of ABSs, there is a corresponding decrease in overall throughput since the same number of ABSs is allocated to MUs with worse channel conditions than that of the FUs. Since the presence of indoor MUs within a building is varied over time, an adaptive interference management with the statistics of indoor MUs in a building rather than the static allocation can help improve radio resource utilization and overall system level capacity. Such adaptive radio resource allocation

can also be exploited in other radio resource domains such as frequency along with time so that even more granular level of resource allocation per RB basis rather than per ABS basis can performed to improve the radio resource utilization further. Further, rather than the static transmit power per FCBS, a dynamic allocation of transmit power can also be exploited to get partial benefit from using the same RB by both the MCBS and FCBSs simultaneously, however at a reduced FCBS transmit power to keep the interference level within a predefined threshold. Since the C-plane traffic do not typically need high data rate demand, adaptive FCBS transmit power control can be exploited if the C-plane of FUs is served by the co-channel microwave. Hence, an adaptive interference management by exploiting 3D radio resources, i.e. time, frequency and transmit power, for the co-channel microwave operated MUs and FUs is indeed an important area of research for SBSA.

C. U-plane transceiver power on and off mechanism

The U-plane receiver is powered on as long as any active U-plane data session exists, otherwise it is powered off. Whereas, the C-plane served transceiver, i.e. the co-channel microwave, is always powered on to ensure a ubiquitous connectivity and cell discovery. An effective discontinuous transceiver operation mechanism to switch the U-plane transceiver's power on and off is necessary to reduce power consumption. Since both the C-plane and the U-plane are co-located at a FCBS, and there is almost no delay in informing the U-plane transceiver by the C-plane one, the timer default value for waiting the next packet arrival can be reduced in SBSA as compared to DBSA which needs additional external signaling for coordination from the MCBS to the FCBS. Hence in DBSA, to reduce the C-plane signaling for switching power on and off of the U-plane transceiver of a FCBS, the timer's waiting period may need to set to be long enough. The shorter duration of the inactivity timer causes to consume less power and improve energy efficiency. Developing an effective U-plane transceiver power on and off mechanism of a FCBS that can trade-off energy efficiency and buffer delay (and hence memory size) for high data rate service is an important research aspect.

D. Cloud radio access network for multi-band FCBS and UE

The C-RAN is a promising technique for centralized radio resource management of split architectures for 5G networks. In C-RAN enabled DBSA, typically the baseband processing of U-plane of all FCBSs within a MC coverage is done centrally in the cloud whereas the C-plane is still served by the MCBS. Through the coordination via X2 backhauls between the baseband processing unit pools of U-plane of all FCBSs and the MCBS, a UE is under the coverage of a FCBS is served. In contrast in SBSA, since both the C-plane and the U-plane of a UE are served by the same FCBS, whether the baseband processing of the C-plane and the U-plane traffic is to be carried out in the cloud centrally or separately, e.g. the C-plane is at the respective FCBS, and the U-Plane is in the cloud, is not well understood. This is because of the fact that if the C-plane of all FCBSs are moved on to the cloud, there is a need for the implementation of an additional X2 backhaul between the baseband processing unit pools and the MCBS as in the case of DBSA for mechanisms such as UE association and handover between the MCBS and FCBSs. On the other hand, if the C-plane is located at the respective FCBS, the capacity requirement of the fronthaul connecting the FCBSs and the baseband processing unit pools needs to be increased because of frequent signaling exchanged between the C-plane and the U-plane of an all FCBSs. This opens an important research direction toward an in-depth investigation and a development of strategies that can address the trade-off between the complexity and the cost from implementing either the fronthaul or an additional X2 backhaul and the overall network performance gain in each case.

5.9 Summary

In this chapter, a multi-band enabled FCBS and UE architecture is proposed for splitting the UL/DL and the C-/U-plane traffic of any UEs within the coverage of any FCBSs by the same BS (i.e., FCBS) based split architecture, i.e. SBSA, in contrast to DBSA for a multi-tier 5G network. The multi-tier network includes FCs and PCs deployed over a large MC coverage where all FCBSs are considered within a 3D multi-

storage building. In SBSA, for any multi-band enabled FCBSs, co-channel microwave and different frequency mmWave bands are considered. Cross-tier co-channel interference of FUs with MUs is considered to be avoided using ABS based eICIC techniques when operating at the co-channel microwave band for each FCBS. The co-existence of co-channel microwave and different frequency 60 GHz mmWave bands at the same FCBS is studied for capacity and spectral efficiency performances to give incentives for enabling FCBSs with multiple bands and identify a suitable band of them on which to operate FCBSs for transporting decoupled UL/DL and C-and U-plane traffic. Since the overall system level capacity and spectral efficiency performances when operating at co-channel microwave band are found lower than that when operating at mmWave band, we propose a FCBS and a UE to be enabled with both types of these bands, i.e. co-channel microwave and different frequency mmWave bands, to serve decoupled UL/DL and C-/U-plane of any UEs within the coverage of any FCBSs based on the respective traffic demand and data rate. More specifically, we consider the mmWave band to serve more and a high data demand traffic whereas the co-channel microwave band to serve less and a low data rate demand traffic of any FCBSs.

A number of SBSAs for the UL/DL and the C-/U-plane splitting, including a disruptive and complete splitting of the UL/DL and the C-/U-plane as well as a combined UL/DL and C-/U-plane splitting for 5G networks, by exploiting dual connectivity on co-channel microwave and different frequency mmWave bands of both a FCBS and a UE are presented. The outperformances of several proposed SBSAs in comparison with DBSA for a number of such performance metrics as system level capacity, average spectral efficiency, energy efficiency, and C-plane overhead traffic capacity on the backhaul are shown. A number of technical and business perspectives and key research issues of SBSA are pointed out. Since respective transceivers of SBSA operated on different bands for the UL/DL or the C-/U-plane can be switched on and off depending on traffic availability, the proposed multi-band enabled SBSA architecture will allow network operators to gain more degrees of freedom for effective resource utilization and higher energy efficiency which will result in a lower associated cost and greater profit margin.

CHAPTER 6
SMALL CELL BASE STATION ARCHITECTURE FOR CONTROL-/USER-PLANE COUPLED AND SPLIT NETWORK

In this chapter, numerous SCBS architectures based on the number of transceivers and operating frequency bands existing in a SCBS for serving the C-/U-plane traffic in indoor environments under both traditional C-/U-plane coupled architecture as well as prospective C-/U-plane split architecture are presented. With a system level simulation of a multi-tier network, the performances of these FCBS architectures in terms of C-plane, U-plane, and an aggregate C-/U-plane traffic capacities for both C-/U-plane coupled and split architectures are evaluated.

6.1 Introduction

The architecture of SCBSs, i.e. FCBSs, for serving the C-/U-plane data traffic is one of the major concerns to address the growing and high data rate mobile traffic demand in indoor environments for next generation, i.e. 5G, mobile networks. As the mobile data traffic demand increases, existing networks have been facing problems from providing necessary capacity to transport this growing data traffic demand. To address such high capacity requirement, SCs are deployed in the coverage of MCs. However, tight coupling of the C-/U-plane in conventional networks, which can also be termed as C-/U-plane coupled architecture (CUCA), restricts the flexibility in network operation and performance management. Because of tight coupling of the C-/U-plane, causes to keep the BSs always active to ensure ubiquitous coverage even though there is no data traffic demand from UEs and results in a poor resource utilization and unnecessary energy consumption [7]. These call for developing a new architecture where the C-/U-plane are decoupled to provide high data rate, to switch the

transmit power of an SCBS on or off based on data traffic demand, and to ensure an always-on connectivity. Such network architecture is termed as CUSA [7, 9] and is considered as one of the major changes in 5G.

In this chapter, we present numerous SCBS, i.e. FCBS, architectures based on the number of transceivers (e.g., single or dual transceiver) and operating frequency bands (e.g., microwave and mmWave bands) existing in a FCBS for serving the C-/U-plane traffic in indoor environments under both traditional CUCA as well as prospective CUSA. With a system level simulation of a multi-tier network, we evaluate the performances of these FCBS architectures in terms of C-plane, U-plane, and an aggregate C-/U-plane traffic capacities.

The chapter is organized as follows. In section 6.2, an overview of a number of SCBS architectures is given. The performance evaluation of all SCBS architectures is presented in section 6.3. In section 6.4, various features of SCBS architectures are pointed out. Finally, we summarize the chapter in section 6.5.

6.2 Small cell base station architectures

In traditional mobile networks, because the C-/U-plane are coupled, their traffic is served simultaneously over the same link between a BS and a UE. However, the C-/U-plane traffic can also be served by decoupling (i.e., splitting) them over separate links for the same UE, which has been proposed for 5G networks. The C-/U-plane coupled networks are typically termed as cell centric networks whereas decoupled ones as device centric networks [95]. In either case, a number of alternative FCBS architectures can be developed based on the number of transceivers and their operating frequencies considered in a FCBS to route the C-/U-plane traffic, explained in the following.

6.2.1 C-/U-plane coupled architecture

In CUCA, MCBSs typically operate at a low microwave frequency. However, FCBSs can be operated either at the same microwave frequency as that of MCBSs with

a proper cross-tier co-channel interference management between the macro-tier and the femto-tier (Figure 6.1(a)) or at a different frequency (e.g., mmWave) (Figure 6.1(b)) from that of MCBSs at the cost of licensing an additional frequency band. Both BSs serve the C-/U-plane traffic to their respective UE.

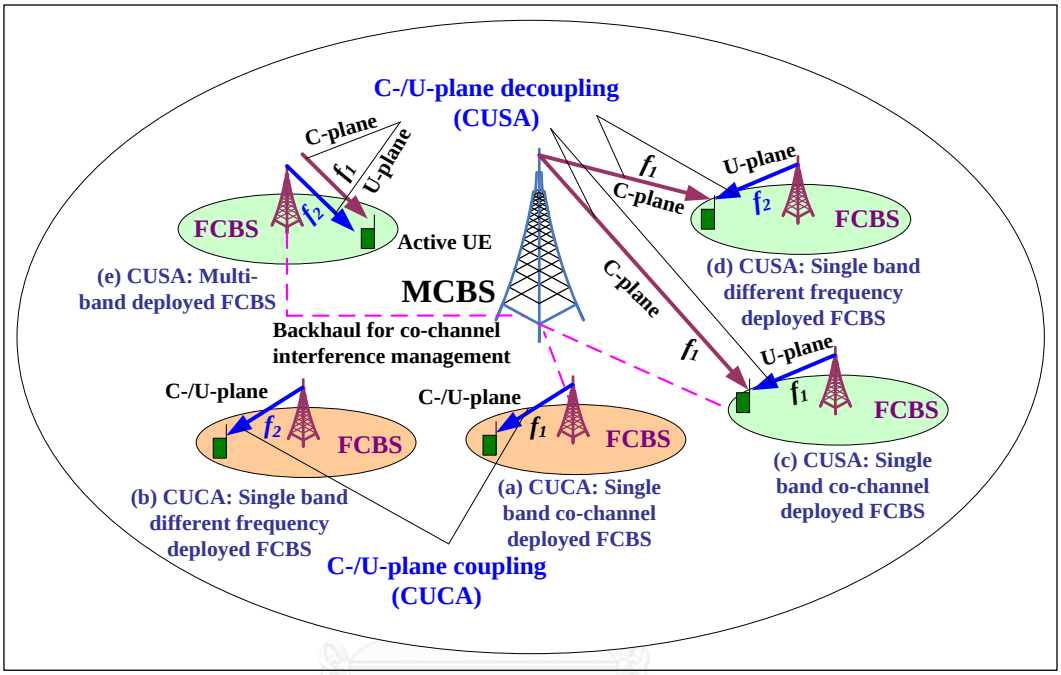

Figure 6.1: FCBS architectures for indoor C-/U-plane traffic.

6.2.2 C-/U-plane split architecture

In CUSA, the C-/U-plane splitting can be done by implementing either single or dual transceivers at a FCBS described as follows.

A. Single transceiver implemented FCBS

In a single transceiver implemented FCBS, the C-/U-plane can be decoupled by operating the FCBS either at the co-channel frequency as (Figure 6.1(c)) or at different frequency from that of its overlaid MCBS (Figure 6.1(d)). Unlike CUCA, C-plane of all UEs is served by the MCBS, and U-plane of FUs is served by the FCBS. However, like CUCA, in co-channel scenario, a proper interference management between the

MC-tier and FC-tier is needed to avoid co-channel cross-tier interference. In contrast, if a FCBS is operating at a different frequency, there is no need for cross-tier interference management. This architecture has been proposed widely for 5G networks [7, 9].

B. Dual transceivers implemented FCBS

In dual transceivers implemented FCBS, a FCBS operates at dual frequencies, e.g. co-channel microwave and mmWave frequencies (Figure 6.1(e)) where each transceiver operates at a different frequency from one another, and decoupling of the C-/U-plane is performed by routing each plane's traffic at a separate frequency. Both the C-/U-plane traffic of FUs are served by the FCBS itself. However, when a UE is out of coverage of a FCBS, the C-/U-plane of the UE is served by the MCBS. Unlike the single transceiver based FCBS architecture in Figure 6.1(d), in this architecture, no coordination signaling is required between C-plane and U-plane BSs. However, it comes at the cost of an additional transceiver at each FCBS as well as UE. Note that single band option is not applicable for dual transceivers implemented FCBS because of more than one transceiver.

6.3 System architecture and performance evaluation

We consider a multi-tier network as illustrated in Figure 6.2, including a single MCBS of a corner excited 3-sectored MC site and a number of indoor FCBSs and outdoor PCBSs within the MC coverage in an urban environment. Each FCBS is deployed in a single room apartment of $10\times10\,m^2$ to serve one FU in any TTIs. A certain percentage of MUs are considered within apartments and offloaded to nearby PCs. All MUs are served by the MCBS only. For a co-channel operated FCBS, all RBs of system bandwidth is reused in each active FCBS. All categories of UE are allocated orthogonally to RBs in any TTIs. If a MU exists within an apartment, TD ABS based eICIC is applied to avoid co-channel cross-tier interference between the indoor MU

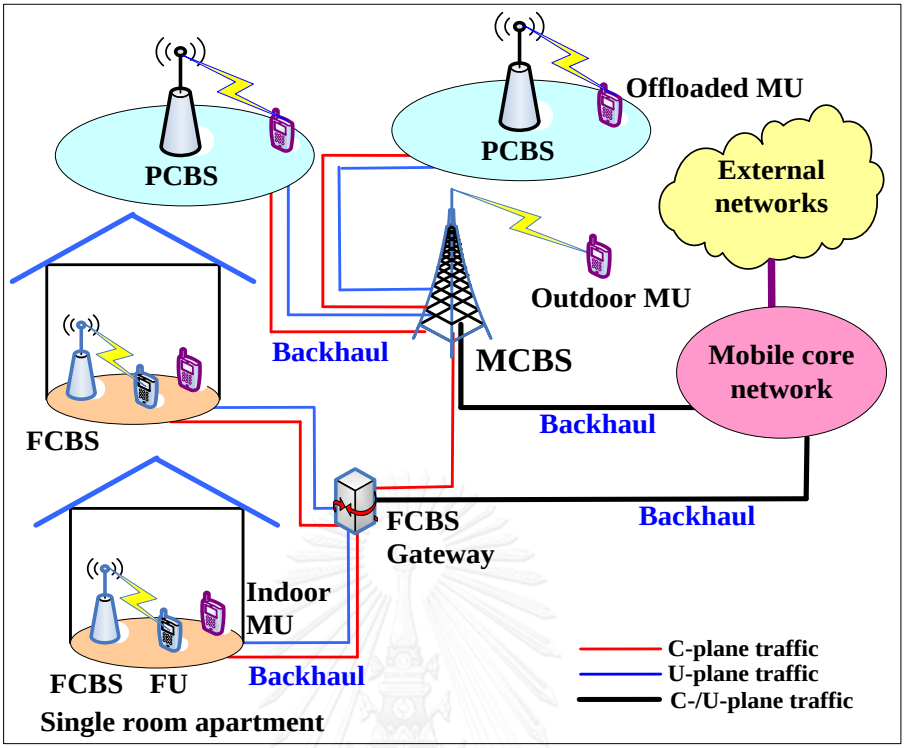

Figure 6.2: System architecture of a multi-tier network.

and FU such that no indoor MUs but FUs can be served only during non-ABSs. However, ABSs are reserved for all MUs. For a different frequency operated FCBS, we consider 60 GHz mmWave band, and no cross-tier interference management between indoor MUs and FUs.

Following the analytical model in section 5.2.2(A) in Chapter 5 and (C.5) in Appendix C, the aggregate capacity of a FCBS operating at the co-channel microwave for a single transceiver based FCBS in CUCA can be expressed as

$$\sigma_{cc} = \sum_{t=1}^{Q} \sum_{i=1}^{M} (1-\varphi)\, \sigma_{t,i}\left(\rho_{t,i}\right)$$

Also for an mmWave based FCBS, $\varphi = 0$ such that the aggregate capacity is given by

$$\sigma_{df} = \sum_{t=1}^{Q} \sum_{i=1}^{m} \sigma_{t,i}\left(\rho_{t,i}\right)$$

Hence, in dual transceivers based FCBS, since both co-channel microwave and mmWave bands exist, the aggregate capacity is given by

$$\sigma_{ccdf} = \sigma_{cc} + \sigma_{df} \tag{6.1}$$

Let x_{cp} denote the percentage of C-plane traffic in CUCA. Table 6.1 shows the C-/U-plane traffic served by all FCBS architectures (in Figure 6.1) for CUCA and CUSA. According to [60], the total control overhead includes 10% for S1 signaling, 4% for handover, and a certain parentage for management signaling. Hence, we assume x_{cp} = 0.25 as an example. Since x_{cp} simply scales the C-/U-plane traffic capacity, considering a different value will not change capacity trends.

Table 6.1: C-plane and U-plane traffic served by a FCBS.

FCBS Architecture	Frequency MCBS : FCBS	U-plane traffic	C-plane traffic	C-/U-plane traffic
CUCA	$f_{cc} : f_{cc}$	$(1-x_{cp})\cdot\sigma_{cc}$	$x_{cp}\cdot\sigma_{cc}$	σ_{cc}
	$f_{cc} : f_{df}$	$(1-x_{cp})\cdot\sigma_{df}$	$x_{cp}\cdot\sigma_{df}$	σ_{df}
CUSA	$f_{cc} : f_{cc}$	σ_{cc}	-	σ_{cc}
	$f_{cc} : f_{df}$	σ_{df}	-	σ_{df}
	$f_{cc} : f_{cc} + f_{df}$	σ_{df}	σ_{cc}	σ_{ccdf}

Default simulation parameters and assumptions used for system level simulation are followed from Table B.1 and Table B.4 in Appendix B. For performance comparison of different FCBS architectures, we focus on only one FCBS since considering many will not alter the evaluation. Figure 6.3 shows C-plane traffic and U-plane traffic capacity of FCBS architectures shown in Figure 6.1. From Figure 6.3, it can be found that CUSA outperforms CUCA for the single transceiver based FCBS operating either at co-channel microwave or mmWave frequencies in terms of effective (i.e., U-plane) user data transmission capacity. This is because of the fact that in CUCA, a certain number of RBs defined by x_{cp} needs to be allocated to serve C-plane traffic. However, in CUSA, C-plane traffic is served by the MCBS so that all RBs of a FCBS can be allocated to serve U-plane traffic, and hence more user data can be served in CUSA than that in CUCA. Certainly in CUSA, the MCBS needs to allocate resources to serve C-plane traffic of the FU, which results in decreasing MUs' data capacity.

However, since most data traffic originate in indoors, and FUs are in more close in-distance from its sFCBS than that of a MU from its serving MCBS, the overall network capacity should increase because of less path loss that cause to improve the received signal quality at the FU.

Further in CUSA, for dual transceivers based FCBS, though U-plane traffic capacity is the same, the overall C-/U-plane traffic capacity is much higher than that of a single transceiver based FCBS. Also, implementing a separate transceiver results in freeing resources at the MCBS for serving C-plane traffic of the FU as in the case of a single transceiver based FCBS such that more resources can be allocated to MUs to increase their data rate and to carry more MU data traffic by the MCBS.

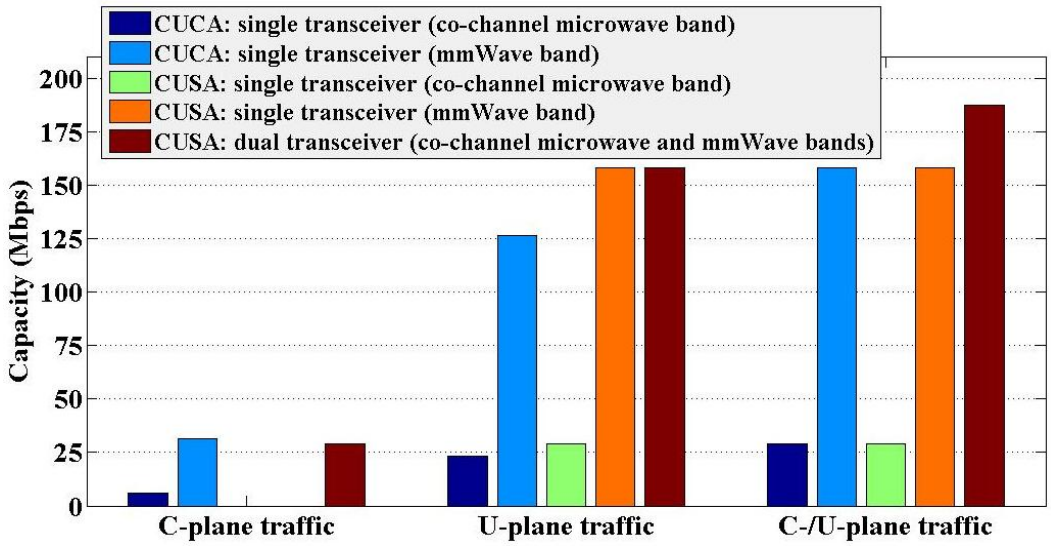

Figure 6.3: C-/U-plane traffic capacity performances of FCBS architectures in Figure 6.1.

6.4 Features of FCBS architectures

The major strength of operating a FCBS in CUCA is reduced or no control signaling overhead for the C-/U-plane cooperation, however it suffers from providing a high data rate in indoor areas. Whereas in CUSA, a FCBS experiences opposite features to that in CUCA, i.e. though a FCBS can address a high data rate in indoor areas, it suffers from generating a huge C-/U-plane cooperation control signaling

overhead, particularly for a single transceiver based FCBS. In Table 6.2, in addition to the strength and weakness, we also discuss other features, e.g. viability challenge and open research issue, of FCBS architectures shown in Figure 6.1.

Table 6.2: Features of various FCBS architectures.

Feature	CUCA	CUSA
Strength and weakness	Resource utilization is low	Resource allocation is maximum for dual transceiver based FCBS
	Low U-plane data traffic capacity	High, since all resources can be allocated to serve U-plane traffic
	No cooperation between MCBS and FCBS is not needed for C-plane traffic	Cooperation between MCBS and FCBS are a must for C-plane traffic to make aligned with U-plane traffic
	MCBS and FCBS transmit powers are always on for a single transceiver based FCBS	Transmit power of MCBS is always on, whereas transmit power of U-plane transceiver of a FCBS is switched on based on FU generated traffic request
Viability challenge	Network operation and management is complex because of the coupled C-/U-plane	Signaling network is complicated when different BSs are used for splitting the C-/U-plane
	SC densification is challenging because of issues, e.g. complex interference and mobility managements	FC discovery and wake up mechanisms is complex for an off-state of transmit power
Open research issue	Scaling of SC densification with a growing traffic demand, increasing per user data rate, and simplifying network operation and management	Simple control signaling network, FCBS discovery and wake up, UE association, and handover mechanisms. For dual transceiver based FCBS, integration and simultaneous operation of dual bands as well as dual band transceiver design

6.5 Summary

In this chapter, we present various FCBS architectures depending on the number of transceivers and their operating frequencies existing in a FCBS in order to serve the

C-/U-plane indoor traffic in both CUCA and CUSA for 5G mobile networks. We carry out an evaluation of capacity performances of a number of FCBS architectures for C-plane, U-plane and an aggregate C-/U-plane traffic with an extensive system level simulation of a multi-tier network, which consists of a MCBS and several outdoor PCBSs and indoor FCBSs. We consider a single transceiver and dual transceivers based FCBS architectures. A single transceiver based FCBS can operate either at the co-channel microwave band or at an mmWave band. However, dual transceivers based FCBS operates at both bands. The simulation results suggest that for a single transceiver based FCBS, CUSA outperforms CUCA in terms of the effective user data transmission capacity, and dual transceivers based FCBS can serve more aggregate C-/U-plane traffic than a single transceiver based FCBS. Finally, we highlight several strengths and weaknesses, challenges, and open research issues associated with CUCA and CUSA for both single and dual transceivers based FCBSs. Because SCs are considered as the major enabler of 5G, findings of this chapter can help network operators and vendors provide insights to understand relative performance capability of various FCBS architectures for serving the C-/U-plane traffic to address the high data rate demand in indoor environments.

CHAPTER 7
CENTRALIZED 3D RADIO RESOURCE ALLOCATION FOR CONTROL-/USER-PLANE SPLIT ARCHITECTURE

In this chapter, we propose a centralized allocation and scheduling strategy for 3D radio resources (namely, time, frequency, and power) for a multi-tier C-/U-plane split architecture by considering schedulers of all BSs located at a central station. We consider a fully blank subframe (FBS) based eICIC to split completely the C-/U-plane such that C-plane can be served only by the MCBS and U-plane by each UE's respective BS. The system bandwidth is reused in FCBSs, and frequency resources are allocated orthogonally per tier basis. We propose a simple FCBS power control mechanism by modeling a FCBS's on-state and off-state power as on and off traffic source model, and derive an optimal value of average activation factor (AAF) of any FCBSs per FBS pattern period to trade-off its serving capacity and transmit power saving.

7.1 Introduction

Radio resource allocation and scheduling plays a crucial role on achievable capacity, spectral efficiency and energy efficiency of cellular networks. Providing a high data rate service demand and network capacity, supporting a large traffic volume, and achieving a high spectral and energy efficiencies of 5G cellular, necessitate the development of an effective radio resource allocation and scheduling strategy for the major 3D radio resources, namely time, frequency, and transmit power due to their limited availability. Though most existing researches addressed either 1-dimensional or 2-dimensional radio resources of these three in decentralized network architectures, a number of researches addressed 3D radio resource allocation and scheduling by now,

e.g. [146] for wireless mesh networks, [147] for low-medium-altitude platforms based WiMAX networks, and [148], for an orthogonal frequency-division multiple access (OFDMA) FC and MC based network. However, decentralized architectures lead to scaling SCBSs with the number of UEs and amount of traffic volume, which causes such architectures to suffer from a number of pitfalls, e.g. increase in network operational expense and severe inter-cell interference. Hence, the idea of centralized cellular architecture has come into being [149]. Numerous proposals on centralized wireless networks exist in literature, e.g. cloud radio access network architecture [56], wireless network cloud [150], and LightRadio [151], which are based on decoupling radio frequency and baseband processing tasks from physical nodes and shifting them to a centralized location. Authors in [149] also proposed a super BS based centralized architecture for 5G where the global centralized resource management center allocates resources to virtual BSs. Recently, software defined networking has been considered as an effective centralized resource management for 5G [152-153].

Besides, because of an expected ultra-densification of SCs in 5G, extensive researches on SC energy efficiency have been ongoing, e.g. an energy efficient SC activation mechanism to reduce network energy consumption in [154], a tradeoff between energy consumption and throughput by considering SCBSs with several power-saving modes in [155], and a study on SCBS on and off operation to enhance energy efficiency in [156], have been addressed. In contrast to traditional CUCAs, CUSAs, also termed as device centric networks [95], have been considered as a potential solution for 5G, and an extensive researches is ongoing on CUSA [7, 9] either by considering to route C-plane traffic of a SC with the SCBS itself or the MCBS [7, 9].

So far, we exploit frequency and time resource allocation and scheduling. Since the transmit powers of SCBSs have a significant impact on the overall network interference phenomenon and energy efficiency, we propose a centralized allocation and scheduling strategy for 3D radio resources (namely, time, frequency, and power) for a multi-tier C-/U-plane split architecture by considering schedulers of all BSs located at a central station. We consider a multi-tier network comprises of a MCBS and a number of outdoor PCBSs as well as indoor FCBSs deployed within a multi-storage building.

In contrast to the conventional ABS, we consider a FBS based eICIC to split completely the C-/U-plane such that C-plane can be served only by the MCBS and U-plane by each UE's respective BS. The system bandwidth is reused in FCBSs, and frequency resources are allocated orthogonally per tier basis. We propose a simple FCBS power control mechanism by modeling a FCBS's on-state and off-state power as on and off traffic source model, and derive an optimal value of AAF of any FCBSs per FBS pattern period to trade-off its serving capacity and transmit power saving. With a system level simulation it is shown that the capacity of a FCBS increases whereas its power saving decreases linearly with an increase in its AAF because of serving increased traffic, and an optimal AAF of 0.5 for the capacity scaling factor $\kappa = 1$ and greater than 0.5 for $\kappa < 1$ is found.

The chapter is organized as follows. In section 7.2, the proposed centralized radio resource allocation and scheduling is discussed. In section 7.3, the transmit power management and modelling of FCBSs are given. Section 7.4 includes radio resource allocation and scheduling and problem formation for evaluation. Simulation parameters and assumptions are given, and performance evaluations are carried out in section 7.5. We summarize the chapter in section 7.6.

7.2 System architecture and operation of centralized radio resource allocation and scheduling

For centralized radio resource allocation and scheduling, the radio resource allocation and scheduling of C-plane and U-plane traffic of all UEs is performed at a central station (Figure 7.1). The central station can be located either at the MCBS or within anywhere the MC coverage based on, e.g. the available backhaul capacity. U-plane traffic of all UEs is served by the respective BS, i.e. outdoor and indoor MUs by the MCBS, offloaded MUs by PCBSs, and FUs by FCBSs. However, C-plane traffic of all UEs under its coverage is served only by the MCBS. For simplicity, we assume separate ideal backhauls from the central station to any BSs. U-plane traffic of all UEs are passed through the respective BS (i.e., FCBSs for FUs, the MCBS for both outdoor and indoor MUs, and PCBSs for offloaded MUs), then central station, mobile core, and

finally to external networks. However, C-plane traffic of all UEs are passed only through the MCBS, then to central station, mobile core, and finally to external networks.

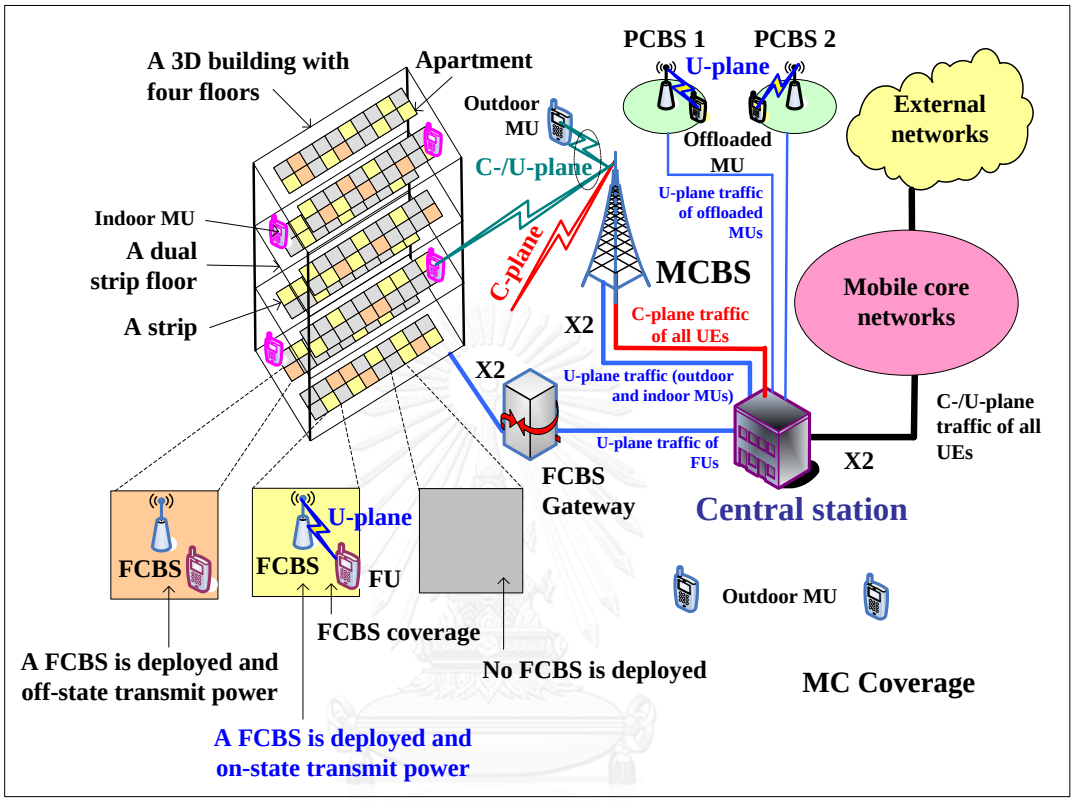

Figure 7.1: System architecture for the proposed centralized radio resource allocation and scheduling.

To serve U-plane traffic, we consider one proportional fair scheduler for all outdoor and indoor MUs, one for all offloaded MUs, and one for all FUs, and to serve C-plane traffic, one proportional fair scheduler for all UEs is considered. Unlike traditional decentralized CUSA [7, 9], the main advantage of centralized radio resource allocation and scheduling is that there is no need for exchanging control signaling between C-plane and U-plane BSs for synchronization, FCBSs' power switching on and off, and SC discovery and wake up, which result in reducing control signaling overhead and increasing user data traffic capacity.

7.3 FCBS power management and modeling

7.3.1 FCBS power management

We consider that FCBSs are not always active and switched on and off based on data traffic requests as shown in Figure 7.2, which is modeled as the on and off traffic source model. Switching on and off any FCBSs is governed by the respective scheduler at the central station. In the absence of any FU's data request, the scheduler sends a *power-off message* to the corresponding FCBS to keep its power switched off until any next requests. In switching any FCBSs to on-state, a FU first sends a random access channel request to the MCBS in the UL. Assuming that a mechanism exists for selecting an appropriate FCBS by the MCBS, the MCBS then informs the corresponding FD scheduler, which schedules resources to the FCBS to which the FU may get connected with. The scheduler then sends a *power-on message* to the corresponding FCBS in the DL and creates necessary data bearers through that FCBS. The scheduler also informs the FU via the MCBS to create relevant RRC connections with the FCBS. After acknowledging the *RRC connection complete message* from the FCBS, the FU starts communicating via the FCBS to mobile core and then to external networks.

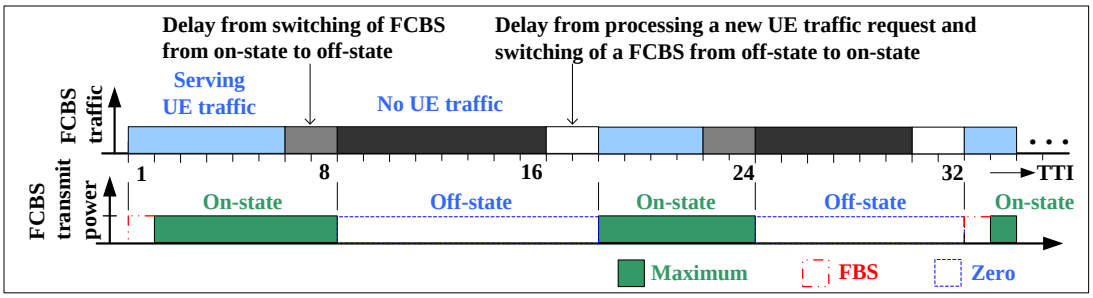

Figure 7.2: An illustration of power on and off scheme of a FCBS.

7.3.2 FCBS power modeling

The 3GPP European Telecommunications Standards Institute traffic model for non-real time Internet data has three layers, namely session, packet call, and packets [157]. BSs need to be active at the upper most layers, i.e. session layer, while a UE is communicating through them. According to [157], sessions or call arrivals can be modeled as a Poisson process. For simplicity, we assume that a BS activity is directly proportional to the cumulative traffic activity from its UEs. Hence, a U-plane BS (i.e., FCBS) power on-state and off-state can be modeled as exponentially distributed continuous time Poisson process such that the amount of time any FCBSs spent on each state is exponentially distributed. Since given the present state, the future state is independent of the past state, any FCBSs transmit power on and off states can be modeled as two state Markov chain as shown in Figure 7.3, where λ_p denotes the power off-state to on-state transition rate, and μ denotes the power on-state to off-state transition rate of any FCBSs.

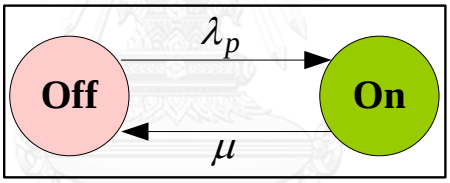

Figure 7.3: Two-state on and off transmit power model for a FCBS.

The randomness in switching any FCBS's transmit power to on and off states can be modeled by the average duration of each state such that the average time at an on-state is given by $1/\mu$ and at an off-state by $1/\lambda_p$ [158]. Hence the AAF, which is defined as the probability that any FCBSs is at the on-state, is given by

$$\alpha = \Pr(\text{on-state}) = (1/\mu)/((1/\lambda_p)+(1/\mu)) = \lambda_p/(\lambda_p+\mu) \quad (7.1)$$

Hence, $$\Pr(\text{off-state}) = 1-\alpha = \mu/(\lambda_p+\mu) \quad (7.2)$$

For a single FU per FCBS, because a FU also has two states (i.e., there is either a traffic request or not at all), the FU state diagram is the same as its FCBS's on and off state diagram (Figure 7.3). Since we consider a single FU per FCBS, the average on and off state probabilities of any FCBSs transmit power are given by (7.1) and (7.2). Hence, for a particular duration of time T_s, the average on-state duration of any FCBSs

is given by $t_{on-state} = \alpha \cdot T_s$, and off-state duration by $t_{off-state} = (1-\alpha) \cdot T_s$. For evaluation, we consider an average value of probabilities given by (7.1) and (7.2) per FCBS per FBS pattern period (FPP) so that an average value is estimated in ratio of the number of TTIs per FPP per FCBS.

7.3.3 Effect of FBS, switching and processing delay

Let $\alpha_{on \to off}$ denote an average aggregate delay per FPP *T* from switching on-state to off-state of any FCBSs, whereas $\alpha_{off \to on}$ denote delay from switching off-state to on-state, for traffic request processing of any FU, e.g. discovery of any FCBSs. Let α_{fbs} denote percentage duration of any FBSs, and α_s and α_{ns} denote percentage average durations of any in-progress active and in-active FU traffic respectively per FPP *T*. The average on and off state durations of any FCBSs can be given by

$$t_{on-state} = \alpha.T = (\alpha_s + \alpha_{on \to off}) \cdot T \tag{7.3}$$

$$t_{off-state} = (1-\alpha) \cdot T = (1-(\alpha_s + \alpha_{on \to off})) \cdot T \tag{7.4}$$

Equivalently, $t_{off-state} = (\alpha_{ns} + \alpha_{off \to on} + \alpha_{fbs}) \cdot T$

Such that, $T = t_{on-state} + t_{off-state}$

7.4 Proposed radio resource allocation and scheduling and problem formation

7.4.1 Radio resource allocation and scheduling

We consider a FBS based eICIC to avoid transmitting any control signals, in contrast to a traditional ABS, in order to switch off the transmit power of a FCBS completely during an FBS. A static allocation of the number of FBSs per FPP, comprising 8 TTIs, by a TD scheduler at the central station is considered. A simple on and off transmit power management strategy is considered. The system bandwidth of

the MCBS is reused in FCs within the building, and like all MUs, the RB allocation to all FUs is also considered orthogonal. If a MU is within a building, the TD FBS based eICIC is applied to FCs to avoid co-channel interference between indoor MUs and FUs. All outdoor MUs are allowed to transmit data during FBSs as well as non-FBSs; however FUs are scheduled only during non-FBSs. Figure 7.4 shows an illustration of radio resource allocation and scheduling with respect to a FCBS. As can be seen, the transmit power of a FCBS has only two states, either zero or maximum, based on the FU traffic requests and other factors as shown in Figure 7.2.

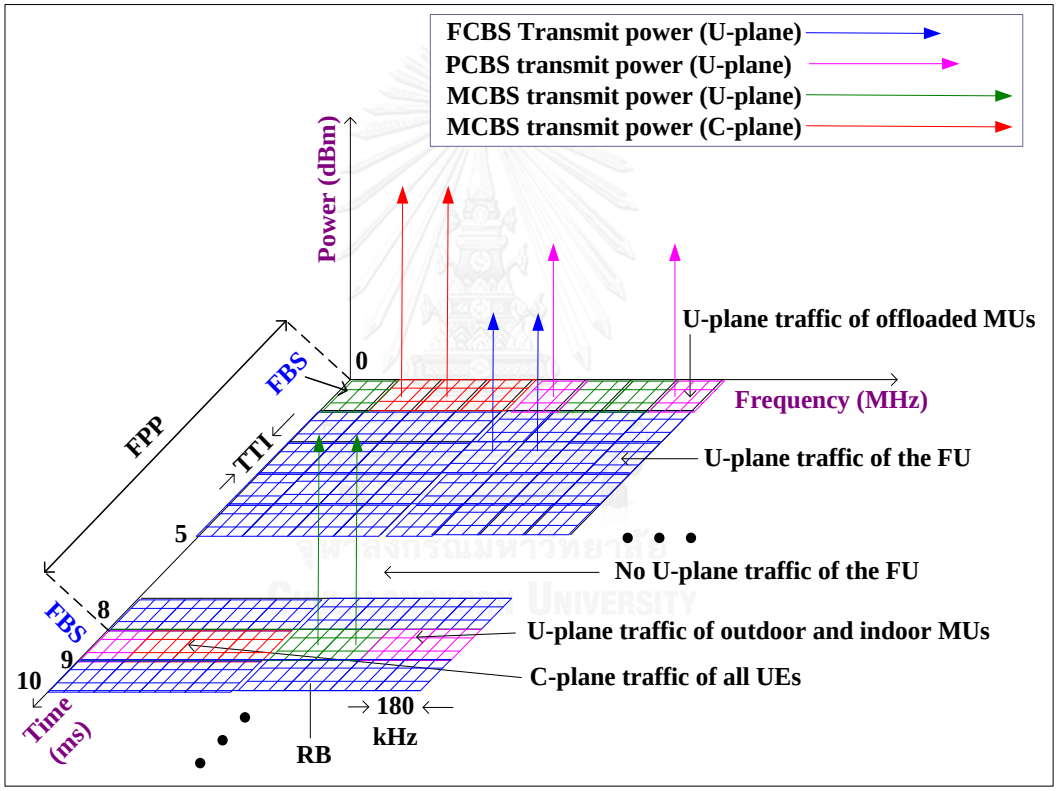

Figure 7.4: An illustration of 3D radio resource allocation and scheduling concerning a FCBS.

7.4.2 Problem formulation

A. Multi-tier network model

Consider that there are M RBs in the system bandwidth. All MUs are partitioned randomly into three disjoint subsets of outdoor MUs, indoor MUs, and offloaded MUs. Consider that all PCs have an equal number of offloaded MUs. Let μ_{iM} denote the ratio of the number of indoor MUs. We consider a multi-storage building within which a number of FCBSs are deployed, and each FCBS serves one UE at any time. All UEs are distributed randomly and uniformly within their respective BS's coverage in a realization, defined as a simulation run time.

Let $\boldsymbol{T}$ denote simulation run time with the maximum time of Q (in time step each lasting 1 ms) such that $\boldsymbol{T} = \{1, 2, 3, \ldots, Q\}$. Let $\boldsymbol{T_{FBS}}$ denote a set of FBS indices over all FPPs for Q TTIs, and T_{FPP} denote the number of subframes per FPP such that $\boldsymbol{T_{FBS}} \subseteq \boldsymbol{T}$ and $\boldsymbol{T_{FBS}} = \{t: t = v.T_{FPP}+n_A; v = 0, 1, 2, \ldots, Q/T_{FPP}; n_A = 1, \ldots, T_{FBS}\}$ where $T_{FBS} = 1, 2, \ldots, T_{FPP}$ corresponds to FBS patterns $\alpha_{fbs} = 1/T_{FPP}, 2/T_{FPP}, \ldots, T_{FPP}/T_{FPP}$ respectively. Let t_{FBS} and $t_{non-FBS}$ denote respectively an FBS and a non-FBS such that $t_{FBS} \in \boldsymbol{T_{FBS}}$ and $t_{non-FBS} \in \boldsymbol{T \backslash T_{FBS}}$.

Let $\boldsymbol{t_{on\text{-}state}}$ denote a set of subframes over all FPPs for $\boldsymbol{T}$, and $t_{on\text{-}state}$ denote the number of subframes per FPP such that $\boldsymbol{t_{on\text{-}state}} \subseteq \boldsymbol{T}$. In general, $t_{on\text{-}state}$ is an integer random variable, which varies from one T_{FPP} to another for Q TTIs and depends mainly on in-progress active UE traffic requests and characteristics over any T_{FPP}.

B. Capacity estimation

The received SINR for a UE at RB i in TTI t at power p can be expressed as

$$\rho_{t,i,p} = \left(P_{t,i,p}/(n_{t,i,p} + I_{t,i,p})\right).H_{t,i,p} \tag{7.5}$$

where $P_{t,i,p}$ is the transmission power; $n_{t,i,p}$ is the noise power; $I_{t,i,p}$ is the total interference signal power; and $H_{t,i,p}$ is the link loss for a link between a UE and a BS at RB i in TTI t at power p, which can be expressed in dB as

$$H_{t,i,p}(\text{dB}) = (G_t + G_r) - (L_F + PL_{t,i,p}) + (LS_{t,i,p} + SS_{t,i,p}) \tag{7.6}$$

where $(G_t + G_r)$ and L_F are respectively the total antenna gain and connector loss, and $LS_{t,i,p}$, $SS_{t,i,p}$, and $PL_{t,i,p}$ respectively denote shadowing effect, small-scale Rayleigh fading or Rician fading, and distance dependent path loss between a BS and a UE at RB *i* in TTI *t* at power *p*. Let β denote implementation loss factor. Using Shannon's capacity formula, a link throughput at RB *i* in TTI *t* at power *p* in bps per Hz is given by [35, 89]

$$\sigma_{t,i,p}\left(\rho_{t,i,p}\right) = \begin{cases} 0, & \rho_{t,i,p} < -10 \text{ dB} \\ \beta \log_2\left(1 + 10^{\left(\rho_{t,i,p}(\text{dB})/10\right)}\right), & -10 \text{ dB} \le \rho_{t,i,p} \le 22 \text{ dB} \\ 4.4, & \rho_{t,i,p} > 22 \text{ dB} \end{cases} \tag{7.7}$$

Using (7.3), the aggregate average capacity of FCBSs is given by

$$\sigma_{FC} = \sum_{t=1}^{Q} \sum_{i=1}^{M} \alpha_s \cdot \sigma_{t,i,p}\left(\rho_{t,i,p}\right) \tag{7.8}$$

where $\sigma_{t,i,p}\left(\rho_{t,i,p}\right)$ denotes the throughput response of all FUs in $t \in \boldsymbol{t_{on\text{-}state}}$ over *M* RBs. The total system capacity is given by

$$\sigma_S = \sum_{t=1}^{Q} \sum_{i=1}^{M} \sigma_{t,i,p}\left(\rho_{t,i,p}\right) \tag{7.9}$$

where σ and ρ are responses of all MUs in $t \in \boldsymbol{T_{FBS}}$, outdoor and offloaded MUs in $t \in \boldsymbol{T \backslash T_{FBS}}$, and all FUs in $t \in \boldsymbol{t_{on\text{-}state}}$.

C. Power saving and optimal value of AAF

Using (7.3) and (7.4), the power saving factor of any FCBSs can be given by the average on-state and off-state durations as follows:

$$\eta = t_{off-state} / \left(t_{on-state} + t_{off-state}\right)$$

$$\eta = \left((1-\alpha) \cdot T\right)/T = 1-\alpha \tag{7.10}$$

Hence, percentage power saving, $\%\eta = (1-\alpha) \times 100$ (7.11)

Since both the capacity and power saving factor of any FCBSs are proportional to AAF, an optimal value of AAF (OAF) that can trade-off these demands can be

defined as its corresponding value of a point where the capacity and power saving responses are equal so that the optimization problem can be formulated as follows:

$$\begin{aligned} &\text{maximize} && \alpha \\ &\text{subject to} && \eta - \left(\sigma_{FC} / \sigma_{FC,\max}\right) = 0 \end{aligned}$$

where $\sigma_{FC,\max}$ denotes the maximum capacity of FUs in $t \in \boldsymbol{T}$ over M RBs.

From (7.7), since σ_{FC} is a function of link quality irrespective of the value of α_s, $\sigma_{FC,\max}$ can be defined and fixed in prior as a system parameter by setting the value of the average link quality of FU σ_{lq} based on, e.g. the operating band of FCBSs. The solution of this problem for $\alpha \cong \alpha_s$ and the capacity scaling factor $\kappa = 1$ is given by

$$\begin{aligned} \alpha^* &= 1 - \left(\sigma_{FC} / \sigma_{FC,\max}\right) \\ &\cong 1/(1+\kappa) \\ &\cong 1/2 \end{aligned}$$ ■

Proof 7.1: From (7.7),

$$\sigma_{FC,\max} = (Q \cdot M) \cdot \alpha_s \cdot \sigma_{lq}$$

Applying the constraint, $\eta = \sigma_{FC} / \sigma_{FC,\max}$

$$\Rightarrow \alpha = 1 - \left(\sigma_{FC} / \sigma_{FC,\max}\right) \tag{7.12}$$

From (7.3), $\alpha = \alpha_s + \alpha_{on \to off}$

Assuming $\alpha_s >> \alpha_{on \to off}$ such that $\alpha \cong \alpha_s$

From (7.7), σ_{FC} can be expressed in terms of $\sigma_{FC,\max}$ such that

$$\sigma_{FC} = \alpha \cdot \left(\kappa \cdot \sigma_{FC,\max}\right)$$

where κ is the capacity scaling factor, $0 < \kappa < 1$. Further from (7.12),

$$\alpha^* \cong 1 - \left(\left(\alpha^* \cdot \kappa \cdot \sigma_{FC,\max}\right) / \sigma_{FC,\max}\right)$$

$$\Rightarrow \alpha^* \cong 1 - \left(\kappa \cdot \alpha^*\right)$$

$$\Rightarrow \alpha^* \cong 1/(1+\kappa)$$

For $\kappa = 1$, $\alpha^* \cong 1/2$ (7.13) ■

7.5 Performance evaluation

Table B.5 and Table B.9 in Appendix B show default simulation parameters and assumptions used for performance evaluation. For simplicity in evaluation, because of considering the average probability of each factor over an FPP, we consider one FCBS for performance evaluation. However, this will not affect the performance trends as indoor channels are less susceptible to Doppler Effect and delay spread because of less movement of objects and small coverage of a FC. We define $\sigma_{FC,\max}$ as the average sum throughputs of FUs in $t \in \boldsymbol{T}$ over M RBs per realization. Since we consider one realization per FBS, $\kappa = 1$. From Figure 7.5, it can be found that the capacity of a FC increases linearly with an increase in its AAF ($\alpha \cong \alpha_s$). The maximum capacity of FC attains when it serves over all TTIs of FPP, which is possible only if there is no

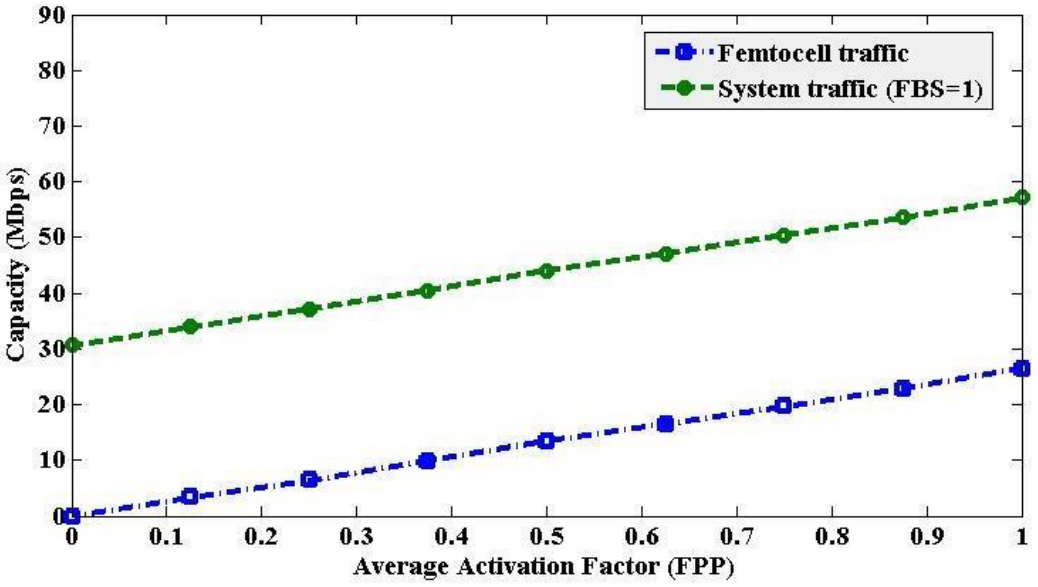

Figure 7.5: Capacity versus AAF.

existence of MU within the building such that the FCBS can transmit in all TTIs of a FPP. As shown in Figure 7.5, the overall system capacity of all UEs is shown for FBS = 1. This is because of the fact that, irrespective of the number of FBSs per FPP, the aggregate capacity of all MUs does not change considerably as shown in Figure 7.6. Hence, the system capacity shows also a linear response and increases with an increase in AAF. Also, the number of FBSs per FPP has a negligible impact on the aggregate capacity of all MUs (Figure 7.6), however has a significant impact on the capacity of FCBS (Figure 7.5). Note that the switching delay from the FCBS's power on and off operation and the UE traffic request processing delay from exchanging control signaling between the MCBS and the FCBS influence greatly the capacity of FCBS, particularly in indoor regions where the movement of UEs is very frequent that causes to originate a large number of UE traffic requests with the FCBS. All these effects are captured in Figure 7.5 by varying the AAF from 0 (always off) to 1 (always on) over an FPP to show how the FCBS capacity varies with a change in environments.

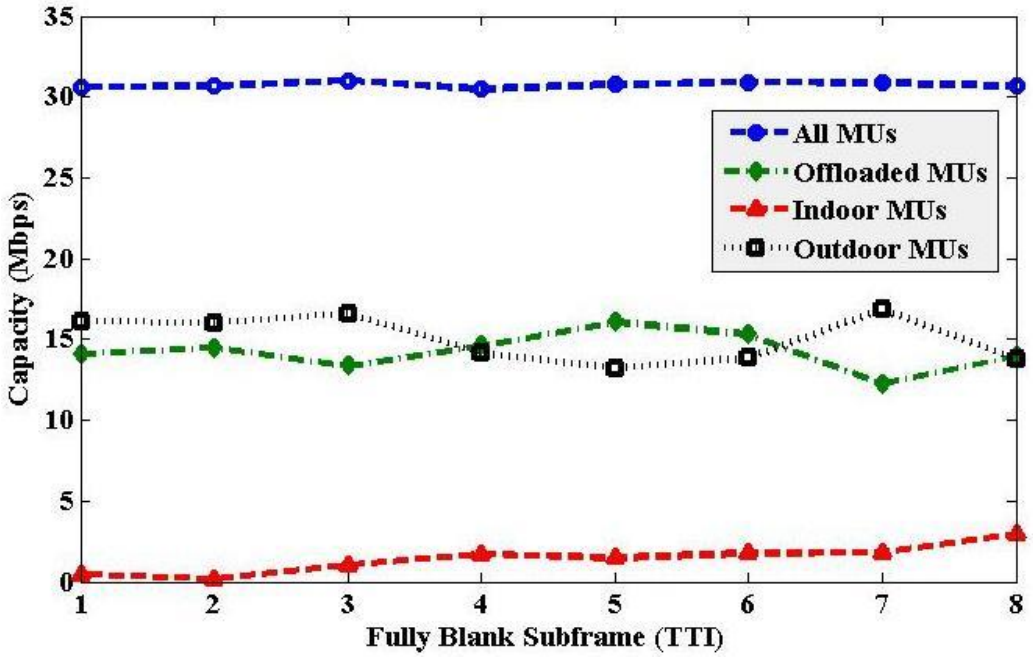

Figure 7.6: Capacity of MUs versus FBS.

In Figure 7.7, the transmit power saving response of the FCBS is shown. As expected, the transmit power saving decreases with an increase in AAF. This calls for

a trade-off between the high capacity and the high power saving demands of a FCBS. We address this issue by deriving an OAF in (7.13). As shown in Figure 7.7, the OAF is about 0.5, which complies with the derived OAF in (7.13). Hence, an optimization of the capacity and energy efficiency of FCBSs can be achieved when each FCBS has on an average an equal or near equal on-state and off-state durations subject to $\kappa = 1$. For $\kappa < 1$, the slope of FC capacity (Figure 7.7) decreases, which results in an obvious increase in the value of OAF from 0.5 in order to compensate the FC capacity corresponding to the amount of decrease of the slope from that of $\sigma_{FC,\max}$.

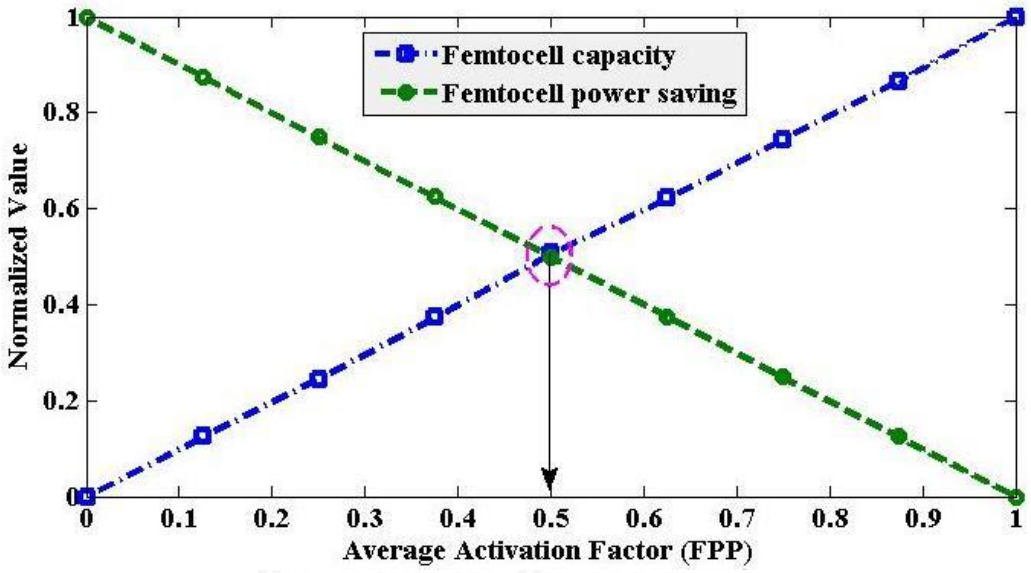

Figure 7.7: FC capacity and transmit power saving and OAF versus AAF.

7.6 Summary

In this chapter, we propose a centralized 3D radio resources, namely time, frequency and power, allocation and scheduling strategy for a multi-tier CUSA. Centralized scheduling is performed by considering schedulers of all BSs located at a central station. The multi-tier network consists of a MCBS and a number outdoor PCBSs and indoor FCBSs deployed in a multi-storage building. The system bandwidth is reused in FCBSs. We propose a FBS based eICIC to split completely the C-/U-plane and to avoid cross-tier interference. Co-tier interference is avoided by allocating

frequency resources orthogonally in each tier. The transmit power of any FCBSs is controlled by proposing a simple power control mechanism, modeled its on-state and off-state as conventional on and off traffic source model. We also derive an OAF over a FPP to trade-off the FCBS capacity and power saving. With a system level simulation, we show that both the capacity of a FCBS and overall system increase, whereas the transmit power saving of the FCBS decreases linearly with an increase in AAF. Further, an OAF of 0.5 for $\kappa = 1$, and greater than 0.5 for $\kappa < 1$, is found. This contribution will give operators insights on scheduling time, frequency, and power centrally in SCs to address the demands of high indoor capacity and energy efficiency of 5G networks.

CHAPTER 8
RECOMMENDED FURTHER STUDY: CONCEPT AND PRELIMINARY RESEARCH OUTCOME

In this chapter, future research directions of the dissertation mainly on the C-/U-plane split architecture based device-centric network for 5G are discussed. A FC clustering approach and static resource reuse and allocation in 3D multi-floor buildings are proposed. The FC clustering approach follows the same as in resource reuse strategy 2 in Chapter 4. However, to reuse resources per cluster, we describe a number of static resource allocation options and propose an algorithm that takes adjacent channel interference into account when allocating resources in FCBSs within a cluster for the resource reuse strategy 1. We evaluate the algorithm for a single floor of a multi-floor building. A number of recommended studies in terms of concepts and preliminary outcomes are discussed and projected approaches are mentioned. Finally, a C-RAN enabled C-/U-plane split architecture based device-centric network for centralized resource allocation in 3D in-building scenario to address the high capacity and spectral efficiency requirements of 5G networks is proposed for further studies.

8.1 Recommended study 01: alternative SCBS architectures

8.1.1 Recommended research proposal

In Chapter 6, as preliminary study we present numerous SCBS architectures based on the number of transceivers and operating frequency bands existing in a FCBS for serving the C-/U-plane traffic in indoor environments under both CUCA and CUSA and evaluate their performances for C-/U-plane traffic capacities. Since there are other aspects than the number of transceivers and operating frequency bands, namely control signaling network overhead for the C-/U-plane BSs, UE association procedure, and

SCBS discovery, wake-up, and transmit power control mechanisms, that can be explored for SCBS architectural alternatives, a deep understanding on these issues will be an effective future research direction in order to address demands of 5G networks, particularly for indoor environments.

8.2 Recommended study 02: FC clustering and static resource reuse and allocation in 3D multi-floor buildings

8.2.1 Recommended research proposal

In Chapter 4, though we have proposed two resource reuse strategies for 3D multi-floor buildings, only resource reuse strategy 2 have been evaluated. As part of further studies, the resource reuse strategy 1 can be evaluated.

8.2.2 Preliminary research progress

As part of preliminary works, we address in the following the resource reuse strategy 1 in detail. The FC clustering approach follows the same as in strategy 2 in Chapter 4. However to reuse resources per cluster, we describe a number of static resource allocation options and propose an algorithm that takes adjacent channel interference into account when allocating RB resources in FCBSs within a cluster for strategy 1. We evaluate the algorithm primarily for a single floor scenario and consider carrying out an evaluation of it for the 3D building as part of further studies.

A. FC clustering approach for resource reuse strategy 1

Clusters of FCBSs are formed based on RoEs constrained by, e.g. link interference, spectral efficiency, and capacity, in both intra-and inter-floor levels as shown in Figure 8.1. Hence, with a change in the constraint type and value, the size of a cluster varies. All clusters within a 3D multi-floor building have the same size, i.e.

the number of FCBSs per cluster for a given constraint is the same. However, the size of each cluster in different buildings may vary with different types and values of any constraints. In CUCA, since the whole system bandwidth can be reused in FCBSs within each cluster, the capacity and spectral efficiency increase with a decrease in cluster size for a given system bandwidth. The RB resource allocation to each FCBS within a RoE is static, i.e. resources allocated to FCBS *r* of cluster *cl*, $S_{r,cl}$ can only be allocated to FCBS *r* of neighboring cluster ($cl+n_c$), $S_{r,cl+n_c}$ where $n_c = 1, 2, 3\ldots$ as shown in Figure 8.1.

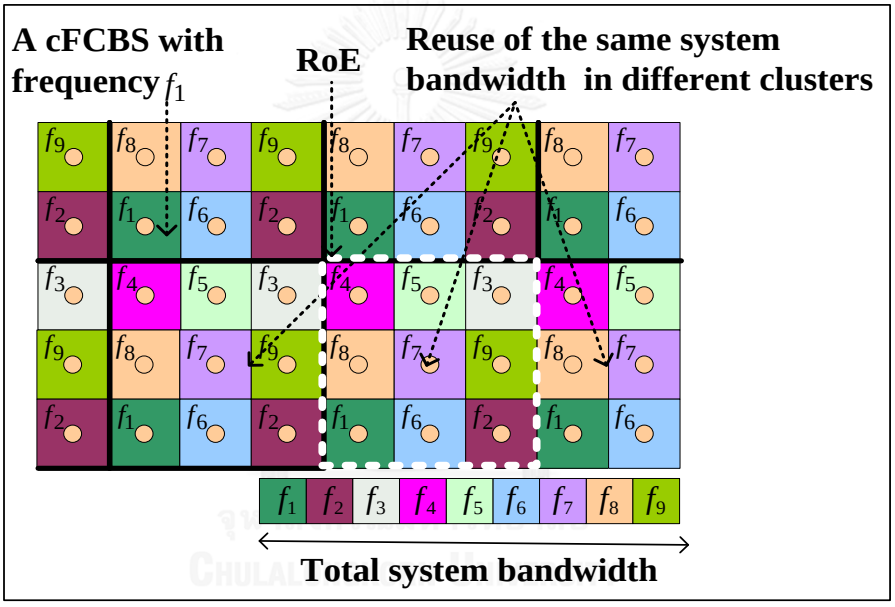

Figure 8.1: Resource reuse strategy 1 and formation of clusters of FCBS (intra-floor level).

B. Resource reuse strategies

The whole system bandwidth is reused in each RoE as shown in Figure 8.1 following a static frequency allocation scheme to avoid co-channel interference, e.g. each FCBS is allocated to the same amount of frequency, such that all FCBSs in any clusters are cFCBSs with respect to neighboring clusters. Since each FCBS serves its own FU, and all FCBSs within a cluster are allocated by an orthogonal frequency allocation, this static resource allocation is analogous to coordinated scheduling CoMP.

The resource schedulers for strategy 1 can be implemented either jointly where all FCBSs in a building can be scheduled by a single FD scheduler or disjointly where FCBSs within each RoE are scheduled by a separate FD scheduler.

Because of the static RB allocation, reuse of RBs becomes dependent on the deployment of FCBSs within any RoEs. This is because reused RBs may be wasted from an absence of any FCBSs within any RoEs such that a certain number of RBs may have already been defined for the absent FCBS and not been possible to reallocate to other FCBSs of neighboring RoEs because of causing co-channel interference. However, since all FCBSs in all RoEs gain advantage from the link capacity constraint enforced by an optimizer, the overall capacity gain from such static resource reuse strategy is expected to be higher than that of the resource reuse strategy 2 proposed in Chapter 4.

C. Static resource allocation

RB resources are allocated equally to each FCBS within a cluster, and the same set of RBs is reused to each cluster. The set of RB indices allocated to any FCBSs is fixed and does not change from one cluster to another. Hence, the same regular pattern of RB indices is followed in allocating RBs to FCBSs in each cluster (Figure 8.1).

For co-channel deployment of the MCBS and FCBSs, in CUCA, a certain percentage of, e.g. m_r RBs, the total number of RBs is kept reserved for the C-plane of all UEs, and the remaining (M-m_r) RBs are allocated following the proposed ORPA or CRPA interference mechanism to FUs per cluster. For CUSA, let M_C denote the number of RBs for the C-plane traffic of all UEs, and M_{iMU} denote the number of RBs for the U-plane traffic of all indoor MUs. Then the number of RBs that can be reused in FCBSs per cluster is $M_{UFC} = M$-(M_C+M_{iMU}). M_{UFC} RBs are reused in each cluster within a building. However, when both the MCBS and FCBSs operate at different frequencies, the whole system bandwidth for FCBSs can be reused in each cluster under both CUCA and CUSA such that $M_{UFC} = M$.

For multiple band co-channel deployment of FCBSs, CUCA is not applicable for this scenario. Let M_{fcbs} and M_{mcbs} denote respectively the high frequency band for

FCBSs only and co-channel low frequency band for both MCBS and FCBSs. *For CUSA*, $M_{UFC} = M_{fcbs}$ for the U-plane traffic in all TTIs, and $M_{UFC} = M_{mcbs}$ for the C-plane traffic of FCBSs in $(1-\varphi)$ TTIs per ABS pattern period.

D. Proposed static RB allocation algorithm for resource reuse strategy 1

Since the minimum constraints must be satisfied in both intra-and inter-floor level, the total system bandwidth must be divided first by the number of floors fl_{3DR} within the RoE for inter-floor level constraint. Each equal number of RBs M is then allocated to FCBSs within any RoEs for intra-floor level constraint per RoE for inter-floor level constraint. The proposed algorithm (Algorithm 8.1) is given in the following and explained with an example (Example 8.1).

Example 8.1: Let $M_T = 48$ and $fl_{3DR} = 3$, $cl_{intra} = 4$, and $fl_T = 15$.

Step 1: $M = 48/3 = 16$, i.e. each inter-floor level cluster has 16 FCBSs.

Step 2: $m_{RB} = \{1, \cdots, 16\}$ and $M/2 = 8$ is an integer. Hence,

$$g = \{1, 2, 3, 4, 5, 6, 7, 8\}$$

$$j = \{9, 10, 11, 12, 13, 14, 15, 16\}$$

Step 3: for $M = 16$, $n_{diag} = 4$.

Step 4: $n_{cl} = 4 + 2 \cdot \sum_{y=1}^{y=3} (4 - y) = 4 + 2 \cdot (3 + 2 + 1) = 16 = M$

Step 5: Total number of orthogonal sets of RB $m_{orth} = 2 \cdot 4 - 1 = 7$

Step 6: The sets $\{g\}$ and $\{j\}$ then include consecutive RB indices of the values:

$$g = \{1, 3, 3, 1\} = 8 \text{ RBs}$$
$$j = \{2, 4, 2\} = 8 \text{ RBs}$$

And RB indices as follows:

$$g = \{\{1\}, \{2, 3, 4\}, \{5, 6, 7\}, \{8\}\}$$
$$j = \{\{9, 10\}, \{11, 12, 13, 14\}, \{15, 16\}\}$$

Algorithm 8.1: Non-adjacent channel interference avoided static radio resource allocation in FCLs in 3D multi-floor buildings.

Step 1: Divide the total number of RBs M_T in the system bandwidth into fl_{3DR} sets of consecutive RBs such that $M = M_T / fl_{3DR}$ number of consecutive RBs are allocated and reused to each RoE (i.e., cluster) for any floors existing within the RoE defined by the number of floors fl_{3DR} for inter-floor interference modeling (Figure 8.2(a)).

Step 2: Now divide the total number of RBs M for any floors into two sets of consecutive RBs denoted as $\{g\}$ and $\{j\}$ such that $m_{RB} = \{\{g\},\{j\}\}$ and $|m_{RB}| = M$. Let $m_{RB} = \{1, \cdots, M\}$ denote the set of RB indices such that (Figure 8.2(a)):

$$|g| = (|j|+1), \quad \text{if } M/2 \text{ is a non-integer}$$
$$|g| = |j|, \quad \text{if } M/2 \text{ is an integer}$$

And $g = \{1, \cdots, (M/2) + x_g\}$; $j = \{(M/2)+1, (M/2)+2, \cdots, M\}$

where $x_g = 1$ for $|g| > |j|$, and $x_g = 0$ for $|g| = |j|$.

Step 3: Find the value of the number of FCBSs along the diagonal of RoE n_{diag} .

Step 4: Estimate the total number of FCBSs in a cluster, i.e. RoE, given by the following expression for intra-floor modeling: $n_{cl} = n_{diag} + 2 \cdot \sum_{y=1}^{y=(n_{diag}-1)} (n_{diag} - y)$

Step 5: Estimate the total number of orthogonal set of RBs m_{RB}, which can be found by the following expression: $m_{orth} = n_{diag} + (n_{diag} - 1) = 2 \cdot n_{diag} - 1$

Step 6: Form the orthogonal set of RBs m_{orth} such that $\{g\}$ and $\{j\}$ include consecutive RB indices of the values as follows (Figure 8.2(b))

$$g = \{1, 3, 5, \cdots, n_{diag} - 1, n_{diag} - 3, n_{diag} - 5, \cdots, 5, 3, 1\}$$
$$j = \{2, 4, 6, \cdots, n_{diag}, n_{diag} - 2, n_{diag} - 4, \cdots, 6, 4, 2\}$$

where each value represents the number of consecutive RB indices.

Step 7: Now allocate consecutive subsets of RB indices to FCBSs alternatively starting from the set $\{g\}$ to $\{j\}$ and then back to $\{g\}$ to $\{j\}$ and so on until the last subset of either $\{g\}$ or $\{j\}$ reaches (Figure 8.2(c)). RB indices are allocated to FCBSs starting from the lower triangle heading towards the diagonal and then to the upper triangle of the square RoE so that adjacent RB indices of the system bandwidth are not allocated to contiguous FCBSs in order to avoid adjacent channel interference. All these steps are explained with an example in the following for an easy of understanding the algorithm. Note that all clusters in a multi-floor building are RB allocated to FCBSs following the same and fixed pattern as explained above.

Step 8: Since the total number of RBs in the system bandwidth M_T is reused in all floors per RoE (inter-floor level) with M RBs per floor, and each floor has the same number of FCBSs, the number of times M_T is reused per 3D RoE can simply be found by the number of RoEs per floor (intra-floor level) cl_{intra}. Hence, the total number of times M_T

(*continued*)

(*continued*)
is reused per building can be found by dividing the total number of floors in a building fl_T by the number of floors per 3D RoE fl_{3DR}. Note that with 3D RoE, we define the RoE that satisfies both intra-floor and inter-floor interference constraints. So, the resource reuse factor can be given by $\xi = (fl_T / fl_{3DR}) \times cl_{intra}$.

Step 7: Allocate consecutive subsets of RB indices to FCBSs alternatively starting from set $\{g\}$ to $\{j\}$ in order to avoid adjacent RB interference.

Note that in intra-floor level (Figure 8.2(c)), there is no contiguous RB indices allocated to FCBSs next to one another except those FCBSs at the edge point along the diagonal of each apartment. However, such effect is negligible as compared to the non-adjacent RB allocations around each side of each square apartment.

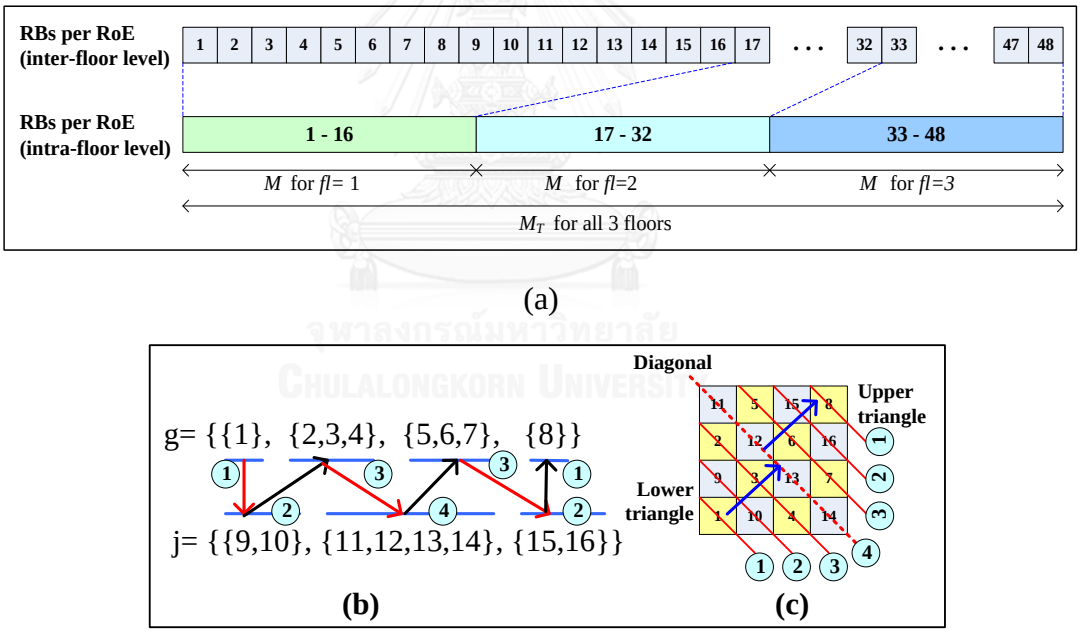

Figure 8.2: Static RB resource allocation to FCBSs with adjacent channel interference avoidance: (a) for M_T = 48 inter-floor level, (b)-(c) for M = 16 for intra-floor level.

Step 8: Resource reuse factor $\xi = (fl_T / fl_{3DR}) \times cl_{intra} = (15/3) \times 4 = 20$. Hence, spectral efficiency can be improved by about 20 times.

E. Performance evaluation

In the following, FC clustering, resource reuse and allocation for 2D intra-floor scenario under CUCA are discussed and evaluated. As shown in Figure 8.1, following a static RB allocation to avoid co-channel interference, the whole system bandwidth is reused in each RoE for 2D intra-floor modeling such that all FCBSs in RoE are cFCBSs with respect to neighboring clusters. We consider an interference constraint to define the RoE. RBs are allocated equally to each FCBS within a cluster, and the same set of RBs is reused to each cluster. The set of RB indices allocated to any FCBSs is fixed and does not change from one cluster to another such that the same pattern of RB indices is followed in assigning RBs per cluster (Figure 8.1). Because of considering any single floors within the building, step 1 in 3D building scenario as described is not needed.

We consider the same multi-tier network as in Chapter 4 in section 4.5.1 and its mathematical model in section 4.5.2(A) for evaluation. To define the RoE, a FU is considered to locate at the farthest radial distance from its sFCBS for the worst-case analysis, and all FCBSs of a single floor of the building are considered for performance evaluation.

Let U_{FC} denote the number of FCBSs per cluster, and M_{FC} denote an equal number of RBs per FCBS per cluster such that $M = U_{FC} \cdot M_{FC}$. Let σ_{thr} corresponds to α_{thr} denote the required link spectral efficiency between sFU and sFCBS within a cluster such that the required capacity constraint for each FCBS can be given by $\sigma_{thr,c} = M_{FC} \times \sigma_{thr}$. Hence, the aggregate capacity from reusing M RBs per cluster on a floor for *Q* TTIs can be given by

$$\sigma_{FC,cl} = U_{FC} \times \sigma_{thr,c} = U_{FC} \times \left(M_{FC} \times \sigma_{thr}\right) \tag{8.1}$$

For all clusters ξ on a floor

$$\sigma_{FC,all} = \xi \times \left(U_{FC} \times \left(M_{FC} \times \sigma_{thr}\right)\right) \tag{8.2}$$

Following (C.5) in Appendix C, the aggregate capacity of all MUs can be given by

$$\sigma_{MC} = \sum_{t=1}^{Q} \sum_{i=1}^{M} \sigma_{t,i}\left(\rho_{t,i}\right) \tag{8.3}$$

where σ and ρ are responses over M RBs of only indoor MUs in $t \in \boldsymbol{T_{ABS}}$ and all outdoor and offloaded MUs in $t \in \boldsymbol{T}$. Since during an ABS, no FCBSs can transmit data signal, the aggregate capacity of FUs for ξ on a floor for any φ is given by

$$\sigma_{FC,fl} = (1-\varphi) \times \sigma_{FC,all} \tag{8.4}$$

Hence, the overall system capacity of the multi-tier network over M RBs for Q TTIs can be expressed as the sum throughput of all UEs as follows

$$\sigma_T = \sigma_{MC} + \sigma_{FC,fl} \tag{8.5}$$

The default simulation parameters and assumptions used for the system level simulation are listed in Table B.5 and Table B.8 in Appendix B. From (4.8) in Chapter 4, it can be found that d^* is independent of the number of reused RBs per FCBS, and any number of RBs can be reused in FCBSs which are located at distances at least $d = d^*$ from one another. A key observation from (4.8) in Chapter 4 is that the aggregate interference at sFU is inversely related to d^* such that by allowing an increase in α_{thr}, d^* between cFCBSs (Figure 8.3), and hence the RoE can be reduced such that more reuse of resources can be obtained. Figures 8.4 and 8.5 show the outperformance of the proposed FC clustering and frequency reuse in FCBSs of each cluster on a floor with 25 FCBSs. For $\alpha_{thr} = 0.1$, $d^*_{tra} = 21.5443$ m is needed. Hence, to enforce d^*_{tra}, up to tier-2 from any FCBSs is to be considered as RoE such that no RBs can be reused in any FCBSs located up to tier-2 around any FCBSs (Figure 8.1). Hence for a floor with 25 FCBSs, the maximum number of 4 clusters, of which one consists of a complete set of 9 FCBSs while each of the remaining three consists of a subset of FCBSs of the complete set, can be formed such that the system bandwidth can be reused about 2.78 times in all 25 FCBSs on the floor. Since both the capacity and spectral efficiency vary directly in proportion to the system bandwidth, the FC capacity and spectral efficiency with the proposed technique can be improved by almost the same factor of 2.78 as compared to the conventional ABS based eICIC as shown in Figures 8.4 and 8.5. Also because of better channel conditions of FUs, most of the capacity of the overall system is contributed by FUs.

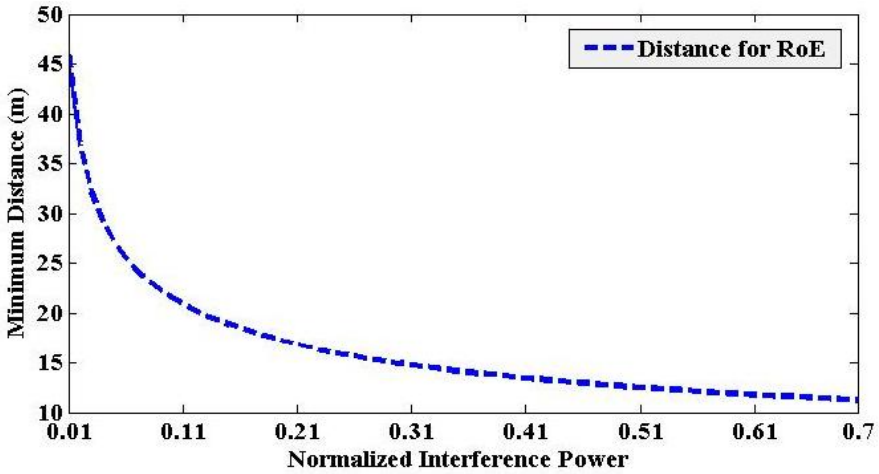

Figure 8.3: Minimum distance versus normalized interference power.

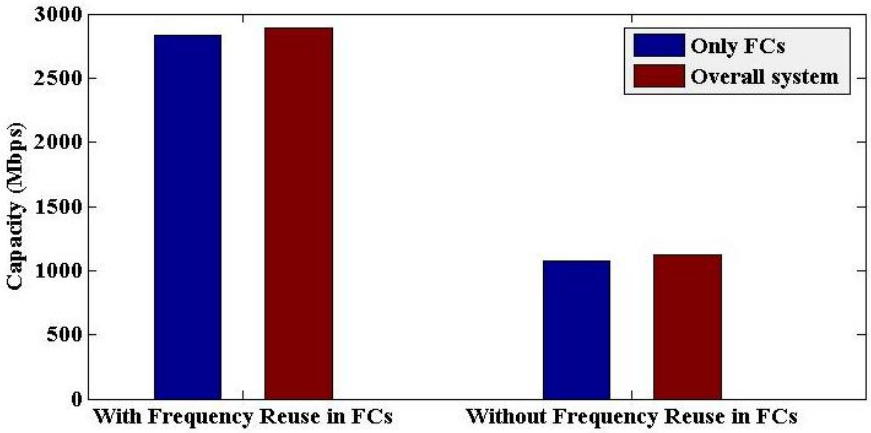

Figure 8.4: Capacity response for the cluster size = 9.

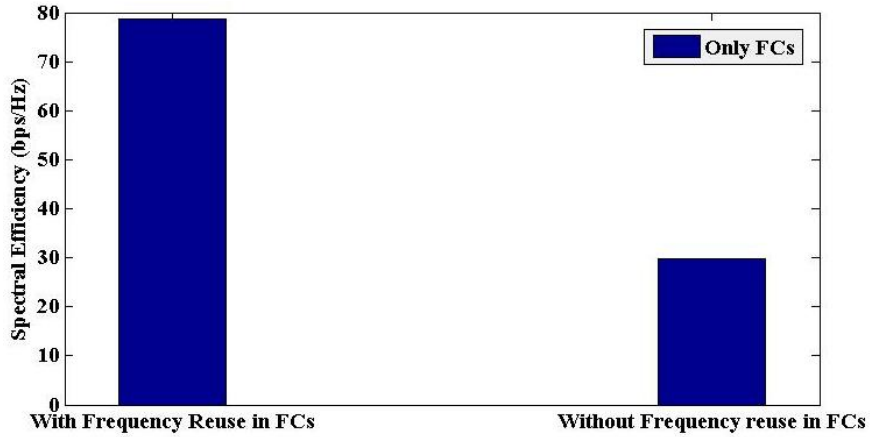

Figure 8.5: Spectral efficiency response for the cluster size = 9.

8.3 Recommended study 03: SCBS transmit power management for multi-user case

8.3.1 Recommended research proposal

In Chapter 7, the modeling of transmit power of FCBSs considers one UE per FCBS such that the explanation for modeling transmit power of FCBSs can be applied directly to find the value of on-state and off-state duration of a FCBS using on and off traffic source model. This is because of the fact that a UE has also two states, i.e. either there is a UE traffic request or not to its associated FCBS. However, in case of multiple users per FCBS, finding the value of on-state and off-state duration is not immediate since there exists more than one UE, and the FCBS may have to be active with an activity factor of 100% at the extreme case, which can be considered for further studies.

8.3.2 Preliminary research progress

In the following, as part of preliminary works toward this direction, a general and simple way to derive on-state and off-state probabilities of a FCBS for multi-user per FCBS scenario is given by estimating the probability of no in-progress UE traffic request such that the probability of off-state can be given by

$$P(\text{off-state}) = 1 - p(0)$$

Similarly, the probability of on-state is given by

$$P(\text{on-state}) = p(1) + p(2) + \cdots + p(N_s)$$

where $p(0), p(1), p(2), \cdots, p(N_s)$ represent the state probabilities for $i = 0, 1, 2, \ldots, N_s$. N_s is the number of users with in-progress traffic with a FCBS. The values of these probabilities can be found using the Birth-Death process as follows.

Consider that there are M_s users per FCBS of which N_s users have in-progress traffic with a FCBS at any time t. Let λ_{N_s} and μ_{N_s} denote the birth rate and death rate respectively. Then, the followings hold.

$$\lambda_{N_s} = (M_s - N_s)\lambda, \quad 0 \le N_s \le M_s$$
$$= 0, \quad \text{otherwise}$$

$$\mu_{N_s} = N_s \cdot \mu$$

The probabilities for any arbitrary N_s (Figure 8.6) can be given by

$$p(N_s) = p(0)\prod_{i=0}^{N_s-1} \lambda(M_s - i)/(i+1)\mu$$

$$p(N_s) = p(0)\cdot(\lambda/\mu)^{N_s} \cdot \binom{M_s}{N_s}$$

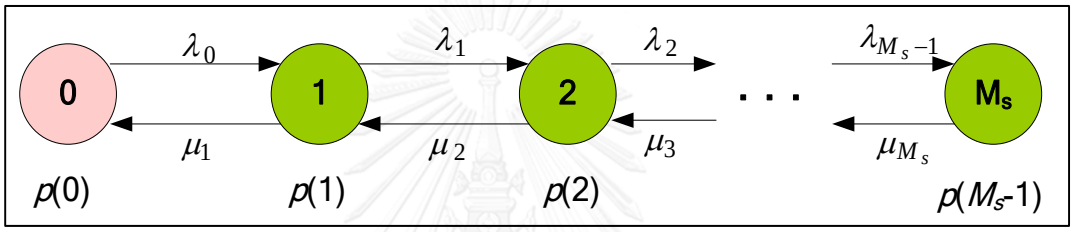

Figure 8.6: Occupancy state diagram of a FCBS.

But $\sum_{N_s=0}^{M_s} p(N_s) = 1$

Such that $p(0) = 1/(1+\lambda/\mu)^{M_s}$

Hence, $P(\text{off-state}) = p(0) = 1/(1+\lambda/\mu)^{M_s}$ (8.6)

$$P(\text{on-state}) = 1 - p(0) = 1 - 1/(1+\lambda/\mu)^{M_s} \quad (8.7)$$

Also, $p(N_s) = \binom{M_s}{N_s} \times \left(\frac{\lambda}{\mu}\right)^{N_s} \Big/ \left(1+\frac{\lambda}{\mu}\right)^{M_s}$

The above model, as an extension to the single user case in Chapter 7, can be evaluated for further studies.

8.4 Recommended study 04: CoMP enabled SCBS transmit power modeling

8.4.1 Recommended research proposal

When energy efficiency is concerned, FCBSs in a RoE (Chapter 6 for multi-floor building) with no active traffic request can be muted for transmission by switching the transmit power off. However, when spectral efficiency is concerned, to overcome wastage of resources, we can consider cooperative or opportunistic resource allocation such that neighboring FCBSs in a RoE with no active traffic request can form a CoMP set to increase the signal strength of a neighboring FCBS with active traffic requests. A FCBS (U-plane BS) can monitor in every certain amount of TTIs to detect if there is any UE traffic request within its coverage. The UE can also be synchronized with the on and off cycle of the FCBS such that it can measure the RSSIs of all U-plane FCBSs around it and inform the scheduler about the inactive FCBSs to form a suitable cooperating set of U-plane BSs for joint transmission CoMP. Hence, an algorithm to tradeoff both spectral efficiency and energy efficiency can be developed. One way to address this issue is to transmit data by neighboring FCBSs in a CoMP set at reduced power. This trade-off can be explored as further studies.

Hence, based on whether or not joint transmission CoMP during transmit power off mode is considered, two schemes can be proposed. In Chapter 6, the scheme without exploiting joint transmission CoMP during power off mode has been discussed. In what follows, we propose a scheme that exploit joint transmission CoMP during power off mode, and can be evaluated as further studies. According to [158], for a traffic service, there is some unused (off) time between their transmitted packets which may be used for other services. We explore this study at the connection level, i.e. UE traffic request, rather than packet level such that during off time, inactive FCBSs can serve other active FCBSs using joint transmission CoMP as described in the following as part of preliminary research progress.

8.4.2 Preliminary research progress

A. Statistical multiplexing/opportunistic scheduling

As explained, we consider cooperative or opportunistic resource allocation such that neighboring FCBSs in a RoE with no active traffic request can form a CoMP set. All FCBSs in a CoMP set transmit the same data to a sFU which literally also termed as joint transmission CoMP. In other words, we exploit networked or cooperative MIMO to serve a FU by multiple FCBSs forming a cooperating set within a cluster. The main essence behind adopting C-RAN is to gain from cooperating among a number of BSs for sharing resources, which we exploit here instead by cooperating among a set of FCBSs transmitting the same data to a FU at different frequency such that the signal strength and hence the capacity improve from multi-point transmissions (i.e., diversity gain or statistical multiplexing gain as shown in Figure 8.7) and is given by

$$\sigma = B_1\left(1+\log_2 \text{SINR}_1\right)+B_2\left(1+\log_2 \text{SINR}_2\right)+, \cdots, +B_{n_f}\left(1+\log_2 \text{SINR}_{n_f}\right) \quad (8.9)$$

where $B_1, B_2, \cdots, B_{n_f}$ denote bandwidths (sets of RB allocated to FCBSs by a static resource allocation strategy as explained before) of neighboring 1, 2, …, n_f FCBSs respectively in the cooperating set. Hence, by combining CoMP features on top of FC clustering based on RoE, an efficient resource usage can be achieved, which can be considered for further studies.

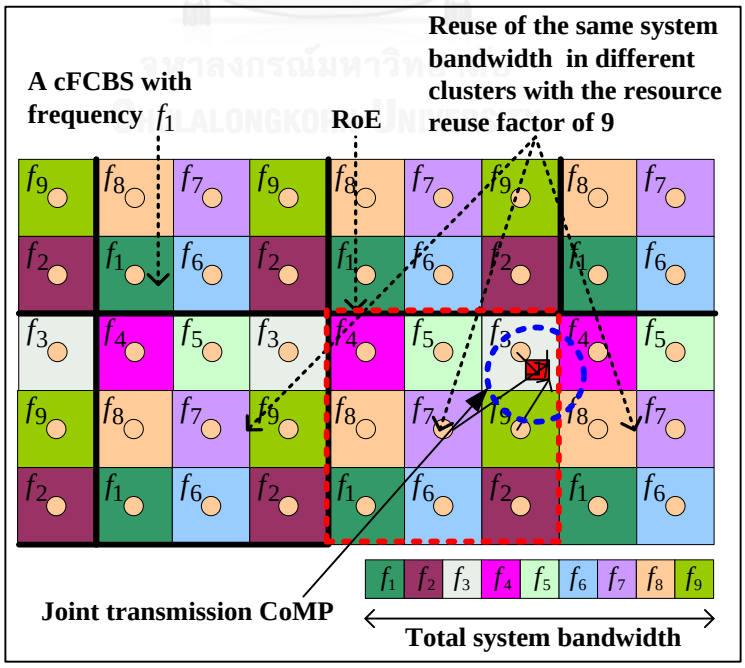

Figure 8.7: Joint transmission CoMP within a cluster.

B. Proposed algorithm for joint transmission CoMP

When an on-state FCBS does not have any data to serve to its own serving UE, it switches from on-state to off-state to save power to improve energy efficiency (Chapter 7). However, if the demand is to enhance spectral efficiency or user throughput rather than energy efficiency, we propose an off-state FCBS to serve other neighbor UEs to increase their throughputs as shown in Figure 8.8. An off-state FCBS serves a UE of one of its nearest neighbor FCBSs. If there exist more than one UE, since the scheduler has all UEs' CSI and traffic data rate demand σ_u, the off-state FCBS is then informed by the scheduler to serve the UE with the maximum service data rate demand $\sigma_{u,\max}$. However, if all neighbor UEs have the same service data rate demand, the off-sate FCBS can serve any of the UEs by choosing randomly.

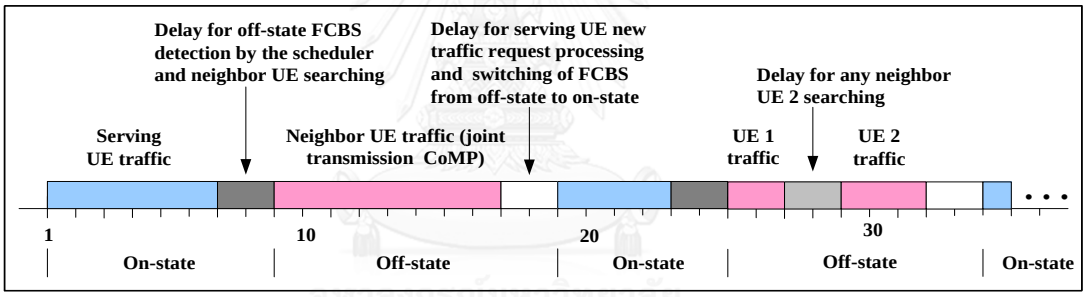

Figure 8.8: Proposed SCBS transmit power on and off mechanism with joint transmission CoMP.

Note that once any off-state FCBS is chosen to serve any neighbor UEs, it continues to serve the same UE as long as either that UE's transmission is finished or until there is a new request from its own serving UE. Hence, if any other neighbor UEs' either CSI or data rate demand is higher than that of the one which has already been chosen by the off-state FCBS, it continues to serve the same UE in order to reduce control signaling overhead. Note also that because of static allocation of frequency resources per FCBS and regular square-grid pattern per cluster, the scheduler has the knowledge of physical cell identity of each FCBS and its location within the cluster to determine and inform any off-state FCBSs. The proposed algorithm for the joint transmission CoMP is given in Algorithm 8.2.

Algorithm 8.2: Joint transmission CoMP for off-state FCBSs.

Step 1: The scheduler in a cluster of FCBSs determines any off-state FCBS' x_{FC} physical cell identity in each TTI based on the CSI responses from all UEs served by the FCBSs.

Step 2: Check the list of neighbor UEs and their service data rate demand $\sigma_{u \in U}$ at the scheduler.

Step 3: Select the UE $U_{\sigma_{u,\max}}$ with the maximum service data rate demand $\sigma_{u,\max}$ to be served by the off-state FCBS x_{FC}.

Step 4: Inform and send the data of $U_{\sigma_{u,\max}}$ to the off-state FCBS x_{FC} to transmit to $U_{\sigma_{u,\max}}$.

Step 5: Continue Step 1 through Step 4 until any new traffic request from the serving UE of the off-state FCBS x_{FC} is made or the data transmission of the ongoing $U_{\sigma_{u,\max}}$ is finished. In the former case, stop transmitting data to $U_{\sigma_{u,\max}}$ and start transmitting data to the serving UE of the off-state FCBS itself. However, in the latter case, stop transmitting data to $U_{\sigma_{u,\max}}$ and start searching other neighbor UEs to serve.

Step 6: Repeat step 1 through step 5 for all UEs per cluster and for all clusters per building.

8.5 Recommended study 05: analysis of the coexistence of multiple bands at SCBS for non-uniform and asymmetric traffic

8.5.1 Recommended research proposal

In order to address high data rate services by employing additional spectrums, the co-existence of a number of frequency bands with diverse propagation characteristics, e.g. microwave and mmWave, within the same system is expected in 5G networks [3]. Besides, traffic is generated non-uniformly network wide because of several issues, including difference in loading of BSs with environment, non-uniform user density, and disparity in high data rate traffic demand with time. Further, as mentioned in Chapter 5, the characteristics of traffic generated in the UL/DL and the C-/U-plane are asymmetric.

These high data rate, non-uniform, and asymmetric traffic demand have a direct impact on a BS capability and the choice of enabling technology resulting the requirement of an adaptive BS which can be configured based on such aspects as area, time, service data rate, the UL/DL and the C-/U-plane traffic volumes. One way to address this adaptive feature of SCBSs is to deploy more than one transceivers implemented with multi-band having diverse propagation characteristics such as microwave and mmWave such that places where the traffic fluctuation is very high, based on the traffic characteristics, each SCBS can switch to mmWave band during a high traffic demand and to microwave band during a low traffic demand. Further, because of shorter distance as compared to a MCBS between a UE and a SCBS and relatively lower traffic of the UL and the C-plane, the UL and the C-plane traffic can be served with a low UE transmit power at microwave frequency, whereas higher traffic volume at a high data rate demand of the DL and U-plane can be served by mmWave frequency.

Because the co-existence of multi-band at a SCBS has manifold benefits, sufficient researches toward this direction is needed in order to adapt a SCBS with traffic characteristic and demand for 5G networks. Though in Chapter 5, we address this issue by proposing a multi-band enabled FCBS architecture where we consider co-channel microwave and mmWave bands, other types of bands than these with more than two bands per FCBS can be explored for further studies to analyze usefulness in view of non-uniform traffic and asymmetric traffic from splitting the UL/DL and the C-/U-plane to enable BS idle mode capability through dual connectivity in 5G networks.

8.5.2 Preliminary research progress

In the following, we extend the proposed architecture in Chapter 5 for non-uniform traffic as shown in Figure 8.9. Since the splitting of the C-/U-plane has been discussed already in Chapter 5, in the following, we discuss only non-uniform traffic and scheduler implementation as part of preliminary research outcomes toward in-depth

further studies. To avoid ambiguity, we consider the same system model as discussed in Chapter 5 for the following discussion.

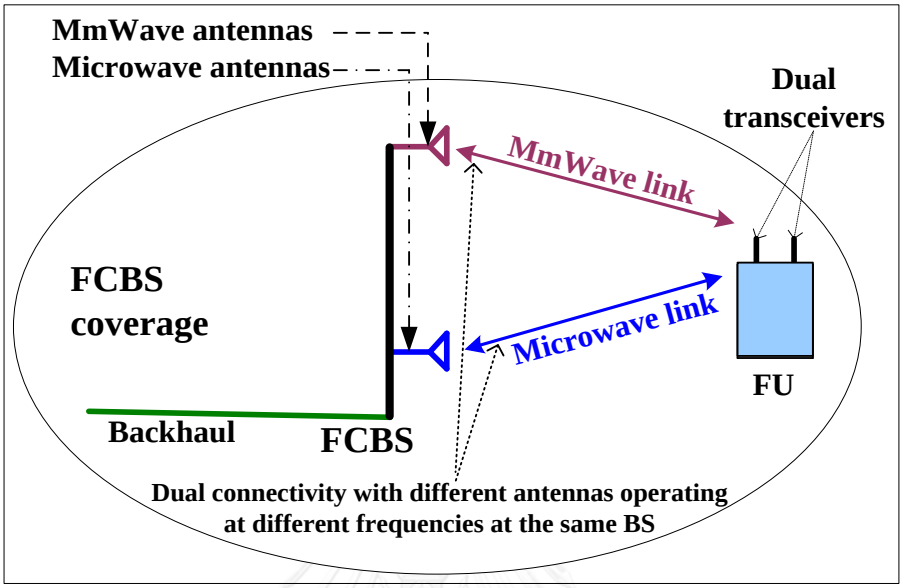

Figure 8.9: Multi-band enabled FCBS architecture.

A. Non-uniform traffic

Though the average traffic demand has been increased by manifold in the last decade, traffic is not generated uniformly network wide because of issues as follows:

- BSs located in urban areas serve more traffic than those in suburban or rural areas.
- In urban environments, all places are not populated uniformly, e.g. bus stations and shopping malls are more likely to be populated than other places. BSs located in these areas need to serve more traffic than others.
- The demand for high data rate services is not uniform since traffic demand largely depends on user profiles, and user characteristics. Hence, it is more probable that a user of upper class residential zones can afford and hence generate more high data rate services than others. Accordingly, more BSs should be installed in such areas.

- Traffic demand varies with time, e.g. most corporate traffic is generated during 8:00-18:00, whereas most residential traffic is generated during 17:00-23:00.

Since both spectrum band and bandwidth have direct impact on the capacity, a FCBS can be implemented with dual spectrums such as microwave and mmWave to address such non-uniformity in traffic demand as aforementioned. As shown in Chapter 5, since an mmWave band provides more capacity than that of a co-channel microwave band, a multi-band enabled FCBS architecture can be operated at mmWave spectrum during a high traffic demand and at co-channel microwave spectrum during a low traffic demand in places where the traffic fluctuation is very high. In both cases, the other off-service transceiver, i.e. co-channel microwave for a high traffic and mmWave for a low traffic, can be switched off to save energy. If necessary, both spectrums can operate at the same time to provide even higher data rate than that when operating at a single spectrum. With such an adaptive scheme for spectrum availability in FCBSs, network operators can provide on-demand data rate services, optimize location specific resource allocation, and maximize profit margin.

B. Scheduler implementation for multi-band enabled FCBS architecture

The scheduler for co-channel microwave spectrum can be implemented either jointly or dis-jointly based on whether the FD scheduler for FCs is implemented either jointly or dis-jointly with the TD scheduler, implemented at MCBS. The TD scheduler allocates subframes to UEs in the system. In dis-joint implementation, the cluster head (as mentioned in Chapter 5) can communicate with MCBS, and the FD scheduler of FUs is implemented at the cluster head (Figure 8.10). However, the FD scheduler for all MUs is implemented at MCBS. FUs can directly report their channel status and traffic demands to the cluster head, and the TD scheduler updates the cluster head about ABS patterns per ABS pattern period. To adapt ABS patterns, an indoor MU in the building during an ABS pattern period informs in the UL to the TD scheduler which in turn informs the cluster head of ABS patterns via X2 backhauls to schedule RBs to FCs

only during non-ABSs. Whereas for no presence of an indoor MU, it informs the cluster head to allocate RBs to FCs in all TTIs over the next ABS pattern period.

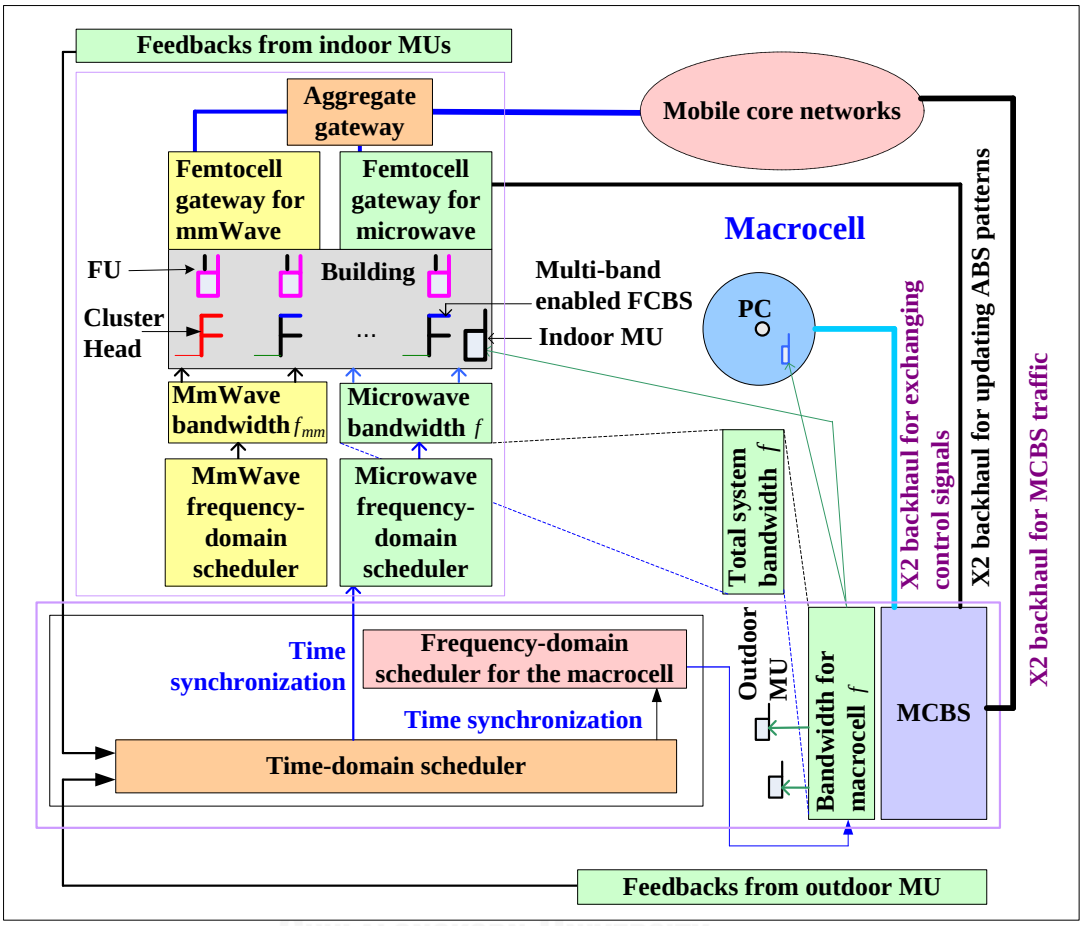

Figure 8.10: Disjoint scheduler implementation for multi-band enabled FCBS architecture.

In joint implementation, all FCBSs inform the cluster head of their traffic demands, which in turn communicates to the FD scheduler for FUs at MCBS. The TD scheduler informs the FD scheduler of ABS patterns for all FCs. Information regarding the allocation of RB resources from the FD scheduler for FCs is then sent over X2 backhaul to the cluster head to relay to FCs of the building. For mmWave, the scheduler implementation is rather straightforward since there is no need for coordination between MC-plus-PC and FC tiers. A disjoint mmWave FD scheduler can be implemented at the cluster head to avoid backhaul control overheads, and the FD scheduler can directly allocate RBs to FCs without taking any concern of the FD

scheduler at MCBS for MUs irrespective of the presence of indoor MUs within the building.

8.6 Recommended study 06: C-RAN enabled CUSA based device-centric networks

8.6.1 Recommended research proposal

The C-/U-plane separation and cloud computing technology based dense HetNets are considered to be promising solutions to address important issues such as centralized interference management and efficient resource utilization for high capacity dense HetNets. In cloud-radio access network, because of centralized processing feature, resource scheduling can be benefitted from centralized interference management, and radio resources of different BSs can be shared with each other whenever necessary.

The general architecture of C-RAN consists of three components, namely a pool of baseband units with centralized processors, RRHs with antennas distributed network wide, and a fronthaul connecting RRHs and centralized baseband units as shown in Figure 8.11. Because of centralized feature, radio resources of different BSs can be shared with each other whenever necessary. The fronthaul is the link connecting baseband unit pool and RRHs that operate on protocols such as CPRI and OBSAI. Fronthaul can be ideal and non-ideal based on its capacity. Non-ideal fronthauls such as microwave or mmWave wireless links are bandwidth, time latency, and jitter constrained. However, ideal fronthauls such as optical fiber is cost inefficient, and hence non-ideal fronthauls are considered to be more viable implementation.

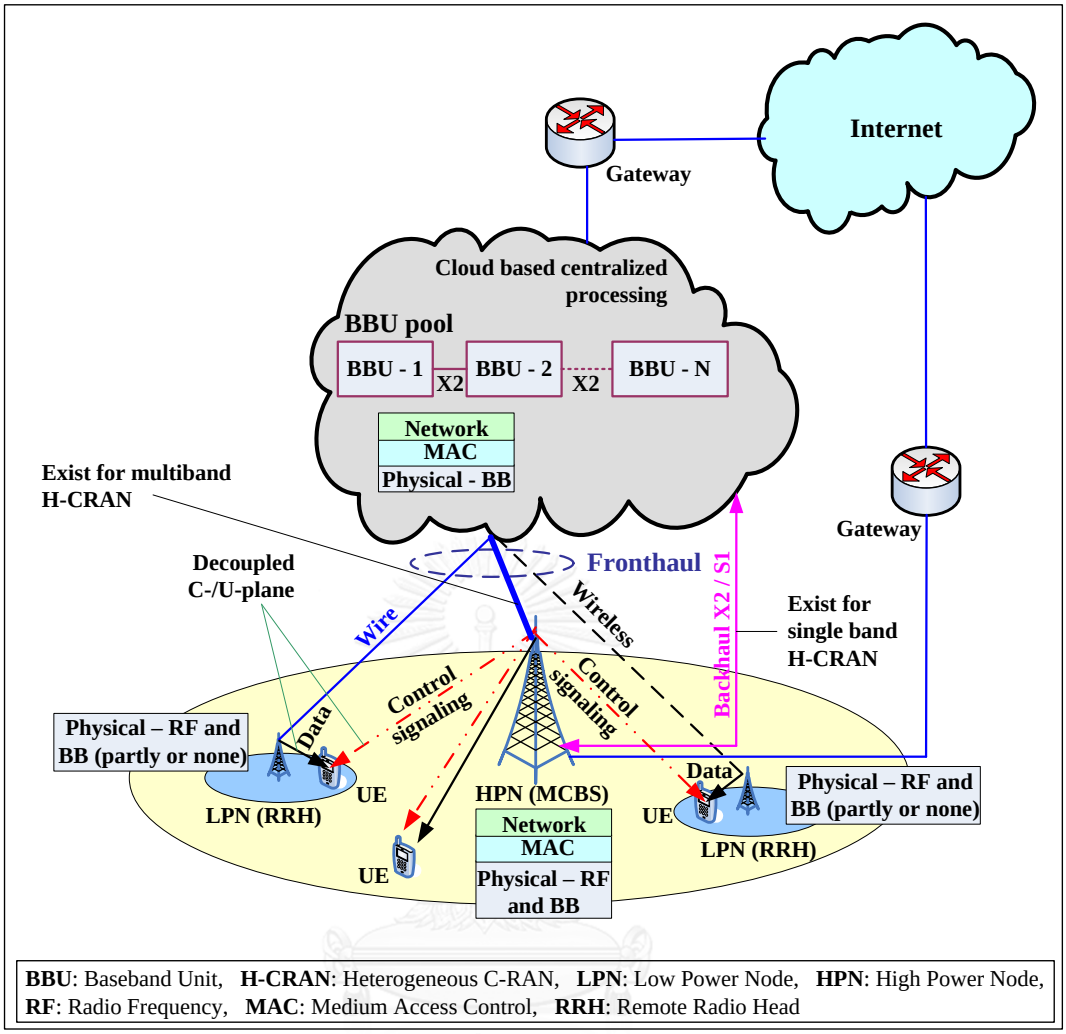

Figure 8.11: C-RAN components and system architecture for single and multiband heterogeneous cloud RAN [159, 161].

Because of high capacity fronthaul requirements, existing C-RANs suffer from poor flexibility and scalability performances owing to unavailability and high cost of optical fibers network wide. The constrain of C-RANs from the fronthaul can be overcome by designing compression technique over the constrained fronthaul, largescale pre-coding and de-coding with low overheads, and radio resource allocation optimization taking the constrained fronthaul into account. In [159], to address the capacity, time delay, and energy efficiency limitations of fronthaul in traditional C-RAN (where the C-/U-plane are coupled), authors proposed decoupling of the C-/U-plane such that all control signaling and system broadcasting data are delivered by high power nodes, i.e. MCBSs, to UEs, and RRHs can be switched on and off based on active

data traffic requests. Like traditional C-RAN, all RRHs are connected to the centralized baseband unit pool which is responsible for layer-1 baseband processing and all upper layer functionalities, and RRHs are responsible for layer-1 radio frequency signal processing. Unlike traditional C-RAN, MCBSs are interfaced with the baseband unit pool to manage interference between MCBSs and RRHs using centralized cloud computing cooperative processing techniques and to allow backward compatibility. MCBSs mainly provide control signaling and seamless coverage network wide in addition to some bursty and low data rate services, and RRHs mainly provide high speed data services. Hence, MCBSs are incorporated into traditional C-RAN by decoupling the C-/U-plane. The architecture is termed as heterogeneous cloud RAN as shown in Figure 8.11 that takes advantages of both HetNets and traditional C-RAN where cloud computing technology is introduced in HetNets to provide large-scale cooperative signal processing and networking functionalities to improve both energy efficiency and spectral efficiency beyond that can be achieved by HetNets or C-RAN operating alone [160].

Rather than cooperative RRM at the centralized baseband unit, the interference between low power nodes, i.e. PCBSs, and MCBSs can also be managed by operating MCBSs and PCBSs at different frequencies, i.e. MCBSs at lower and PCBSs at higher frequencies. In [132], the C-/U-plane decoupled multiband HetNets architecture was proposed where MCBSs at 2 GHz provide all control signaling functionalities, and PCBSs at 3/60 GHz mainly provide high data rate services. Both MCBSs and PCBSs are connected to the C-RAN via CPRI interface, and MCBSs mange mobility and traffic of all UEs and assist UEs for cell discovery via C-RAN as shown in Figure 8.11. Like single band heterogeneous cloud RAN, parts of layer-1 baseband processing and all upper layer functionalities are performed centrally.

C-RAN enabled CUSA brings with a number of advantages over conventional networks as follows:

- CUSA allows low energy consumption by switching SCBSs off (when there is no active data traffic request), ubiquitous coverage by large MCs, high data rate

services by SCBSs, and adaptive traffic service mechanisms both in time and space.

- CUSA provides flexible mobility management since less handover is required for C-plane because of a large MC coverage, and for U-plane, handover is required only for active data requests, and no handover requests are required for inactive UEs for both planes. These result in a reduced overhead signaling.
- CUSA can be scaled easily to adapt with a growing traffic demand. U-plane can be flexibly scaled without concerning C-plane such that more SCBSs can be added on the existing network wherever and whenever necessary.
- Spectral efficiency can be increased because of reduced control signaling interference from the smaller number of control MCs as well as data plane interference from the inactive SCBSs.
- Because MCBSs and SCBSs operate at different frequencies, cross-tier interference between them can be avoided.

Furthermore, in dense HetNets, existing interference management techniques may not be sufficient and responsive enough such that a centralized coordinator with a global view may be helpful to control and mange efficiently radio resources among dense BSs. In this aspect, MCBSs, i.e. C-plane BSs, can play the role of a centralized coordinator to control SCBSs, i.e. U-plane BSs under their respective coverage, and C-RAN is a promising candidate for this kind of centralized network control and management [9]. Hence, in future studies, the problem of interference modeling, resource reuse and allocation, and densification limit of 3D in-building SCs in cloud-radio access network enabled CUSA can be addressed. A centralized resource allocation algorithm can considered to develop that can exploit and schedule time, frequency, and transmit power resources to SCBSs optimally for a given set of constraints such as fronthaul, degree of centralization, and operating frequency to show comparative performances of the traditional cell-centric network architecture and cloud-radio access network enabled CUSA in terms of achievable capacity of 5G networks.

8.6.2 Preliminary research progress

In Figure 8.12, a C-RAN enabled CUSA based device-centric network for centralized resource allocation in FCBSs and PCBSs is illustrated for further studies. In the following, how different tasks to address centralized resource allocation can be performed by a number of elements at various sections of the architecture, which can be considered to investigate, is briefly described.

A. Centralization and degree of cooperation

Baseband units of a number of SCBSs are decoupled first from their radio frequency functionalities to locate them centrally as a single grouped resource to address lightly and heavily loaded BSs balanced and to allow easy of cooperation for exchanging information among BSs in order to implement cooperative communication easily. Cooperative communication has a high potential for managing interference and allocating resources to BSs and hence improving overall network capacity, which is considered to investigate over the coupled baseband unit and the C-/U-plane cell-centric architecture. After processing in the centralized baseband units, U-plane IP traffic are transported to the mobile core network over backhaul links, e.g. X2 backhauls, followed by which are then sent to the external networks, e.g. Internet.

B. Fronthaul constraints

The link between SCBSs and centralized baseband units is called fronthaul, and the link that connects centralized baseband units to the mobile core network is called backhaul link. Fronthaul mobile architecture has been recently proposed for NGMN architecture. The capacity requirement of fronthauls is much higher than IP backhauls since real time in-phase and quadrature sample signals, which are jitter and delay sensitive, are carried over fronthauls. Optical fiber is the best solution for fronthauls, however because of a high cost of fiber, other alternative solutions such as microwave, wavelength division multiplexing, and passive optical network can be considered based

on system requirements. Since cluster size impacts greatly on the performance gain from C-RAN (the larger the cluster size, the more the C-RAN gain), investigations

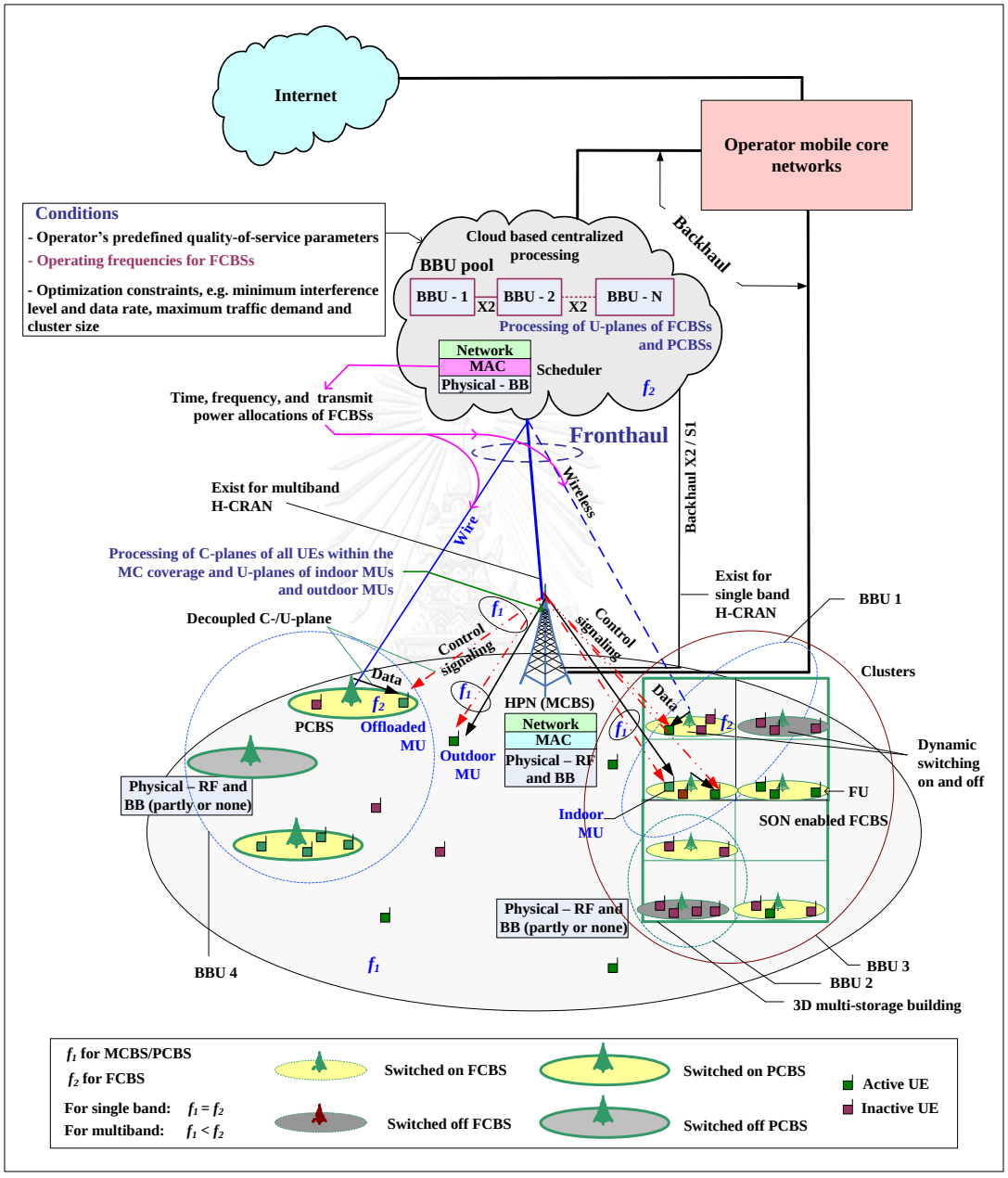

Figure 8.12: Proposed device-centric network architecture for centralized resource allocation for further studies.

under fronthaul constraints, e.g. alternative solutions as aforementioned, can be considered to carry out further.

C. Optimal cluster size

Clustering of FCBSs in 3D buildings can be done in a number of ways. A straightforward way is the proposed clustering approach as described in Chapter 3 for conventional networks, i.e. considering all FCBSs deployed within a 3D building as a cluster. A baseband unit per cluster is needed at the centralized baseband units. Since, the number of floors as well as apartments is varied from one building to another, and so is the density of FCBSs per building, clustering can be exploited based on traffic demand of FUs rather than buildings. For highly dense buildings, more than one cluster can be considered such that in place of one baseband unit, multiple baseband units per building can be considered at the centralized baseband units. Typical practice of a cluster size is to consider a minimum of 15 BSs and preferably 30 BSs per baseband unit. Since more gain can be achieved by increasing the cluster size, it is always preferable to increase the cluster size to as big as possible. However, since all in-phase and quadrature samples are to be transported over fronthauls, because of fronthauls' capacity constraint, it is not possible to group as many SCBSs as possible into a cluster. Depending on fronthauls' capacity and availability by the operator, the proper size of a cluster can be set. Hence, considering that an operator has a number of alternative fronthaul solutions, an in-depth investigation with a variable fronthaul capacity for an optimal cluster size can be considered to carry out further.

D. Operating frequency bands

The proposed architecture considers both single band and multiband deployment scenarios. In multiband scenario, both the C-/U-plane of MCBS operate at the lower frequency f_1 typically 2 GHz to provide a large coverage, and U-plane of all PCBSs and FCBSs operate at a higher frequency f_2, e.g. 6 GHz to provide a high data rate within small coverages. The advantage of operating BSs on multi-band over a single band is to overcome cross-tier interference between MCBS tier and FCBS-plus-PCBS tier for U-plane, however at the cost of an additional band to be licensed for FCBS-plus-PCBS tier. In contrast, single band outperforms multiband by reusing the

same frequency in FCBS tier, however at the cost of generating co-channel cross-tier interference with MCBS-plus-PCBS tier for both the C-/U-plane. Hence, interference management is more crucial for single band scenario than that in multiband. Both scenarios are incorporated in the proposed architecture to investigate and to find an optimal tradeoff these two scenarios. Note that resources are considered to reuse for U-plane in FCBSs only, and for U-plane of PCBSs, an orthogonal resource allocation at frequency f_2 is considered. Since C-plane of all UEs operate at the same frequency f_1, interference among all tiers, i.e. MCBS-tier, PCBS-tier, and FCBS-tier for C-plane traffic needs to be properly managed. Since schedulers for C-plane are located at the MCBS, a straightforward way to address C-plane interference is to allocate resources orthogonally both in time and frequency to all UEs. However, since typically only a fraction of total system bandwidth is allocated for C-plane traffic, and there is a huge number of FUs, such orthogonal resource allocation may not seem to be a viable solution. Hence, a new mechanism to address C-plane interference needs to be developed and can be considered to investigate.

E. Processing C-/U-plane traffic and degree of centralization

The MCBS is solely responsible for processing and serving all UEs' C-plane traffic to ensure ubiquitous coverage. In addition, the MC processes and serves U-plane traffic of all outdoor MUs and indoor MUs. FCBSs are deployed in 3D buildings only and are responsible for U-plane traffic of FUs only. All PCBSs are responsible for serving U-plane traffic of offloaded MUs. All U-plane baseband traffic of both FCBSs and PCBSs are processed centrally by forming clusters, i.e. a group of corresponding SCBSs, such that each baseband unit in the pool of baseband units at the central station represents the U-plane traffic of all SCBSs within the corresponding cluster. Both PCBSs and FCBSs possess only radio frequency functionalities of U-plane traffic. The degree of centralization of any baseband units can be changed by changing the number of SCBSs per cluster as well as an average traffic generated per SCBS. An appropriate mechanism to define the degree of centralization, for a given set of constraints, needs to be developed and can be considered to address.

F. Resource scheduling

A scheduler for U-plane traffic of all SCBSs in a cluster, i.e. a baseband unit, schedules time, frequency, and transmit power based on the conditions as shown in Figure 8.12. Note that all schedulers for U-plane traffic of all SCBSs within the MC coverage are resided at the central station, and there is one scheduler per baseband unit. Information about the scheduled UEs in any time at any RB along with transmit power level are sent to the cluster head of any clusters, which in turn then forwards to those SCBSs in a cluster to which the scheduled UEs are communicating with. Note that we consider one cluster head per cluster whose function is to transmit information to UEs from the baseband unit of the corresponding cluster in the DL and receive information from UEs and transmit to the baseband unit in the UL over the fronthaul on CPRI interface. No additional processing is considered at the cluster head. The cluster head could be any FCBSs within a cluster of FCBSs, and any PCBS within a cluster of PCBSs. For the MCBS, there are separate schedulers for scheduling C-plane traffic. The number of schedulers required at the MCBS needs to be investigated. One way to address could be to consider one scheduler per category of UEs, i.e. FU and MU. However, since the number of FUs far exceeds the number of other categories of UEs, more than one scheduler for all FUs, e.g. one scheduler per cluster of FUs, could be required. However, this may result in additional and unnecessary costs and hence is left for getting investigated further.

G. Opportunistic time, frequency and transmit power control

Both FCBSs and PCBSs are switched to active mode if there exists traffic requests from at least one UE. Otherwise, they are considered to switch off and keep inactive until there is a new traffic request from a UE in order to reduce wastage of radio resources, e.g. time, frequency, and transmit power. Further, the number of active FUs per FCBS is considered more than one simultaneously. All FCBSs are enabled with the SON features to configure and optimize their transmit powers such that the

maximum allowable interference power (aggregate) at any FUs does not exceed the predefined value. In contrast to exploiting only frequency resources, opportunistic time, frequency and power control using SON for FCBSs can be considered to exploit in the proposed architecture in order to gain the most network capacity and spectral efficiency.

Hence, a centralized resource allocation algorithm that can exploit and schedule time, frequency, and transmit power resources for SCBSs, for a given set of constraints such as fronthaul, cluster size, degree of cooperation and centralization, resource scheduler, and operating frequency, to allocate to UEs optimally to address key issues, e.g. aggregate interference threshold, minimum data rate, traffic dynamics, overall traffic demand, and so on is indeed a crucial need for high capacity and spectral efficient NGMN, which can be considered to develop in the next up studies. A number of key features of the proposed architecture are as follow:

- It is independent of the dimension of the physical structure where FCBSs are considered to deploy, e.g. 2D flat and 3D in-building structures.
- It can address randomness in placement of FCBSs.

These can be achieved by the SON features of FCBSs and employing intelligent mechanisms at the central station for time and frequency resources allocation to FCBSs. This is because of the fact that resources are centrally allocated to distributed-physical-access nodes, i.e. FCBSs, from the central station, i.e. centralized baseband units, rather than from the access nodes. To address so, centralized baseband units take help CSI feedback from of a FU to adjust the power level of its sFCBS such that the aggregate interference level toward neighboring FCBSs is within a limited threshold value. Further, with cooperation within a cluster, neighboring FCBSs can be informed of tuning up or down their transmit power levels from the central station such that the interference constraint is satisfied. The SON features of FCBSs can help such self-optimization features to enable. Moreover, with an intelligent mechanism to allocate time and frequency resources orthogonally to FCBSs within a cluster, interference can be avoided, given that other constraints such as per UE data rate is satisfied.

Hence, irrespective of where and how randomly FCBSs are deployed, by sensing the surrounding environment with SON features of FCBSs and by employing intelligent mechanisms for time and frequency resources allocation to FCBSs within a cluster, interference can be managed by adjusting transmit powers, and allocating conflict-free subframes and RBs to FCBSs. Hence, the proposed architecture can be considered independent of randomness in placement of FCBSs and dimension of deployed FCBSs' physical structures.

8.7 Summary

In this chapter, numerous recommended further studies on this dissertation research are discussed in terms of research proposals and preliminary research progress, mainly for CUSA based device-centric networks for 5G. Particularly, alternative SCBS architectures, FC clustering and static resource reuse and allocation approach for FCs deployed in multi-floor buildings, SC transmit power management for the multi-user case, CoMP based SC transmit power modeling, coexistence of multiple bands at SCs to address non-uniform and asymmetric traffic, and finally the C-RAN enabled CUSA based device-centric networks are highlighted as part of further studies. Each recommended study is explained with reasonable details, and wherever necessary, relevant illustrations, analytical models, and performance evaluation results from the preliminary research studies are also given.

CHAPTER 9
CONCLUSION

This chapter summarizes the dissertation research as a whole, including its objectives, system architectures, investigation scenarios, major contributions, and further research directions.

9.1 Research overview

The dissertation entitled “analysis of high capacity mobile network with 3D in-building dense small cell” is addressed as part of the Ph.D. degree requirements. Key system architectural investigation scenarios of the dissertation are twofold for densely deployed SCBSs in 3D multi-floor buildings as follows:

- Conventional cell-centric control mobile network architecture with coupled C-/U-plane and decentralized RAN.
- New device-centric control mobile network architecture with decoupled C-/U-plane and centralized RAN.

Major objectives of the dissertation comprises of the followings. An extensive survey on enabling technologies of NGMN is carried out first. For cell-centric control networks, an ORRA to SCBSs deployed in 3D multi-floor buildings distributed over MC coverage is investigated. Further, a tractable analytical model is developed for interference characterization and minimum distance enforcement between SCBSs deployed densely in a 3D multi-floor building to reuse and allocate spectrum resources non-orthogonally (i.e., NORRA) in SCBSs for a number of optimization constraints such as link level interference, spectral efficiency, and capacity. The minimum distance enforced between SCBSs gives an upper limit of SCBS densification. A novel

clustering approach and a number of resource reuse strategies for dense SC networks deployed in 3D in-building scenario are proposed. For device-centric networks, a novel multi-band enabled SC and UE architecture for the UL/DL and the C-/U-plane splitting, a number of SCBS architectures for performance comparison between the C-/U-plane coupled and split architectures are proposed and evaluated. Finally, a centralized 3D radio resource allocation and scheduling approach for the C-/U-plane split architecture is proposed and evaluated.

Major system level scopes of investigation to carry out the objectives of the dissertation are limited to the followings. For system model, a square-grid based FC coverage area where each FCL consists of a number of 2D floors, and each floor consists of a number of square-grid apartments are considered. Each apartment has one FCBS placed in the center of the apartment and assumed static. A fixed free space around its building of a FCL and some free spaces between two neighboring FCLs are assumed. A UE per FCBS is considered. FCBSs are dropped as a set of groups of them within MC coverage. A single MC of a corner excited 3-sectored MC site and a number of SCs, including outdoor PCs and indoor FCs are considered. A certain percentage of MUs are assumed within FCLs. All indoor MUs are served by the MC. In addition, a certain percentage of outdoor MUs are offloaded to nearby PCs. ABS based eICIC techniques are considered to manage interference between MC-plus-PC and FC tiers both for NORRA and ORRA schemes. Proportional fair scheduler is considered for resource allocation to UEs. For modeling path loss of indoor FCs, empirical models recommended for evaluation by the 3GPP are considered. The default simulation parameters and assumptions used for system level simulation are based on 3GPP recommendations for system level performance evaluation. The validity of any research result is primarily based on MATLAB® simulator based simulation and analytical results.

9.2 Research contributions and further studies

Major contributions of this dissertation research in terms of journal and conference articles, which are either published or under-review to date are given as follows:

- In (journal) article 1 based on Chapter 2, an extensive review has been carried out on the trends of existing as well as proposed potential enabling technologies that are expected to shape 5G mobile wireless networks. Based on the classification of the trends, we develop a 5G network architectural evolution framework that comprises three evolutionary directions, namely, (i) radio access network node and performance enabler, (ii) network control programming platform, and (iii) backhaul network platform and synchronization. In (i), we discuss node classification including low power nodes in emerging machine-type communications, and network capacity enablers, e.g., mmWave communications and massive multiple-input multiple-output. In (ii), both logically distributed cell/device-centric platforms, and logically centralized conventional/wireless software defined networking control programming approaches are discussed. In (iii), backhaul networks and network synchronization are discussed. A comparative analysis for each direction as well as future evolutionary directions and challenges toward 5G networks are discussed. This survey will be helpful for further research exploitations and network operators for a smooth evolution of their existing networks toward 5G networks.

- In (journal) article 2 based on Chapter 3, we address mainly an important issue of reusing frequency resource in FCs deployed in dense multi-floor buildings over a large urban MC coverage to enhance network capacity and spectral efficiency using ABS based eICIC technique. FC clustering and modeling an OPNA are however two major challenges to reuse frequency in FCs deployed in buildings using ABS based eICIC. We address these challenges by exploiting the high external wall penetration loss of any buildings and in-between distance of neighboring buildings and propose a FC clustering approach by considering

all FCs per building as a FCL to avoid additional computational complexity from clustering. We develop a FRSA for an arbitrary value of ABS for a multi-tier network which consists of in-building FCs and outdoor PCs in the coverage of an urban MC. We then propose a model for estimating an OPNA and derive an OPNA per FCL basis under two schemes, namely adaptive OPNA and non-adaptive OPNA, in order to vary the number of ABSs imposed on FCs within a building dynamically based on the presence of indoor MC users within a building to avoid cross-tier interference with FCs. An optimization algorithm for OPNA schemes is developed, and its implementation aspects are discussed. The impact of varying the number of ABSs and FCs per building on the throughput performance of FRSA is analyzed through an extensive system level simulation, and the capacity outperformance of the adaptive over the non-adaptive OPNA scheme is shown. A schematic of the scheduler implementation for FRSA is developed, and the capacity outperformance of FRSA over a number of existing works is evaluated. Finally, a number of technical and business perspectives of the proposed FRSA are discussed.

- In (journal) article 3 based on Chapter 4 we address mainly two important issues, namely characterizing co-channel interference and enforcing a minimum distance between FCBSs for reusing resources in FCBSs deployed in a 3D multi-floor building. Each floor is modelled as a group of square-grid apartments, with one FCBS per apartment. We propose a simple yet reasonable analytical model using planar-Wyner model for intra-floor interference and linear-Wyner model for inter-floor interference modeling in a 3D multi-floor building in order to derive a minimum distance between cFCBSs for optimization constraints, namely link level interference, spectral efficiency, and capacity. As opposed to ORRA where resources are reused once, using the proposed model, we develop two strategies for reusing resources more than once, i.e. NORRA, within a multi-floor building. An algorithm of the proposed model is developed by including an application of the model to an ultra-dense deployment of multi-floor buildings. With an extensive numerical analysis and system level simulation, we demonstrate the capacity outperformance of

NORRA over ORRA by manifold. Further, with a fairly accurate yet realistic estimation, we show that the expected spectral efficiency of 5G networks can be achieved by applying the proposed model to an ultra-dense deployment of FCBSs.

- In (journal) article 4 based on Chapter 5, a multi-band enabled FCBS and UE architecture is proposed in a multi-tier network that consists of SCs, including FCs and PCs deployed over the coverage of a MC for splitting the UL/DL as well as the C-/U-plane for 5G mobile networks. Since splitting is performed at the same FCBS, we define this architecture as SBSA. For multiple bands, we consider co-channel microwave and different frequency 60 GHz mmWave bands for FCBSs and UEs with respect to the microwave band used by their over-laid MCBS. All FCs are assumed to be deployed in a 3D multi-storage building. For co-channel microwave band, cross-tier co-channel interference of FCs with MC is avoided using ABS based eICIC techniques. The co-existence of co-channel microwave and different frequency mmWave bands for SBSA on the same FCBS and UE is first studied to show their performance disparities in terms of system capacity and spectral efficiency in order to provide incentives for employing multiple bands at the same FCBS and UE and identify a suitable band for routing decoupled the UL/DL or the C-/U-plane traffic. We then present a number of disruptive architectural design alternatives of multi-band enabled SBSA for 5G mobile networks for the UL/DL and the C-/U-plane splitting, including a disruptive and complete splitting of the UL/DL and the C-/U-plane as well as a combined UL/DL and C-/U-plane splitting, by exploiting dual connectivity on co-channel microwave and different frequency mmWave bands. The outperformances of SBSA in terms of system level capacity, average spectral efficiency, energy efficiency, and C-plane overhead traffic capacity in comparison with DBSA are shown. Finally, a number of technical and business perspectives as well as key research issues of SBSA are discussed.

- In (conference) article 5 based on Chapter 6, we present numerous SCBS, i.e. FCBS, architectures based on the number of transceivers (e.g., single or dual transceiver) and operating frequency bands (e.g., microwave and mmWave bands) existing in a FCBS for serving the C-/U-plane traffic in indoor environments under both traditional CUCA as well as prospective CUSA. With a system level simulation of a multi-tier network, we evaluate the performances of these FCBS architectures in terms of C-plane, U-plane, and an aggregate C-/U-plane traffic capacities. The simulation results show that because of serving only U-plane traffic by a FCBS in CUSA, CUSA outperforms CUCA for a single transceiver based FCBS in terms of U-plane traffic capacity irrespective of operating frequency. However, the presence of dual bands at a dual transceiver based FCBS results in higher aggregate C-/U-plane traffic capacity than that of a single transceiver based FCBS. Finally, we discuss a number of strengths and weaknesses, viability challenges, and open issues of these FCBS architectures.

- In (conference) article 6 based on Chapter 7, radio resource allocation and scheduling plays a crucial role on achievable capacity, spectral efficiency and energy efficiency of cellular networks. Providing a high data rate service demand and network capacity, supporting a large traffic volume, and achieving a high spectral and energy efficiencies of 5G cellular, necessitate the development of an effective radio resource allocation and scheduling strategy for the major 3D radio resources, namely time, frequency, and transmit power due to their limited availability. So far, we exploit frequency and time resource allocation and scheduling. Since the transmit powers of SCBSs have a significant impact on the overall network interference phenomenon and energy efficiency, we propose a centralized allocation and scheduling strategy for 3D radio resources (namely, time, frequency, and power) for a multi-tier C-/U-plane split architecture by considering schedulers of all BSs located at a central station. We consider a multi-tier network comprises of a MCBS and a number of outdoor PCBSs as well as indoor FCBSs deployed within a multi-storage building. In contrast to the conventional ABS, we consider a FBS based eICIC

to split completely the C-/U-plane such that C-plane can be served only by the MCBS and U-plane by each UE's respective BS. The system bandwidth is reused in FCBSs, and frequency resources are allocated orthogonally per tier basis. We propose a simple FCBS power control mechanism by modeling a FCBS's on-state and off-state power as on and off traffic source model, and derive an optimal value of AAF of any FCBSs per FBS pattern period to trade-off its serving capacity and transmit power saving. With a system level simulation it is shown that the capacity of a FCBS increases whereas its power saving decreases linearly with an increase in its AAF because of serving increased traffic, and an optimal AAF of 0.5 for the capacity scaling factor $\kappa = 1$ and greater than 0.5 for $\kappa < 1$ is found.

- In (conference) article 7 based on Chapters 5 and 8, an analysis of the coexistence of multiple bands at SCBS for non-uniform and asymmetric traffic are carried out. For the co-channel microwave band, the cross-tier co-channel interference between FCBSs and the MCBS is avoided using ABS based eICIC techniques. An extensive system level simulation is carried out, and outperformances of millimeter-wave over co-channel microwave bands in multi-band enabled FCBS architecture are shown in terms of system capacity and spectral efficiency. We analyze the applicability of multi-band enabled FCBS architecture to address non-uniform traffic and asymmetric traffic from splitting the UL/DL as well as the C-/U-plane at a high data rate to introduce BS idle mode capability by exploiting dual connectivity feature in 5G networks. Finally, outperformances of multi-band enabled FCBS architecture over the single band enabled FCBS architecture proposed in existing literatures in terms of energy efficiency, system capacity, and spectral efficiency are shown.

- In (conference) article 8 based on Chapters 4 and 8, a FC clustering approach and static resource reuse and allocation in 3D multi-floor buildings are proposed. The FC clustering approach follows the same as in resource reuse strategy 2 in Chapter 4. However, to reuse resources per cluster, we describe a

number of static resource allocation options and propose an algorithm that takes adjacent channel interference into account when allocating resources in FCBSs within a cluster for the resource reuse strategy 1. We evaluate the algorithm for a single floor of a multi-floor building.

Finally, a number of potential further research directions on this dissertation are pointed out in Chapter 8 in terms of concepts and preliminary results, namely as follows:

- Alternative SCBS architectures
- FC clustering and static resource reuse and allocation in 3D multi-floor buildings
- SCBS transmit power management for multi-user case
- CoMP based SCBS transmit power modeling
- Analysis of the coexistence of multiple bands at SCBS for non-uniform and asymmetric traffic and scheduler implementation
- C-RAN enabled C-/U-plane split architecture based device-centric networks

REFERENCES

[1] Perez, D. L., Güvenç, I., Roche, G. D. L., Kountouris, M., Quek, T. Q. S., and Zhang, J. Enhanced inter-cell interference coordination challenges in heterogeneous networks. IEEE Wireless Communications 18, 3 (2011): 22-30.

[2] Tomovic, S., Pejanovic-Djurisic, M., and Radusinovic, I. SDN based mobile networks: concepts and benefits. Wireless Personal Communications 78, 3 (2014): 1629-1644.

[3] Boccardi, F., Heath Jr., R. W., Lozano, A., Marzetta, T. L., and Popovski, P. Five disruptive technology directions for 5G. IEEE Communications Magazine 52, 2 (2014): 74-80.

[4] Ishii, H., Kishiyama, Y., Takahashi, H., A novel architecture for LTE-B: c-plane/u-plane split and phantom cell concept. Proceedings of IEEE GC Wkshps'12, IEEE, (2012): 624-630.

[5] Jagadeesan, S., Riihijarvi, J., and Petrova, M., Impact of three-dimensionality of femtocell deployments on aggregate interference estimation. Proceedings of IEEE PIMRC'15, IEEE, (2015): 737-742.

[6] Hwang, I., Song, B., and Soliman, S. S. A holistic view on hyper-dense heterogeneous and small cell networks. IEEE Communications Magazine 51, 6 (2013): 20-27.

[7] Mustafa, H. A. U., Imran, M. A., Shakir, M. Z., Imran, A., and Tafazolli, R. Separation framework: an enabler for cooperative and d2d communication for future 5G networks. IEEE Communications Surveys & Tutorials 18, 1 (2016): 419-445.

[8] Ge, X., Tu, S., Mao, G., Wang, C. X., and Han, T. 5G ultra-dense cellular networks. IEEE Wireless Communications 23, 1 (2016):72-79.

[9] Abdelrahim, M., Onireti, O., Imran, M. A., Imran, A., and Tafazolli, R.

Control-data separation architecture for cellular radio access networks: a survey and outlook. IEEE Communications Surveys & Tutorials 18, 1 (2016): 446-465.

[10] Chin, W. H., Fan, Z., and Haines, R. Emerging technologies and research challenges for 5G wireless networks. IEEE Wireless Communications 21, 2 (2014): 106-112.

[11] Hossain, E. and Hasan, M. 5G cellular: key enabling technologies and research challenges. IEEE Instrumentation & Measurement Magazine 18, 3 (2015): 11-21.

[12] Cheng, H., Leng, X., Tang, Y., and Liu, Y., Experimental study on UE-oriented frequency reuse for indoor DAS networks. Proceedings of IEEE PIMRC'15, IEEE (2015): 1100-1104.

[13] Liu, Z., Sørensen, T., Wigard, J., and Mogensen, P., DAS, uncoordinated femto and joint scheduling systems for in-building wireless solutions. Proceedings of IEEE VTC'11, IEEE, (2011): 1-5.

[14] Alade, T., Zhu, H., and Osman, H., Spectral efficiency analysis of distributed antenna system for in-building wireless communication. Proceedings of IEEE VTC'11, IEEE, (2011): 1-5.

[15] Alade, T., Zhu, H., and Wang, J. Uplink spectral efficiency analysis of in-building distributed antenna systems. IEEE Transactions on Wireless Communications 14, 7 (2015): 4063-4074.

[16] Dan, H., Hong-jia, L., Xiao-dong, X., and Xiao-feng, T. Inter-femtocell interference coordination in 3D in-building scenario. The Journal of China Universities of Posts and Telecommunications 19, 2 (2012): 36-42.

[17] Li, W., Zheng, W., Xiangming, W., and Su, T., Dynamic clustering based sub-band allocation in dense femtocell environments. Proceedings of IEEE VTC'12, IEEE, (2012): 1-5.

[18] Liu, J., Wu, J., Chen, J., Wang, P., and Zhang, J., Radio resource allocation in

buildings with dense femtocell deployment. Proceedings of ICCCN'12, (2012):1-5.

[19] Chen, J., Wang, P., and Zhang, J. Adaptive soft frequency reuse scheme for in-building dense femtocell networks. Proceedings of IEEE ICCC'12, IEEE, (2012): 530-534.

[20] Wu, J. Y., Liu, J., Chen, J., and Chu, X., Cooperative interference mitigation for indoor dense femtocell networks. Proceedings of the 7th international ICST conference on CHINACOM, (2012): 93-98.

[21] Abdelnasser, A., Hossain, E., and Kim, D. I. Clustering and resource allocation for dense femtocells in a two-tier cellular OFDM network. IEEE Transactions on Wireless Communications 13, 3 (2014): 1628-1641.

[22] Cho, S. and Choi, W. Coverage and load balancing in heterogeneous cellular networks with minimum cell separation. IEEE Transactions on Mobile Computing 13, 9 (2014): 1955-1966.

[23] Cho, S. and Choi, W. Energy-efficient repulsive cell planning for heterogeneous cellular networks. IEEE Journal on Selected Areas in Communications 31, 5 (2013): 870-882.

[24] Capone, A., Fonseca dos Santos, A., Filippini, I., and Gloss, B., Looking beyond green cellular networks. Proceedings of the 9th Annual Conference on WONS, (2012): 127-130.

[25] Xu, X., He, G., Zhang, S., Chen, Y. and Xu, S. On functionality separation for green mobile networks: concept study over LTE. IEEE Communications Magazine 51, 5 (2013): 82-90.

[26] Savic, Z. 2011. LTE Design and Deployment Strategies available from: http://www.cisco.com/web/ME/expo2011/saudiarabia/pdfs/LTE_Design_and_Deployment_Strategies Zeljko_Savic.pdf, 2011.

[27] Dunlop, J., Girma, D., and Irvine, J. Digital mobile communications and the TETRA system. John Wiley & Sons, NY, 1999.

[28] Boccardi, F., Andrews, J., Elshaer, H., Dohler, M., Parkvall, S., Popovski, P., and Singh, S., Why to decouple the uplink and downlink in cellular networks and how to do it. Unpublished Manuscript, https://arxiv.org/ftp/arxiv/papers/1503/1503.06746.pdf, 2015.

[29] Nagata, S., Takeda, K. and Takahashi, H. LTE-advanced release 12 standardization technology overview. NTT DOCOMO Technical Journal 17, 2 (2015): 31-35.

[30] CISCO. Visual networking index. CISCO White Paper (2 2014).

[31] Andrews, J. G., Buzzi, S., Choi, W., Hanly, S. V., Lozano, A., Soong, A. C. K., and Zhang, J. C. What will 5G be?. IEEE Journal on Selected Areas in Communications 32, 6 (2014): 1065-1082.

[32] Osseiran, A., Boccardi, F., Braun, V., Kusume, K., Marsch, P., Maternia, M., Queseth, O., Schellmann, M., Schotten, H., Taoka, H., Tullberg, H., Uusitalo, M. A., Timus, B., and Fallgren, M. Scenarios for 5G mobile and wireless communications: the vision of the METIS project. IEEE Communications Magazine 52, 5 (2014): 26-35.

[33] Hossain, E., Rasti, M., Tabassum, H., and Abdelnasser, A. Evolution toward 5G multi-tier cellular wireless networks: an interference management perspective. IEEE Wireless Communications 21, 3 (2014): 118-127.

[34] Wang, C. X., Haider, F., Gao, X., You, X. H., Yang, Y., Yuan, D., Aggoune, H. M., Haas, H., Fletcher, S., and Hepsaydir, E. Cellular architecture and key technologies for 5G wireless communication networks. IEEE Communications Magazine 52, 2 (2014): 122-130.

[35] 3rd Generation Partnership Project; technical specification group radio access network; evolved universal terrestrial radio access (E-UTRA); FDD home eNode B (HeNB) radio frequency (RF) requirements analysis (release 12). 3GPP TR 36.921/12.0.0 (2014): 1-45.

[36] Golaup, A., Mustapha, M., and Patanapongpibul, L. B. Femtocell access

control strategy in UMTS and LTE. IEEE Communications Magazine 47, 9 (2009): 117-123.

[37] 3rd Generation Partnership Project; technical specification group radio access network; evolved universal terrestrial radio access (E-UTRA); further advancements for E-UTRA physical layer aspects (release 9). 3GPP TR 36.814/9.0.0 (2010): 1-104.

[38] Yunas, S. F., Valkama, M., and Niemelä, J. Spectral and energy efficiency of ultra-dense networks under different deployment strategies. IEEE Communications Magazine 53, 1 (2015): 90-100.

[39] Rost, P., Bernardos, C. J., Domenico, A. D., Girolamo, M. D., Lalam, M., Maeder, A., Sabella, D., Wübben, D. Cloud technologies for flexible 5G radio access networks. IEEE Communications Magazine 52, 5 (2014): 68-76.

[40] Jafari, A. H., L´opez-P´erez, D., Ding M., and Zhang, J., Study on scheduling techniques for ultra small cell networks. Proceedings of IEEE VTC'15, IEEE, (2015): 1-6.

[41] Thurfjell, M., Ericsson, M., and Bruin, P. D., Network densification impact on system capacity. Proceedings of IEEE VTC'15, IEEE, (2015): 1-5.

[42] Asp, A., Sydorov, Y., Keskikastari, M., Valkama, M., and Niemela, J., Impact of modern construction materials on radio signal propagation: practical measurements and network planning aspects. Proceedings of IEEE VTC'14, IEEE, (2014): 1-7.

[43] Bhushan, N., Li, J., Malladi, D., Gilmore, R., Brenner, D., Damnjanovic, A., Sukhavasi, R. T., Patel, C., and Geirhofer, S. Network densification: the dominant theme for wireless evolution into 5G. IEEE Communications Magazine 52, 2 (2014): 82-89.

[44] Jungnickel, V., Manolakis, K., Zirwas, W., Panzner, B., Braun, V., Lossow, M., Sternad, M., Apelfröjd, R., and Svensson, T. The role of small cells, coordinated multipoint, and massive MIMO in 5G. IEEE Communications Magazine 52, 5 (2014): 44-51.

[45] Soret, B., Pedersen, K. I., Jørgensen, N. T. K., and Fernández-López, V. Interference coordination for dense wireless networks. IEEE Communications Magazine 53, 1 (2015): 102-109.

[46] Xu, J., Wang, J., Zhu, Y., Yang, Y., Zheng, X., Wang, S., Liu, L., Horneman, K., and Teng, Y. Cooperative distributed optimization for the hyper-dense small cell deployment. IEEE Communications Magazine 52, 5 (2014): 61-67.

[47] Hu, R. Q. and Qian, Y. An energy efficient and spectrum efficient wireless heterogeneous network framework for 5G systems. IEEE Communications Magazine 52, 5 (2014): 94-101.

[48] Letourneux, F., Corre, Y., Suteau, E., and Lostanlen, Y. 3D coverage analysis of LTE urban heterogeneous networks with dense femtocell deployments. EURASIP Journal on Wireless Communications and Networking 2012, 319 (2012):1-14.

[49] Condoluci, M., Dohler, M., Araniti, G., Molinaro, A., and Zheng, K. Toward 5G dense HetNets: architectural advances for effective machine-type communications over femtocells. IEEE Communications Magazine 53, 1 (2015): 134-141.

[50] Performance of eICIC with control channel coverage limitation. 3GPP TSG RAN WG1 Meeting#61, R1-103264 (2010): 1-8.

[51] Sawahashi, M., Kishiyama, Y., Morimoto, A., Nishikawa, D., and Ta, M. Coordinated multipoint transmission/reception techniques for LTE-advanced. IEEE Wireless Communications 17, 3 (2010): 26-34.

[52] Kreutz, D., Ramos, F. M. V., Verı´ssimo, P. E., Rothenberg, C. E., Azodolmolky, S., and Uhlig, S. Software-defined networking: a comprehensive survey. Proceedings of the IEEE 103, 1 (2015): 14-76.

[53] Koponen, T., Casado, M., Gude, N., Stribling, J., Poutievski, L., Zhu, M., Ramanathan, R., Iwata, Y., Inoue, H., Hama, T., and Shenker, S., Onix: a distributed control platform for large-scale production

networks. Proceedings of the 9th USENIX conference on OSDI'10, USENIX Association, (2010): 1-6.

[54] Evolved universal terrestrial radio access (E-UTRA) and evolved universal terrestrial radio access network (EUTRAN); overall description. 3GPP TS 36.300/10.7.0 (2012): 1-204.

[55] Andrews, J. The seven ways HetNets are a paradigm shift. IEEE Communications Magazine 51, 3 (2013): 136-144.

[56] China Mobile. C-RAN: the road towards green RAN. China Mobile Research Institute White Paper (9 2013).

[57] Ericsson. It all comes back to backhaul. Ericsson White Paper (8 2014).

[58] Ericsson. Non-line-of-sight microwave backhaul for small cells. Ericsson Review (2 2013).

[59] Ericsson. Heterogeneous networks. Ericsson White Paper (9 2014).

[60] Ge, X., Cheng, H., Guizani, M., and Han, T. 5G wireless backhaul networks: challenges and research advances. IEEE Network 28, 6 (2014): 6-11.

[61] Dehos, C., González, J. L., Domenico, A. D., Kténas, D., and Dussopt, L. Millimeter-wave access and backhauling: the solution to the exponential data traffic increase in 5G mobile communications systems?. IEEE Communications Magazine 52, 9 (2014): 88-95.

[62] Benedetto, V., Zaffaroni, M., rui, D., and zhichao, Q. Huawei e-band rtn380-field trial report. Huawei White Paper (10 2013).

[63] Hashemi, H. The indoor radio propagation channel. Proceedings of the IEEE 81, 7 (1993): 943-968.

[64] Tan, S. Y., Tan, M. Y., and Tan, H. S. Multipath delay measurements and modeling for interfloor wireless communications. IEEE Transactions on Vehicular Technology 49, 4 (2000): 1334-1341.

[65] Austin, A. C. M., Neve, M. J., Rowe, G. B., and Pirkl, R. J. Modeling the effects of nearby buildings on inter-floor radio-wave propagation. IEEE Transactions on Antennas and Propagation 57, 7 (2009): 2155-2161.

[66] Jo, H., Mun, C., Moon, J., and Yook, J.-G. Self-optimized coverage coordination in femtocell networks. IEEE Transactions on Wireless Communications 9, 10 (2010): 2977-2982.

[67] Brown, T. Cellular performance bounds via shotgun cellular systems. IEEE Journal on Selected Areas in Communications 18, 11 (2000): 2443-2455.

[68] Baccelli, F., Klein, M., Lebourges, M., and Zuyev, S. Stochastic geometry and architecture of communication networks. Telecommunication Systems 7, 1 (1997): 209-227.

[69] Haenggi, M., Andrews, J., Baccelli, F., Dousse, O., and Franceschetti, M. Stochastic geometry and random graphs for the analysis and design of wireless networks. IEEE Journal on Selected Areas in Communications 27, 7 (2009): 1029-1046.

[70] Andrews, J. G. Baccelli, F., and Ganti, R. K. A tractable approach to coverage and rate in cellular networks. IEEE Transactions on Communications 59, 11 (2011): 3122-3134.

[71] Dhillon, H. S., Ganti, R. K., Baccelli, F., and Andrews, J. G. Modeling and analysis of K-tier downlink heterogeneous cellular networks. IEEE Journal on Selected Areas in Communications 30, 3 (2012): 550-560.

[72] Kim, Y., Lee, S., and Hong, D. Performance analysis of two-tier femtocell networks with outage constraints. IEEE Transactions on Wireless Communications 9, 9 (2010): 2695-2700.

[73] Yin, C., Gao, L., Liu, T., and Cui, S. Transmission capacities for overlaid wireless ad hoc networks with outage constraints. Proceedings of IEEE ICC'09, IEEE, (2009): 1-5.

[74] Mukherjee, S. Distribution of downlink SINR in heterogeneous cellular networks. IEEE Journal on Selected Areas in Communications 30, 3 (2012): 575-585.

[75] Mukherjee, S., UE coverage in LTE macro network with mixed CSG and open

access femto overlay. Proceedings of IEEE ICC'11, IEEE, (2011): 1-6.

[76] Mukherjee, S. Downlink SINR distribution in a heterogeneous cellular wireless network with biased cell association. Proceedings of IEEE ICC'12, IEEE, (2012): 6780-6786.

[77] Cheung, W. C., Quek, T. Q. S., Kountouris, M. Throughput optimization, spectrum allocation, and access control in two-tier femtocell networks. IEEE Journal on Selected Areas in Communications 30, 3 (2012): 561-574.

[78] Zhuang, W. and Ismail, M. Cooperation in wireless communication networks. IEEE Wireless Communications 19, 2 (2012): 10-20.

[79] Meulen, E. C. V. D. Three-terminal communication channels. Advanced Applied Probability 3, 1 (1971): 120-154.

[80] Cover, T. M. and Gamal, A. E. Capacity theorems for the relay channel. IEEE Transactions on Information Theory 25, 5 (1979): 572-584.

[81] Li, Q., Hu, R. Q., Qian, Y., and Wu, G. Cooperative communications for wireless networks: techniques and applications in LTE-Advanced systems. IEEE Wireless Communications 19, 2 (2012): 22-29.

[82] Technical report 3rd Generation Partnership Project; technical specification group radio access network; coordinated multi-point operation for LTE physical layer aspects (release 11). 3GPP TR 36.819/11.2.0 (2013): 1-70.

[83] Sun, S., Gao, Q., Peng, Y., Wang, Y., and Song, L. Interference management through CoMP in 3GPP LTE-advanced networks. IEEE Wireless Communications 20, 1 (2013): 59-66.

[84] Pérez, D. L., Ding, M., Claussen, H., and Jafari, A. H. Towards 1 Gbps/UE in cellular systems: understanding ultra-dense small cell deployments. IEEE Communications Surveys & Tutorials 17, 4 (2015): 2078-2101.

[85] Elsherif, A. R., Chen, W. P., Ito, A., and Ding, Z. Adaptive resource allocation

for interference management in small cell networks. IEEE Transactions on Communications 63, 6 (2015): 2107-2125.

[86] Davaslioglu, K., Coskun, C. C., and Ayanoglu, E. Energy-efficient resource allocation for fractional frequency reuse in heterogeneous networks. IEEE Transactions on Wireless Communications 14, 10 (2015): 5484-5497.

[87] Ullah, R., Fisal, N., Safdar, H., Khalid, Z., and Maqbool, W., Fractional frequency reuse for irregular geometry based heterogeneous cellular networks. Proceedings of the 5th National Symposium on Information Technology: Towards Smart World, (2015): 1-6.

[88] Simulation assumptions and parameters for FDD HeNB RF requirements. 3GPP TSG RAN WG4 (Radio) Meeting #51 R4-092042 (2009): 1-8.

[89] Ellenbeck, J., Schmidt, J., Korger, U., and Hartmann, C. A concept for efficient system-level simulations of OFDMA systems with proportional fair fast scheduling. Proceedings of IEEE Globecom Workshops, IEEE, (2009): 1-6.

[90] Saha, R. K. and Saengudomlert, P., Novel resource scheduling for spectral efficiency in LTE-advanced systems with macrocells and femtocells. Proceedings of ECTI-CON'11, (2011): 340-343.

[91] Wang, Y., Pedersen, K. I., Sørensen, T. B., and Mogensen, P. E. Carrier load balancing and packet scheduling for multi-carrier systems. IEEE Transactions on Wireless Communications 9, 5 (2010): 1780-1789.

[92] Bang, H. J., Ekman, T., and Gesbert, D. Channel predictive proportional fair scheduling. IEEE Transactions on Wireless Communications 7, 2 (2008): 482-487.

[93] Radio frequency (RF) system scenarios. ETSI TR 136 942/8.2.0 or 3GPP TR 36.942/8.2.0 (2009): 1-87.

[94] Saquib, N., Hossain, E., and Kim, D. Frequency reuse for interference

management in LTE-advanced hetnets. IEEE Wireless Communications 20, 2 (2013): 113-122.

[95] Saha, R. K., Saengudomlert, P., and Aswakul, C. Evolution toward 5G mobile networks - a survey on enabling technologies. Engineering Journal 20, 1 (2016): 87-119.

[96] Wang, X., Zheng, W., Lu, Z., Wen, X., and Li, W. Dense femtocell networks power self-optimization: an exact potential game approach. International Journal of Communication Systems 29, (2016): 16-32.

[97] Tahalani, M., Sathya, V., Ramamurthy, A., Suhas, U. S., Giluka, M. K., and Tamma, B. R., Optimal placement of femto base stations in enterprise femtocell networks. Proceedings of IEEE ANTS'14, IEEE, (2014): 1-6.

[98] Liu, J., Kou, T., Chen, Q., and Sherali, H. D. Femtocell base station deployment in commercial buildings: a global optimization approach. IEEE Journal on Selected Areas in Communications 30, 3 (2012): 652-663.

[99] Khan, M. F. and Wang, B. Effective placement of femtocell base stations in commercial buildings. Proceedings of ICUFN'14, (2014): 176-180.

[100] Wang, S., Guo, W., and O'Farrell, T., Optimizing femtocell placement in an interference limited network: theory and simulation. Proceedings of IEEE VTC'12, IEEE, (2012): 1-6.

[101] Guo, W. and Wang, S. Interference-aware self-deploying femto-cell. IEEE Wireless Communications Letters 1, 6 (2012): 609-612.

[102] Langar, R., Secci, S., Boutaba, R., and Pujolle, G. An operations research game approach for resource and power allocation in cooperative femtocell networks. IEEE Transactions on Mobile Computing 14, 4 (2015): 675-687.

[103] Kao, S. J. and Wang, H. L. Dynamic orthogonal frequency division multiple

access resource management for downlink interference avoidance in two-tier networks. International Journal of Communication Systems 28, (2015): 281-295.

[104] Bouras, C., Diles, G., Kokkinos, V., and Papazois, A. Transmission optimizing on dense femtocell deployments in 5G. International Journal of Communication Systems (2015).

[105] Wang, X., Han, Q., Guan, X., Ma, K. Price-based interference management in dense femtocell systems. International Journal of Communication Systems 28, (2015): 19-37.

[106] Simulation assumptions and parameters for FDD HeNB RF requirements. 3GPP TSG RAN WG4 (Radio) Meeting #50bis, R4-091422 (2009): 1-7.

[107] Tukmanov, A., Ding, Z., Boussakta, S., and Jamalipour, A. On the impact of network geometric models on multicell cooperative communication systems. IEEE Wireless Communications 20, 1 (2013): 75-81.

[108] Molkdar, D. Review on radio propagation into and within buildings. IEE Proceedings H – Microwaves, Antennas and Propagation 138, 1 (1991): 61-73.

[109] Vu, T. K., Kwon, S., and Oh, S. Cooperative interference mitigation algorithm in heterogeneous network. IEICE Transactions on Communications E98-B, 11 (2015): 2238-2247.

[110] Kim, W., Kaleem, Z., and Chang, K. H. Power headroom report-based uplink power control in 3GPP LTE-A hetnet. EURASIP Journal on Wireless Communications and Networking 233, (2015): 1-13.

[111] Kaleem, Z., Hui, B., and Chang, K. H. QoS priority-based dynamic frequency band allocation algorithm for load balancing and interference avoidance in 3GPP LTE HetNet. EURASIP Journal on Wireless Communications and Networking 185, (2014): 1-18.

[112] Kim, B., Malik, S., Moon, S., You, C., Liu, H., Kim, J. H., and Hwang, I.

Performance analysis of coordinated multi-point with scheduling and precoding schemes in the LTE-A system. Wireless Personal Communications 77, 4 (2014): 2615-2630.

[113] Wang, Y., Lu, W. J., and Zhu, H. B. Propagation characteristics of the LTE indoor radio channel with persons at 2.6 GHz. IEEE Antennas and Wireless Propagation Letters 12, (2013): 991-994.

[114] Wunderlich, S., Welpot, M., and Gaspard, I. Indoor radio channel modeling and mitigation of fading effects using linear and circular polarized antennas in combination for smart home system at 868 MHz. Advances in Radio Science 12, (2014): 53-59.

[115] Ricknäs, M., Operators ready to open up femtocells. Available from: http://www.pcworld.com/article/200164/operators_ready_to_open_up_femtocells_says_ubiquisys.html, 2010.

[116] Liang, H., Wang, B., Liu, W., and Xu, H. A Novel transmitter placement scheme based on hierarchical simplex search for indoor wireless coverage optimization. IEEE Transactions on Antennas Propagation 60, 8 (2012): 3921-3932.

[117] Time delay between physical channels of different scrambling codes. 3GPP TSG-RAN WG1 (Radio) Meeting #7, TSGR1#7(99)b53 (1999): 1-10.

[118] Hekmat, R. Ad-hoc networks: fundamental properties and network topologies. Springer, The Netherlands, 2006.

[119] Andersen, J. B., Rappaport T. S., and Yoshida, S. Propagation measurements and models for wireless communications channels. IEEE Communications Magazine 33, 1 (1995): 42-49.

[120] Honcharenko, W., Bertoni, H. L., and Dailing, J. Mechanisms governing propagation between floors in buildings. IEEE Transactions on Antennas Propagation 41, 6 (1993): 787-790.

[121] Seidel, S. Y. and Rappaport, T. S. 914 MHz path loss prediction models for

indoor wireless communications in multifloored buildings. IEEE Transactions on Antennas Propagation 40, 2 (1992): 207-217.

[122] Saha, R. K. Modified proportional fair scheduling for resource reuse and interference coordination in two-tier LTE-advanced systems. International Journal of Digital Information and Wireless Communications 3, 2 (2013): 9-28.

[123] Saivichit, C., Graph theory and combinatorial optimization. Lecture notes, Department of Electrical Engineering, Chulalongkorn University, 2015.

[124] Brueninghaus, K., Astley, D., Salzer, T., Visuri, S., Alexiou, A., Karger, S., and Seraji, G-A., Link performance models for system level simulations of broadband radio access systems. Proceedings of PIMRC'05, IEEE, (2005): 2306-2311.

[125] Yaun, G., Zhang, X., Wang, W., and Yang, Y. Carrier aggregation for LTE-advanced mobile communication systems. IEEE Communications Magazine 48, 2 (2010): 88-93.

[126] Ericsson. Ericsson mobility report. Ericsson (11 2012).

[127] Falaki, H., Lymberopoulos, D., Maharajan, R., Kandula, S., and Estrin, D., A first look at traffic on smartphones. Proceedings of IMC'10, ACM, (2010): 281-287.

[128] NSN. Nokia solutions and networks TD-LTE frame configuration primer. NSN White Paper (11 2013).

[129] Chen, S. and Zhao, J. The requirements, challenges, and technologies for 5G of terrestrial mobile telecommunication. IEEE Communications Magazine 52, 5 (2014): 36-43.

[130] Feng, Z., Feng, Z., Li, W., and Chen, W., Downlink and uplink splitting user association in two-tier heterogeneous cellular networks. Proceedings of IEEE Globecom'14, IEEE, (2014): 4659-4664.

[131] Elshaer, H., Boccardi, F., Dohler, M., and Irmer, R., Downlink and uplink

decoupling: a disruptive architectural design for 5G networks. Proceedings of IEEE Globecom'14, IEEE, (2014): 1798-1803.

[132] Sakaguchi, K., Sampei, S., Shimodaira, H., Rezagah, R., Tran, G. K., and Araki, K., Cloud cooperated heterogeneous cellular networks. Proceedings of ISPACS'13, (2013): 787-791.

[133] Geng, S., Kivinen, J., Zhao, X., and Vainikainen, P. Millimeter-wave propagation channel characterization for short-range wireless communications. IEEE Transactions on Vehicular Technology 58, 1 (2009): 3-13.

[134] Yilmaz, T., Fadel, E., and Akan, O. B., Employing 60 GHz ISM band for 5G wireless communications. Proceedings of IEEE BlackSeaCom'14, IEEE, (2014): 77-82.

[135] Daniels, R. C. and Heath Jr., R. W. 60 GHz wireless communications: emerging requirements and design recommendations. IEEE Vehicular Technology Magazine 2, 3 (2007): 41-50.

[136] GTI. 4G Multi-mode multi-band device requirements and architectures. GTI White Paper (9 2012).

[137] Rysavy Research. LTE and 5G innovation: igniting mobile broadband. 4G Americas White Paper (8 2015).

[138] Smiljkovikj, K., Elshaer, H., Popovski, P., Boccardi, F., Dohler, M., Gavrilovska, L., and Irmer, R., Capacity analysis of decoupled downlink and uplink access in 5G heterogeneous systems. Unpublished Manuscript, http://arxiv.org/abs/1410.7270, 2014.

[139] Zhang, H. Separation of data and control planes. TNO innovation for life, 5Green Summer School - KTH (8 2014).

[140] Jungnickel, V., Jaeckel, S., Börner, K., Schlosser, M., and Thiele, L., Estimating the mobile backhaul traffic in distributed coordinated multi-point systems. Proceedings of IEEE WCNC'12, (2012): 3763-3768.

[141] Jungnickel, V., Manolakis, K., Jaeckel, S., Lossow, M., Farkas, P., Schlosser, M., and Braun, V., Backhaul requirements for inter-site cooperation in heterogeneous LTE-Advanced networks. Proceedings of IEEE ICC'13, IEEE, (2013): 905-910.

[142] Robson, J. Small cell backhaul requirements. NGMN White Paper (6 2012).

[143] Yang, L. L. and Park, M. Multi-band gigabit mesh networks: opportunities and challenges. International Journal on Advances in Networks and Services 2, 1 (2009): 88-99.

[144] 4G Americas. Wireless handset RF front-end optimization. 4G Americas Report (10 2014).

[145] Akyildiz, I. F., Gutierrez-Estevez, D. M., and Reyes, E. C. The evolution to 4G cellular systems: LTE-advanced. Physical Communication 3, (2010): 217-244.

[146] Cheng, H. T. and Zhuang, W. Joint power-frequency-time resource allocation in clustered wireless mesh networks. IEEE Network 22, 1 (2008): 45-51.

[147] Zhao, L., Cong, L., Liu, F., Yang, K., and Zhang, H. Joint time-frequency-power resource allocation for low-medium-altitude platforms-based WiMAX networks. IET Communications 5, 7 (2011): 967-974.

[148] Ngo, D. T., Khakurel, S., and Le-Ngoc, T. Joint subchannel assignment and power allocation for OFDMA femtocell networks. IEEE Transactions on Wireless Communications 13, 1 (2014): 342-355.

[149] Qian, M., Wang, Y., Zhou, Y., Tian, L., and J. Shi. A super base station based centralized network architecture for 5G mobile communication systems. Digital Communications and Networks 1, 1 (2015): 152-159.

[150] Lin, Y., Shao, L., Zho, Z., Wang, Q., and Sabhiki, R. K. Wireless network cloud: architecture and system requirements. IBM Journal of Research and Development 54, 1 (2010): 4:1-4:12.

[151] Segel, J. and Weldon, M. LightRadio. Alcatel-Lucent White Paper - Technical

Overview, 2011.

[152] Duan, X., Akhtar, A. M., and Wang, X. Software-defined networking-based resource management: data offloading with load balancing in 5G hetnet. EURASIP Journal on Wireless Communications and Networking 181, (2015):1-13.

[153] Zhang, F., Sun, S., Chen, N., and Huang, H., Radio resource management based on NFV and SDN in 4G and 5G hetnet. Proceedings of ICSON'15, LNICST 149, S. Sun and J. Li (Eds.), Springer, (2015): 165-172.

[154] Prasad, A., Maeder, A., and Ng, C., Energy efficient small cell activation mechanism for heterogeneous networks. Proceedings of IEEE GC Wkshps'13, IEEE, (2013): 754-759.

[155] Liu, C., Natarajan, B., and Xia, H. Small cell base station sleep strategies for energy efficiency. IEEE Transactions on Vehicular Technology 65, 3 (2016): 1652-1661.

[156] Lee, G. and Kim, H., Green small cell operation using belief propagation in wireless networks. Proceedings of IEEE GC Wkshps'14, IEEE, (2014): 1266-1271.

[157] Universal Mobile Telecommunications System (UMTS); Selection procedures for the choice of radio transmission technologies of the UMTS. ETSI, TR 101 112 UMTS 30.03/3.1.0 (1997-2011): 1-80.

[158] Chimeh, J. D., Hakkak, M., and Alavian, S. A., Internet traffic and capacity evaluation in UMTS downlink. Proceedings of FGCN'07, (2007): 547-552.

[159] Peng, M., Li, Y., Jiang, J., Li, J., and Wang, C. Heterogeneous cloud radio access networks: a new perspective for enhancing spectral and energy efficiencies. IEEE Wireless Communications 21, 6 (2014): 126-135.

[160] Peng, M., Li, Y., Zhao, Z., and Wang, C. System architecture and key technologies for 5G heterogeneous cloud radio access networks. IEEE Network 29, 2 (2015): 6-14.

[161] Peng, M., Wang, C., Lau, V., and Poor, H. V. Fronthaul-constrained cloud radio access networks: insights and challenges. IEEE Wireless Communications 22, 2 (2015): 152-160.

[162] Iwamura, M., Takahashi, H., and Nagata, S. Relay technology in LTE-Advanced. NTT DOCOMO Technical Journal 12, 2 (2010): 29-36.

[163] Wang, C. X., Hong, X., Ge, X., Cheng, X., Zhang, G., and Thompson, J. Cooperative MIMO channel models: a survey. IEEE Communications Magazine 48, 2 (2010): 80-87.

[164] Yilmaz, O. N. C., Li, Z., Valkealahti, K., Uusitalo, M. A., Moisio, M., Lundén, P., and Wijting, C., Smart mobility management for D2D communications in 5G networks. Proceedings of IEEE WCNCW'14, IEEE, (2014): 219-223.

[165] Doppler, K., Rinne, M., Wijting, C., Ribeiro, C. B., and Hugl, K. Device-to-device communication as an underlay to LTE-Advanced networks. IEEE Communications Magazine 47, 12 (2009): 42-49.

[166] Study on LTE device to device proximity services. 3GPP TSG RAN Meeting#58 RP-122009 (2012): 1-6.

[167] Technical specification group services and system aspects; feasibility study for proximity services (ProSe) (release 12). 3GPP TR 22.803/12.2.0 (2013): 1-45.

[168] Zakrzewska, A., Ruepp, S., and Berger, M. S., Towards converged 5G mobile networks-challenges and current trends. Proceedings of the 2014 ITU Kaleidoscope academic conference: living in a converged world-impossible without standards?, (2014): 39-45.

[169] Goncalves, V. and Dobbelaere, P., Business scenarios for machine-to-machine mobile applications. Proceedings of ICMB-GMR'10, (2010): 394-401.

[170] Shih, M. J., Pang, Y. C., Lin, G. Y., Wei, H. Y., and Vannithamby, R.,

Performance evaluation for energy-harvesting machine-type communication in LTE-A system. Proceedings of IEEE VTC'14, IEEE, (2014): 1-5.

[171] Han, C. L. I, S., Chen, Y., and Li, G., Trillions of nodes for 5G!?. Proceedings of IEEE/CIC ICCC'14, IEEE, (2014): 246-250.

[172] Taleb, T. and Kunz, A. Machine type communications in 3GPP networks: potential, challenges, and solutions. IEEE Communications Magazine 50, 3 (2012): 178-184.

[173] Wu, G., Talwar, S., Johnsson, K., Himayat, N., and Johnson, K. D. M2M: from mobile to embedded internet. IEEE Communications Magazine 49, 4 (2011): 36-43.

[174] Service requirements for machine-type communications (MTC), stage 1, release 12. 3GPP, TS 22.368/12.3.0 (2013).

[175] Astely, D., Dahlman, E., Fodor, G., Parkvall, S., and Sachs, J. LTE release 12 and beyond. IEEE Communications Magazine 51, 7 (2013): 154-60.

[176] Technical specification: machine-to-machine communications (M2M); functional architecture. ETSI TS 102 690/2.1.1 (2013): 1-332.

[177] Architecture enhancements to facilitate communications with packet data networks and applications. ETSI TS 123 682/11.4.0 (2013): 1-31.

[178] Osa, V., Herranz, C., Monserrat, J., and Gelabert, X. Implementing opportunistic spectrum access in LTE-advanced. EURASIP Journal on Wireless Communications and Networking 99, (2012): 1-17.

[179] Chen, Y. and Wang, W., Machine-to-machine communication in LTE-A. Proceedings of IEEE VTC'10, IEEE, (2010): 1-4.

[180] Jo, M., Maksymyuk, T., Batista, R. L., Maciel, T. F., Almeida, A. L. F. D., and Klymash, M. A survey of converging solutions for heterogeneous mobile networks. IEEE Wireless Communications 21, 6 (2014): 54-62.

[181] Castanheira, D. and Gameiro, A. Distributed antenna system capacity scaling. IEEE Wireless Communications 17, 3 (2010): 68-75.

[182] Zhang, X., Sundaresan, K., Khojastepour, M. A., Rangarajan, S., and Shin, K. G., NEMOx: scalable network MIMO for wireless networks. Proceedings of MobiCom'13, ACM, (2013): 453-464.

[183] Zong, Z., Feng, H., Yang, T., and Hu, B., Distributed framework of downlink CoMP MU-MIMO transmission with adaptive mode switch and power allocation. Proceedings of ICNC'14, (2014): 611-615.

[184] Larsson, E. G., Edfors, O., Tufvesson, F., and Marzetta, T. L. Massive MIMO for next generation wireless systems. IEEE Communications Magazine 52, 2 (2014): 186-195.

[185] Marzetta, T. L. Massive MIMO: an introduction. Bell Labs Technical Journal 20, (2015): 11-22.

[186] Qiao, D., Wu, Y., and Chen, Y., Massive MIMO architecture for 5G networks: co-located, or distributed?. Proceedings of ISWCS'14, (2014): 192-197.

[187] Marzetta, T. L. Noncooperative cellular wireless with unlimited numbers of base station antennas. IEEE Transactions on Wireless Communications 9, 11 (2010): 3590-3600.

[188] Rappaport, T. S., Sun, S., Mayzus, R., Zhao, H., Azar, Y., Wang, K., Wong, G. N., Schulz, J. K., Samimi, M., and Gutierrez, F. Millimeter wave mobile communications for 5G cellular: it will work!. IEEE Access 1, (2013): 335-349.

[189] Rappaport, T. S. Wireless communications: principles and practice. Prentice-Hall, Englewood Cliffs, NJ, 2002.

[190] Gutierrez, F., Agarwal, S., Parrish, K., and Rappaport, T. S. On-chip integrated antenna structures in CMOS for 60 GHz WPAN systems. IEEE Journal on Selected Areas in Communications 27, 8 (2009): 1367-1378.

[191] Rappaport, T. S., Ben-Dor, E., Murdock, J. N., and Qiao, Y., 38 GHz and 60

GHz angle-dependent propagation for cellular and peer-to-peer wireless communications. Proceedings of IEEE ICC'12, (2012): 4568-4573.

[192] Rappaport, T. S., Murdock, J. N., and Gutierrez, F. State of the art in 60 GHz integrated circuits & systems for wireless communications. Proceedings of the IEEE 99, 8 (2011): 1390-1436.

[193] Rusek, F., Persson, D., Lau, B. K., Larsson, E. G., Marzetta, T. L., Edfors, O., and Tufvesson, F. Scaling up MIMO: opportunities and challenges with very large arrays. IEEE Signal Processing Magazine 30, 1 (2013): 40-60.

[194] Qiao, J., Shen, X., Mark, J. W., Shen, Q., He, Y., and Lei, L. Enabling device-to-device communications in millimeter-wave 5G cellular networks. IEEE Communications Magazine 53, 1 (2015): 209-215.

[195] Zheng, K., Liu, F., Lei, L., Lin, C., and Jiang, Y. Stochastic performance analysis of a wireless finite-state Markov channel. IEEE Transactions on Wireless Communications 12, 2 (2013): 782-793.

[196] Pi, Z. and Khan, F. An introduction to millimeter-wave mobile broadband systems. IEEE Communications Magazine 49, 6 (2011): 101-107.

[197] FCC. Millimeter wave propagation: spectrum management implications. Office of Engineering and Technology (7 1997).

[198] Seidel, S. Y. and Arnold, H. W., Propagation measurements at 28 GHz to investigate the performance of local multipoint distribution service (LMDS). Proceedings of IEEE Globecom'95, IEEE, (1995): 754-757.

[199] Zhao, Q. and Li, J., Rain attenuation in millimeter wave ranges. Proceedings of the 7th international symposium on antennas, propagation & EM theory, (2006): 1-4.

[200] Roh, W., Seol, J. Y., Park, J., Lee, B., Lee, J., Kim, Y., Cho, J., Cheun, K., and Aryanfar, F. Millimeter-wave beamforming as an enabling technology for 5G cellular communications: theoretical feasibility

and prototype results. IEEE Communications Magazine 52, 2 (2014): 106-113.

[201] Li, Q., Niu, H., Wu, G., and Hu, R. Q., Anchor-booster based heterogeneous networks with mmWave capable booster cells. Proceedings of IEEE GC Wkshps'13, IEEE, (2013): 93-98.

[202] Taori, R. and Sridharan, A. Point-to-multipoint in-band mmWave backhaul for 5G networks. IEEE Communications Magazine 53, 1 (2015): 195-201.

[203] Paolini, M. Crucial economics for mobile data backhaul-an analysis of the total cost of ownership of point-to-point, point-to-multipoint, and fiber options. Senza Fili Consulting White Paper (2011).

[204] Webb, R. Macrocell mobile backhaul equipment and services market share and forecasts. Infonetics Research (2012).

[205] Innovation Observatory. Spectrum and technology issues for microwave backhaul in Europe. White Paper, Innovation Observatory Ltd. (2010).

[206] Schwartz, R. and Rice, M. Rethinking small cell backhaul: a business case analysis of cost-effective small cell backhaul network solutions. Wireless 20/20 White Paper (7 2012).

[207] Monturus, E., A Practical look at LTE backhaul capacity requirements. Available from: http://www. slideshare.net /allabout4g/apracticallookatltebackhaulrequir ementspdf, 2011.

[208] Pietraski, P. J., The bandwidth crunch: can wireless technology meet the skyrocketing demand for mobile data. Proceedings of IEEE LISAT'11, IEEE, (2011): 1-6.

[209] Kim, H. and Feamster, N. Improving network management with software defined networking. IEEE Communications Magazine 51, 2 (2013): 114-119.

[210] Qadir, J., Ahmed, N., and Ahad, N., Building programmable wireless

networks: an architectural survey. Unpublished Manuscript, http://arxiv.org/pdf/1310.0251.pdf, 2014.

[211] ON.LAB: ONS - SDN controller, Available from: http://onlab.us/tools.html

[212] Gude, N., Koponen, T., Pettit, J., Pfaff, B., Casado, M., McKeown, N., and Shenker, S. NOX: towards an operating system for networks. ACM SIGCOMM Computer Communication Review 38, 3 (2008): 105-110.

[213] Sherwood, R., Gibb, G., Yap, K. K., Appenzeller, G., Casado, M., McKeown, N., and Parulkar, G., FlowVisor: A network virtualization layer. Technical Report Openflow tr-2009-1, Stanford University, 2009.

[214] Yap, K. K., Sherwood, R., Kobayashi, M., Huang, T. Y., Chan, M., Handigol, N., McKeown, N., and Parulkar, G., Blueprint for introducing innovation into wireless mobile networks. Proceedings of VISA'10, ACM, (2010): 25-32.

[215] McKeown, N., Anderson, T., Balakrishnan, H., Parulkar, G., Peterson, L., Rexford, J., Shenker, S., and Turner, J. OpenFlow: enabling innovation in campus networks. ACM SIGCOMM Computer Communication Review 38, 2 (2008): 69-74.

[216] Costa-Requena, J., SDN integration in LTE mobile backhaul networks. Proceedings of ICOIN'14, (2014): 264-269.

[217] Jin, X., Li, L. E., Vanbever, L., and Rexford, J., SoftCell: scalable and flexible cellular core network architecture. Proceedings of CoNEXT'13, ACM, (2013): 163-174.

[218] Gudipati, A., Perry, D., Li, L. E., and Katti, S., SoftRAN: software defined radio access network. Proceedings of HotSDN'13, ACM, (2013): 25-30.

[219] Yap, K. K., Kobayashi, M., Underhill, D., Seetharaman, S., Kazemian, P., and McKeown, N., The Stanford OpenRoads deployment. Proceedings of WiNTECH'09, ACM, (2009): 59-66.

[220] Sama, M. R., Said, S. B. H., Guillouard, K., and Suciu, L., Enabling network programmability in LTE/EPC architecture using OpenFlow. Proceedings of the 12th international symposium on WiOpt'14, (2014): 389-396.

[221] Wen, H. Virtualization and software-defined infrastructure framework for wireless access networks. Master's Thesis, Department of Electrical and Computer Engineering, McGill University, 2014.

[222] Seidel, S. Y, Rappaport, T. S., Feuerstein, M. J., and Blackard, K. L., The impact of surrounding buildings on propagation for wireless in-building personal communications system design. Proceedings of IEEE VTC'92, (1992): 814-818.

[223] Tarng, J. H. and Perng, D. W. Modelling and measurement of UHF radio propagating through floors in a multifloored building. IEE Proceedings-Microwave, Antennas, and Propagation 144, 5 (1997): 359-363.

[224] Cheung, K. W., Sau, J. H. M., and Murch, R. D. A new empirical model for indoor propagation prediction. IEEE Transactions on Vehicular Technology 47, 3 (1998): 996-1001.

[225] Austin, A. C. M., Neve, M. J., and Rowe, G. B., Modelling inter-floor radio-wave propagation in office buildings. Proceedings of IEEE AP-S'08, IEEE, (2008): 1-4.

APPENDIX A
5G MOBILE NETWORK ARCHITECTURE

Appendix A includes relevant information, mainly additional RAN nodes, massive MIMO, mmWave communications, WSDN, CUSA, and in-building cellular mobile communications based on the existing research works with corresponding citations as part of literature review for the completeness and clarity in Chapter 2. This appendix is included for gaining additional information and insights, not necessarily prerequisites or parts of the main research works carried out in this dissertation.

A.1 Radio access network node and performance enabler

A.1.1 Radio access network node

In addition to the nodes explained in Chapter 2, a number of potential access nodes are discussed in this section. The relays are also low power nodes that relay signals from a MCBS to UEs and vice versa [1]. Relays are of two categories, namely, fixed relays and mobile relays. For fixed relaying, a relay node uses the wireless backhaul to connect to a MCBS. The link that exists between a UE and a relay node is called an access link, and the link that exists between a MCBS and a relay node is called a backhaul link. Relays can be classified based on a number of aspects, namely, spectrum usage, UE awareness, type, and degree of processing [1, 37, 162]. For example, based on the usage spectrum in access and backhaul links, relays are classified as inband relays and outband relays. When the relay operation is performed at the same frequency on the access link as that on the backhaul link, the relay is termed as inband relay; however, if performed at a different frequency, the relay is termed as outband relay. For mobile relaying, relays are usually of two types: moving network-relays and mobile user relays [163]. In moving network-relays, dedicated relay nodes are set up on moving vehicles such as trains and buses to exchange data between MCBSs and UEs

onboard in order to improve cell coverage in moving vehicles. In mobile user relays, distributed UEs can relay information in an ad-hoc fashion that can complement existing cellular networks. Given a sufficient level of infrastructures, theoretical studies [163] have proved that mobile user relays can improve the sum throughput of users. However, mobile user relays can be disadvantageous from such constraints as power consumption of UE batteries and complicated billing problems.

Device-to-device communications are expected to be deployed in 5G networks [164]. Device-to-device communications have been paid attention by research communities for years [165] and studied in 3GPP Releases 12 and 13 particularly on device-to-device discovery and communication [166]. Two scenarios are defined in 3GPP [167], namely, direct data path and locally routed data path. In the former scenario, devices exchange information without any involvement of network elements for the U-plane; however in the later scenario, devices involve controlling nodes for relaying data to exchange locally without routing through the core networks. Hence, other nodes can have control on signal transmissions and receptions with assistance from the network. Specifically, nodes in cell-edge areas where the communication link between a UE and a MCBS is typically weak but the link between two cell-edge UEs can be very good such that one of these two UEs can act as a transmitter for the other. A MCBS carries out all control signaling operations, e.g., synchronization.

Machine-type communications or machine-to-machine communications are one of the enabling technologies for 5G networks that will allow devices such as cars and health monitoring devices to connect to the Internet [168]. Consumer electronic devices can be networked, interconnected, and accessible or controllable remotely. That results in innovation shifting from products to services delivered by these devices [169]. In machine-type communications, a number of devices communicate to one another or to a central controller even without any human intervention [170]. The machine-type communication is generally characterized by a small packet size, a low mobility, a group based communication, a secure connection, and a transmission delay tolerant [171-172]. A few applications of machine-type communication are health care, tracking, sensor monitoring, vehicular telematics, and smart grid [173]. For supporting machine-type communication in 4G LTE-Advanced systems, service requirements for network improvements for machine-type communication are specified in [174] by the

3GPP to address the requirements of 5G networks [175]. Further, the European Telecommunications Standards Institute has already defined the overall end-to-end machine-to-machine functional architecture [176].

Machine-type communication applications are typically hosted by an application server which may be connected directly with a cellular network or may use service capability servers to offer additional control and data services [177]. Devices in machine-to-machine communications can share and operate on unlicensed spectrums of cellular networks and help reduce transmission loads and improve performances of cellular networks [178-180]. There are a number of scenarios for the convergence of machine-to-machine networks and cellular networks as presented in [180]. For example, the most advanced convergence scenario is a fully connected machine-to-machine network that allows a single data flow to be routed through multiple machine-to-machine connections and all machine-to-machine devices can act at a time as cellular consumers as well as machine-to-machine communication providers.

A.1.2 Radio access network performance enabler

A. Cooperative multi-antenna systems

Employing multiple antennas at both a transmitter and a receiver is one of the most useful technologies to increase spectral efficiency and system capacity, and literally the configuration is called MIMO. To avoid ambiguity, we refer to a BS as transmitter and a UE as receiver in the DL and in the UL a UE as transmitter and a BS as receiver in a cellular system. At the system level, the major concepts of multiple-antenna system implementation are either centralized or distributed. In the centralized concept, a number of antennas are collocated at the same BS with a few wavelengths apart from one another. Centralized systems usually work best in terms of performance improvements in capacity and diversity when channels, observed by each antenna, are highly scattered such that the correlation between channels from an antenna array system is the least or none at all. However in reality, because of implementation specific constraints (e.g., physical limitations at transceivers), a large number of antennas are

implemented within a limited space. This causes a high correlation between channels and a low degree of freedom which results in a poor performance. However, if the same number of antennas are distributed geographically and are jointly processed at a central station via ideal backhaul links such as optical fibers, a high degree of independent channels can be achieved [181]. Because of spatial diversities, channel characteristics from these antennas varies significantly from one to another at the same UE and hence results in an improved capacity from achieving a high received signal diversity gain. Further, a reduction in transmission power and path loss can be achieved from spatial diversities of these distributed antennas. This type of multi-antenna system is called DAS [181] and is illustrated in Figure A.1(a).

In MIMO systems, when there is only one user in a BS coverage, we refer to the scenario as a single user-MIMO (SU-MIMO) system as shown in Figure A.1(b). An SU-MIMO system suffers from a high channel correlation since multiple antennas are spaced apart by a short distance both at a BS and a UE. Further, the capacity of a SU-MIMO system is limited by the number of antennas of a UE. This is because the capacity of a MIMO system varies proportionally with spatial multiplexing gain of the link between a BS and a UE, where the gain is directly proportional to the lesser the number of antennas of a transmitter (BS) and a receiver (UE) in the DL, and a UE usually has fewer antennas than a BS. To overcome this problem, a high diversity in spatial channels needs to be achieved. One way to do this is to employ MIMO principles to more than one UE by exploiting randomness of UE distributions in the coverage of a BS, and the resulting system is called multi-user-MIMO (MU-MIMO) as shown in Figure A.1(c). However, the inter-cell interference experienced by UEs, particularly cell-edge UEs, from nearby BSs and UEs is the major bottleneck to an improvement in the overall system capacity.

Cooperation between nearby BSs can be exploited to keep this interference at a minimal or zero level. By introducing coordination between BSs, a higher degree of freedom can be achieved. This configuration is called networked MIMO where a group of BSs coordinate with each other to form a virtual massive multi-antenna system for the DL transmission as shown in Figure A.1(d). In a networked MIMO system [182], data streams from multiple BSs are simultaneously transmitted to multiple UEs within or beyond their cell coverage by cancelling cross-talk interferences. This results in

achieving a spatial multiplexing gain that scales system capacity with cluster size (i.e., the density of cooperating BSs). However, it requires a tight synchronization in terms of transmission time, carrier frequency, sampling clock-rate, and sharing of user data between cooperating BSs for cancelling cross-talk interferences. Since overheads from cooperating BSs increase with cluster size, a networked MIMO system is feasible for small networks. As proposed in [183], CoMPs with MU-MIMO can also be exploited to improve capacity by taking advantages from both the spatial multiplexing gain of MU-MIMO systems and the interference avoidance (nullification) of CoMP systems.

However, 5G networks are expected to support 1000 times the volume of data as the current networks do. In order to address the high capacity demand of 5G networks, a large number of antennas, e.g., hundreds are expected to be deployed in 5G networks. This antenna configuration is called massive MIMO or large antenna systems as shown in Figure A.1(e). A massive MIMO system relies on a high spatial multiplexing gain, and hence it is assumed that a BS has channel knowledge of both

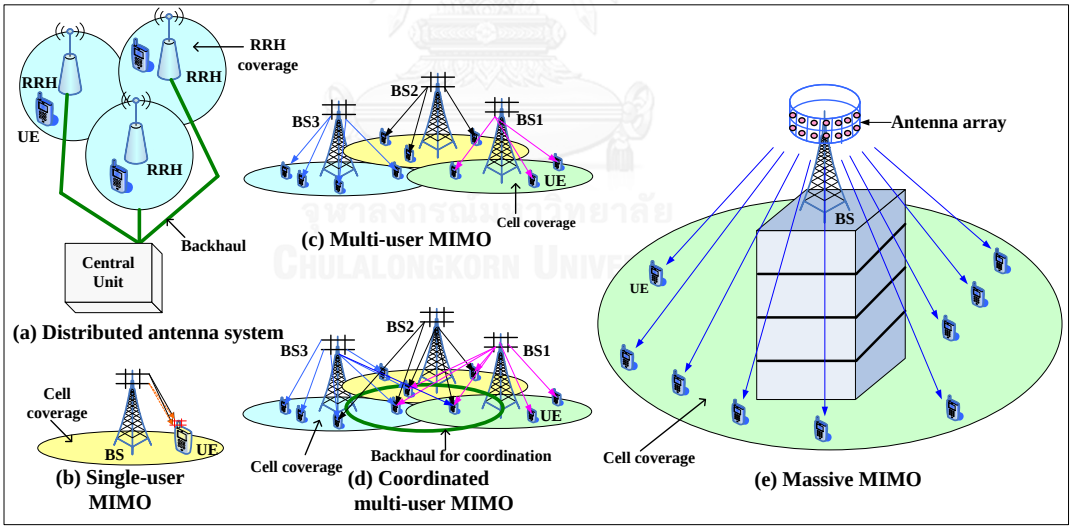

Figure A.1: Multi-antenna configurations.

UL/DL. In the UL, UEs can send pilots, and a BS can measure the channel response of each UE based on these pilot signals. However, the DL channel measurements are not easy. In a frequency division duplex based current LTE systems, BSs send pilots to UEs; UEs then estimate channels based on pilots; and after quantizing estimated channels, UEs send them back to BSs [184]. However, this process is challenging in

the case of a massive MIMO system, particularly for high-mobility users, mainly for two reasons. Firstly, it requires 100 times more resources in the DL than in conventional systems to ensure mutually orthogonal pilots between antennas. Secondly, there is a proportional increase in the number of channel responses with BS antennas for UL. That is why massive MIMO systems are expected to be operated on a time division duplex mode where it can use channel reciprocity between the UL/DL [184]. A number of representative features and challenges of massive MIMO systems are discussed in the followings.

1. Features of massive MIMO systems

- *Operation*: In massive MIMO systems, multiple data streams are sent using the spatial-division multiplexing technique such that different data streams can use the same time and frequency resources. The spatial-division multiplexing is performed with a large number of independently-controlled antennas. Data streams are precoded before transmitting based on the channel responses which are sent in the UL by UEs and received at each antenna of the antenna-array. The precoding matrix is chosen such that the desired signal is strong enough as compared to the interference and noise signals at each intended UE [185]. Similarly, in the UL, each UE transmits its data stream using the same time and frequency resources. The sum data from UEs is received at each antenna and then decoded to retrieve the received signals to produce individual data streams.
- *Architecture*: Massive MIMO systems can be deployed using an array of antennas which are either co-located at the same BS or distributed to cover a certain area [186]. Further, a MCBS can be replaced by a large number of low power antennas.
- *Scalability*: Massive MIMO ensures the scalability issue by employing the time division duplex method. In contrast to the frequency division duplex method, time division duplex is used because of the fact that the time required to collect the channel responses is independent of the number of antennas [185], and there

is almost no bound on the maximum number of antennas that is to be considered in massive MIMO systems with time division duplex [3].

2. Challenges of massive MIMO systems

- *Channel estimation*: Estimating the channel responses accurately is critical to update the precoding matrix, and is one of the major limitations of massive MIMO systems [3]. This is because of the fact that the UE velocity puts a limit on the time interval during which the channel response must be acquired. This in turn limits the maximum number orthogonal pilots that can be obtained and the maximum number of UEs that can be served simultaneously [185].
- *Pilot contamination*: Because of the limited number of pilots for channel estimations, pilots are to be reused in nearby cells. Hence, the pilot sequence of one cell to serve its UEs can be interfered by another cell that uses the same pilot sequence to serve its UEs. This phenomenon is called pilot contamination [185, 187], and is another major challenges for the massive MIMO system implementation.
- *Economic and standardization impacts*: The cost effectiveness of developing massive MIMO systems is not explicitly justified yet [3]. In addition, the real implementation of massive MIMO systems may require a new standard [185].

B. Millimeter wave communications

1. Incentives and features of mmWave

One of the major enablers to address the high traffic demands of 5G networks is to increase system bandwidth by using spectrum aggregation techniques. Current microwave frequencies ranging from 700 MHz to 2.6 GHz [188] for cellular wireless are almost saturated by their practices. Currently, the global bandwidth allocation for cellular wireless is limited to 780 MHz, and an approximate maximum bandwidth of 200 MHz for each major wireless provider across different bands [188-189]. This

motivates the use of mmWave spectrums for 5G networks. According to [188], one of the major differences of 5G systems from 4G systems will be in the use of greater spectrum allocations at mmWave bands. In addition, backhaul networks will be implemented at mmWave bands instead, by replacing existing copper and fiber backhauls. The implementation of a high gain and steerable antenna both at a UE and a BS makes mmWave communications viable over the wireless medium [188, 190, 191]. Noticeable features of mmWave [188] that make the movement toward mmWave communications are as follows:

- An availability of a large amount of usable spectrums in mmWave bands results in achieving a high data rate
- An expansion of channel bandwidth beyond 20 MHz [192]
- A small wavelength of mmWave results in an exploitation of new spatial processing techniques such as massive MIMO, adaptive beamforming [193]
- An availability of a large amount of bandwidth allows handling capacity for BS-to-UE link and BS-to-BS backhaul link in highly populated areas greater than the current 4G systems
- Wireless features result in flexibility and quick deployment of backhauls in dense urban areas
- A small coverage by mmWave results in an exploitation of spatial frequency reuse techniques and new cooperative techniques such as networked MIMO, cooperative relays

2. Propagation characteristics of mmWave

MmWave spectrums have a number of essential propagation characteristics that make the mmWave difficult to achieve seamless coverage and reliability [133, 194-195]. Firstly, an mmWave signal experiences a much higher propagation loss than a microwave signal, which can be compensated by a high-gain directional antenna. Secondly, an mmWave signal faces difficulty in diffracting around obstacles because of its small wavelength. Further, LOS propagations can be blocked by obstacles, and

non-LOS can be blocked from a shortage of multiple paths and a significant attenuation. All these result in a possibility for a link outage if a LOS path does not exist. Thirdly, an mmWave propagation faces difficulty from penetrating solid materials (e.g., a 178 dB attenuation at 40 GHz for brick walls [194]).

3. Spectrums of mmWave

MmWave spectrums range from 3 GHz to 300 GHz with corresponding wavelengths range from 1 mm to 100 mm [196]. However, from this range of mmWave spectrums, the oxygen absorption band which ranges from 57 GHz to 64 GHz with attenuation of about 15 dB/km, and the water vapor absorption band which ranges from 164 GHz to 200 GHz with an attenuation about tens of dBs are to be excluded for mmWave communications. Assume that 40 percentages of the remaining 252 GHz can be potentially explored for the use of mmWave communications, and then a possible new 100 GHz of spectrum [196-197] can be exploited for 5G mobile communications. In an announcement by the Federal Communications Commissions in October 2003, 71-76 GHz, 81-86 GHz, and 92-95 GHz frequencies that constitute aggregately a total of 12.9 GHz bandwidth became available for ultra-high-speed-data communications [196].

Further, the licensed 28 GHz and 38 GHz bands have an available bandwidth of over 1 GHz that could be used for mobile access and backhaul networks [188, 198]. Even though rain and atmospheric attenuations are the major unavoidable drawbacks for mmWave spectrums, the impact from them is not significant enough for 28 GHz and 38 GHz bands because of small mmWave cell sizes. There is only a 1.4 dB attenuation from a heavy rain fall over 200 m distance at 28 GHz. For small distances, typically less than 1 km, the rain attenuation has a minimal effect on mmWave propagations at 28 GHz and 38 GHz [188, 199]. Further, for 28 GHz and 38 GHz, the atmospheric absorption is insignificant for an mmWave cell size of 200 m.

4. Access link and backhaul link of mmWave

MmWave technologies have been proposed for 5G mobile networks [200]. MmWave BS and backhaul systems are expected to be deployed on urban utility poles, street lamps, and building frontages. Access links of mmWave will be assisted by a MCBS for control signaling and synchronization purposes, while user data at a high speed will be provided to a UE by an mmWave BS. Hence, C-plane will be served by a MCBS and U-plane will be served by an mmWave BS. With a multi-hop short distance (up to 100 m - 200 m) LOS mmWave backhaul, a peak capacity of 10-25 Gbps can be provided, and the backhaul can be extended up to 1 km. For such a long distance backhaul, high-end solutions with highly directive antennas (e.g., 30 dBi to 52 dBi gain) are emerging at E-bands [61-62]. Data rates up to 2.5 Gbps using 64 quadrature amplitude modulation on a 500 MHz wide channel has already been announced [61].

Moreover, mmWave backhauls are now commonly accepted among the main network equipment providers, and several prototype network implementations for measurement campaigns have been carried out, e.g., Nokia Siemens Networks in New York at 72 GHz, Samsung in New York, Austin, and Korea at 28 GHz and 38 GHz [61]. However, the main constraints for access link come from UE requirements. For example, UEs are equipped with multi-radio support capabilities such as WiFi and global positioning system, each operating at a distinct frequency with multiple antennas. Further, there is a disproportionate advancement in the development of UE battery technologies with applications. All these make mmWave a technology to be embedded at a minimal impact on the existing hardware of a UE with a minimal space for setting up of a new mmWave radio and antenna. Furthermore, an mmWave access link needs to communicate with a larger coverage in outdoor environments than in indoor environments. This larger coverage in outdoor can be addressed with a high gain antenna and a high transmission power where a UE's size and power consumption can be relaxed [61].

5. Applications of mmWave to emerging technologies

MmWave wavelengths are attractive for new emerging technologies such as massive MIMO to enhance spectral efficiency since more antennas can be located with

a reduced antenna array size. A large gain from beamforming with a large number of antennas can supplement high path losses of mmWave spectrums. However, cell discoveries in mmWave face problems from the directivity. To overcome this problem, SC discoveries at mmWave can be done in a number of ways [201]. One way is that a MCBS handles the cell discovery process. In this case, a MCBS knows a SC's coverage and a UE location. The MCBS informs a SC as a UE heads toward the SC such that the SC can steer its beam toward the UE. The MCBS then informs the UE so that the UE can also steer its antenna beam toward the SCBS. The other way would be to implement both a SCBS and a UE with a capability to operate on both below 3 GHz and mmWave frequencies. In this case, cell discoveries are provided at a frequency below 3 GHz. Once a UE gets connected to a SC, the SC can transmit user data at an mmWave frequency by steering its antenna beam toward the UE. MmWave spectrums can also be applied to new emerging technologies such as device-to-device communications. There are two kinds of device-to-device communications that can be enabled in mmWave spectrums, i.e., local device-to-device and global device-to-device communications. In a local device-to-device communication, two devices communicate to one another via the same BS or via a relay node if a LOS signal is present between them. However, in a global device-to-device communication, two devices are typically associated with two different BSs and can communicate to one another via mmWave backhauls [194].

Further, to address the high capacity demand of 5G networks, SCs are expected to be deployed densely. But, a dense deployment of SCs raises several issues. One of the major concerns is a high cost of fiber backhauls for every SC which in turn raises the practicability of deployment of backhauls to SCs using fibers. However, using wireless backhauls at microwave frequencies to reduce cost is already a well-accepted approach, and an extensive number of microwave point-to-point links are in operation in 4G systems [202-206]. Authors in [202] have proposed a point-to multipoint in-band mmWave wireless solution where both access and backhaul links are multiplexed on the same frequency to address low cost and low latency requirements of ultra-dense 5G networks. Note that usually out-of-band backhauls are dominant in wireless industry [205-206] to overcome an extreme capacity demand in licensed access frequency bands [207-208]. However, in mmWave backhauls, a channel bandwidth can be large so that

inband backhaul approach can be deployed [202]. In Table A.1, a comparative analysis for network capacity improvement approaches, i.e., cooperative communications, multi-antenna systems, dense HetNets, and mmWave communications is given.

A.2 Network control programming platform

A.2.1 Logically centralized programmable control network platform

SDN is a new networking paradigm which provides flexibility, simplicity, and evolvability in network operation, control, and management with a software platform. It principles on separating network intelligences to a logically centralized entity called controller from network processing units called data plane switches to simplify policy enforcement and network configuration and evolution [209]. Though the SDN principle was initially evolved around wired networks, recently it has got a significant momentum in wireless networks. Numerous research projects on wireless SDN (WSDN) are ongoing, and research approaches are proposed to address several issues of WSDN.

A. Conventional SDN concept

The concept of SDN is based on split architecture with the following characteristics [2]

- Network control functions are separated from network forwarding functions.
- Network intelligence is moved to a logically centralized single entity called SDN controller.
- Controller maintains global abstracted network views on which control and management applications work.

Table A.1: A comparative analysis for network capacity improvement approaches.

Features	Cooperative communicat-ion	Multiple antenna system	mmWave communication	Dense HetNet
Enablers	CoMP, eICIC	Massive MIMO, networked MIMO	mmWave spectrums	SCs
Objectives	Interference management	Spatial multiplexing, spatial diversity	Spectrum aggregations	Frequency reuse
Improvement	Spectral efficiency	Spectral efficiency	Bandwidth extension	Capacity
Taking advantages from	Coordination among spatially separated BSs	A massive number of antennas that can be implemented at a BS either centralized or distributed manner	An enormous amount of available bandwidth	Short distance between a UE and a BS
Requirements	Strict backhaul	Maximization of the minimum between the numbers of transmit and receive antennas	Small coverage area typically with 200 m cell radius	Maximizat-ion of frequency reuse
Methodologies	By exchanging CSI and information of data among BSs	By creating multiple parallel data streams and beamforming between a BS and a UE	By enabling highly directive LOS link between a UE and a BS	By deploying SCs as densely as possible in MCs
Enabling degrees-of-freedom	CoMP (e.g., Joint processing) and eICIC (e.g., TD and FD)	Number of antennas for a massive MIMO and cluster size for a networked MIMO system s	28 GHz, 38 GHz, 60 GHz, 71-76 GHz, 81-86 GHz, and 92-95 GHz	PC, FC, RRH, and relay
Applications	MC and SCs	MC and SCs	Backhaul and SCs	SCs

- SDN controller communicates with forwarding nodes using a standard protocol, e.g., OpenFlow.
- Network operators can control and manage network requirements through SDN control and the management programs in SDN controller to be free from vendor agnostic processes.

Because of programmable features of SDN controller, these networks are referred to as software defined [210]. Figure A.2 [211] shows a typical SDN architecture. SDN consists of three planes: a forwarding plane that includes forwarding elements, a control plane that includes network operating system and network hypervisor, and an application plane that includes network control and management applications. In addition, there are two interfaces: southbound (e.g., OpenFlow) and northbound (e.g., XML) interfaces. In the following, we give an overview on components of SDN architecture.

A network operating system, like an ordinary computer operating system, provides an ability to observe and control the network [212]. A network operating system also keeps network states and provides a global view to the controller. The network operating system and applications run on servers. POX, a network operating system written in python, is an example of network operating system. Applications are control and management programs that are usually implemented on top of the network operating system and perform all control and management tasks. The global network view contains results of the network operating system, and applications use it for control and management decisions. Example applications are routing and mobility management. A network hypervisor is used to virtualize physical resources into a number of virtual resources such that multiple users can use the same physical resources concurrently without intervening one another. A hypervisor is software that is installed on a server. An example hypervisor is FlowVisor [213] that acts as a proxy such that all traffic to and from the controller and forwarding switches pass through the FlowVisor in order to enforce a proper policy on packets in each flow to provide isolation between virtual network resources.

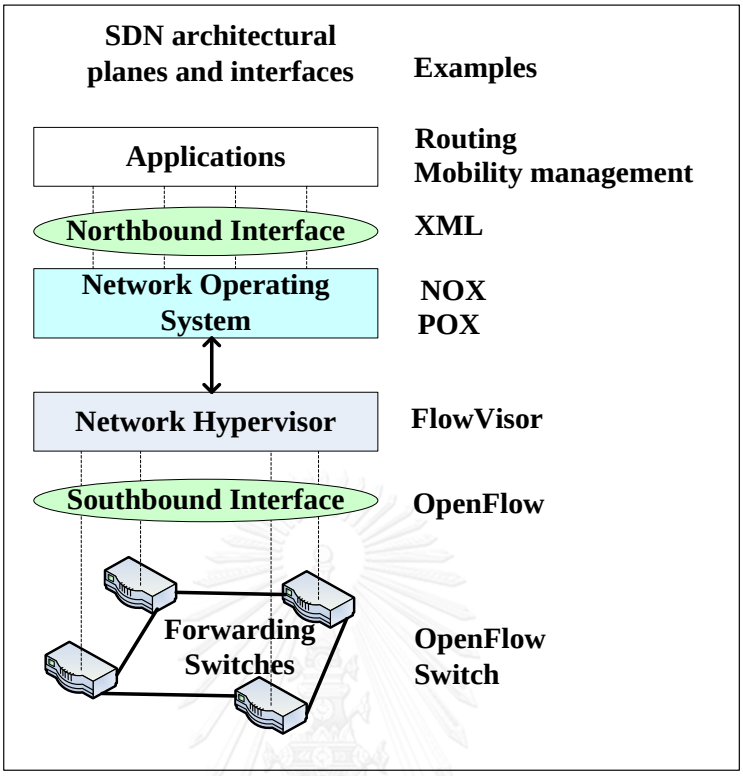

Figure A.2: Typical SDN architecture [211].

A southbound interface provides a necessary medium to communicate the controller with forwarding switches. A well accepted southbound interface is OpenFlow. OpenFlow is a protocol that provides a way to communicate the controller with data paths using match-action rules [214]. When a packet arrives at a data path switch, its packet header is first matched with a flow entry in a flow table resided in each data path switch, and a corresponding action is taken on the packet following OpenFlow specifications for match-action rules such as forward, drop, modify, or send the packet to the controller. A northbound interface allows applications to communicate with the network operating system. There is no standardized northbound interface yet. XML can be used as a northbound interface. SDN forwarding switches are responsible for switching a packet from an ingress port to an egress port. An example forwarding switch is OpenFlow switch that contains a forwarding table incorporating a number of flow entries. Each flow entry has three fields: a packet header defining a flow, an action defining how a packet should be processed, and statistics that keep record on the

number of bytes and packets in each flow and the time since the last packet matched a flow [215]. Each flow is controlled by the controller.

B. WSDN

In wireless networking, there is no single dominant technology. Rather several technologies, e.g., cellular, WiFi, and worldwide interoperability for microwave access (WiMAX), are deployed in a particular scenario. Diversification in technology, distributed network management paradigm, unpredictable wireless medium, and multitude user requirements make current wireless networks hard to manage. SDN with its capability to separate control plane from data plane and to control data plane by providing a physical data plane network abstraction to control and management programs can provide flexibility and simplicity in wireless network control and management tasks. More importantly, it is the physical network abstraction which is the key in SDN that makes a significant impact on decisions of the controller and hence the overall efficiency. Before we discuss applications of SDN to wireless networks, we justify the following properties of SDN regarding wireless technologies.

- *Property 1 - Control plane and data plane can be separated*: In current wireless distributed networking paradigms, network intelligences and processing functionalities of most network entities (e.g., SGW, PGW, and RAN in LTE) are distributed across the network. Through a proper interface (e.g., OpenFlow), the intelligence part of these network entities can be separated from the processing part, and be moved to a logically centralized entity – the controller. All management and decision applications can be implemented on top of the controller and can communicate with physical U-plane of these entities through a proper interface (e.g., XML).
- *Property 2 - SDN controller is technology independent*: SDN controller simply takes decisions based on an abstraction given to it. So, SDN controller is technology independent. Though underlying network abstractions of LTE, WiMAX and WiFi are different, this technology distinction does not have any

impact on the controller operation since the controller works simply on whatever an underlying abstraction it is provided with. Given simply an abstraction of underlying networks, SDN controller takes necessary decisions based on operator's goals provided through applications.

- *Property 3 - Abstracted network can be segmented, and modular implementation can be introduced*: In mobile networks, based on geographical regions, e.g., urban and suburban, we can segment the global view of an underlying network. And since each region has different characteristics replicated in the abstraction of that part of the network, SDN controller can set modular implementation such that there is a module for each region: urban-module, suburban-module, rural-module, and dense HetNet-module. Each module is responsible for that particular region and updates itself according to a change in the network abstraction of that region. This can simplify the controller decision and network management tasks since if there is any change needed for a particular region, only the corresponding module needs to be updated by leaving the rest of the network update unchanged.

A number of WSDN architectures for LTE cellular [216-218] and WiFi/WiMAX [219] have been proposed, mostly by separating access networks from core networks. Few LTE architectures leave legacy LTE networks almost unmodified while others propose changes on current networks and are explained in the following.

1. WSDN architectures without changing existing LTE core networks

A number of architectures have been proposed in [216] based on an integration of SDN with core network entities, e.g., MME, SGW, and PGW. SDN can be integrated as part of either MME for more awareness of mobility requirements, or it can be integrated as part of SGW and PGW to control transport networks. One of these proposed architectures is based on decoupling logical and data planes of SGW and PGW, as shown in Figure A.3 [216]. Logical parts of SGW and PGW are separated and are integrated with an SDN controller. The controller manages data planes of SGW and

PGW. The MME interacts with logical parts of SGW and PGW. The rest of the elements in the network are kept unchanged.

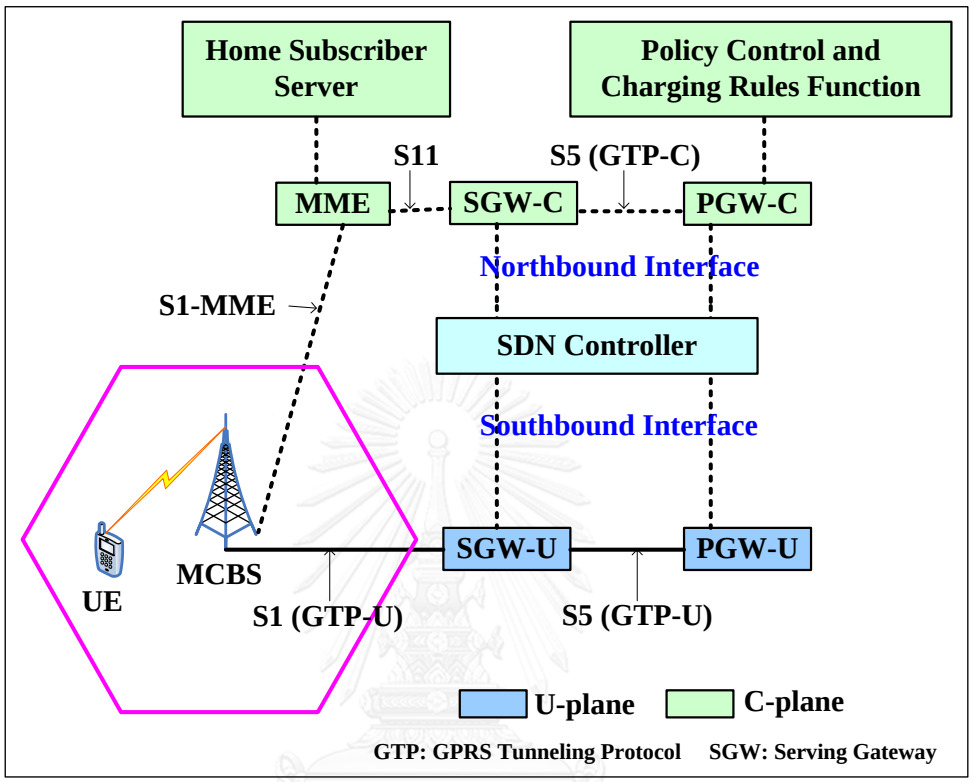

Figure A.3: Integration of SDN with S/P-GW [216].

2. WSDN architectures with changing existing LTE core networks

Softcell architecture has been proposed in [217] which considers changing current LTE core networks by removing core network elements such as SGW, PGW and point-to-point tunneling (Figure A.4). Instead, it considers supporting stateful middleboxes such that all packets in both directions of a connection must traverse the same instance. A controller implements high level service policy to direct traffic through middleboxes by using switch level rules. Each BS is associated with an access switch that is responsible for fine-grained packet classifications on a UE's traffic. The rest of the network consists of core switches, including a few gateway switches. Core switches are responsible for traffic forwarding functions through appropriate middleboxes [217]. The controller directs traffic over the network and middlebox paths

based on service policies which are abstracted at a high level depending on subscriber's attributes and applications. A service policy includes multiple clauses that specify which traffic should be handled in what way. An example service policy clause is: VoIP traffic must go through an echo canceller followed by a firewall.

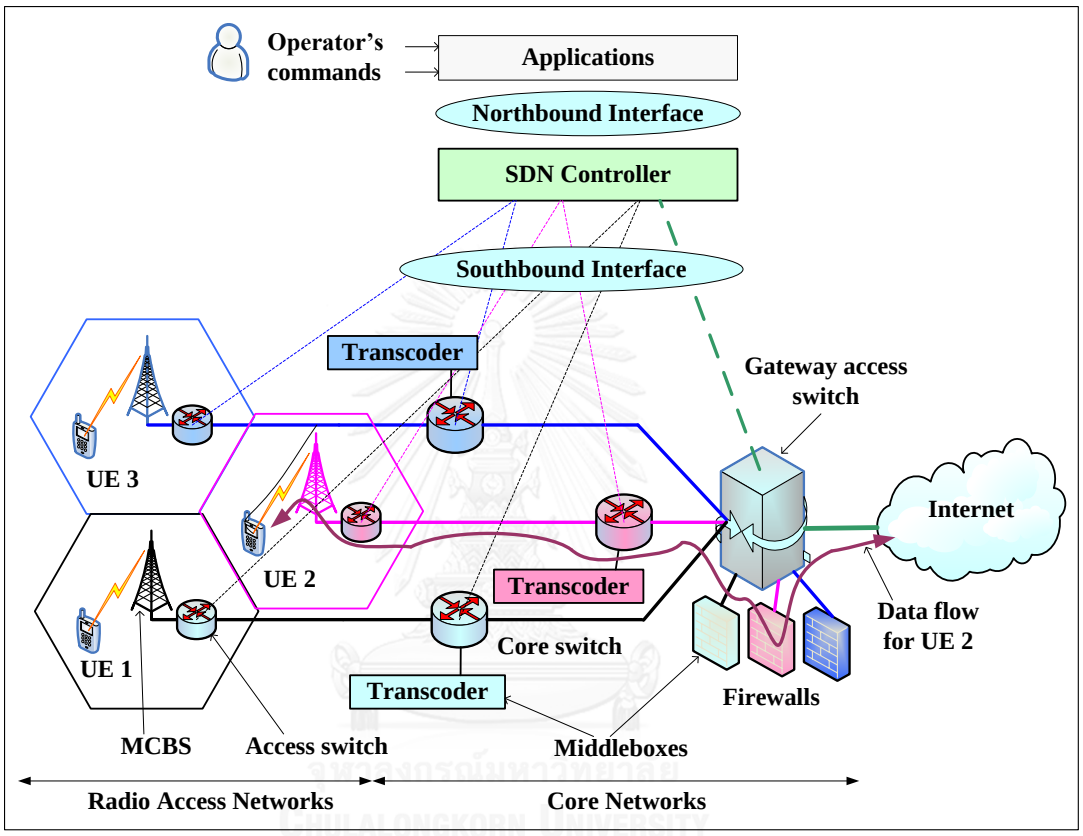

Figure A.4: Softcell network architecture [217].

3. WSDN architectures on existing LTE access networks

SoftRAN architecture which is a result of an application of SDN principle on the LTE RAN is shown in Figure A.5 [218]. SoftRAN is software defined centralized control plane for access networks that abstracts all physical BSs in a geographical area as a virtual big BS. Rather than controlling radio resources of each BS by itself in a distributed manner, all resources are allocated by a central controller among neighboring BSs. Radio resources are abstracted in three dimensions, including space (BS identifier), time, and frequency and are programmed by a logically centralized

controller. In each time-frequency block, the controller needs to make a decision that is conveyed to each BS, and to assign an appropriate transmission power and the flow to

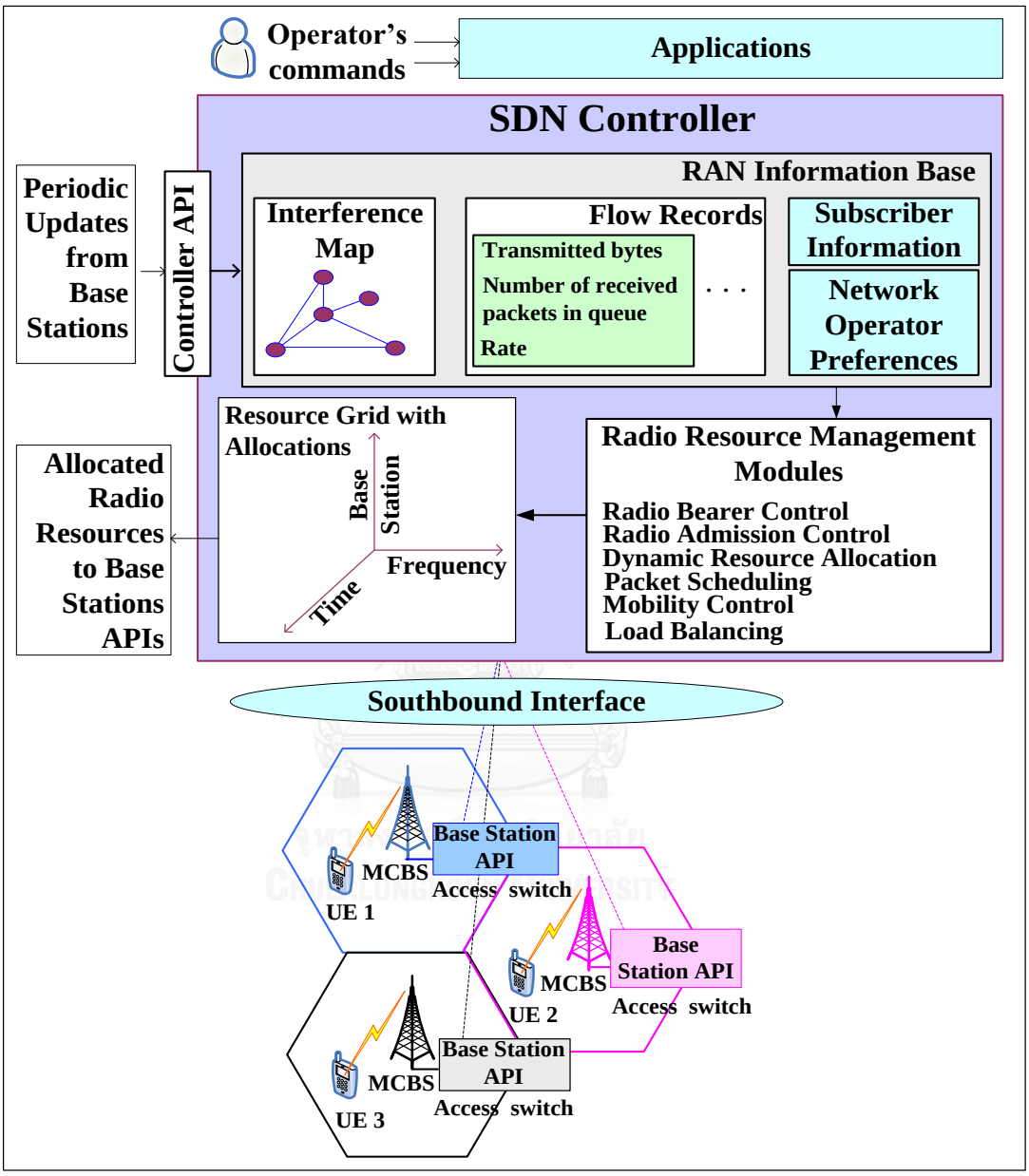

Figure A.5: SoftRAN architecture [218].

be served by a BS. A centralized controller receives local network states periodically from all BSs in a local geographical area. The controller then updates and maintains the global network state in the form of a database called RAN Information Base that contains information on interference maps (in the form of weighted graph), flow records

(e.g., in the form of the number of bytes transmitted), and network operator's preferences (e.g., for priority services) which is accessed by various control modules to take decisions on the radio resource management.

4. WSDN architectures on WiFi/WiMAX networks

OpenRoads or OpenFlow Wireless is a mobile wireless platform for experimental network researches and realistic deployment of networks and services using virtualization techniques as shown in Figure A.6 [219]. OpenFlow Wireless uses

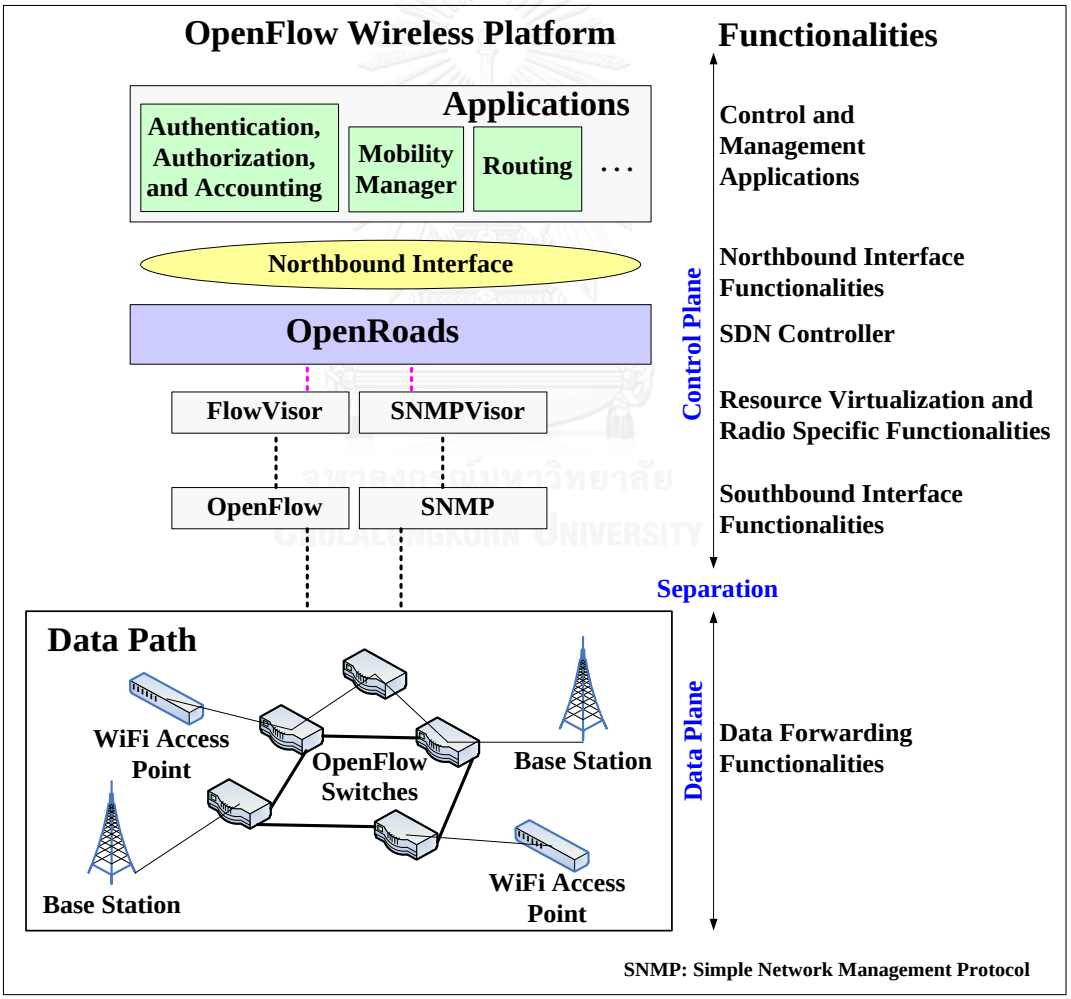

Figure A.6: OpenFlow Wireless architecture [219].

OpenFlow protocols to separate control plane from an underlying data path. A network hypervisor called FlowVisor is used to virtualize data plane to create network slices and to provide isolation between slices such that multiple experiments can co-exist and run in parallel with production networks without any intervention. In addition, a SNMPVisor is also used to configure radio specific problems [219]. All control and management applications communicate with the controller with a standard interface, and their decisions are conveyed to data paths by the OpenFlow protocol.

A.2.2 WSDN implementation requirements and challenges

Even though an adoption of SDN concept is highly desirable for wireless networks, there are several challenges that are to be addressed for the viability of WSDN from experimentation through technology development to policy level. A few of these requirements and challenges are outlined below.

- SDN was developed with wired networks in mind. But characteristics of a wireless medium are far different and unpredictable. Adopting wireless medium characteristics in SDN is very challenging and requires considerable researches on this issue.
- SDN is now in its early stage, and hence most elements of SDN are either under development or not broadly available in commercial markets. For example, the popular OpenFlow protocol specification is under the developing phase and still does not provide all radio configuration related functionalities.
- SDN has so far been proposed to be integrated with current 4G mobile architectures without major changes on current networks (e.g., as proposed in [220]). A full advantage from the adoption of SDN is yet to be proven toward a higher 5G target and beyond.
- Technology-specific bindings of virtualization are important due to a need to preserve efficiency in an unpredictable multi-user multi-access wireless medium [221]. It is also important to understand that not all these technologies benefit equally from various wireless virtualization perspectives [221]. Benefits

of virtualization are mostly apparent in technologies where the bandwidth and the supported number of users are relatively high, leaving enough room for dynamic sharing of resources, such as in 802.11 WLAN and cellular networks.

- OpenFlow does not provide any feature to configure data path elements, e.g., transmission power management and channel allocation. Therefore, an efficient wireless resource allocation and interference management cannot be achieved without more enhancements in the radio hardware. A comparative analysis for distributed and centralized network control programming approaches is given in Table A.2.

Table A.2: A comparative analysis for network control programming approaches.

Features	**Logically distributed programmable control networks**		**Logically centralized programmable control networks**
	Cell-centric control	**Device-centric control**	
Network architecture	Cell-centric	Device-centric	WSDN controller-centric
Network programming	Networking device level	Networking device level	WSDN controller level
Network control assessment	Based on a local network view	Based on a local network view	Based on a global network view
Network control mechanism	Both logically and physically distributed	Both logically and physically distributed	Logically centralized but physically distributed
Control plane and data plane of a networking device	Integrated in the same networking device	Integrated in the same networking device	Control plane is separated from data plane
UE control mechanism	Fully networked controlled	Both network and device controlled	Fully controlled by a WSDN controller
Control and management of network requirements	Vendor agnostic	Vendor agnostic	Free from vendor agnostic processes

A.3 Control-and user-plane separation architecture

In CUSA, C-plane is provided by MCs operating typically at low frequencies such as below 3 GHz to provide a large coverage, and U-plane is provided by SCs (e.g., FCs) operating typically at high frequencies such as mmWave to provide a high data rate services to UEs. MCs may also be responsible for a low data rate services. C-plane is responsible for system configuration and management [7] to provide system information to access network, synchronization information for timing frames and symbols, and reference signals for CSI. Whereas, U-plane is responsible mainly for providing on-request data traffic and some acknowledgement information such as hybrid automatic repeat request. Note that some control signaling of both planes cannot be decoupled completely since they are UE traffic request specific such as CSI and timing frame and symbol levels, and hence they are present in both planes. In CUSA, the definition of coverage is twofold, namely area coverage and service coverage [9]. Area coverage can be defined as the coverage that is provided by MCBSs (i.e., C-plane BSs) for network access and service request, whereas service coverage can be defined as the coverage provided by SCBSs (i.e., U-plane BSs) with promised quality-of-service, e.g. data rate. Hence, a user with no active-data request can have area coverage without having had any service coverage.

A.4 In-building cellular mobile communications

A.4.1 Multi-floor and floor material attenuation

As reported in [222], the attenuation caused by multi floors is a non-linear function of the number of floors between transmitter and receiver, with a standard deviation ranges from 3.2 dB to 10.5 dB for the measurements taken in 3 different buildings. With an increase in floor number, an additional path loss experienced by the received signal per floor decreases, i.e. the difference of path loss between floors 1 and 2 is greater than that between floors 3 and 4. This implies an existence of additional

sources of signal such as multi-path scattering from surrounding buildings. Information on building layouts and so on can be found in [222]. From [222], it can be concluded that the measurement based statistical/empirical results, e.g. for attenuation factor, are site specific and deviate considerably from one building to another.

The same result for floor attenuation response has been reported by the authors in [120] by considering two paths for signal propagation of which one involves transmission through floors, and the other comprises of paths having segments outside buildings as well as involved diffraction at window frames. The authors showed that the measured signal falls by about 12 dB per floor at the receiver for the first six floors of separation. Further, with an increase in separation distance by more than eight floors, the received signal declines gradually, i.e. non-linear response of signal attenuation with the number of floors. This statistic of attenuation is used for modeling attenuation factor within a 3D building in this research.

A.4.2 Indoor propagation modeling

There are two major approaches to predicting indoor propagation [224], namely empirical modeling and theoretical modeling. However, empirical modeling has a number of limitations as follows:

- Measurement data must first be obtained in order for the empirical parameters to be determined.
- Propagation models can generally only model propagation phenomena which do not set out radically from propagation in free space.
- The use of this model restrictive, and the transportability of the model cannot be guaranteed even for similar environments [223].

Empirical or statistical approaches to predicting path loss take the following form [224],

$$\mathrm{PL}(d)\,[\mathrm{dB}] = 10\log_{10}(d/d_0)^{n_{\exp}} + \sum_{p=1}^{\mathrm{WL}} WAF(p) + \sum_{q=1}^{\mathrm{FL}} FAF(q) \qquad \text{(A.1)}$$

where WL and FL are the number of walls and floors respectively between the transmitter and receiver. The empirical parameters $n_{\exp}$, $WAF(p)$, and $FAF(q)$ are termed as path loss exponent, wall attenuation factor, and floor attenuation factor respectively [224].

In theoretical modeling, electromagnetic theory is applied more rigorously using ray-tracing techniques such as the uniform theory of diffraction which invokes detailed site specific information about the particular building. Predictions based on ray tracing can predict complex propagation phenomena such as diffraction and reflection. However, it suffers from such limitations as long computational time and consideration for alteration of the permittivity constants to match with the measured values, resulting its advantages over empirical models questionable.

A number of works applied theoretical modeling. For instances, authors in [223] proposed a general 3D theoretical model using the ray-tracing technique to estimate radio loss. Authors in [64] have also presented a comprehensive 3D ray-tracing model for inter-floor and measurements of power delay profiles for two-floor scenario. Due to the complexity of fully electromagnetic models and the necessity for comprehensive information of the physical geometry and layout, a number of approaches have already been proposed to develop a model in the middle ground between empirical and ray tracing techniques. Authors in [224] have proposed a new empirical propagation model which incorporates much of the propagation phenomena that is suggested by electromagnetic theory such as uniform theory of diffraction, but still retains the straightforwardness of the empirical approach. Also, authors in [225] have proposed a mechanistic model that maintains the precision of their electromagnetic fundamentals. It is however suitable for system design.

A.4.3 Types of building and their impact on signal propagation

Owing to a strong dependency of the received signal statistics on the types of buildings, different types of buildings need to be classified to provide bounds on the received signal statistics. Since a detail description of a building under test would make the classification of similar types of buildings difficult, in [108], authors attempted to

provide a classification which, to some extent, disregards the detailed structure of any particular building. A classification of buildings has been proposed in [108]. Based on this classification, the received signal statistics and channel models for any particular type of building are given by treating narrowband and wideband measurements separately. In general, as reported in [108], it has been found that

- Penetration loss is dependent on the construction materials of a building, building orientation with respect to transmitter, internal layout, floor height, and the percentage of windows in a building. Therefore, the variability of penetration loss makes the indoor environment different from that of land mobile radio as far as interference is concerned.
- Spatial and temporal distributions are also different in an indoor environment from a land mobile radio. The spatial fading rate is much lower in an indoor environment because of the slower motion of the receiver. Nulls between 20 and 30 dB are observed when the receiving antenna is moved through small distances. The temporal fading is much higher in an indoor environment because the antennas are not shielded and not at a high elevation as is the case in land mobile radio. Burst type fading of the order of 17-30 dB with 20 to 40 seconds duration has been measured.

The wide variability of the values and models of these parameters make it difficult to determine exact models for different parameters which can be used for different types of buildings [108]. As reported in [108],

- The rate of decay varies between 0.45 and 8.6 depending on the types of buildings, the relative position between transmitter and receiver, conditions of transmission, types of materials used in a building, and frequency.
- Penetration loss varies widely for different types of buildings as well as frequencies ranging from -2 to 38 dB.

These changes which are mainly due to the characteristics of buildings make the system planning quite difficult. The plan for modeling the wideband (i.e., not necessarily a frequency flat response) portable channel is to some extent similar to that of terrestrial mobile radio channel [108]. This plan consists of two major phases as follows:

- In the first phase, the available data should be used to model the channel on small scale basis, e.g. over a building. This modeling should be carried out by estimating the statistical parameters such as root mean square time delay spread in conjunction with appropriate statistical distributions for individual paths, e.g. distribution of amplitude, phase, and time delay for each path.
- In the second phase, the derived small scale statistical parameters should be used to put bounds on their values over the similar types of buildings [108]. This can lead to large area characterization similar to that of terrestrial mobile radio channel.

A detail description on narrow band and wideband modeling can be found in [108].

A.4.4 In-building signal propagation modeling to enforce a minimum distance between small cells

There are mainly two approaches that can be considered for modeling propagation for in-building scenario:

- One approach is to consider the nearby building reflection effects particularly in urban environments where buildings are in close proximity to one another.
- The other approach is not to consider the nearby buildings' reflection effects such that an isolated building is concerned, and only in-building propagation of signals through floors, reflected signals from walls, ceilings, and floors, and diffracted signals from edges of buildings through windows are to be considered. This is, to a great extent, a valid assumption when the transmitter

and receiver are both inside the buildings such that there is sufficient building attenuation to make the effects of the surroundings insignificant [108].

Certainly, considering the second approach will make the modeling simpler but less accurate particularly for dense urban environments. However, simplification of modeling indoor propagation is worthy enough to address the issue of enforcing minimum distance for reusing resources within a building where both transmitter and receiver are located in close proximity.

APPENDIX B

DEFAULT SIMULATION PARAMETER AND ASSUMPTION

In this appendix, default simulation parameters and assumptions used for system level simulations for each chapter are given in Tables. Since a number of parameters and assumptions are common for different simulation scenarios, in order to avoid repetition, we categorize them into two segments, one which includes all the common parameters and assumptions, and the other which includes those used only for any specific simulation scenarios. Because CUCA and CUSA are the two major system architectures considered in this work, both common and specific parameters and assumptions are tabulated chapter wise based on whether any simulation scenarios belongs to CUCA and CUSA as follows.

Table B.1: Default and common simulation parameters and assumptions for the C-/U-plane split architectures.

Parameter and assumption			Value
E-UTRA simulation case[1]			3GPP case 3
Cellular layout[2] and Inter-site distance[1,2]			Hexagonal grid, dense urban, 3 sectors per MC site and 1732 m
Carrier frequency[2,3] and transmit direction			2 GHz (microwave), 60 GHz (mmWave line-of-sight) and DL
System bandwidth			5 MHz (for both 2 GHz and 60 GHz)
Type of FCs			CSG
Total BS transmit power[1] (dBm)			46 for MC[1], 37 for PC[1], 20 (for 2 GHz) and 17.3 (for 60 GHz) for FC[1,3]
co-channel fading model[1]			Frequency selective Rayleigh for MC and PC and Rician for FC
Path loss	MCBS and a UE[1]	outdoor MU	PL(dB) = 15.3 + 37.6log$_{10}R$, R is in m
		indoor MU	PL(dB) = 15.3 + 37.6log$_{10}R$ + L$_{ow}$
	PCBS and a UE[1]		PL(dB) = 140.7+36.7log$_{10}R$, R is in km

(*continued*)

Table B.1 (*continued*)

Parameter and assumption		Value
Path loss	FCBS and a UE[1,2,3]	PL(dB) = 127+30log$_{10}$(R/1000), R is in m (for 2 GHz), PL(dB) = 68+21.7log$_{10}$(R), R is in m (for 60 GHz)
Lognormal shadowing standard deviation (dB)		8 for MCBS[2] , 10 for PCBS[1], 10 (for 2 GHz) and 0.88 (for 60 GHz) for FCBS[2,3]
Antenna configuration		Single-input single-output for all BSs and UEs
Antenna pattern (horizontal)		Directional (120^0) for MC[1] and omnidirectional for PC[1] and FC[1]
Antenna gain plus connector loss (dBi)		14 for MCBS[2], 5 for PCBS[1], 5 (for 2 GHz) and 5 (for 60 GHz, Biconical horn) for FCBS[1,3]
UE antenna gain[2,3]		0 dBi (for 2 GHz), 5 dBi (for 60 GHz, Biconical horn)
UE noise figure[2,4] and UE speed[1]		9 dB, 3 km/hr
Total number of MUs and number of UEs per FC		30 and 1
PC coverage and MUs offloaded to all PCs[1]		40 m (radius), 2/15
Percentage of indoor MUs[1], external wall penetration loss[1] (L_{ow})		35% , 20 dB
CSI		Ideal
Scheduler and traffic mode		Proportional Fair and full buffer
TTI[1], T, and scheduler constant (t_c)		1 ms, 8 ms, and 100 ms
Simulation run time for any ABS pattern T and total simulation run time		8 ms and ($T \times \lvert\varphi\rvert$)

taken [1]from [93] , [2]from [88], [3]from [133], and [4]from [134].

Table B.2: Default and specific simulation parameters and assumptions for the C-/U-plane split architecture in Chapter 5.

Parameter and assumption	Value	
Number of cells	One MC, two PCs, and 10 FCs	
FC building model[1] (3GPP dual strip FC model)	Number of apartments per floor	40
	Number of floors	4
	Total number of FCBSs	10

taken [1]from [93].

Table B.3: Default and specific simulation parameters and assumptions for the C-/U-plane split architecture for non-uniform and asymmetric traffic in Chapter 8.

Parameter and assumption	Value	
Number of cells	One MC, two PCs, and 5 FCs	
FC building model[1] (dual strip FC model)	Number of apartments per floor	40
	Number of floors	4
	Total number of FCs	5

taken [1]from [93].

Table B.4: Default and specific simulation parameters and assumptions for the C-/U-plane split architecture in Chapter 6.

Parameter and assumption	Value
Number of cells	One MC, two PCs, and 1 FC
[5]The value of β	0.6

taken from [5][90].

Table B.5: Default and common simulation parameters and assumptions for the C-/U-plane coupled architectures.

Parameter and assumption			Value
E-UTRA simulation case[1] and transmission direction			3GPP case 3 and DL
Cellular layout[2] and inter-site distance[1,2]			Hexagonal grid, dense urban, 3 sectors per MC site, and 1732 m
Carrier frequency[2] and system bandwidth			2 GHz and 5 MHz
Total BS transmit power[1]			46 dBm for MC[1], 37 dBm for PC[1], and 20 dBm for FC[1]
Fading model[1]			Frequency selective Rayleigh for MC and PCs and Rician for FCs
Distance-dependent path loss	MCBS and a UE[1]	MU is outside	PL(dB) = 15.3 + 37.6log$_{10}$*R*, where *R* is in m
		MU is inside an apartment	PL(dB) = 15.3 + 37.6log$_{10}$*R* + L_{ow}, where *R* is in m, and L_{ow} is the penetration loss of an outdoor wall
	PCBS and a UE[1]		PL(dB) = 140.7+36.7log$_{10}$*R*, where *R* is in km
	FCBS and a UE[1,2]		PL(dB) = 127+30log$_{10}$(*R*/1000), where *R* is in m
Lognormal shadowing standard deviation			8 dB for MCBS[2], 10 dB for PCBSs[1], and 10 dB for FCBSs[2]
Antenna configuration			Single-input single-output for all BSs and all UEs
Antenna pattern (horizontal)			Directional (120^0) for MC[1] and omnidirectional for PCs[1] and FCs[1]
Antenna gain plus connector loss			14 dBi for MCBS[2], 5 dBi for PCBSs[1] and FCBSs[1]
UE antenna gain[2], UE noise figure[2] and UE speeds[1]			0 dBi, 9 dB, and 3 km/hr
Total number of MUs			30
PC coverage and fraction of MUs offloaded to all PCs[1]			40 m (radius) and 2/15
Percentage of indoor[1] MUs and external wall penetration loss[1]			35% and 20 dB (for indoor MUs)
ABS pattern and APP			1/8, 8 ms
Scheduler and traffic model[2]			Proportional Fair and full buffer
TTI[3] and Proportional Fair scheduler time constant t_c			1 ms and 100 ms

taken [1]from [37], [2]from [88] and [3]from [84].

Table B.6: Default and specific simulation parameters and assumptions for the C-/U-plane coupled architecture in Chapter 4.

Parameter and assumption			Value
Number of cells			1 MC, 2 outdoor PCs, and 250 indoor FCs
3D multi-floor building and FC network modeling	Number of buildings		1
	Number of floors		10
	Number of apartments per floor		25
	Number of FCBSs per apartment		1
	FCBS activation ratio		100%
	FCBS deployment ratio		1
	Total number of FCBSs per building		250
	Number of UEs per FCBS		1
	Area of an apartment		10×10 m^2
	Minimum horizontal distance between sFU and sFCBS		5 m
	Location of a FCBS in an apartment		Center
	Reused frequency per cFCBS		1 MHz and 2 MHz
	Link capacity constraint for cFCBSs		3.459 bps (for resource reuse strategy 2)
	Maximum number of cFCBSs	Intra-floor level	8
		Inter-floor level	Single-sided 1
			Double-sided 2
Simulation run time			8 ms

Table B.7: Default and specific simulation parameters and assumptions for the C-/U-plane coupled architecture in Chapter 3.

Parameter and assumption	**Value**
Number of cells	One MC, four outdoor PCs, and 10 indoor CSG FCLs
FCL model[1]	320 FCs for 10 FCLs where $U_F = 32$ FCs per FCL with an activation ratio of 100%
Simulation run time for any ABS pattern, T and total simulation run time	8 ms and $(T \times \lvert\varphi\rvert)$
Side length of a square-grid apartment[2], a	10 m
Free space around its building of a FCL[2]	10 m
ABS pattern period, T_{APP}	8 ms
Implementation loss factor[3,5], β	0.6

taken [1]from [37] and [2]from [88] and [3]from [93], [4]from [95], [5]from [90].

Table B.8: Default and specific simulation parameters and assumptions for the C-/U-plane coupled architecture in Chapter 7.

Parameter and assumption	Value	
Number of cells	1 MC, 2 outdoor PCs, and 25 indoor FCs	
FC building	Number of buildings and floors	1 and 1
	Number of apartments/floor and FCBSs/apartment	25 and 1
	Number of FCBSs/apartment and UEs/FCBS	1 and 1
	Location of a FCBS in an apartment	Center
ABS pattern, APP, and simulation run time	1/8, 8 ms, and 8 ms	

Table B.9: Default and specific simulation parameters and assumptions for the C-/U-plane coupled architecture for FC clustering and resource reuse in 3D buildings in Chapter 8.

Parameter and assumption	Value
Number of cells	1 MC, 2 PCs, and 1 FC
[3]the value of β	0.6
FC model[2]	3GPP dual strip
TTI[1], T, and scheduler constant (t_c)	1 ms, 8 ms, and 100 ms
Simulation run time for any FBS pattern T and total simulation run time	8 ms and ($T \times \lvert \alpha_{fbs} \rvert$)

taken [1]from [93] , [2]from [88], and [3]from [90].

APPENDIX C

GENERIC SCHEDULING ALGORITHM AND CAPACITY ESTIMATION OF A MULTI-TIER NETWORK

In this Appendix C, we describe the generic proportional fair scheduler and the capacity estimation of a multi-tier network model, which we consider to carry out performance analysis and refer to this appendix whenever necessary in any chapters.

C.1 Proportional fair scheduling

Because of ensuring an optimal trade-off between fairness in resource allocation and throughput per user performances in comparison with other conventional schedulers such as Round Robin and max-SINR, we consider proportional fair scheduler to schedule radio resources, specifically time and frequency among UEs. Based on the current and past average throughputs of a UE, a proportional fair scheduler schedules a UE with the maximum performance metric given by [91]

$$x_i(t) = \arg\max_x \left(\sigma_{x,i}(t)/\tilde{\sigma}_{x,i}(t)\right) \tag{C.1}$$

where $\sigma_{x,i}(t)$ and $\tilde{\sigma}_{x,i}(t)$ represent respectively the current and past average throughputs of UE x at RB i in TTI t. Let $x_i(t)$ denote the UE scheduled in TTI t at RB i. The past average throughput $\tilde{\sigma}_{x,i}(t)$ at RB i is updated in every TTI as [92]

$$\tilde{\sigma}_{x,i}(t+1) = \begin{cases} \tilde{\sigma}_{x,i}(t)(1-1/\mathrm{t_c}) + \sigma_{x,i}(t)(1/\mathrm{t_c}), & x = x_i(t) \\ \tilde{\sigma}_{x,i}(t)(1-1/\mathrm{t_c}), & x \neq x_i(t) \end{cases} \tag{C.2}$$

where $\mathrm{t_c}$ denotes adjustable time constant.

C.2 Capacity estimation of a multi-tier network

The received SINR for a UE at RB *i* in TTI *t* can be expressed as

$$\rho_{t,i} = \left(P_{t,i} / (n_{t,i} + I_{t,i})\right).H_{t,i} \quad \text{(C.3)}$$

where $P_{t,i}$ is the transmission power; $n_{t,i}$ is the noise power; $I_{t,i}$ is the total interference signal power; and $H_{t,i}$ is the link loss for a link between a UE and a BS at RB *i* in TTI *t*. The channel response $H_{t,i}$ can be expressed in dB as

$$H_{t,i}(\text{dB}) = (G_t + G_r) - (L_{\text{F}} + \text{PL}_{t,i}) + (\text{LS}_{t,i} + \text{SS}_{t,i}) \quad \text{(C.4)}$$

where $(G_t + G_r)$ and L_F are respectively the total antenna gain and connector loss, and $\text{LS}_{t,i}, \text{SS}_{t,i}$, and $\text{PL}_{t,i}$ respectively denote large-scale shadowing effect, small-scale Rayleigh fading or Rician fading, and distance dependent path loss between a BS and a UE at RB *i* in TTI *t*.

Using Shannon's capacity formula, a link throughput at RB *i* in TTI *t* in bps per Hz is given by [89-90]

$$\sigma_{t,i}(\rho_{t,i}) = \begin{cases} 0, & \rho_{t,i} < -10\,\text{dB} \\ \beta \log_2\left(1 + 10^{(\rho_{t,i}(\text{dB})/10)}\right), & -10\,\text{dB} \le \rho_{t,i} \le 22\,\text{dB} \\ 4.4, & \rho_{t,i} > 22\,\text{dB} \end{cases} \quad \text{(C.5)}$$

where β = 0.6 denotes implementation loss factor.

APPENDIX D
LIST OF PUBLICATIONS

In this Appendix D, we list out all the published, accepted, and under-review journal and conference articles based on this dissertation research by mentioning the chapter which contents are used for any articles.

D.1 Published/accepted journal articles

1. *Saha, R. K., Saengudomlert, P., and Aswakul, C.* Evolution toward 5G mobile networks – a survey on enabling technologies. Engineering Journal 20, 1 (2016): 87-119. [Indexed in ISI Web of Science/SCOPUS]. Content taken from Chapter 2 and Appendix A.

2. *Saha, R. K., and Aswakul, C.* A novel frequency reuse technique for in-building small cells in dense heterogeneous networks. IEEJ Transactions on Electrical and Electronic Engineering, Wiley Blackwell, USA (Accepted on 14 OCT 2016) [Indexed in ISI Web of Science/SCOPUS]. Content taken from Chapter 3.

3. *Saha, R. K., and Aswakul, C.* A tractable analytical model for interference characterization and minimum distance enforcement to reuse resources in 3D in-building dense small cell networks. International Journal of Communication Systems, Wiley Blackwell, USA, (In publication, accepted on 14 OCT 2016) [Indexed in ISI Web of Science/SCOPUS]. Content taken from Chapter 4.

4. *Saha, R. K., and Aswakul, C.* Incentive and architecture of multi-band enabled small cell and UE for up-/down-link and control-/user-plane splitting for 5G

mobile networks. Frequenz Journal of RF Engineering and Telecommunications, Degruyter, Berlin, Germany, (Published online ahead of print on 28 NOV 2016). [Indexed in ISI Web of Science/SCOPUS]. Content taken from Chapter 5.

D.2 Accepted conference articles

5. *Saha, R. K., and Aswakul, C.,* Capacity analysis of control-/user-plane traffic of different small cell base station architectures for 5G cellular. IEIE/IEEE International Conference on Electronics, Information and Communication (ICEIC), 2017 (accepted on 02 NOV 2016). [Indexed in IEEEXPlore]. Content taken from Chapter 6

6. *Saha, R. K., and Aswakul, C.,* Centralized 3D radio resource allocation and scheduling in control-/user-plane split architecture for heterogeneous 5G cellular. IEIE/IEEE International Conference on Electronics, Information and Communication (ICEIC), 2017 (accepted on 02 NOV 2016). [Indexed in IEEEXPlore]. Content taken from Chapter 7

7. *Saha, R. K., and Aswakul, C., A* novel clustering, frequency reuse and allocation technique for 2D regular grid-based dense urban femtocell deployment for 5G mobile networks. IEIE/IEEE International Conference on Electronics, Information and Communication (ICEIC), 2017 (accepted on 02 NOV 2016). [Indexed in IEEEXPlore]. Content taken from Chapter 8

8. *Saha, R. K., and Aswakul, C.,* Micro-and millimeter-wave enabled small cell for non-uniform and asymmetric traffic in 5G mobile network. IEIE/IEEE International Conference on Electronics, Information and Communication (ICEIC), 2017 (accepted on 02 NOV 2016). [Indexed in IEEEXPlore]. Content taken from Chapter 8

REFERENCES

VITA

Mr. Rony Kumer Saha is currently a Ph.D. student at the department of Electrical Engineering, Chulalongkorn University (CU), Thailand. He received the Master of Engineering in Information and Communications Technologies (ICT) from Asian Institute of Technology (AIT), Thailand in 2011 and the Bachelor of Science in Electrical and Electronic Engineering (EEE) from Khulna University of Engineering and Technology (KUET), Bangladesh in 2004 with distinct CGPAs in both levels. Mr. Saha has been awarded the 100th anniversary CU Fund for Doctoral Scholarship and EECU-PhD Honors Program Scholarship in PhD study level. He was also the recipient of AIT scholarship and AIT fellowship in graduate level and university merit based scholarship in undergraduate level.

Mr. Saha worked as Lecturer in the department of EEE at American International University-Bangladesh (AIUB), Bangladesh during January 2005-July 2008 where he rejoined in May 2011 and worked until August 2013. He worked at East West University, Bangladesh as Senior Lecturer in the department of EEE from 01 September 2013 to 25 July 2014. His research interests mainly include indoor small cell network densification, 5G ultra-dense HetNets, and radio resource allocation and scheduling.